Parametric Studies of Cavitation Dependence on Hydrocarbon and Biodiesel Fuel Injection Flows

Nadia NDAMUSO, ***M.Eng***

A dissertation submitted in fulfilment of the requirements for the degree of

Doctor of Philosophy

City University of London

School of Mathematics, Computer Science and Engineering

September 2017

Blank Page

TABLE OF CONTENTS

Blank Page

LIST OF FIGURES

Blank Page

LIST OF TABLES

Blank Page

I hereby declare that the work presented in this thesis is wholly my own and that all material extracted from other sources or developed in a joint effort with other members of the research group is clearly stated and referenced in the text accordingly.

I grant powers of discretion to the University Librarian to allow this thesis to be copied in whole or in part without further reference to me. This permission covers only single copies made for study purposes, subject to normal conditions of acknowledgement.

London, September 2017

Nadia Ndamuso

ACKNOWLEDGEMENTS

I dedicate this work to my dad – Thank you for your kind words of encouragement and for always believing in me even when I did not believe in myself at times. You have been my role model all my life and continues to play a tremendous part in it.

A big thank you to the City University Center of Energy and Transport Team: to Mr. J Hooker for the kindness he showed me and the support he offered me during my time at City University from my first year as undergraduate to my last year as a PhD candidate. To my supervisor Dr. R. Lockett for having believed in me enough to offer me the opportunity to work alongside him. For his support, all through my time at the university and for his guidance and understanding when things did not go accordingly. To Mr. M. Smith, Mr. G. Clow and Mr. J. Ford for their technical advice and support all through my PhD.

I acknowledge the financial support of Shell Global Solutions who has been the main sponsor for this study. To Mr. Trevor Davies and Mr. Richard Price thank you for your collaboration.

I would also like to thank all those who, along the way have helped me through highs and lows – To my husband, thank you for your patience. To my mum, sisters and brothers, thank you for the time taken to take care of my beautiful girls in order for me to concentrate on the thesis. To friends and to all those I did not mention by name, I had tremendous help and enjoyed my time as a PhD candidate at the university because of you. Thank you for being there!

N. Ndamuso

Blank Page

ABSTRACT

The parametric studies investigated the cavitation phenomena occurring in Diesel Fuel Injection Equipment using immersed jets. The studies looked at cavitation from the incipient stage, to the fully developed stage, to leaving the fuel to cavitate for a sustained period of time. The studies were conducted with the aim of understanding the cavitation phenomena occurring inside the Fuel Injection Equipment making use of purposed built continuous flow rigs.

The **first part** investigated the onset of cavitation taking place inside a mechanical 80 bar continuous recirculated flow rig that mimicked the flow inside the injectors spill valves as well as the flow inside the high-pressure pumps spill valves during the first stages of cavitation.

High velocity jets of variable concentration were considered, from the incipient stage to the fully developed stage, focusing on the impact that changing the fuel composition has on the jets as well as on the impact it has on the geometrical parameters of the nozzle valves. The rig made use of custom made Acrylic, Brass and Aluminum-steel nozzles of Cylindrical, Hemispherical and Conical geometries respectively.

The n-Octane, n-Decane, n-Dodecane, n-Tetradecane and n-Hexadecane mixtures were directed into an optically accessible receiver using single hole injector nozzles of 0.14mm and 0.25 mm hole diameters respectively. Parameters such as the fuel composition, the geometry and the material of the nozzles, as well as the operating conditions of the fuels were looked into where 25 repetitive sets of measurements were completed taking into consideration each parameter respectively. Incipient cavitation was associated with the flow outside of the nozzle and was visually observed at the top of the nozzle hole. Cavitation additionally occurred between the layers of the turbulent high immersed jet flow and the stagnant fluid inside the receiver.

The onset of cavitation was obtained using the fuel Upstream Pressure to Downstream Pressure ratio. At the point of onset, the results showed that the Upstream Pressure to Downstream Pressure ratio decreased with the increase of n-Octane percentage in the mixture when considering the Cylindrical and the Hemispherical nozzles. When considering the Conical nozzle on the other hand, the critical Upstream Pressure to Downstream Pressure ratio increased with the increase of n-Octane concentration. The results also showed that the jet length and width increased when varying the diameter of the nozzle hole from 0.14 mm to 0.25 mm.

Furthermore, the total Saturated Vapour Pressure increased with the increase in n-Octane concentration, where the increase in the propensity of the flowing fuel through the Cylindrical and Hemispherical nozzles, to cavitate was noted. On the other hand, the propensity of the Conical nozzles to cavitate decreased with the increase in Saturated Vapour Pressure.

The **second part** of the study investigated the sustained hydrodynamic cavitation taking place inside a mechanical 1650 bar continuous recirculated flow rig, mimicking the flow inside the injectors spill valves and high-pressure pumps spill valves at a later stage of cavitation as the fuel was left to cavitate for a longer period of time, leading to the degradation of the fuel due to changes in the fuel's chemical composition taking place during cavitation.

A needleless 0.213 mm single hole diameter Cylindrical nozzle was considered, as the Commercial Diesel fuel, the biofuel Rape Methyl Ester and the Gas to Liquids paraffin blend were left consecutively to cavitate for a period of 30 hours. The volume flow rate was obtained as 1.129 Liter per minutes considering a Discharge Coefficient of 0.8.

The results showed that by passing a 405nm laser over the 30 hours period through the cavitated fuel mixtures, a decrease with time of the transmission signal of the laser beam penetrating all tested fuels respectively was noticed. The laser beams experienced a decrease in strength due to the changes in the chemical composition of the fuel as high pressures and high temperatures took place inside the receiver. The effect of heating the fuels overnight inside a modified Water Bath tea urn at 60 degrees Celsius was looked into in order to separate the impact of temperature to the impact of cavitation alone. The effect of subjecting to fuel to cavitation and heating was greater than the effect of subjecting the fuel to heating alone.

The Gas to Liquids fuel was visually transparent compared to the commercial Diesel fuel and had the highest laser transmission signal.

Of all three fuels, the Commercial Aged Diesel fuel had the lowest laser transmission signal as the impurities inside the fuel changed the chemical composition of the fuel due to sustained hydrodynamic cavitation.

Blank Page

NOMEMCLATURE

– *Acronyms*

abs	absolute
BDC	Bottom Dead Center
BOC	British Oxygen Company
Ca	Cavitation Number
CAD	Computer Aided Design
Cd	Coefficient of discharge
CEB	Collapse Energy Breakup
CFD	Computational Fluid Dynamics
CI	Compression Ignition
CO	Carbon Monoxide
CO_2	Carbon Dioxide
CN	Cetane Number
CVC	Constant Volume Chamber
DI	Direct Injection
DPFs	Diesel Particulate Filters
ECU	Engine Control Unit
EDC	Electronic Diesel Control
EDU	Electronic Driver Unit
EGR	Exhaust Gas Recirculation
EIP	Enhanced Injection Pressure
EUI	Electronic Controlled Unit Injector

EUP	Electronic Unit Pump
FIE	Fuel Injection Equipment
FIS	Fuel Injection System
FUEL A	Commercial Diesel Fuel
GC	Gas Chromatography
GHG	Greenhouse Gas
GTL	Gas To Liquid
HC	Hydrocarbons
HCCI	Homogeneous Charge Compression Ignition
HPP	High Pressure Pump
HSDI	High Speed Direct Injection Diesel engine
H_2SO4	Sulphuric acid
ICCD	Charge-Coupled Device
ICE	Internal Combustion Engines
IDI	In Direct Injection
ITC	Injection Timing Control
KE	Kinetic Energy
LDV	Laser Doppler Velocimetry
LIF	Laser Induced Fluorescence
LNG	Liquefied Natural Gas
LPP	Low Pressure Pump
LSD	Laser Sheet Dropsizing
MIE	Mie Scattering

NO	Nitrogen Monoxide
NO_X	Nitrogen Oxides
NO_2	Nitrogen Dioxide
N_2O	Nitrous Oxide
O_3	Tropospheric Ozone
PAH	Polycyclic Aromatic Hydrocarbons
Pb	Lead
PC	Personal Computer
PDF	Probability Density Function
PIV	Particle image velocimetry
PM	Particulate Matters
RME	Rape Methyl Ester
RTWI	Real Time Water Injection
SI	Spark-Ignition
SMD	Sauter Mean Diameter
SO_2	Sulphur Dioxide
SQRT	Square Root
STDEV	Standard Deviation
TDC	Top Dead Center
UBHC	Unburned Hydrocarbon
UK	United Kingdom
VCO	Valve Cover Orifice
VOCs	Volatile Organic Compounds

– *Symbols*

A	Antoine’s Equation Constant
B	Antoine’s Equation Constant
C	Antoine’s Equation Constant
$Ca_{Critical}$	Critical Cavitation Number
$Ca_{FullyDevl}$	Fully Developed Cavitation Number
C_f	Collision Frequency
D	Density
d	Diameter
E	Young's Modulus
K	Tapered hole coefficient
k_b	Boltzmann’s Constant
L	Liter
l	Length
$l_{FreePath}$	Mean free path
I_{in}	Intensity In
I_{Out}	Intensity Out
I_{Ref}	Reference Intensity
M	Molar Mass of Nitrogen
$\dot{m}$	Mass Flow Rate
M_4	Screw Bolts
M_6	Screw Bolts

N_2	Unoxidised Nitrogen gas
P	Pressure
P_{avg}	Average transmitted Power/reflected power
P_D	Delivery Pressure
P_{Down}	Downstream Pressure
P_{in}	Internal Pressure
P_{max}	Maximum Power
P_{min}	Minimum Power
P_{out}	External Pressure
P_R	Received Pressure
$P_{Sat\ Vap}$	Saturated Vapour Pressure
P_{Up}	Upstream Pressure
Q	Volumetric Flow rate
R	Universal gas constant
Re	Reynolds number
T	Temperature
t	Time
V	Velocity
V_B	Bernoulli Velocity
Vol	Volume
v_{rms}	Root Mean Square Velocity
1G	First Generation Biofuel
2D	2 Dimensions

2G	Second Generation Biofuel
3G	Third Generation Biofuel
α	Attenuation Coefficient
$\propto_{absorbed}$	Absorbed Attenuation Coefficient
$\alpha_{Scattered}$	Scattered Attenuation Coefficient
ΔP	Pressure difference
$\boldsymbol{\varepsilon_{\theta}}$	Circumferential Strain
$\boldsymbol{\varepsilon_{r}}$	Radial Strain
$\boldsymbol{\varepsilon_{z}}$	Longitudinal Strain
σ_{θ}	Circumferential stress
σ_{r}	Radial Stress
σ_{z},	Longitudinal Stress
^{0}C	Degree Celsius
%	Percent

Blank Page

CHAPTER I. INTRODUCTION

Over the recent years, engineers, scientists and engine manufactures have found themselves increasingly under pressure to constantly improve the design of the Fuel Injection System (FIS) in order to comply with automotive fuel emission regulations. The impact of cavitation on the FIS is today the focus of a good number of researches as cavitation is seen to increasingly affect the injector nozzle flow; Injector Nozzle Flow cavitation research in today's society is of the high essence as the complex nature of phenomena occurring inside the combustion system is still puzzling a good number of scientists and engineers struggling to fully understand what happens during the combustion process [1] – Among many, cavitation plays an important role in the atomization process of the fuel inside the Internal Combustion Engine (ICE).

The pressure control system in most ICE diesel fuel injection systems is made up of a primary nozzle as well as a secondary nozzle system. The secondary injector is made up of a one way solenoid needle valve that acts as a nozzle which enables the fuel out of the injection system and back into the tank – as the engine control module signal is sent to open the solenoid spill valve, the fuel coming from the feed pump is sent to the pressure chamber at low pressure. As a second signal is sent to close the solenoid needle spill valve, the fuel is directed towards the injection system. The magnetic solenoid/ piezo-electric valve is installed on each injector of the common rail and is used to control the fuel injection timing and the amount of fuel being injected – this is done as the difference of pressures inside the injector and at the top of the needle generates a lift of the actuator pin. I.e. The new Denso Diesel fuel injection pump makes use of solenoid spill valves to control the volume of the fuel injected inside the ICE and prevents spillage taking place. [2]

As the appropriate amount of fuel is injected, the excess fuel is returned to the tank – due to the internal pressure equalization system used to precisely control the amount of fuel being injected inside the ICE.

The returned excess fuel is subjected to large pressure ratios causing the flow across the valve to cavitate. As often enough the engine fuel pump will provide more fuel to the injector than needed, part of the cavitated fuel experiencing this very tense situation is returned to the tank unburned and subjected to exiting regions of high pressures and low pressures, leading to an increase in deposit formation. The deposits formed act as blockage and can greatly affect the injector systems impacting the filter, nozzle hole, as a whole. [3]

Hence understanding how and when the pressure ratios affect the cavitation phenomena inside and/or near the valves, helps in controlling the cavitation taking place at the vicinity of the valves.

The ICE recirculated closed system was designed to allow the cavitated fuel to be returned to the tank and be reused for combustion. Researchers have discovered that the fuel subjected to recirculated cavitation tends to degrade over time [4], leading to the formation of harmful particles due the chemical reactions taking place inside the FIS.

The phenomenon occurs in most Diesel internal combustion injection systems. i.e motorcycles, automobile, ships, aircraft, etc. and remains a problem to be properly tackled and resolved.

Hence, a combination of experimental studies [5-7], in parallel with numerical research studies [8-20] of the FIS is being conducted by a great number of researchers in order to tackle the "still" mystery that is "cavitation" – Researchers at City University London are looking closely at the effect of cavitation on the FIS where academics such as Arcoumanis *et al.* [21-26] and Lockett *et al.* [27-29] have been working on cavitation research inside City University laboratories. As a result, City University

researchers have teamed up with scientists at Shell Global Solutions, in order to study the cavitation phenomena in great detail.

Hence, in relation to *the present study*[1], Shell has shown a particular interest in controlling the flow mechanism responsible for cavitation taking place in and/or around the injector and pump spill control valves, looking at the start of the cavitation phenomena, the fully developed cavitation as well as looking at the effect of leaving the fuel to cavitate for a longer period of time. Researches are conducting these studies in order to fully understand what happens inside the injector valve when cavitation takes place. By changing the working fuel composition – scientists at Shell are particularly keen in finding ways of increasing the overall consumption efficiency of the hydrocarbon fuel. They are furthermore interested in the impact of subjecting the fuel to recirculation as it is being cavitated.

Hence *the present study*, is divided into two parts.

Part **A**, focused on the impact that the changes in the fuel composition has on the onset of cavitation when varying the pressures upstream and downstream of the injector nozzle, in order to understand how pressure variation impacts the cavitation formation. Part A additionally looked at the effect that submerged cavitated jets, formed when varying the Upstream and Downstream pressures, have on the surrounding stagnant fluid inside a receiver. This was mainly because, a better understanding of the changes in the jets geometrical parameters led to a better understanding of the impact of the cavitation inception on shear jet flows inside Diesel Fuel Injection Equipment (FIE) such as control valves. [3,30-33].

Part **B** on the other hand, looked closely at the development of the cavitation phenomena after the onset of cavitation has taken place, focusing particularly on the impact of the sustained hydrodynamic

[1] The PhD thesis will often be referred to as "*the present study*" all throughout.

cavitation on Diesel and Biodiesel fuels [34,35] inside FIE. By understanding the impact of cavitation on the fuel as it is recirculated over a long period of time inside the ICE, the study helped in finding ways of controlling the degradation of the fuel caused by cavitation taking place as the fuel existed the injectors and pumps spill control valves.

The incipient cavitation [36] denotes the onset of cavitation – as cavitation occurs, small microbubbles are observed as liquid air is pulled from the working fluid due to a reduction of pressure, leading to the formation of vapour and gas mixtures.

A number of studies has been conducted on incipient cavitation experimental as well as numerical research. *The present study* made mostly use of experimental techniques, I.e. experimental rigs, in order to control the pressures in and/or around the nozzle. However, when using numerical simulations in the study of incipient cavitation, various techniques may similarly be employed. For example, Incipient Cavitation Index is sometimes used to simulate the incipient cavitation formation. Other techniques may likewise be used. As an example, in their study Falculcci *et al.* [37] have recently demonstrated that cavitation clouds could be simulated by using the Boltzmann lattice simulations of multiphase flows. The authors have discovered that cavitation number (Ca), when used on its own is not able to predict the incipient cavitation. Similarly to *the present study*, the authors have found that the structure of the cavitated bubble is very much affected by the surface tension. In *the present study*, collusion was observed between the bubbles formed as cavitation took place. A similar observation was pointed out by Mansoor *et al.* [38] who have recently worked on the onset of cavitation taking place as collision occurred between a given sphere and a solid surface inside a Newtonian fluid layer. From their experiment, the authors have observed the behavior of newly formed bubbles on the surface of the sphere as the bubbles entered the fluid layer.

White Cloud formation was observed in *the present study* as the jet passed through the nozzle and penetrated the stagnant fuel inside the Fused Silica receiver used during the experiment. Sou *et al.* [39] in their study of the transparent cavitation sheet as well as in their study of cloud cavitation bubbles, looking precisely at the transient cavitating flow, have discovered that cloud cavitation takes place inside the Diesel fuel injector as incipient cavitation is simulated. The authors have made use of a combination of simulation codes in their studies such as, the Large Eddy Simulation (LES) and the Rayleigh–Plesset (RP) equations.

Comparably to the experimental rigs uses during *the present study*, devices which can simulate a submerged jet flow are being used in various engineering applications. Fang *et al.* [40] have worked on submerged flow field experiments making use of the Organ pipe nozzle. The authors have taken into account various structures in order to study the performances of the Organ pipe nozzle when varying the pressure. The authors have discovered that the optimum parameters at the exit of the organ pipe nozzle as well as the characteristics of the nozzle were affected by the working pressure, the length of the cavity as well as the diameter of the cavity. The authors have concluded that cavitation increased due to the formation of a separated circular vortex inside the shear layer of the jet. Using a submerged nozzle, Straka *et al.* [41] have likewise been able to observe the cavitation inception behaviour, looking at cavitation inception numbers for quiescent, near-quiecent and co-flow submerged jets. The authors have managed to separately control the jet flow as well as the freestream velocities. The authors have concluded, as noticed in *the present study*, that the change in the flow mechanisms does affect the cavitation inception formation location and pattern.

Erosion damage which can sometimes take place inside Diesel injector nozzles [42] as the fuel recirculates inside the FIE, was not taken into consideration in *the present study* because the selected

materials used for the rig and the nozzles during the experiment were not prone to cavitation erosion. Although cavitation erosion [43] can sometime be seen as a destructive source of energy as water cavities formed near and/or inside the injector system (the formed cavities can have a detrimental impact on the surrounding area of the device), it is often made use of in various fields of engineering such as surface cleaning, material crushing and industrial cutting. Chahine *et al.* [44]

Despite the fact that the mechanical rig employed in the first part of *the present study* made use of liquid alkane as the working fluid, the rig has equally been designed for experiments conducted with water as the working fluid. Hence *the present study* could be compared, to some extent, to the different researches conducted with the use of water as the working fluid.

Henceforth, the study which has been conducted by Wright *et al.* [45] was seen valuable to the present work and was used as a means of comparison to *the present study*. The authors have recently worked on cloud cavitation formation of a submerged water jet in a tank of quiescent water at high pressures, using a 27.6 MPa pressurized nitrogen discharger. Similarly to *the present study*, the authors have observed an increase in the propagated distance of the formed cloud caused by an increase in the pulsation of the cavitation clouds due to the increase in the jet diameter. The authors have measured a 30 percent increase in the propagated distance when increasing the jet nozzle diameter from 1.0 mm to 2.0 mm. The increase was due to the pulsated cavitated bubbles moving away from the nozzle proportionally to the Re, until they collapsed.

Chemloul [46] has focused on bubble breakup where the jet is injected perpendicularly to a subsonic crossflow and is subjected to atomisation. By changing parameters such as the orifice diameters, the injection pressure differentials as well as the orifice entrance geometry, the author has been able to visualise the similarities in the jet trajectory of the cavitated flows as well as the similarities in the jet trajectory of the non-cavitated flows. The author has discovered that where hydraulic flip occurred

the trajectory of the liquid jet followed a different path. When visualising the hydraulic flip, the author has been able to observe small breakup length. Equally to *the present study*, the author has found out that an increase in turbulence caused a decrease in the Coefficient of discharge (Cd) as cavitation bubbles developed around the sharp-edged orifice geometry.

The Cd represents the ratio of the actual discharge to the theoretical discharge of the flow. The ratio can be used for comparing one nozzle's efficiency to another. It is derived from the Bernoulli equation.

$$C_d A = \frac{\dot{m}}{\sqrt{2\rho\Delta P}}$$

Equation 1 - Coefficient of discharge

String (or vortex) cavitation can sometimes take place inside the FIS. String cavitation has been studied by authors such as Reid *et al.* [47] Making use of a 2000 bar pressure rig, the authors have worked on string cavitation formed inside an optically accessible diesel fuel injector nozzle. By adjusting the position of two adjacent nozzle holes, the authors were able to observe string cavitation vortices caused because of the existing nozzle hole interaction. The authors have observed a change in the holes interaction of vortices as well as the holes formation of vortices when working in a steady state regime compared to a transient regime. Comparing their numerical results to experimental results the authors have concluded that no cavitation was found in vortices. However, cavitation was present for the transport of the gas-phase constituents by the vortices inside the injector flow.

Although it is troublesome to reproduce to absolute detail the design of the FIS, in order to study the effect of cavitation inside and/or around the nozzle [48-54], the innovative designs that have been used up to date by researchers in the study of cavitation are seen to reproduce the real conditions to near perfection – However, there is still more work to be done. In that regard, new technologies are constantly emerging with changes made to the geometry and/or the material of the nozzle. The variable orifice design, by Tiam [55], where the nozzles are manufactured in such a way that they can exhibit high spray velocities is an example of such design. Furthermore, there is the multistage nozzle tip, the rotating nozzle tip and the double needle which are manufactured with the aim to improve the design of the injector.

The overall sets of results obtained during *the present study,* focusing on understanding the cavitation phenomena taking place in and around spill vales, were beneficial to researchers. By being able to control parameters such as the fuel composition inside the internal combustion engine as well as the geometry of the nozzle valves, researchers could be able to control the combustion fuel quality subjected to cavitation, hence researchers could likewise be able to control the combustion fuel spray quality. Researchers could additionally be able to control the timing and quantity of the combustion fuel entering the spill valves regions, leading to a control of the amount of fuel subjected to degradation, preventing in turn FIS failure, as well as controlling the rate of pollution generated from automobiles.

Below is a table of definition of the type of cavitation mentioned in *the present study*.

Cavitation	Definition
Bubble cavitation	cavitation formed due to the pressure distribution around the device leading to high suction pressures
Cavitation erosion	Cavitation formed as a result of high pressure water jets – a process leading to the deterioration of metal surfaces
Cavitation Number	Cavitation Number represents the potential of the flow to cavitate. A higher value of Cavitation Number often denotes a non-cavitating flow
Cavitation Onset	The starting point of cavitation
Cloud Cavitation	Cavitation taking place as the sheet cavitation bubbles collapse, can have devastating consequences as the collapse of the bubbles can lead to damage formation. White Cloud formation often takes place during incipient cavitation due to the presence of very low pressures downstream of the injector nozzle.
Critical Cavitation Number	Cavitation number obtained at the start of cavitation
Desinent cavitation number	The end point of cavitation which represent the point of cessation of cavitation
Geometric cavitation	Cavitation caused due to the geometry of the device.
Root cavitation	Cavitation taking place around the roots of the propeller blades – when strong root cavitation takes place, erosion damage can be observed.

Shear Layer Cavitation	Cavitation occurring within the boundary layers of two fluids
Sheet cavitation	Cavitation formed due to the flow separation caused by strong adverse pressure gradients. Sheet cavitation takes place due to the buildup of the large suction pressures near the leading edge of the blade. The unsteady sheet cavitation is often found behind the fully developed sheet cavities and can be extremely damaging to the object being cavitated.
String Cavitation	Vortex cavitation
Tip vortex Cavitation	Cavitation caused due to the low pressure formation occurring within the vortex sheet.
Ultrasound Cavitation	Cavitation formed as an ultrasound effect is generated due to the increase of chemical activities within the fluid mixture

Table 1 Cavitation Definition

Thesis outline: The present thesis comprises 7 different chapters, where;

Chapter I comprises the motivation as well as a summary of a number of researches conducted on the subject of cavitation.

Chapter II. introduces the reader to a background of the FIS. It furthermore presents a literature review of the different studies and challenges faced by engineers and scientists working on the FIS's research area – the intensive literature review focuses on a broad aspect of the ICE Diesel fuel research. It additionally focuses on alternative sources of power, on the incipient cavitation jet and the sustained hydrodynamic cavitation research, as well as on the imagining techniques currently being used to study the cavitation phenomena. moreover, this part of the thesis put emphasis on the destructive power of the cavitation phenomenon as well as on its growing usage in various areas of engineering.

Chapter III on the other hand focuses on the experimental study of the effect of incipient cavitation on n-Hexadecane based fuels, using a mechanical rig capable of sustaining pressures of up to 80 bar upstream of the nozzle and 15 bar downstream of the nozzle – Acrylic, Brass and Aluminum-steel nozzles, and making use of a combination of hydrocarbon paraffin based homogenous fuel mixtures. The cavitation inception of each mixture was obtained based on the changes in the chemical composition of the paraffin fuels, as the fuels flew respectively into the stationary liquid inside the receiver, leading to the formation of shear flows around the boundary layer of the jet. **Chapter IV** presents the results obtained during the experimental analysis conducted for the Incipient Cavitation research study. The chapter is mainly divided into two different parts: - Firstly, focusing on the pressure results obtained from the mixtures of increasing n-Octane percentage in n-Hexadecane based fuel as well as the pressure results obtained from the mixtures of n-Octane, n-Decane, n-Dodecane, n-Tetradecane and n-Hexadecane.

- Secondly, looking at a range of parameters such as the volumetric flow rate (Q), the Ca, the Cd, the jet speed (V) as well as the Reynolds number (Re) in order to understand the effects that varying the geometrical parameters of the nozzle has on the cavitated jet.

Chapter V looked at the sustained hydrodynamic cavitation of Diesel and biodiesel fuels, using the Commercial Diesel (Fuel A), the Gas to Liquids (GTL) and the Rapeseed Methyl Ester (RME) fuels. This part of the study made use of a 1650 bar gauge high pressure recirculating rig, where the experiment focused on determining the resulting effects of leaving the fuels to cavitate for 3 days (30 hours) versus the resulting effects of heating the fuels overnight inside a modified commercial tea urn at 60 degrees Celsius. **Chapter VI**, focused on the experimental results of the sustained hydrodynamics cavitation study. The different graphs plotted represent the variation of the Normalized and Self-Normalized Transmissivity Signal as well as the Spectral Attenuation Coefficient and Self-Normalized Attenuation Coefficient. The chapter moreover focused on the results obtained from the fuel heating tests.

Chapter VII is the conclusion of the work, highlighting the main findings of *the present study*. This part of the thesis in addition contains various suggestions for future work.

REFERENCES is made up of a series of carefully selected references used in relation to the present work is presented in this section. It comprises references from books, journal papers as well as conference papers. It also contains a list of carefully selected internet website which were found useful for *the present study*.

APPENDIX comprises the appendix A and Appendix B section, which contain series of remaining graphs, tables, figures and photographs which were used during *the present study.*

Blank Page

Chapter II. GENERAL BACKGROUND AND LITERATURE REVIEW

The General Background and Literature Review is a collection of years of intensive researches relevant to the present research work, summarized for a better understanding of where cavitation research fits in, in today society – The review looks into the past, the present as well as the future of the FIE subjected to cavitation.

The review starts with a general overview of the work done on the ICE [56-57] and looks precisely at the Diesel development [58-63], fuel and energy consumption and alternative fuels – a considerable number of studies are presently focusing on alternative fuels research, [64-67] however at present time, the Diesel and the Gasoline fuels are considered to have no plausible adversary. [68] Going further, the focus of the review is directed toward the impact of incipient cavitation on Diesel flow conditions, bubble dynamics as well as the study of Diesel fuel spray using high speed video imaging techniques. Henceforth the review is narrowed down to the study of high speed jet flows and immerged jet shear flows. The study additionally touches on the subject of fuel and gas mixture solubility as well as the different measurement techniques that have been made used of over the years.

2.1. Internal Combustion Engine

It is hard to imagine the world today without the Internal Combustion Engine (ICE) as it is one of the invention that revolutionized the engine technology [56], e.g. the automobile technology.

The ICE, likewise known as the explosion engine was first developed before the 19th century where a great number of scientists and engineers contributed to its development; Scientists such as Alessandro Volta [69] around 1780 built an electric pistol toy where a mixture of air and hydrogen was

detonated, using an electric spark, and François Isaac de Rivaz [70-71] around 1807 looked into the ICE powered with a mixture of hydrogen and oxygen. Scientists such as Etienne Le Noir [72] a Belgian engineer first successfully commercialized the ICE in 1860 – modifying the boiler of a steam engine. However, it is only around 1861 that French Engineer Alphonse Beau de Rochas [73] proposed the idea of a piston compressing the air-fuel mixture before ignition. Hence scientist Nicholaus Otto [74] a German inventor, was later able to modify the first ICE to efficiently burn fuel using a piston chamber. Because Otto's engine where too large, around 1883, German engineer, Gottlieb Daimler [75-76] invented a much smaller engine making use of the highly volatile petrol fuel, and hence revolutionized the use of the car; the first ICE car required work to be done as it was still considered uneasy to manipulate and quite inefficient. It is only after the introduction of the FIS made up of a row of electric valves used to spray the fuel inside the cylinder i.e. better fuel consumption, that the ICE was considered a powerful power unit. [77-79]

The ICE can be characterized based on its layout comprising: the reciprocating engine, the rotary engine, the continuous combustion engine, e.g. Gas turbine, the jet engine and the Rocket engine.

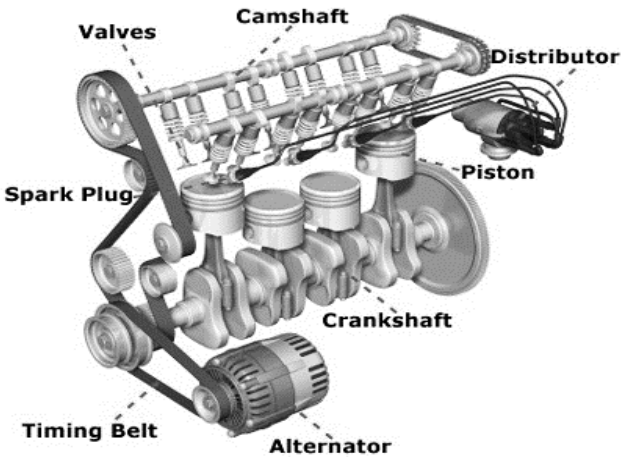

Figure 1 The ICE model [80]

The reciprocating engine equally called the heat engine, makes use of a cylinder piston devise which, with the aid of a crankshaft, helps to transform the fuel chemical energy into a more useful mechanical energy – The ICE very much differs from the steam engine as it follows a mechanism which burns fuel inside the engine instead of outside the engine. [81-82]

The Diesel cycle, the ideal cycle for the Compression Ignition (CI) engine, was first developed by the German engineer Rudolf Diesel, [83] in 1896, with the aim of increasing the efficiency of the steam engine. The very early models of the CI engine were big in size and bulky. Smaller and more robust engines only surfaced around 1908 – Around 1930, the CI engine was used for construction tractors. The CI engine found great importance during the World War I and Word War II where it was used for military purposes [84], with applications on electric plants, road transportation and marine propulsion engines. The CI engine is one of the most efficient ICE with, a very low fuel consumption and high reliability and durability characteristics – Today, the CI engine is used in numerous applications such as in small robust automobiles [85]. The engine performance is measured based on parameters such as the energy efficiency and the fuel consumption. [60, 86].

2.1.1. Combustion System

The combustion process which takes place inside the CI engine is until today, not well understood. The process has been the subject of a vast number of research studies over the years. [56-57, 61-63, 87-89]

To date, engineers and scientists have resorted to the use of powerful computational codes/modelling devises and high speed imaging techniques such as Laser Sheet Imaging, in the aim to understanding the combustion process taking place inside the engines. [90] Hence, today, a considerable number of researches focuses on injector nozzle design, particularly on the DI engines nozzle design [34, 88]. Based on recent researches, it is believed that the current combustion processes can reach temperatures above 2000C and fuel injection pressures of over 2,000 bar [91].

The 4-stroke Diesel engine combustion processes are: Induction stroke, Compression stroke, Power stroke, and Exhaust stroke. [62, 92] At the end of the fourth stage the cycle restarts as the new air is drawn inside the cylinder – The crankshaft rotates to 180 degrees during each of the engine strokes, as a total of two revolutions must occur at the end of the four strokes. In the 2-Stroke engine however, only one revolution of the crankshaft is needed to complete the cycle. Air is pressurized using a turbocharger. The combustion of the premixed fuel causes a raise of the pressure and the temperature as the ignition of the fuel provides the power energy which is transformed into useful mechanical energy. When looking at the CI engine combustion process, it is vital to take into account the temperature and the kinetic energy of the air drawn inside the cylinder; parameters such as the design of the intake port, the nozzle hole geometry, the spray angle as well as the fuel properties affect the combustion temperature and kinetics energy [88] – The energy as well as the efficiency of the engine can be calculated from the values obtained from the specific heats as well as the cycle temperatures. The injection process and the combustion process must be completed in a short time duration in order to reach the optimum engine performance – The heterogeneous combustion takes place after the air-fuel mixture process is done where the chemical energy stored in the fuel is transformed into mechanical work. [93] A good number of scientists and engineers have been working toward shortening the ignition lag. Kobori *et al.* [94], found out that the Diesel ignition delay time could be shortened by increasing the ambient gas temperature as well as the ambient gas pressure inside the cylinder. The authors additionally found out that a reduction in the orifice diameter of the injector nozzle led to a decrease in the ignition time delay – In the CI engine, the ignition lag, a process lasting around 1 millisecond, is defined as the period passed between the end of the injection and the start of the combustion. It is a function of the Cetane Number (CN) which represent the fuel's ignition

quality, the air intake temperature as well as the compression ratio – As the premix fuel-air causes an increase in the pressure during the combustion process, it is vital to limit the contact between the fuel and the air in order to achieve an effective combustion process. Due to the use of high injection pressures and temperatures inside the Diesel engine, the rate of heat release is proportional to the efficiency of the air-fuel droplet evaporation and mixture i.e. the stoichiometric point. Due to the existing time delay between the end of the injection and the start of the combustion process, as the fuel flows through the combustion chamber, the pressure and the temperature are seen to be at their lowest at this stage

As more fuel than needed is often supplied to the engine during the combustion process, increasing the amount of air inside the ICE can reduce the likelihood of cavitation taking place downstream of the injector spill valve. Hence, the CI Engine are often equipped with turbochargers and aftercoolers which promote a rapid mixing of the fuel and air by forcing an extra amount of air inside the combustion chamber. Hence the turbochargers and aftercoolers help to increase the overall performance of the engine by reducing the noise and the pollutant resulting from the combustion. [95-96]

Tamilporai *et al.* [97] observed an increase in the overall performance of the engine as well as a reduction in the engine smoke emission with the use of aftercoolers. For single injection Diesel combustion, part of the fuel is sprayed during the time delay in order to keep the pressure, the temperature and the reaction rates from dropping. The downside in doing so is that the high pressures can lead to engine knock formation. Techniques such as the “Pilot injection”, where a control of the auto-ignition intensity reduces the pressure and the temperature to near ambient conditions can be used. Zhang [98].

For many years, scientists and engineers have worked toward improving the design of the combustion chamber [99] as this plays a major role in the performance of the CI engine. Parameters such as the thermal efficiency, the fuel consumption and the power output have often been looked into when it came to improving the CI engine.

Two types of combustions chambers can be distinguished: The DI chamber, a combustion chamber where the fuel is injected directly into the combustion cavity using a piston cylinder devise, as well as the Indirect Injection (IDI) chamber. One of the advantages of using the DI chamber is the fact that there exist very low pressure differences within the combustion chamber – because of its lower surface area to volume ratio, the DI chamber contributes to the increase of the engine efficiency by reducing the heat loss taking place during the compression phase. Zhao [88]

When considering the Indirect Injection (IDI) chamber however, the combustion chamber is made up of multiples compartments joined by a means of restricted passages; the prime compartment is a pocket inside the cylinder while the secondary compartment(s) is designed inside the cylinder head. Up to 15 percent more fuel can be consumed when using the IDI chamber compared to using the DI chamber. However, the IDI chamber is less costly to produce than the DI chamber; an engine fitted with the IDI chamber often produces a minimum amount of noise. Hence, these engines are often used for passenger cars as they tend to produce a lower HC and NO_X level – The use of techniques such as the air swirl in the IDI in order to regulate the relative velocity between the fuel droplets and air has tremendously increased the performance of the IDI chamber [100].

2.1.2. Diesel Fuels and Alternatives

This part of the thesis summarizes a number of literatures written by researchers on the use of Diesel and alternatives fuels – as *the present study* looked at conventional Diesel and alternative fuel

mixtures, the reviews helped in understanding the importance of alternative sourced of energy in the automotive industry.

The production of alternative fuels can often be costlier than the production of the crude oil. Thus, scientists and engineers are constantly debating on the global benefits of using alternative fuels as compared to using the HC based fuels as a balance has to be met between the cost of production and the impact on GHG emissions.

Even though much efforts are put in place in regard to the use of alternative sources of energy, petroleum is still up to date the highest contributor to the world energy production; the United Kingdom (UK)'s Petroleum production has greatly decreased mainly because most of its reservoirs and infrastructures are aging. Hence the UK found itself having to rely on petroleum importation.

The Diesel fuel has 15 percent more energy density than the Gasoline fuel, making it less volatile than the latter. The minimum quality standards for the Diesel fuel grades are established by the American Society for Testing Materials.

Although the UK has been experiencing a decline in the production of its petroleum as it consumes more petroleum than what it produces, it is as of date, one of the leading petroleum exporters of the European Union – As an estimate, the UK consumed 1.6 million barrels and produced 1.4 million barrels per day of oil. [101]

The Diesel fuel is obtained from the processing of the petroleum crude oil in refinery oil production plants using techniques such as, the distillation which separates the crude oil into a number of HC.

As the distillation process takes place, the fuel properties such as the CN, the viscosity, the density and the sulfur level can be obtained – the boiling points of the HC distillates varies between 150°C and 380 °C [101]. The regular Diesel, the Biodiesel blend and the synthetic Diesel have a CN of 48, 50 and 55 respectively. [32]

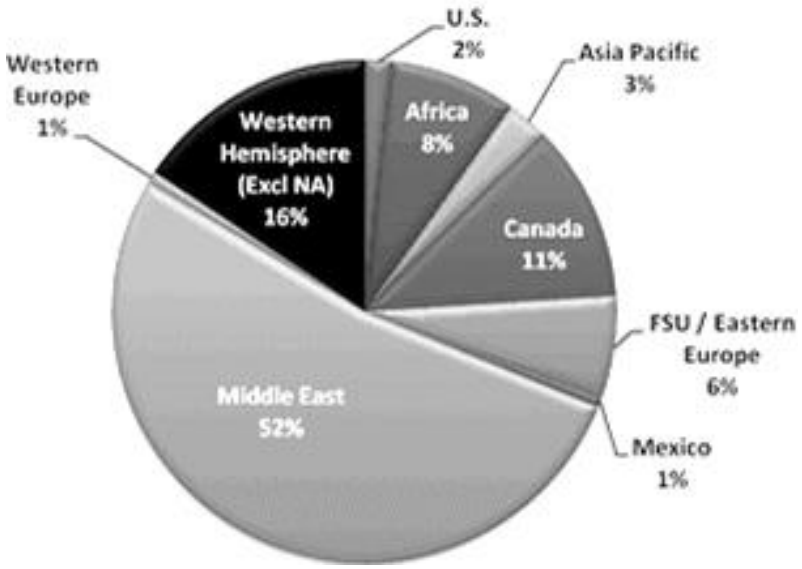

Figure 2 Diesel Distillation Process [102]

Figure 2. shows that more than 50 percent of the world's oil reserve is located in the Middle East. The Western European regions on the other hand have the lowest percentage.

Increasing price of the Diesel and petrol oil from 2000 to 2013 – The Diesel fuel has always maintained a higher price than the Gasoline. [103]

As major concerns are continually noted in regard to the Diesel fuel pollution, researchers are repeatedly put under pressure to improve the efficiency of the Diesel fuel. [104-109]

Hence, researchers are focusing on improving the fuel operation management system of automobiles, constantly looking at alternative fuels as one of the biggest challenges faced today by the automotive industry is the reduction against fossil fuels being used as the primary source of energy – A number of researches, by Schumacher L. and Gerpen [64], Zawadzki *et al.* [65] and Hervé *et al.* [110], have been conducted on the use of Biodiesel, ethanol, natural gas as well as electricity [111] as valuable sources

of alternative fuel. The UK has greatly invested in renewable energy and proud itself for being the main offshore wind supplier in the world. [112]

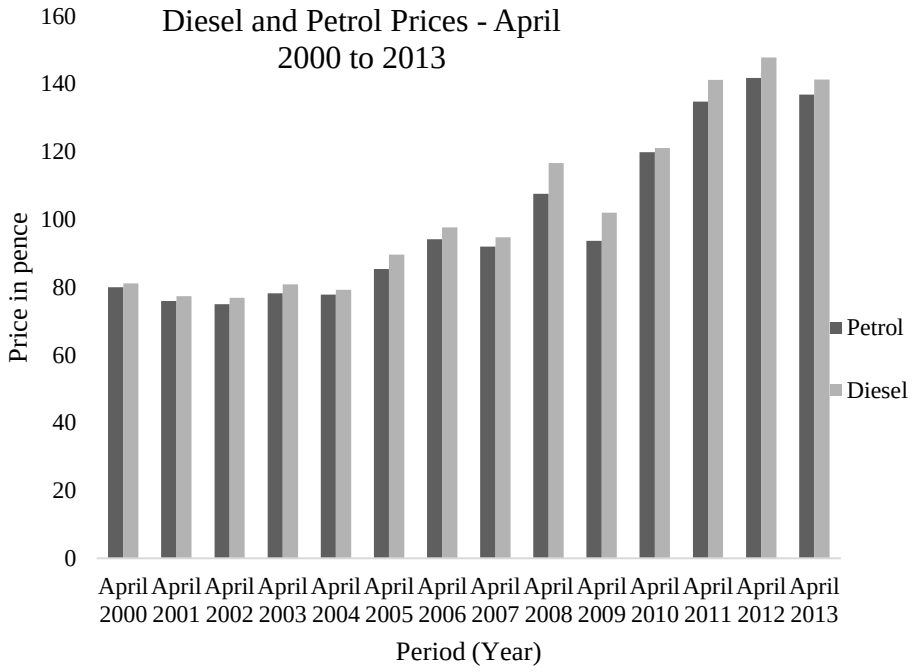

Figure 3 Diesel and Petrol Prices [106]

Natural Gas: Nowadays the gas industry is booming, with drilling processes taking place through the earth layers in various locations around the world.

The UK is today consuming more natural gas than it is producing. Since 2000, the UK has experienced a decrease in the production of natural gas making it one of the major importer of natural gas. As it takes billions of years to produce natural gas, most of the UK's reserves cannot satisfy the demand of the population at present. In 2010, the UK experienced a 5 percent decrease in the production of natural gas, and an increase of around 7 percent in the total natural gas consumed. As a result, the UK is importing an increasing amount of Liquefied Natural Gas (LNG). The UK is

importing most of its natural gas from the Norway. Hence the government is currently putting in place new energy policies focusing on improved gas recovery techniques. [113]

The work done by researches such as Lee *et al.* [114] can be considered as a step forward toward the use of alternative fuel such as natural gas. The authors looked at compressed natural gas and how it is used in heavy duty engines. They focused their work on mixture distributions, conducting a parametric study using the KIVA-3V model. [88] In their research, the authors looked at three specific features; the cycle equivalence ratio, the injection timing and the engine speed. The authors found out that by adding fresh air to the fuel-air mixture, progressively inside the cylinder, it was possible to observe the stratification phenomenon, this considering a closed valve injection. By varying the cycle equivalence ratios and the engine speeds, the authors additionally found out that there is a close similarity in the calculated distributions of the mixture inside the cylinder. The authors were able to observe a uniform velocity profile of the fully developed turbulent flow at the nozzle exit. They discovered that the open valve injection technique, compared to the closed-valve injection technique, resulted in a homogeneous distribution inside the cylinder at the ignition timing.

Biofuel: Today the number of engines running on the Biodiesel is seeing a sharp growth [107] as the Biofuel is the more and more considered as a safer alternative source of energy as oppose to the conventional Petroleum based fuel. [115] Biofuel is likewise seen as a source of diversity in terms of the global world energy supply.

As the use of Biofuel was considered in *the present study*, it was useful to review researches conducted on the subject. The review written by Schumacher and Gerpen [64] is a collection of real world data tests done from 1991 to 1995, which addressed the many problems encountered by scientists and engineers on the use of the Biodiesel as a better and a safer alternative to the

conventional HC fuels. The authors considered the use of the vegetable oil and the animal fat Biodiesel (alkyl monoester) as well as the use of the Methyl Soyate, which is a mix of the soybean oil and the methanol – made from a blend of the Biodiesel and the low sulfur Petroleum Diesel fuels. [67]

In their study, Schumacher and Gerpen discovered a number of issues related to the use of the Biodiesel when gathering data from four scientific sources: The Urban Bus Data Collection, the 5.9L Cummins Engines in Dodge Pickups, the Diesel Locomotive and the Farm Tractors.

The authors considered a range of 0 percent to 99.9 percent Biodiesel concentration in fuel mixtures. Among the issues reported by the authors were the mixing of the Biodiesel and the Low Sulfur Diesel Fuel, called “splash blending”. The report stated that the mix had an impact on the fuel economy. Among the proposed solution to the problem was the use of different mixing temperature. The authors additionally reported the need for a better cooling system was necessary. Other reported issues were; a cold start occurring when mixing the conventional fuel with a 20 percent Biodiesel blend, an increase in the NOx (with a decrease in CO, HC, and Particulate Matters **(**PM)), a 7 percent decrease in the fuel economy when using the soybean oil Methyl Ester, an increase in the smoke and a reduction in the engine power when using more than 50 percent Biodiesel, injector failures as well as changes in the fuel quality.

Although the use of Biofuels comes with pros and cons, a number of scientific sources has stated that due to the world economic growth leading to the growth of its energy demande, and due to the decline in the petrolum based oil demand, Biofuels renewable energy productions is increasingly growing. [110]

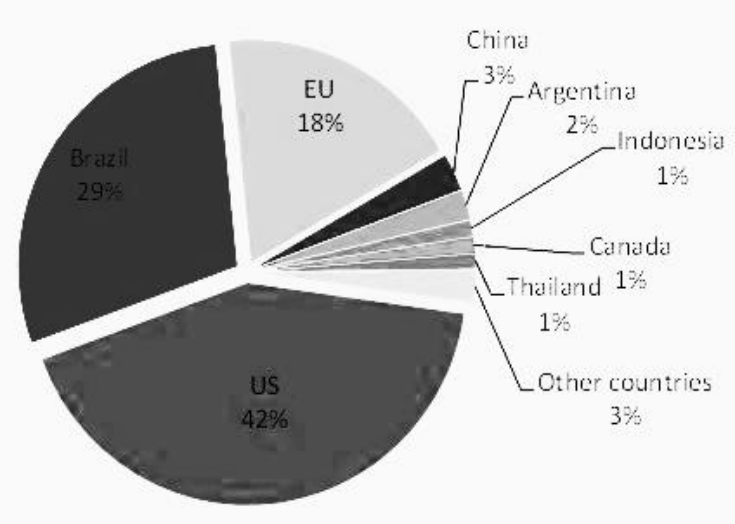

Figure 4 World Biofuel Production [107] [110].

However, much efforts are still to be made in order to keep up with the growing population as agriculture supplies are to sustain, not only the needs of the population but also the need for the energy production[110]. In their studies, Hossain *et al.* [116] described how algae can easily grow in a CO_2 enriched air and can be converted into an oily substance. This technique can be a useful means of maintaining the production of the Biofuel.

Electricity: Electricity is nowadays used as an alternative source of energy for electric vehicles and plug-in hybrid electric vehicles. Electric cars are defined as electric motors driven cars, making use of rechargeable batteries, in order to store the electricity coming from the central grid electric power source. One of the benefits of using the electric and the plug-in hybrid electric vehicle is the fact that they contribute less to the GHG emissions due to their higher fuel efficiency [117].

2.1.3. Energy Consumption and Optimization

The cavitation taking place inside the ICE is partly responsible for the increase in the production of harmful pollutants. Hence, this part of the thesis looked at the fuel emission generated by the transport sectors responsible for air pollution.

Today, air pollution is one of the major problems facing the Great Britain and the rest of the world. [118-119] Although the subject of "air pollution" is considered as a top priority, the government health standards regulations are often not accurately followed by the general public as the regulatory limit figures imposed to them are continually exceeded – This is a major problem for the UK; currently because of air pollution, a great number of incidents occur each year as thousands of lives are claimed due to the premature deaths occurring within the UK. The government is working hard towards reinforcing the imposed regulations in order to properly tackle the current problem. [119] Among researchers who have worked on the subject are Patz *et al.* [120] who have looked at the effect of hazardous chemicals on the human life.

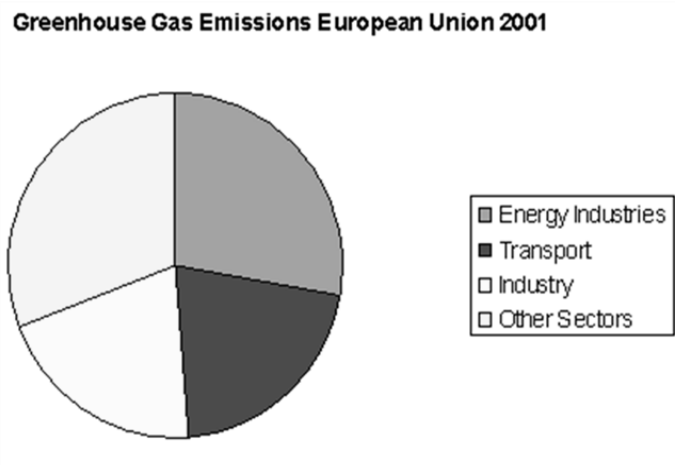

Figure 5 Green Gas Emissions 2001 [110]

The transport sector – mostly the domestic transport sector, is among those responsible for the increase in the GHG emissions. It is currently the third largest growing source of harmful pollutants responsible for over 20 percent of the world's emissions, with CO_2 as the major pollutant at 85 percent [112, 119, 121] The transport sector was responsible for one fifth of the total GHG generates in the UK in 2001. [118]

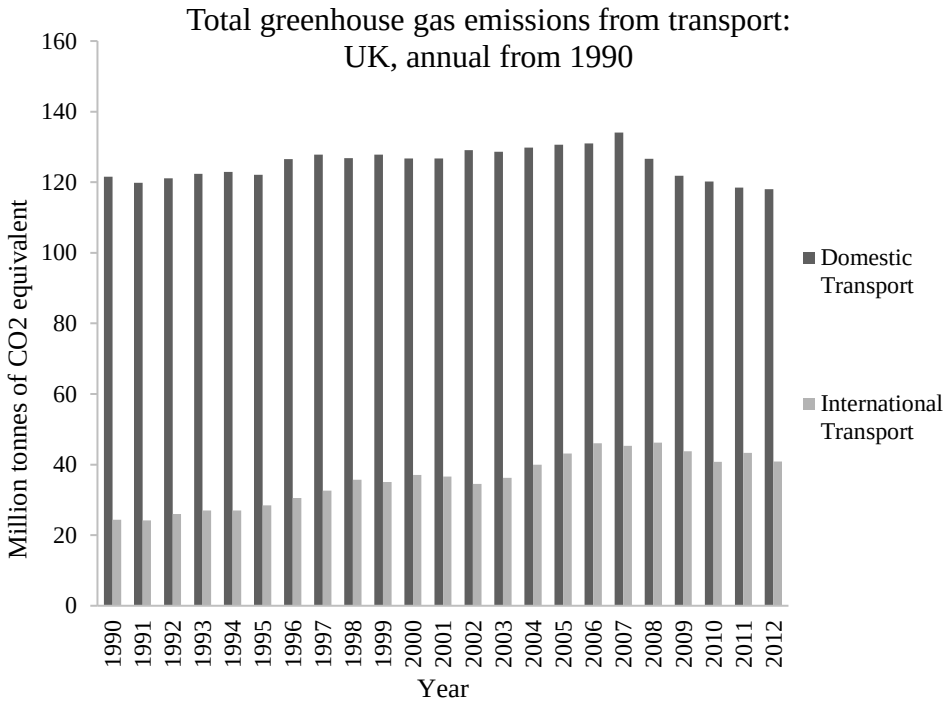

Figure 6 Transport Green Gas Emission – 1990 to 2001 [103]

Around 99% of CO, 76% of NO_X and 90% of HC are produced in London due to road traffic:

The UK is responsible for around 2 percent of nearly 30 billion tons of CO_2 produced from human activity. Since 1750, a 31 percent raise in CO_2 has been noted. Road transport fuel emission is responsible for about 5 percent of the Methane produces [92].

The use of Lead (Pb) is today seen as a minor risk for the population; since the year 2000 the majority of European automobiles make use of the unleaded fuel. Road transport is likewise seen as the leading cause of Pb pollution [103, 122]

In order to suitably tackle the problem surrounding CI engine emissions, it is vital to control the amount of fuel burned during the combustion as the air-fuel ratio must be kept near the stoichiometric value [123] – the stoichiometric mixture takes place as a sufficient amount of air is provided to completely burn the fuel during the combustion process. Hence, a small amount of excess fuel will go through the injector's return spill valve, reducing the amount of fuel subjected to cavitation.

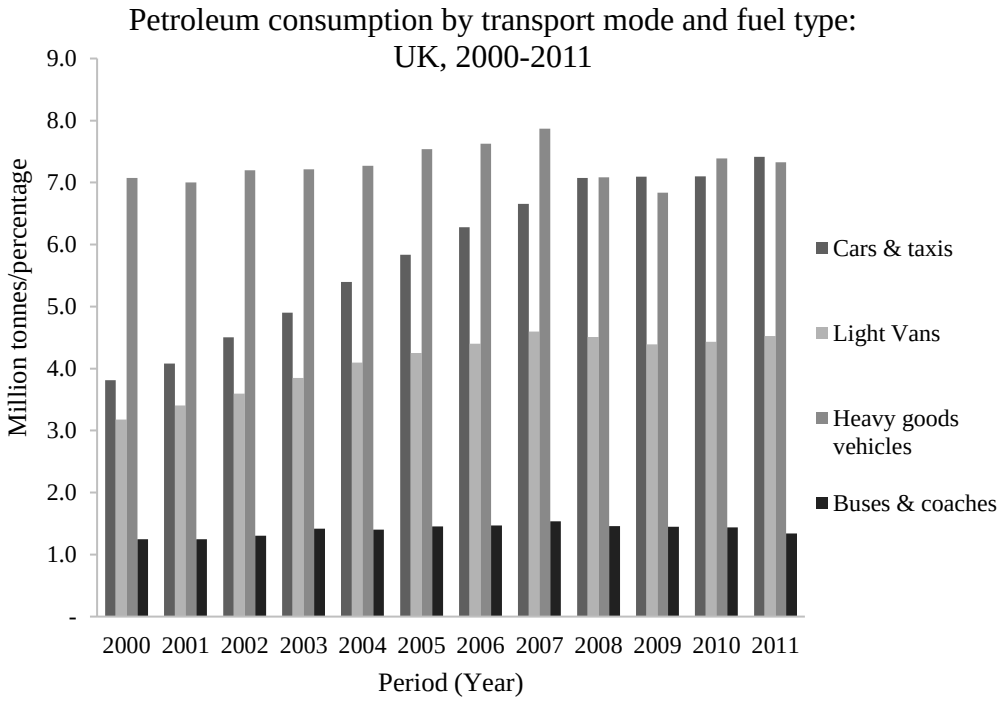

Figure 7 UK Petroleum Consumption [103]

When comparing the CI engine to the SI engine, the CI engine provides better fuel economy – this is mainly because of the fact that the CI engine uses considerably less fuel compared to the SI engine. Hence the CI engine is seen to produce low levels of CO and CO_2 emissions. [103]

Nonetheless, few inconveniences are noted with the use of the CI engine compared to the SI engine – The engine produces slightly more PM, NOx and soot particles. The problem is often solved with the use of a catalytic converter placed inside the engine exhaust gas to convert the NOx, CO and HC into N_2, H_2O and CO_2 in order to accelerate the chemical processes taking place as the gas leaves the engine exhaust. [123] When considering 20 percent of the total emissions, with CO_2 as the major pollutant, 32 percent comes from heavy duty vehicle – this amount to 8 percent of the UK CO_2 emissions. [124]

Researches such as Rumsey *et al.* [106] worked on of the combustion modeling of an Off-Highway Heavy Vehicle Diesel with the aim to improving the efficiency of the combustion process – The authors focused on the fuel emissions process as well as on the low fuel consumption with the aim to meeting the Tier 3 emissions standards.

2.1.4. Fuel Injection System

A key component in the study of the ICE is the control of the FIS as the need to further one's understanding of the fuel spray formation, development, and atomization process is increasing over the years [88] – A rising number of studies have been conducted on the development of the Diesel injector's performance. However, the difficulty still resides in obtaining "fine spray atomization and quality". [125-128] The cavitation phenomenon can greatly impact the atomization structure and hence impact the spray quality due to the presence of impurities in the fuel form as the fuel degrades. [4]

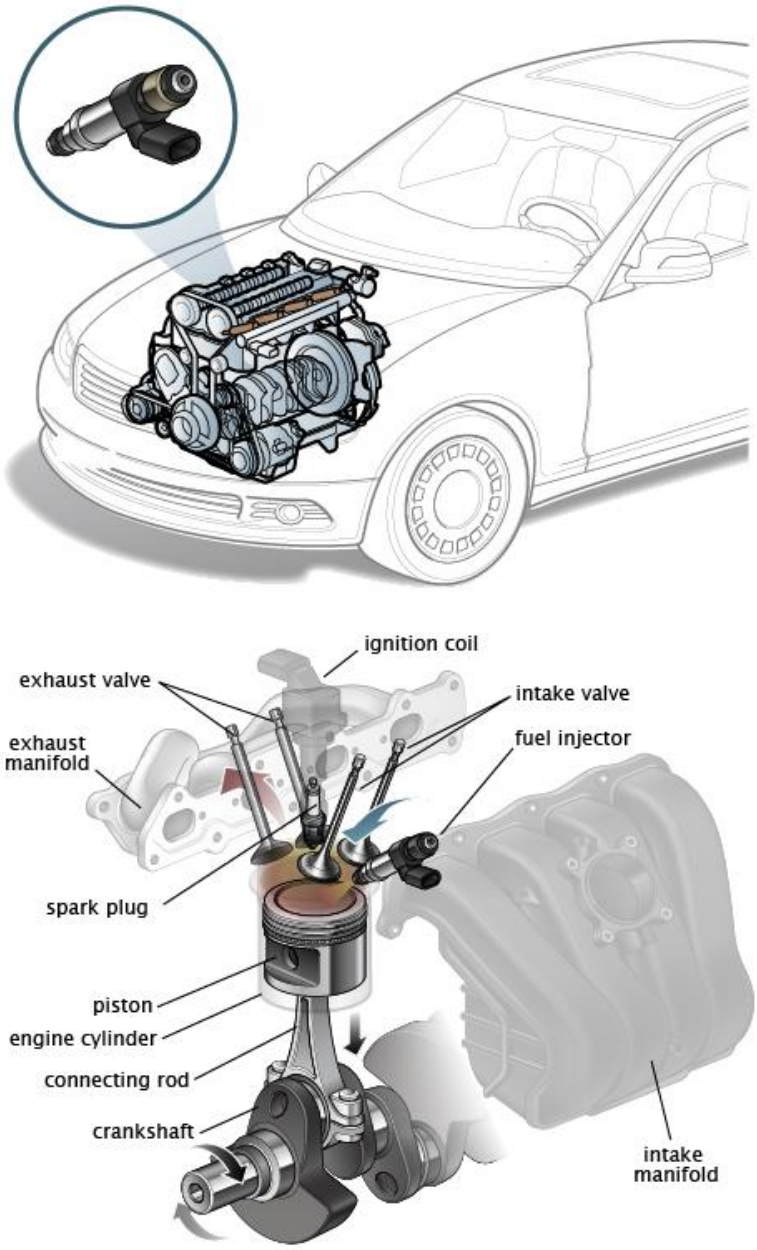

Figure 8 Diesel FIS [129]

Among the different types of injection systems that exist are:

- The Single Point Injection: likewise known as the throttle body injection which has replaced the use of the carburetor. The single point injection system makes use of a single injector.
- The Multi Point Injection: which comprises a combination of single injector nozzles connected to each cylinder, replaced the use of the intake manifold. The multi point injection is used to assist in the control of the air-fuel ratio and hence, it allows for a better metering of the fuel.
- The Direct Injection: Here the fuel is directly injected inside the combustion chamber. [130]

A considerate amount of research time is today dedicated to the design and the analysis of the injector system, looking at its geometric parameters as well as at the materials used during the manufacturing processes [23, 35]. The Diesel FIS is designed so as to supply the fuel to the ICE at a precise time; the fuel is sprayed at high pressures inside the injector [21,25,127,131-132] and is dependent on factors such as the piston position and the crank angle. [133]

The majority of commercial vehicles and passenger's automobiles makes use of the Electronic Diesel Control (EDC) system [60]. The use of the EDC system led to the industrialization of the engine system and so led to the birth of the FIS where, the injection pressure is independent of the engine speed and the engine load [134] – the new technology made use of the hydraulic actuation system made up of a pressure intensifier giving rise to the preferred pressure by varying the oil pressure. This could be done independently of the engine lubrication system and the solenoid valve, in order to control the start and the end of the injection; the solenoid spill valve is used to connect the highly pressured oil to the intensifier plunger. [135]

2.1.4.1. Common Rail Injection System

This chapter comprises a summary of the history of the common rail system from the early 19th century to the present time. The chapter presents detailing mechanism of the electromagnetic solenoid as well as the piezo electric injector citing manufacture companies such as Vickers, Bosch, Denso and Magneti Marelli.

2.1.4.1.1. History of the Common Rail System

In 1913, the first attempt to what is today called the common rail system was developed by Vickers Ltd. The system was made up of a multi plunger pump which was used for the delivery of the fuel to the accumulator. A relief valve was used in order to maintain the fuel pressure of the mechanically operated injector at 35 bar. [136] Its only around 1980, with the emergence of the high speed actuator by Lucas Epic (Electronically Programmed Injection Control), necessary for the control of multiple injectors, that the common rail technology was first used for light duty engine cars. With the development of the High Speed Direct Injection Diesel engine (HSDI), an improvement of the fuel injection process was noticed, mainly an improvement of the small pilot injection, leading to the control of the cylinder pressure rate at the start of the combustion process; this was mainly done with the aim to control the combustion knock occurring inside the early HSDI. Although the control of the injection timing and quality over the engine load and the engine speed was dealt with using the electronically controlled distribution pumps, it was vital to tackle the fact that the injection pressure was still a function of the engine speed. It's only around mid-1980s that Magneti Marelli invented the first FIS completely independent of the engine speed and engine load using the common rail. [137] In 1995, Denso was able to manufacture more powerful common rail systems. [138]

The Common rail system is classified in term of “generation”, whereas the generation marks the maximum pressure inside the rail; the first generation of common rails came from an agreement made between Bosch and Fiat on the development of the common rail system. The first generation could not reach 1600 bar pressure. It was made up of a High Pressure Pump (HPP), a high pressure rail, an Engine Control Unit (ECU) and number of solenoid injectors. Bosch was able to further develop the system which later on reached pressures of around 1600 bars. However, the second generation of common rails encountered severe leakage complications even though the sole focus of the new developed product was on the improvement of the material and the manufacturing processes. The third generation on the other hand, did not have continuous system leakage and was able to reach pressure above 1800 bar. Now a day however, the fourth generation of common rail injectors systems can reach pressures above 2000 bar [87, 139] – Delphi is today one of principal producers of the DI as well as the IDI Diesel injectors, making use of techniques such as the Enhanced Injection Pressure (EIP) with the Electronic Unit Pump EUP) systems and reaching injection pressures above to 2,000 bar.

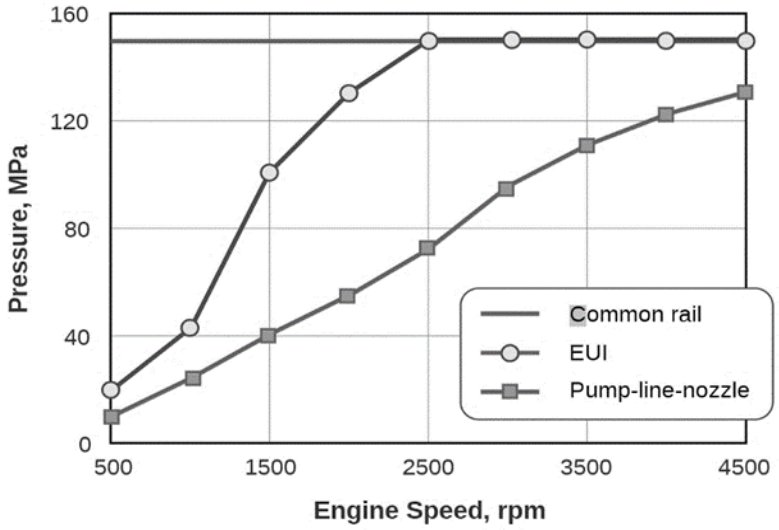

Figure 9 Pressure variations for corresponding changes in Engine Speed – Common Rail, Electronic Controlled Unit Injector (EUI), Pump-Line Nozzle [140]

As shown in Figure 9 Contrary to the use of the EUI and the Pump-Line Nozzle, with the use of common rails the pressure inside the engine remains unaffected by the change in engine speed.

2.1.4.1.2. Mechanism of the Common Rail System

The DI engine common rail makes use of a pipeline where the fuel is injected into the cylinder through a series of injectors connected together. The common rail system makes use of the injection spray momentum delivering short and multiple injections at a precisely controlled time in order to maintain a high injection pressure inside the nozzle, focusing on the operating speed of the injection taking place. The EDC is often used as a fuel injection control system that helps to calibrate with high precision the amount of fuel supplied to the combustion chamber [141].

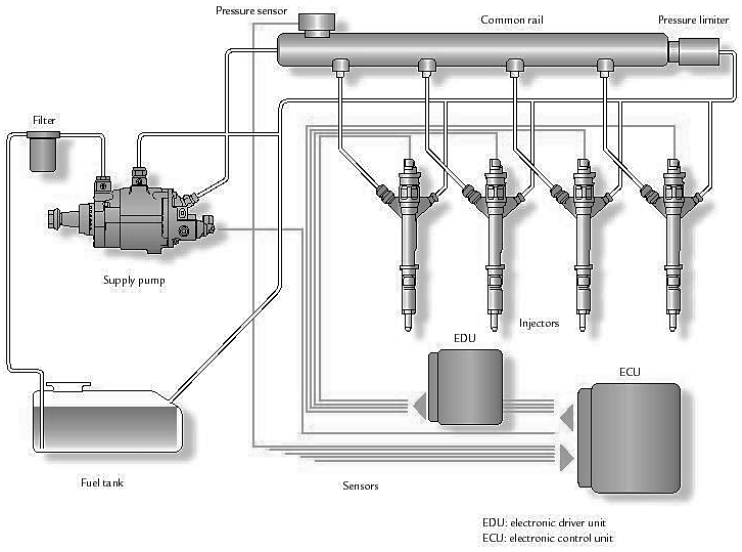

Figure 10 The Diesel FIS [142]

The electronically driven highly pressurized fuel located inside the fuel reservoir is directed into the injector nozzle holes leading to the movement of the injector needles. And hence, the fuel is directed

into the engine. The modern common rail system is mainly made up of Injectors, a HPP, an Electronic Control Unit (ECU) and an Electronic Driver Unit (EDU), a high pressure rail and a fuel tank. The use of servo hydraulic fuel injectors has dramatically improved the combustion system fuel efficiency, where the rapid opening and closing of the nozzle needle allow for a precise injection flow rate control. [143] The introduction of the EDC system helps to control the high demand of increase engine efficiency. Hence, the use of the EDC has dramatically increased the engine's performance and has contributed to the control of the GHG emissions [144-145]

Two types of actuators are considered when it comes to the FIS; the Electromagnetic Solenoid Injector and the Piezoelectric Ceramic Injector.

As the current moves through the coil, the solenoid valve converts into an electromagnet – Hence, the electromagnetic force produced in the magnetic material is used to move the plunger.

Among the advantages of using the Electromagnetic Solenoid Injector is that it is solider than the piezoelectric injector as a result has a low-cost construction demand. Among the disadvantages of the using the Electromagnetic Solenoid Injector however, is the fact that only up to five injection pulses per cycle is made at a time, making it harder to control the fuel delivery system.

With the use of piezoelectric actuators, which convert the inputted energy into a mechanical movement, common rail pressures of more than 2000 bar can be achieved.

Among the advantages of using the Piezoelectric Ceramic Injector is the faster response time noticed in comparison to using the Electromagnetic Solenoid Injector. The main disadvantage however is the fact that the Piezoelectric Ceramic Injector is often found to be costly.

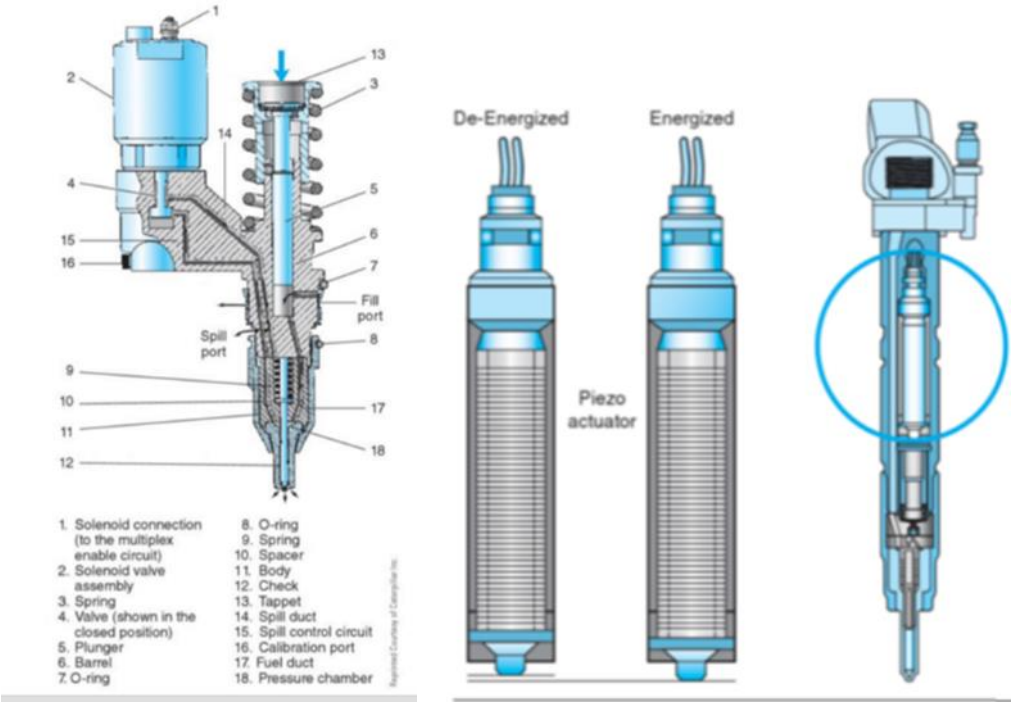

Figure 11 Electromagnetic solenoid and Piezoelectric Ceramic Injectors [146]

A number of researchers have conducted studies on the Piezoelectric Ceramic Injectors. Authors such as Giannadakis *et* al. [147] conducted research on the Pintle Piezo injector nozzle. Lee *et al.* [148] worked on the impact that the Piezo-driven needle opening has on the flow inside the nozzle. Among today's manufactures of the Piezoelectric Ceramic Injector are Robert Bosch and Magneti Marelli. Denso currently develops both, the Solenoids and the Piezo actuators. The Solenoid and the Piezo actuators observe a similar mode of operation. However, the main difference is seen in the way they are manufactured – The highly pressurized fuel inside the common rail will exert a force above and below the needle valve acting as a spring-loaded device. Hence, the release vale is activated between injections in order to control the fuel delivery system. [149-150]

2.1.4.2. Nozzle Design

The injector nozzle constitutes the main component of the FIS. The injector needle movement as well as the geometry of the nozzle are key parameters taken into consideration when it comes to the design of the CI engine nozzle. [22,28-29, 50, 133, 148] Factors affecting the fuel spray are often the fuel injection pressure, the cavitation phenomenon inside the injector spill valve, the nozzle geometry, the fuel composition as well as the ambient conditions being taken into account. The level of performance of the engine operation is determined by the optimization of the fuel atomization process. Hence the design of the nozzle is done with great care as it defines the way the engine operates. [151]

Great care and attention to detail is needed when designing the nozzle holder, also known as the body of the injector, due to the extremely high pressures occurring during the combustion process.

Three different types of nozzle holders can be considered: The standard nozzle holder also known as the single-spring nozzle holder, the two-spring nozzle holder and the stepped nozzle holder. [121]

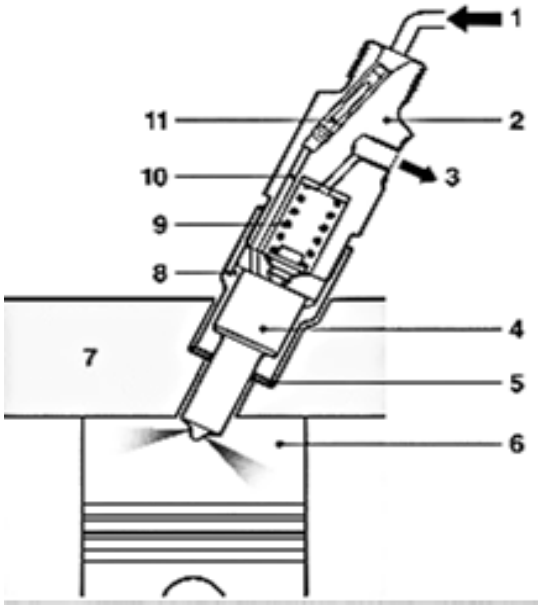

Figure 12 Injector nozzle – The FIS. [59]

The nozzle holder is made up of the nozzle retaining nut (8), the spring valve (9), the fuel supply (10) and return pipe and the filter (11). From Figure 12, other components such as the fuel inlet (1) and the injection nozzle (4) can be seen – the primary nozzle is located at the top of the nozzle holder and is positioned inside the combustion chamber – The nozzle needle is located inside the nozzle body and is used for orifices fuel blockage. [59] Furthermore, the cylinder (6) and the cylinder head (7) are likewise shown.

Two main injector nozzle types are often used by car manufacturers; the hole nozzle and pintle nozzle.

- The ***hole nozzle*** commonly used for the DI engine and frequently used with the in-line injection pump is further characterized into two different types;
  - The Sac-hole nozzle: Here the spray holes are arranged in the sac hole – The sac volume (located below the needle valve) and diameter may vary. Carefulness is observed when designing the tip of the nozzle as well as the sac hole. The advantage of using the sac type nozzle is the presence of a uniform flow field through the nozzle holes. However, the disadvantage of using the sac-hole nozzle is the fact that the fuel sometimes remains inside the sac as the injection has taken place. As a consequence, the remaining fuel when not completely directed toward the nozzle spill valve, tends to leak leading to soot emission. [152]
  - The seat hole nozzle or Valve Covered Orifice (VCO): The design of the VCO, plays a role in the reduction of the residual volume inside the sac as the volume of the VCO sac is inferior in comparison to the volume of the sac-hole nozzle.
- The ***pintle nozzle*** often used for the IDI engine: Due to the buildup of carbon deposits taking place with the use of the pintle nozzle, leading to an increase in the combustion noise, pintle nozzles are not often the manufacturer's preferred chose. [152]

Nozzle Tip design – based on the geometry of the nozzle, two types of tip designs can be considered: The ***Round nozzle*** tip design: The spray holes are drilled mechanically or with the use of appropriate electrochemical devices. The ***Cylindrical and Conical*** tip design: For design purposes, an electrochemical device is used. The sac hole is Cylindrical/semispherical and allow for a high level of design freedom.

When designing the nozzle, care must be considered when it comes to the nozzle geometry and sharpness, as well as the consistency of the flow under standardized test conditions. The Cd variation depends on the automotive manufacturer and on the device's application – As an example, when considering 101 bar upstream of the nozzle and 1 bar downstream of the nozzle, the Cd could vary between 0.80 and 0.88 [153]

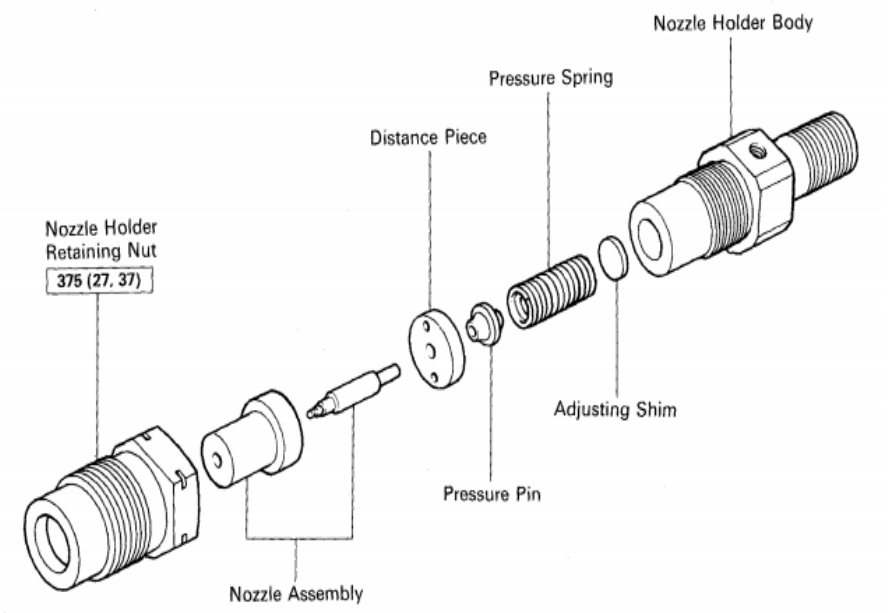

Figure 13 Exploded view of the CI injector Nozzle [154]

A number of Scientists such as Akagawa *et al.* [155] made use of pintle nozzles in their studies, focusing on the difficulties encountered when using the pre-mixed lean Diesel combustion. The authors discovered that the use of the pintle nozzle may reduce the overall HC and CO emissions. Marsh *et*

al. [156] likewise worked with pintle nozzles considering 8 degrees and 30 degrees pintle angles. The authors made use of High-speed spark photographs in order to visualize the spray in the air and discovered that the pintle angle does not have a greater impact on the spray cone angle.

As great design consideration must be observed when it comes to the spray hole length and quantity as well as the spray injection angle, a number of scholars in the field of ICE tend to focus on the study of the Diesel spray. Bae *et al.* [35] worked on the Influence of Injector Parameters on the Diesel spray, Karrholm *et al.* [126] looked into the turbulence interaction and combustion of Diesel spray, Habchi *et al.* [127] made use of a Diesel spray atomization and break up model in their study.

The use of the VCO technique, where the sac volume between the injector needle valve and the nozzle hole is dramatically reduced, has helped to reduce the amount of Unburned HC pollutants caused by the combustion process. By controlling the sac volume, it is possible to control the quantity of fuel located downstream of the needle valve, exposed to combustion when left inside the sac volume. [153] Making use of optical imaging devices, noticeable differences in the spray in relation to the VCO and the sac-hole techniques can be observed. When using the VCO technique, a non-symmetric spray with detailed atomization features can be observed – For identical nozzle hole diameter, the VCO configuration tends to induce high turbulence in order to assist the spray atomization process, making it more susceptible to flow separation and cavitation. The use of the VCO technique likewise produces a low value of Cd. [153]

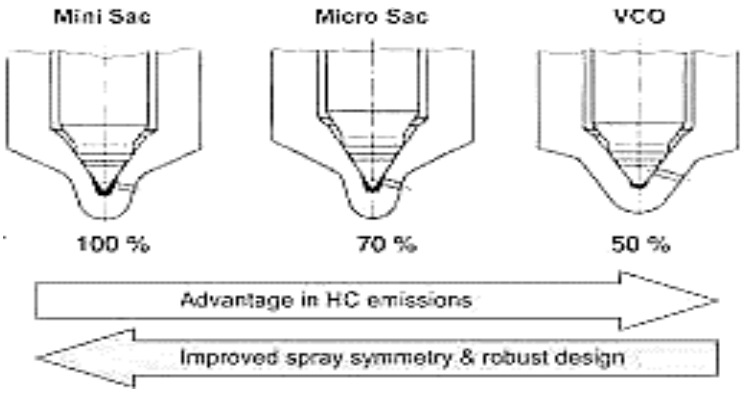

Figure 14 HC emission comparison of 3 different types of Nozzle design [157]

Some of the Delphi injectors are designed using the VCO technique, making use of a mechanically/electronically controlled pump line. The pump line is mechanically closed using a high stress-capable spring. With a typical nozzle diameter of 250 microns and with the fluid moving at several hundreds of meters per second, obtaining completely accurate experimental flow measurements can sometimes come as a challenge.

Authors such as Bae *et al.* [35] made use of a common-rail system configuration, and a 30 bar pressurized chamber in order to study the spray characteristics of the Sac and the VCO (double guided needle) nozzles. Considering different nozzle geometries, the authors made use of video imaging techniques in order to visualise the spray characteristics. The authors were able to observe the behavior of the high pressure injection measured spray penetration and spray angle. Looking at the spray surface structure and the primary breakup, the authors were able to use the Sauter Mean Diameter (SMD) to obtain the Fuel droplet sizes. The authors found out that, by varying the nozzles geometries – increasing the K factor (which represent how tapered the hole can be), and by decreasing the exit hole sizes, an increase in the spray penetration was noticed at a smaller spray angle. [35]

2.2. Cavitation

As *the present study* focused on the effect of cavitation on the FIE – from the inception phase to the fully developed phase, it was important to highlight the various studies conducted by scholars on the subject over the years.

2.2.1. What is Cavitation?

Cavitation can be defined as the phenomenon that occurs in liquids during the nucleation process, where low pressure regions of the flow field result in the vapourization of localized pockets inside the liquid, Wright *et al.* [45] Cavitation can be compared to boiling which happens during the nucleation process due to the raise of temperature taking place above the saturated vapour temperature. The process of cavitation is dependent on the quality of the working fluid as micro bubbles are considered.

Cavitation can be classified as being dynamic as well as static with both cases leading to bubble formation inside the fluid. The dynamic cavitation induces high levels of stresses which causes the flowing fluid to rupture leading to extreme pressure excursions. During the occurrence of the static cavitation on the other hand, the local pressure of the fluid drops to a level lower than its vapour pressure.

2.2.2. Cavitation Research

In his paper dated 1984, Osborne Reynolds was able to demonstrate that the cavitation phenomenon could occur within a converging-diverging glass tube, using water as the working fluid – As the water moved through the constriction area of the tube, based on Bernoulli's law, a decrease in pressure was observed in the narrow region of the tube, allowing for the formation of cavitation in that region. [158]

During the nineteenth century, as the cavitation phenomenon started to puzzle the scientific community, a growing interest in the study of the damages caused to materials due to cavitation emerged. As a result, scientists were able to determine how, under certain flow configurations, cavitation was indeed responsible for the solid material's corrosion. Parsons and Cook [159] looked at the causes of corrosion/erosion on propellers, looking precisely at the effect of sea water on the magnesium bronze. Based on the jet atomization technique proposed by Kong *et al.* [125], the main factors affecting the internal nozzle flow were cavitation and turbulence. The turbulence phenomenon is often better understood; it is known as one of the leading causes of the primary atomization breakup process as it finds its source from the shear stresses created at the wall boundaries. On the other hand, the cavitation phenomenon, which often occurs under severe dynamic conditions, is still not properly understood. Wright *et al.* [45] Due to its impact on the nozzle exit velocity and pressure, and due to its transient properties, the cavitation behavior is assumed to likewise play a role on the primary atomization breakup processes. Giannadakis *et al.* [52]

2.2.2.1. Incipient Cavitation Bubble Formation

It is hard to predict what will happen to the bubbles formed as they move through the flow from one point to another – when near the flow-specific critical value, vapour cavities begin to emerge from nucleation sites. They may expand and merge into a cavitation cloud, or they may shrink in size, this taking into consideration parameters such as the internal temperature and pressure as well as the rate at which boiling, and condensation takes place. The bubbles formed as cavitation takes place may collide with other particles in the flow in order to form new growing bubbles – As the flow velocity eventually decreases, the pressure will rise back above the vapour pressure and the cavities will begin to collapse. The cavities may furthermore attach themselves to the wall boundaries.

As described in the "Cavitation in Control Valves" by Samson [160], the spherical cavitation nuclei can be considered when an equilibrium state is observed between the pressures inside the bubbles and, the liquid pressure on the surface of the bubbles and the surface tension.

$$P_G + P_{V=} \frac{2\alpha}{R} + P \quad \textit{Equation 2}$$

Where P is the fluid pressure, P_G is the pressure of the gas inside the bubble, P_V the vapour pressure and $\frac{2\alpha}{R}$ the surface tension considering radius R and constant α.

Based on the spherical nuclei general gas law, the isothermal change of volume can be described in Equation 3.

$$P_G = \frac{N\, R_G\, T}{\frac{4}{3}\pi R^3} = \frac{G}{R^3} \quad \textit{Equation 3}$$

Where G represents the gas concentration. G is proportional to the gas volume inside the bubble.

Merging Equation 2 in Equation 3 gives:

$$P - P_{V=} = \frac{G}{R^3} - \frac{2\alpha}{R} \quad \textit{Equation 4}$$

Hence Incipient cavitation formation can be obtained when $\frac{d(P-P_V)}{dR} = 0$, which is equal to:

$$(P - P_V)_{crit} = -\frac{4\alpha}{3\sqrt{3}}\sqrt{\frac{2\alpha}{G}} \quad \textit{Equation 5}$$

Wang *et al.* [54] were able to observe string cavitation which often occurs as a strong cavitation flow takes place near the nozzle exit – string cavitation plays a significant role in the fuel atomization process and may occur as a result of hydraulic flip. The authors made use of pressure forces from a compressed air device in order to drive the water through the nozzle. The incipient cavitation as well as the string cavitation phenomena were observed inside an axisymmetric large scale sharp-edged acrylic nozzle. Similarly to *the present study*, the authors concluded that cavitation was very much dependent on Re as an increase in the Re gave rise to an increase in the cavitation. With the use of CFD simulations and high speed video imaging techniques, Andriotis *et al.* [53] were able to study the cavitation structure inside the Diesel nozzles. Comparably to *the present study*, the authors made use of purposely built transparent large scaled Diesel nozzles with converging tapered conical holes and cylindrical holes. Taking into consideration low needle lifts, the authors were able to visualise string cavitation [161] near the region of large-scale vortices – Parameters such as the flow rate and the Re were made use of, enabling the authors to obtain images of the string cavitation, the frequency of appearance, the lifetime and the size of the vortex. The authors managed to compare their work to phenomena occurring in real life-size Injectors. As they could visualise geometric cavitation at the entrance of the cylindrical holes, the authors furthermore discovered that cavitation erosion occurred where string cavitation took place.

Using the modified version of the Multi-Dimensional CFD KIVA-3V model, the "Cavitation bubble Collapse Energy Breakup (CEB) model", Nishimura and Assanis [50] were able to study cavitation bubbles. The authors were able to study the movement of the bubbles inside the injector and the liquid core using the modified model. Comparable to *the present study*, the authors were able to observe the

spray tip penetration and spray cone angles, and found out that their were easily obtained when considering a 25 microns mean bubble radius as the specified radius corresponded to the primary breakup child droplets.

The key method employed in *the present study* in order to induce incipient cavitation – the manipulation of the Upstream and/or the Downstream Pressures of the flow through an injector nozzle, has likewise been used by scientists such as O'Hern [32]. The author worked on the cavitation inception taking place inside a turbulent shear layer. Using high speed video imagining techniques, the author found out that the cavitation inception occurred inside the turbulent shear layer structures giving rise to spanwise and streamwise vortex structures. The author also found out that the turbulent shear flow cavitation was at the root cause of the cloud cavitation formation and as such was one of the main causes of the observed cavitation erosion. Iyer and Ceccio [31] experimented with the shear layer cavitation with the aim to study the impact that the growth and the collapse of the cavitated bubble has on the dynamic of the shear flow. The authors worked on cavitation inception as well as on fully developed shear flow. By setting a constant exit velocity and a constant working fluid temperature and by varying the Ca, the authors were able to demonstrate that the development and the collapse of the cavitated bubbles located inside a plane shear layer, affected the dynamic characteristics of the shear layer – An increase in the velocity is often observed downstream of the cavitated region as the fluid flows through the nozzle. The increase in the flow velocity was likewise observed while conducting *the present study*.

Ganippa *et al.* [162] also worked on the cavitation inception where they were able to observe bubbles inside the flow. Comparably to *the present study*, the authors detected that the bubbles were not attached to the wall boundary. They furthermore observed an increase in the flow that led to the formation of a denser group of bubbles, leading therefore to cloud cavitation formation – The

cavitation formed as the flow increased, gave rise to a change in colour of the flow from a white cloudy appearance to a glassy appearance. A symmetric cavitated spray was first observed inside the nozzle hole. As the flow further increased however, cavitation was perceived at the exit of the hole. Depending on the geometry of the hole, for some cases, the authors observed the appearance of cavitation on one side of the hole – an atomized jet was observed only on the heavily cavitated side of the hole.

Chaves *et al.* [163] made use of transparent purposely build injectors for their study of the cavitation inception. Reflecting the same conditions as those found inside the Diesel injector, and making use of the video imaging techniques such as the modified laser-two-focus-velocimeter, the authors were able to observe the flow inside the nozzle. The discharge measurements as well as the flow velocity measurements were obtained considering a maximum pressure of 100 Mpa. The authors additionally found out that for certain conditions, an increase in the flow pressure led to the cavitation moving from the inside corner of the nozzle to the outside of the nozzle.

Aside from the incipient cavitation occurring inside the ICE, the study of the cavitation inception has also been conduction on the various subject area of engineering. Making use of the axially symmetric caliber ogive-nosed bodies, Parkin and Holl [164] focused on visually studying the incipient cavitation occurring around the nose. In order to simulate cavitation around the nose, the authors decreased the free-stream static pressure and kept the tunnel velocity constant. Hence the pressure was increased up to the point where the incipient cavitation was observed.

Often making use of water as the working fluid, a number of scientists have worked on the stress induced cavitation research – Cavitation sometimes takes place around the sharp edge corner of the inlet of the nozzle, this may occur as the pressure drops around the edges of the nozzle. Such cases

may cause the formation of a detached flow as the liquid detached itself from the wall of the nozzle. As the liquid completely detach itself from the nozzle wall, hydraulic flip takes place [46, 52, 165] Stress induced cavitation can lead to poor performance due to material deterioration, corrosion and/or erosion taking place. It can also lead to noise vibration which can have a detrimental impact on the device being used.

With the aid of a 2D model Wang *et al.* [54] worked on stress induced cavitation looking at the cavitation occurring near the tips of the nozzle. Dabiri *et al.* [51] focused on detecting the stress induced cavitation occurring on the liquid flowing through an atomizer orifice, this considering a two-phase incompressible flow. The authors worked on the Re ranging between 100 to 2000. The configuration of the nozzle orifice was so that the upstream corner was rounded and the downstream corner was sharpened. A strong correlation between the change in the viscous stress and the impact it has on cavitation was observed. The authors furthermore looked at the effects of changing the nozzle geometry as well as the existence of hydraulic flip inside the orifice.

2.2.2.2. Immersed Jet Cavitation

As the study of the immersed jet flowing through an injector inside a stagnant fuel receiver was one of the main focus of *the present study*, it was vital to emphasise on the impact of the cavitation on the jet and on its surrounding.

Bergwerk [166] worked on the impact of cavitation on the jet. The author observed jet perturbations occurring during noncavitating conditions as well as during cavitating conditions. Considering the later conditions, cavitation occurred as the jet was no longer attached to the wall. Similarly to *the present study*, the Cd varied with the change in in the Re and with the change in the Ca – The speed, the pressure as well as parameters such as the Ca are paramount to the study of the cavitated jet flow. Authors such as Giannadakis *et al.* [24] made use of the Lagrangian and Eulerian CFD models in order

to investigate the Diesel nozzle hole. The results were compared to experiments done on real-size six-hole mini-sac nozzles. Using high-speed video cameras and Laser Doppler Velocimetry (LDV) measurements techniques, the authors were able to study the start and the development of cavitation. A significant void zone was observed inside the injection hole when making use of the Eulerian models, making it impossible to visualise the changes occurring as cavitation developed. The Lagrangian model however was seen to predict with more details, the onset of the flow as well as the transition to the fully developed flow. The authors discovered that an increase in the flow velocity as well as a decrease in the Cd occurred as cavitation took place.

Scientists and engineers have intensively studied the flow characteristics of cavitation occurring on self-oscillating jets. Liao *et al.* [167] made use of a pulsed flow capable of changing the pipe's flow into fluctuation motions in order to increase the speed of a drilling oil well. Chahine *et al.* [168] in their study of self-resonating cavitation jets made use of a self-excited cavitating jet assembly for the study of underwater sound generation. The authors made use of a feedback mechanism which matched the natural frequency of the submerged jet with that of the resonant chamber. Parameters such as the pipe length, the pressure drop across the nozzle as well as the Ca were taken into account. The scholars found out that the efficiency of the self-resonating cavitating jet was two orders of magnitude greater than that of a typical cavitating jet. The authors took into consideration a number of parameters impacting the cavitation structure such as the geometrical parameters of the nozzle.

Researchers have been looking at mixing the Diesel fuel with water as an alternative source of power in order to tackle harmful pollutant formed as a result of combustion. Making use of a heavy-duty Diesel inline six-cylinder engine with overhead camshaft, Chadwell *et al.* [169] focused on the performance of the engine as well as on the emission control looking precisely at the reduction of soot formation. The authors made use of the modified Real Time Water Injection (RTWI) method to

incorporate the water addition passages, in combination with the Exhaust Gas Recirculation (EGR) system – The EGR is a system that controls Diesel engines NOx emissions making use of the heat absorption in order to decrease the oxygen concentration in the combustion chamber. The method was seen to reduce the NOx emission by 82 percent. However, a reduction of 42 percent was noted when using the RTWI alone – It is to be noted that the author over simplified their design in order to reach the ideal conditions taking place during the mixing of water and fuel near the needle seat. Due to the complex nature of the water and fuel interactions inside the nozzle prior to, during and past the injection period, the effect of stratification within the spray cloud was not predicted. The authors had trouble maintaining the water injection hardware unchanged for every cylinder used as constant efforts were required to maintain a balanced water injection when considering the cylinders consecutively.

A number of studies have showed that cavitation can be observed in turbulent shear flows when the local liquid pressure drops below the liquid vapour pressure and vapour bubbles form in the low-pressure cores of fluid vortices, the phenomenon was likewise observed in *the present study*; as the liquid expends and ruptures, it experiences high tensile strengths due to negative pressures taking place causing instable equilibrium within the liquid leading to the accumulation of gas molecules in concerned regions. Some of the newly formed nuclei will expend to a point where their diameters will surpass the critical diameter. Cerutti *et al.* [170] worked on incipient cavitation rate focusing on regions of high Re. The authors used an axisymmetric jet modeled using an axisymmetric vorticity-stream function with a semi empirical Lagrangian bubble dynamics solution. During their experiment, microscopic bubbles were injected from the inlet of the jet. Katz *et al.* [171] likewise worked on cavitation inception taking place within the streamwise vortices of the shear layer. The authors discovered that pressure at the core of the vortex reduced due to the presence of the

streamwise vortices alongside the spanwise vortices. As the whole flow was subjected to a reduction of pressure, the presence of cavitation was noted in the streamwise vortices. Gopalan *et al.* [172] discovered that incipient cavitation took place in the core of the streamwise vortices as they conducted experiments on the incipient cavitation jet focusing on the differences between the distorted spherical bubbles and the inclined cylindrical bubbles. The authors measured the near field of the jet, the streamwise vortices strength distribution and the velocity profile within the boundary layers. Xing *et al.* [173] looked at the effect of the cavitated planar submerged laminar jet on the dynamics of the vortex using a homogeneous cavitation model. The authors were able to consider the non-linear bubble dynamics taking place, as well as the interactions between spherical bubbles. By varying parameters such as the Ca and Re, the authors were able to observe cavitation within the core of the primary vortices. They furthermore discovered that the core vortex was lifted vertically due to cavitation. Choi *et al.* [174] studied the growth, the oscillation and the collapse of the vortex cavitation bubbles by varying parameters such as the pressure between the bubble, the Re, the applied tension rate distribution and the spatial distribution using 2D and 3D models. The authors were able to observe the change in the shape of some bubbles as they elongated along the vortex axis to fill the vortex core up to the point where they collapsed and split radially when subjected to high tensions. On the other hand, in their work, Iyer and Ceccio [31] discovered that cavitation does not affect the formation of the vortex within the shear layer. They discover however, as it was equally discovered in *the present study*, that the development of cavitation impacts the turbulence. For the study of incipient cavitation, the authors proposed the use of the single phase simulation of shear flow to further examine the impact of cavitation on the shear flow.

Yang *et al.* [30], conducted research experiment with the use of a non-plunger central-body nozzle with square outlet where the impact of the nozzle configuration on the jet properties was analyzed.

The authors were able to simulate a number of submerged jet discharges from the central-body nozzle and found out that by keeping a constant central-body diameter, an optimal contraction degree of nozzle's outlet was observed leading to an increase in the jet cavitation. Comparable to *the present study*, the authors discovered that the jet profiles were affected when changing the size of the relative diameter from a larger size – where most of the bubbles took place in the core of the jet, to a smaller size – where the bubbles were observed between the jet and the surrounding fluid. The energy coming from the cavitated jet as a result of bubble collapse, increased the impacts of cavitation on the jet. [21] By studying the effect of the structural parameters of the cavitated non-plunger nozzle jet, the author aimed to provide a solid basis for the design of the injector nozzle.

Researches also worked on the angular nozzle structures of the submerged cavitation. Hutli *et al.* [175] made use of a nanosecond high speed Intensified Charge-Coupled Device (ICCD) camera, the 4-Quik-05, in the study of the jet's structure and the temporal and special behavior of cloud cavitation. For a closer view and for a uniform observation of the jet, an endoscope producing a homogeneous light distribution inside a test chamber, was utilized enabling a clear visualization of the highly submerged cavitating water jet. As compared to *the present study*, parameters such as the Upstream and the Downstream Pressure as well as the Ca of the jet were looked into. Additionally, the authors worked on the effect of temperature on sono-luminescence. In the second part of their work, Hutli *et al.* [176] made use of a submerged jet inside a test rig containing a combination of pumps, valves, temperature sensors and transducers, heat exchanger and gauges. The authors were able to observe the temporal and spatial random behavior of cavitation clouds formed from the cavitating jet. The study made use of a photodiode connected to an oscilloscope which captured images within the order of microseconds. However, the authors found out that the using an endoscope did not yield to

satisfactory results as the image were seen to have very poor resolutions – the jet's breaking point position was observed at various location. The jet was seen to exhibit turbulent behaviors with micro jets and shock waves taking place due to bubbles formation, growth and collapse. The phenomena caused a change in the pressure distribution. Similar to the observations made in *the present study*, the authors were able to observe fully spherical bubbles where the size of the jet as well as the penetration of the jet increased as a decrease in the nozzle Downstream Pressure was noticed. The authors additionally noticed an increase in the number of bubbles. Sono-Luminescence phenomena occurring due to the collapse of the bubbles were also observed.

Both, the experimental and the numerical studies have their perks and drawbacks – the modelling sometimes requires making numerous assumptions to the code(s) in order to describe the flow to near enough perfection as scientists are still trying to understand the existing relationship between the nozzle spray characteristics and the injector nozzle. Not only that, in multi-dimensional codes, high density difference between the vapour and liquid can lead to significant instabilities taking place. On the experimental side, due to the complicated nature of the design and mechanism of the fuel injectors and due to the high speed processes taking place during combustion, the experimental measurements techniques being used so far are not totally adequate to mimic the difficulties faced when using injectors in real life. [177]

2.3. Other Relevant Studies

This section focuses on the different studies relevant to *the present study*, where the solubility of the fuel and gas mixture is looked into as well as the different measurement techniques used in relation to injector nozzle cavitation.

2.3.1. Fuel and Gas Mixture Solubility

As *the present study* made use of Unoxidised Nitrogen gas (N_2) in order to move the working fluid through the nozzle hole – where an accurately measured mixture percentage of five alkanes fuels made up of n-Octane, n-Decane, n-Dodecane, n-Tetradecane and n-Hexadecane respectively was used, it was paramount to analyze the effect of convection as well as the effect of diffusion on the Nitrogen-alkane mixing.

Pressurized N_2 systems have been used by a number of scientists for experimental purposes. Wright *et al.* [45]

Care must be taken when making use of Alkane solutions such as n-Octane due to its highly volatile state. Hence, in such case, the use of N_2 is one of the preferred choices due to its inert state lowering the risks of combustion – N_2 is a colorless and odorless gas which does not undergo chemical reactions in low temperature conditions. It is inexpensive and can be found in high reserve in nature and can moreover be used for different applications such as drilling and oil and gas wells. As part of his work, Weiguo [178] made use of compressed N_2. Contrary to the work done by Weiguo, in *the present study*, the alkane mixtures were maintained at the same temperature (in order to avoid the risk of evaporation), taking into consideration the time it took for the fuel mixture to stabilize – The fuels were properly stirred to allow for a homogeneous mixture. Not only that, all through the experimental procedures, the rig mechanism allowed for a continuous movement of the fuel in order to greatly reduce the probability of fuel stratification – As the different alkanes fuels used in *the present study* had variable densities, it was important to make sure that flow stratification did not occur as an imbalance in the density of the mixture could have impacted the cavitation onset pressure readings.

As N_2 was used to pressurised the fuel in *the present study*, it was important to make sure that the N_2 did not mix with the alkane solutions as an increase of the N_2 in the fuel mixture would have impacted the end results. Moreover, a vigorous control of the highly pressures N_2 was paramount to avoid cases of physical injuries to the members of the personnel involved as well as physical damages to the equipment being used.

A Diffusion-Controlled Evaporation model was made use of by Brereton [179] while working on the dissipation of injected N_2. The author made a number of assumptions in his study. Among them were; the rate of dissipation of N_2 was dependant upon the surface rate of diffusion, the Nitrogen bubbles were spherical, evaporation took place as soon as the N_2 molecules were in contact with the liquid surface because the dissipation of the N_2 is considered dependent only on the motion of the Nitrogen molecules as the intermolecular forces are not considered. Based on that, a few assumptions were furthermore considered when looking at the dissipation rate of N_2 used in *the present study*. The diffusion of the N_2 was taken into account in order to obtain the time it took for the N_2 to diffuse in the fluid as injection took place.

The mean free path (averaged length traveled by the N_2 molecules between collusions) of the N_2 was obtained considering

- Minimum pressure of 11 bar and maximum pressure P of 61 bar
- Cylinder Temperature T = 17^{o}C
- Diameter of Nitrogen molecule d = 3.8×10^{-10}m
- Molar Mass of Nitrogen M = 28.0134 kg/kmol
- Nitrogen Molecular Mass = 0.028 kg
- Boltzmann's Constant k_b = 1.37 x 10^{-23} JK^{-1}

– Universal gas constant R = 8.3 Jmol-1k-1

Hence considering a minimum pressure of 11 bar, the mean free path was obtained using Equation6.

$$l_{FreePath} = \frac{k_b T}{\sqrt{2}\,\pi d^2 P} \quad \textit{Equation 6}$$

$$l_{FreePath} = \frac{1.37 \text{ x } 10^{-23} \times 290}{\sqrt{2} \times 3.14 \times (3.8 \text{ x } 10^{-10})^2 \times 11 \times 10^6}$$

$$l_{FreePath} = \frac{3973 \times 10^{-24}}{7.0570^{-12}}$$

$$l_{FreePath} = 5.6298^{-10}\ m$$

Considering the ideal gas law, the Root Mean Square was obtained using Equation 7

$$v_{rms} = \sqrt{\frac{3RT}{M}} \quad \textit{Equation 7}$$

$$v_{rms} = \sqrt{\frac{3 \times 8.3 \times 290}{0.0280134}}$$

$$v_{rms} = 507.71\text{m/s}$$

The collision Frequency C_f was thus obtained using Equation 8

$$C_f \frac{v_{rms}}{l_{FreePath}} \quad \textit{Equation 8}$$

$$C_f = \frac{507.71}{5.6298^{-10}}$$

$$C_f = 9.01826 \times 10^{11}\text{hz}$$

The time between two successive Nitrogen molecules collisions was obtained using Equation 9.

$$\text{t} = \frac{l_{FreePath}}{v_{rms}} \quad \textit{Equation 9}$$

$$\text{t} = \frac{5.6298^{-10}}{507.71}$$

$$\text{t} = 1.1089 \times 10^{-12}\,\text{s}$$

The partial pressure of N_2 is significantly lower then that of the alkane fuel mixture. Based on Henry's law, this meant that soon after the N_2 was used to pressurise the fuel, the gas inside the tanks was promptly directed through a secondary hose connected to the laboratory ventilation system. Moreover, as the N_2 was pressurized through a small hose diameter, 6 mm ID, a smaller contact surface area between the N_2 and the fuel was impacted, reducing the chances of increased N_2 penetration inside the fuel. And hence the contact surface between the N_2 and the fuel was considered fairly minimal as to greatly impact the end results.

In their work, Battino *et al.* [180] presented a review of different studies conducted on the solubility of Nitrogen in n-alkanes HC. Hence, looking at the standard deviation of the curve and using the regression analysis of the data as a function of the temperature and the number of carbon atoms, the authors were able to obtain a fitted equation from statistical solubility data from the worked done by a number of scholars. For the majority of studies, a rise in the temperature led to an increase in the solubility of Nitrogen in water – as temperature remind constant in *the present study*, the likelihood of N_2 dissolving in the fuel was further reduced.

Furthermore, the authors discovered that an increase in the number of carbon led to a decrease in the solubility of Nitrogen. Using the Bunsen absorption coefficient, Thomsen *et al.* [181] also concluded that an increase in the number of carbon led to a decrease in the Nitrogen solubility. This was paramount for *the present study* as it meant that, mixing n-Octane with hydrocarbons such as Hexadecane further reduced the ability of N_2 to dissolve inside the fuel. Wakefield and Marsh [182] were able to measure the viscosities as well as the densities of mixture of 9 different n-alkanes making use of the Utube Ostwald viscometer and the pycnometer respectively. The authors worked on Hexane, Heptane, Octane, Nonane, Decane, Dodecane, Tetradecane, Hexadecane, and Tetracosane, looking at a temperature range of 303 K to 338 K. On the other hand, making use of the high-pressure burette and the viscometer, Tanaka *et al.* [183] studied the viscosity and density of alkanes. The authors worked with the mixture of n-Octane, n-Dodecane, and n-Hexadecane with Cyclohexane, considering temperatures ranging between 298 K, 323 K, and 348 K respectively at 150 MPa. De Lorenzi *et al.* [184] moreover worked with a mix of Paraffin and Cycloparaffin. The authors measured the density of the fuel using the vibrating tube densimeter as well as the kinetic viscosity of the fuel using the Ubbelohde Capillary Viscometer at atmospheric pressure and temperature (around 298.15K). Weiguo

[178] conducted work on pure liquids, on binary mixtures as well as on ternary mixtures. The author was able to conduct measurements of the static vapour pressures considering temperatures ranging between 298.15K and 303.15K, using a densimeter to obtain the densities of pure compounds as well as the densities of the different mixtures. Similarly, Lacher *et al.* [185] worked on binary mixtures – the Chlorobenzene-Ethylene Bromide and 1-Nitropropane-Ethylene Bromide looking specifically at the chemical potentials of the liquid phase, considering the total and the partial measurement. Kay *et al.* [186], looked into the existing relationships between vapour-liquid equilibrium of n-Butane and n-Pentane as well as n-Butane and N-Hexane.

2.3.2. Measurement Techniques and Diagnostics

This chapter comprises a brief history of laser spectroscopy highlighting the interaction between matters and electromagnetic radiations as well as the different spectroscopy measurement techniques currently being used by scientists and engineers – As a 405 nm laser was utilized in the study of the sustained hydrodynamic cavitation, it was important to highlight the significance of the use of laser in cavitation studies.

In 1901 Planck discovered that the energy's frequency v was represented by random discrete variables nhv instead of random continuous variables – As atoms of active elements are pumped using an electrical discharge or an optical discharge, they experience excitation and jump to a higher level of energy emitting the absorbed energy as they return to the ground state. The energy emitted as a form of light with the same wavelength as the incident photon, conveys detailed information of the tested substances.

The energy emitted by the photon can be represented using Equation 10.

$$h\nu = E_2 - E_1 \quad \textit{Equation 10}$$

Where E_1 is the lower energy level and E_2 is the upper energy level.

In 1916, Albert Einstein explained the concept of photons, explaining how electromagnetic energy can be quantified. He also explains how the process of emission can take place by means of induced/stimulated photon or can occur spontaneously. His work allowed him to explain the presence of black body radiation – During thermal equilibrium, the spontaneous decay will take place at a greater rate than the stimulated emission creating an incoherence in conventional light sources – as the spontaneous decay takes place, a photon of frequency hν is emitted to a lower level. Spontaneous decay takes place as an atom located at the upper level is decayed emitting a stimulated photon with equivalent properties to the incident photon that caused it. As Einstein made use of Born's theory (to calculate the electron's energy level), he was able to conduct further experiments on stimulated emissions and hence he was able to demonstrate how photons and black body radiation can be compatible.

The first optical laser effect was demonstrated around May 1960 – The pulsed operation laser had a wavelength of 694.3 nm. Ruby was used as the amplifier to amplify the beam of light at a specified wavelength. The use of amplifiers has greatly improved spectroscopy enabling the use of the infrared as well as the ultraviolet spectrum of light.

Lasers are classified based on their light concentration: Spatial concentration denotes the low divergence considered when designing lasers as this enables the projection of light at a closer/further maximum distance to/from the source. It likewise accounts for accurate distance calculation. Spectral concentration looks at the accurate frequency level considered for the emission of radiation reaching

relative precision $\Delta v/_v$ of 1014. Temporal concentration on the other end focuses on the interaction mechanism taking place inside a number of lasers in a matter of milliseconds or less – hence lasers are often utilized in the study of chemical reaction looking closely at the formation of free radicals. [3]

Among other applications of lasers are, but not limited; to materials treatment, drilling measurements, telecommunication, laser weapons medicine, instrumentation cutting.

Although there exist a significant number of spectroscopy measurement techniques at present, it has been noted that, the Laser Induced Fluorescence (LIF), the MIE Scattering, the Laser Sheet Dropsizing (LSD) as well as the LDV, are the four main methods often employed by scientists and engineers – Although the use of these spectroscopy techniques was not paramount to *the present study*, it was import to enclose a brief summary of the different techniques utilized nowadays – the rig was designed and setup in such a way that the different techniques could be employed if needed. However, for the purpose of *the present study*, the high resolution imaging camera used to obtain high resolution pictures of the nozzles and the cavitated jet flow as well as the 405 nm laser were appropriate for the purpose of the experiment.

- LIF: The volume dependent technique is often used for temporal and spatial study of molecular structures as well as flow visualization. As the laser light is emitted, the species is exited emitting in turn a defined level of excitation classified by its excitation wavelength. A photomultiplier can be used to record the fluorescent light, and hence it can be used to record the data for spectrum analysis. There exist two types of LIF techniques:
  - Diverse where the position of the laser wavelength is fixed
  - Excitation where light is collected for a fixed emission wavelength.

- MIE: The surface dependent technique takes place as electromagnetic radiations are scattered by a sphere, forcing the light to deviate from a straight trajectory and hence forcing particles to collide. Elastic Mie is the elastic light scattering that takes place as the KE is conserved. Here the direction is modified leading to less energy being transferred.
- LSD, is often a combination of LIF and MIE and is generally used when studying a 2Dimensional (2D) spray's droplet size and size distribution, providing accurate spatial and temporal measurements.
- LDV The optical technique makes use of a monochromatic laser light to measures the instantaneous velocity of the flow. Although the technique offers a very accurate set of data, the disadvantages of using such technique is that it only considers a single point of focus and can be quite costly in terms of the equipment being used.

Making use of an air assisted fuel injector inside a Constant Volume Chamber (CVC) of an optical test engine, Boretti *et al.* [49] were able to study the fuel spray transient behaviour of a two phase injector flow. The authors made use of the LSD imaging techniques and were able to obtain experimental results using the CFD Eulerian and Lagrangian codes. The authors discovered that the use of a 10 μm droplets low pressure width led to a low penetration as well as an intensified spray atomization. In their study, Sou *et al.* [39] likewise studied transient cavitation behavior. The authors were able to investigate the turbulent velocity occurring inside a rectangular nozzle with the use of a high speed camera. A LDV technique was used to validate the model. Maurice *et al.* [187] worked on a combination of LIF and Particle image velocimetry (PIV) measurements techniques as well as LDV in the modelling of turbulent flows cavitation taking place inside rocket engine turbopumps inducers.

2.4. Motivation and Significance of the Present study

The present study provides a well-rounded depiction of the cavitation phenomenon occurring not only inside the FIE but also inside a broad range of engineering devices that are subjected to high speed cavitation jet flow.

The first part of *the present study* is quite unique in the way it tackles the incipient cavitation caused by the jet traveling through the nozzle – The experiment was setup as to mimic the flow through the injector and the pump spill control valves. Although a good number of scholars have done work on incipient cavitation occurring inside the nozzle, as of date, there has not been an experimental study focusing on the effect of incipient cavitation on the spill control valves due to the changes in the fuel composition as well as the changes in parameters such as the Saturated Vapour Pressure and the Ca. Therefore, the first part of *the present study* is quite unique as it does not mimic the work done by past authors on the subject of injector cavitation but presents a novel method of controlling incipient cavitation as there exists a gap to be filled as scientists are still struggling to fully control the cavitation occurring inside the injector system.

Controlling the fuel composition in order to control the cavitation process based on the Upstream and Downstream Pressures, is a new method not yet looked at by scientists mainly because of the complexity involved in reproducing such experiment when using real injector nozzles. To go around the imposed complexity, the first part of *the present study* has made used of purposely manufactured acrylic and metal nozzles which replicate real flow conditions taking place in and around the injector and the pump spill control valves. This study represents a solid base for computationalists working on injector flow simulation as the results obtained can be used as a means of comparison. The present work moreover finds its use in the study of immersed high speed jet flows, analyzing the effect of cavitation on jet shear flow through a stagnant liquid – the jet will experience friction when travelling

through the stagnant liquid inside the receiver. The present work presents a new insight on the impact of changing the fuel composition on the cavitated jet and can be applicable to devices that experience high pressures fluid discharge.

By focusing on the damages caused as a result of the sustained hydrodynamic cavitation occurring in and around injectors and pumps spill control valves, considering the Diesel and the Biodiesel fuels, the second part of *the present study* aimed to find ways of controlling the fuel emission pollution inside the ICE. This part of the thesis finds its use in the monitoring of the FIE, mainly in the monitoring of common rails injectors, diesel injectors and diesel pumps in order to investigate how they are affected by sustained cavitation of a recirculated flow over a long period of time. It also presents a means of comparison between Diesel fuels and Biodiesel fuels, looking at the different ways they are affected by the cavitation process.

The FIE makes use of high pressures and habitually reach very high temperatures – As the fuel is often recirculated for hours inside the ICE, leading to changes in its chemical composition due to ultrasound cavitation taking place inside the ICE, the formation of new elements can lead to the deterioration of the FIE as high temperatures often lead to irreversible pyrolysis processes; during pyrolysis, thermochemical decomposition takes place due to the absence of oxygen. As the production of particulates such as soot [152] during the combustion process is still one of the leading cause of pollution, it is sensible to say that scientists have not yet mastered the complete mechanism taking place during the combustion process.

This part of the thesis is an extension of the work previously conducted by researchers such as Lockett *et al.* [188] and Jeshani *et al.* [3]. However, contrary to the previous work where pressures of up to 550 bar are made use of, *the present study* makes use of pressures similar to those encountered inside real ICE at 1650 bar.

Blank Page

CHAPTER III. EFFECT OF INCIPIENT CAVITATION ON N-HEXADECANE BASED FUEL JET – EXPERIMENTAL INVESTIGATION

3.1. Introduction

The study of incipient cavitation in turbulent jet is one that is puzzling engineers and scientists due to the complex nature of the multiphase flows taking place inside and around the jet. i.e. axisymmetric jets can sometimes display different form of vortices; helix, toroidal and linear. [15]

Due to the complexity of the design of the ICE injector and pump system, the hydrodynamic phenomena occurring as the jet flows through the ICE components often takes place at a fast rate making it difficult to observe the incipient cavitation phenomena. This means that making small scale changes on the Re, the mass flow rate, the Ca or even making small scale changes on the pressures when conducting experiments on such devices, can greatly affect the end results.

Moreover, the lack of literature in the field has made it difficult to compare the cavitation phenomena taking place when considering different working fluids – As most data obtained from literature reviews make use of water as the working fluid, a valid comparison of the work conducted with the use of fuels rather than water is often difficult to establish. [18]

The key features of this experiment were observed as incipient cavitation took place primarily solely outside the injector nozzle. Secondarily, cavitation took place between the layers of the n-Hexadecane based stagnant fuel mixtures and the fuel jet flowing through it – Jet cavitation will often take place as the jet is submerged in regions of separating flow and is dependent on the non cavitated flow structure [18]

The cavitation taking place just outside of the nozzle was affected by the composition of the fuel as well as by the geometry of the injector nozzle. However, it is the second type of cavitation occurring due to the growth and the collapse of cavitation bubbles between the fluid layers, which impacted the dynamic of the flow [31] as shear cavitation took place – Due to the high speed at which the eddies rotate (shear cavitation takes place next to the attached cavities and can lead to the formation of strong eddies), a drop in pressure was expected in the vicinity of the jet.

Depending on the shape of the bubbles, and depending on the forces that pulls the bubbles together or draws them apart, the formation of bubbles can be categorized in three groups: For bubbles of Re less than 1 and bubble radius less than 0.1 mm, solid spheres, will raise within the liquid without oscillating. For Re ranging between 1 and 800, and bubble radius between 0.1 mm and 1 mm, the bubbles tend to exhibit a helical shape when moving. For Re equal or greater than of 800 and radius greater than 1 mm, the bubbles will move in an ellipsoidal shape and hence they are considered ellipsoidal. Often the third case will occur in nature, when considering complex geometries. For such case, a thermal equilibrium will often not take place. [189]

The theoretical analysis of the mechanism responsible for incipient cavitation in a jet is represent below based on the analysis by Franc and Michel. [190] By modelling the turbulent flow, and considering the liquid pressure as the superposition of the mean pressure and the fluctuation pressure, the local pressure responsible for destabilizing the bubble is obtained using Equation 11.

$$\bar{P} - P' = P_c \quad \textit{Equation 11}$$

Where $\bar{P}$is the mean pressure, $P'$is the fluctuation pressure and P_c is the critical pressure.

Considering only the negative value of the fluctuations – P' is always greater than zero and considering the pressure coefficient Cp, Equation 12 can be obtained.

$$C_{\bar{P}} = \frac{\bar{P} - P_{ref}}{\frac{1}{2}\rho V^2} \quad \textit{Equation 12}$$

The non-dimensional form can be written as

$$\sigma_V < -C_{\bar{P}} - \frac{P_V - P_C}{\frac{1}{2}\rho V^2} + \frac{P'}{\frac{1}{2}\rho V^2} \quad \textit{Equation 13}$$

Where $-C_{\bar{P}}$ is used to obtain the mean pressure field,

$\frac{P_V - P_C}{\frac{1}{2}\rho V^2}$ is used to obtain the static delay to incipient cavitation caused by the difference between the vapour pressure and the critical pressure – the static delay is often not taken into consideration as it reduces with the reduction of velocity.

$\frac{P'}{\frac{1}{2}\rho V^2}$ is used to obtain the incipient cavitation due to fluctuation.

An existing correlation between the root mean square and the turbulent kinetic energy was taken into considering in order to obtained a simplified solution to the third term derived from Equation 13, which represents the incipient cavitation formed due to fluctuation,

$$k = \frac{1}{2}\left[\overline{u'^2} + \overline{v'^2} + \overline{w'^2}\right] \quad \textit{Equation 14}$$

Where k turbulent kinetic energy

Assuming that the root mean square velocities are equal as isotropic turbulence takes place, the equation can be re-written as

$$k = \frac{1}{2}\left[3\overline{u'^2}\right] \quad \textit{Equation 15}$$

And considering a linear relationship existing between the fluctuation pressure and the turbulent kinetic energy,

$$\sqrt{\overline{P'^2}} = C.\frac{2}{3}\rho k \quad \textit{Equation 16}$$

Where C is a constant varying depending on the experiment.

Hence the fluctuation pressure can be obtained using Equation 17.

$$\sqrt{\overline{P'^2}} = C.\rho u'^2 \quad \textit{Equation 17}$$

By changing parameters such as the operating pressures and by varying the nozzle geometry and material, the present parametric study has presented a comprehensive array of data on the geometric cavitation occurring near the nozzle [153], applicable to the ICE injector design and fuel efficiency researches.

The flow conditions' mechanism as established for the purposely built mechanical rig used in *the present study*, could be compared to same extend, to what is seen inside the turbine's crankshaft used to generate high velocity water jet inside the propeller. The jet considered in this case is similar to a

high speed liquid jet generated from a garden hose immersed into a bathtub, but is different to the jet seen from the wake of a propeller blade.

3.1.1. Fuel Matrix

A fuel matrix was provided by Shell, where the mixture of hydrocarbon fuel samples was completed simultaneously with great care inside the City University Thermodynamics Laboratory.

The results of the saturated vapour pressure provided by Shell were later on used as a means of comparison to the results obtained in *the present study*.

13 fuels mixtures were first considered at the beginning of the experiment.

- First Set: Homogeneous solutions considering an increase in n-Octane concentration in n-Hexadecane based fuel: Fuel 1, Fuel 9 to Fuel 13, (0.1%, 0.5%, 1%, 2% and 5% n-Octane).
- Second Set: Homogeneous solutions of n-Octane, n-Decane, n-Dodecane, n-Tetradecane and n-Hexadecane: Fuel 2 to Fuel 8. Refer to Table 2 and Table 3 below.

Considering the uncertainty of each hydrocarbon fuel to be $\Delta C \pm 0.05\%$, the propagation error of each mixture was obtained. Hence using Fuelα (representing the fuel mixture) and C_A, C_B, $C_C \ldots C_Z$ (representing the hydrocarbons) Equation 18 was obtained.

$$Fuel\alpha = C_A + C_B + C_C + \cdots + C_Z \quad \textit{Equation 18}$$

The propagation error of each mixture concentration was therefore obtained using Equation 19.

$$\Delta Fuel_\alpha = \sqrt{(\Delta C_A)^2 + (\Delta C_B)^2 + \Delta(C_C)^2 + \cdots + (\Delta C_Z)^2} \quad \textit{Equation 19}$$

Subsequently, Fuel 14, Fuel 15 and Fuel 16 where added towards the end of the experiment where 10%, 15% and 20% n-Octane concentration were added to 90%, 85% and 80% n-Hexadecane fuel correspondingly. The selected range of n-Octane concentration, from 0.1% to 20% was chosen in an effort to cover a broader spectrum of the mixture.

Matrix1 **n-Alkane**	**Fuel 1** %v	**Fuel 2** %v	**Fuel 3** %v	**Fuel 4** %v	**Fuel 5** %v	**Fuel 6** %v	**Fuel 7** %v	**Fuel 8** %v
C_8	5.5	4.0	1.0	3.0	0.0	0.0	0.0	0.0
C_{10}	0.0	15.0	41.0	0.0	22.0	15.0	0.0	0.0
C_{12}	0.0	10.0	28.0	0.0	10.0	75.0	0.0	4.0
C_{14}	0.0	5.0	0.0	14.0	0.0	0.0	29.0	96.0
C_{16}	94.5	66.0	30.0	83.0	68.0	10.0	71.0	0.0
Viscosity at 293K (mm^2/s)	3.964	2.983	2.008	3.968	2.997	2.002	4.001	3.007
Flash point (°C)	48	49	53	57	67	64	117	97
V_p (at 343K) (kPa)	1.53	1.56	1.53	0.85	0.78	0.74	0.0	0.1
Mixture Concentration **Percentage Error %**	0.0707	0.1118	0.1	0.0866	0.0866	0.0866	0.0707	0.0707

*Table 2 F*uel Matrix 1 provided by Shell Global Solutions – Mixture composition of the paraffin based Fuel 1 to Fuel 8 respectively

Due to the danger surrounding the manipulation of high percentages of n-Octane while working under high pressures, mixing 20% n-Octane with 80% n-Hexadecane was considered an appropriate limit – as far as safety was concerned, 20% n-Octane was considered as the maximum amount that could be handled inside the laboratory without endangering the equipment being used as well as the laboratory's personnel.

Matrix2 n-Alkane	Fuel 9 %v	Fuel 10 %v	Fuel 11 %v	Fuel 12 %v	Fuel 13 %v
C_8	0.1	0.5	1	2	5
C_{16}	99.9	99.5	99	98	95
Viscosity at 293K (mm^2/s)	4.482	4.440	4.390	4.290	4.008
Flash point (^0C)	110	85	74	63	50
V_p (at 343K) (kPa)	0.039	0.153	0.296	0.577	1.394
Mixture Concentration Percentage Error %	0.0707	0.0707	0.0707	0.0707	0.0707

Table 3 Fuel matrix 2 provided by Shell Global Solutions– Mixture composition of the paraffin based Fuel 9 to Fuel 13 respectively

3.1.2. Chemical Properties, Purity and Source

The fuel samples were purchased from Sigma Aldrich where 99.9% pure n-Hexadecane as well as 98% pure n-Octane were first made use of. A sample of 95% Hexadecane was used to flash the rig as needed throughout the experiment.

n-Hexadecane and n-Octane formulae were based on the molecular structure of Alkane:

$$C_nH_{2n+2}$$

n-Hexadecane – Chemical Formulae: $C_{16}H_{34}$, Structural Formula: $CH_3(CH2)_{14}CH_3$

$$H_3C - CH_2 - CH_2 - CH_2 - CH_2 - CH_2 - CH_2 - CH_2 - CH_2 - CH_2 - CH_2 - CH_2 - CH_2 - CH_2 - CH_3$$

n-Octane – Chemical Formulae: C_8H_{18}, Structural Formula: $CH_3(CH2)_6CH_3$

$$H_3C - CH_2 - CH_2 - CH_2 - CH_2 - CH_2 - CH_2 - CH_3$$

The experiment was conducted for approximately 2 years where a total of 14 nozzles were tested. The fuel was first tested with the use of acrylic nozzles – one of the main reasons for choosing acrylics was to be able to observe the cavitation occurring inside the nozzle hole passages through the transparent nozzle. However, it was later noticed that cavitation occurred outside of the nozzle hole.

3.2. Schematic Model and CATIA Rig design

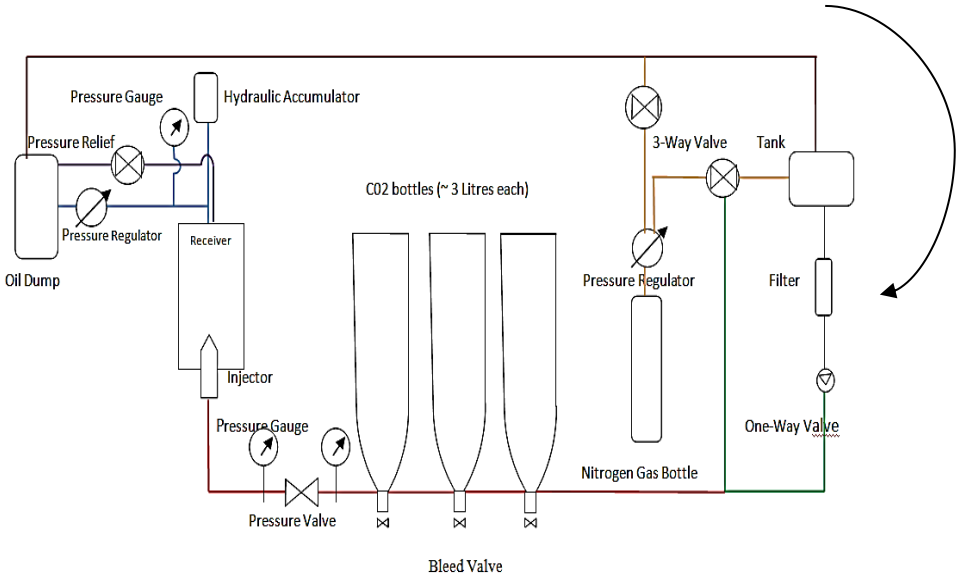

Figure 15 Incipient Cavitation Rig Schematic (image not to scale)

Figure *15* above shows the closed loop mechanical rig where the fuel moved in a clockwise direction. The fuel inside the tank was pushed by the N_2 bottle through the filter and was directed towards the High Pressure Bottles ($C0_2$ bottles). Hence the fuel was observed inside the Fused Silica Receiver before being collected inside the oil Dump. Based to some extent on the design of an existing cavitation rig inside City University Laboratory, a schematic model was drawn at the start of the experiment, representing the design of the mechanical rig used for the study of incipient cavitation

structure and development – the schematic of the existing rig was to some extent a modified version of the rig used for a series of experiments on the characterization of Diesel Cavitation inside City University laboratory. The presented rig was designed and built insitu.

Prior to starting the experiment, using the Computer Aided Design (CAD) software such as: CATIA and SolidWorks, the drawing of the mechanical rig was done from the schematic model in Figure 15, enabling the design and the manufacture the rig's component to be completed. i.e. Receiver, injector nozzle, hose, tank etc.

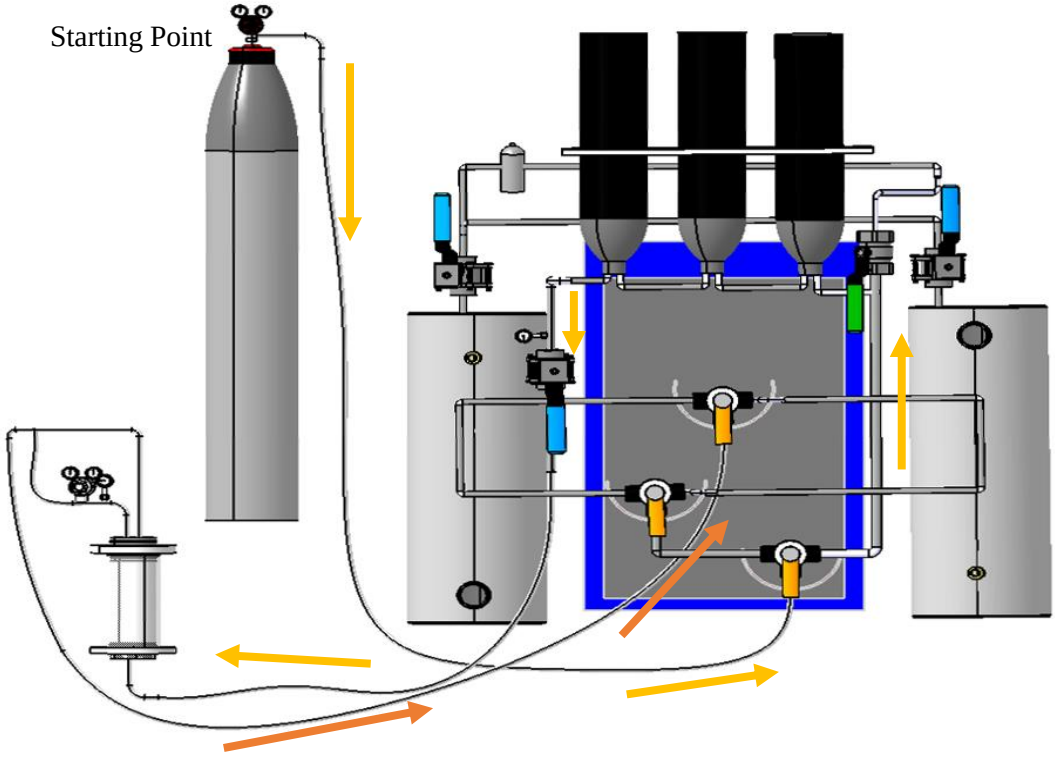

Figure 16 CATIA design of the mechanical rig used for the study of incipient cavitation.

Figure 16 is a CATIA representation of the mechanical rig showing the Fused Silica Receiver to the left, the fuel tanks on each sides of the rig plate, the black high pressure bottles placed on top of the rig plate as well as the different valves made use of during the experiment. The movement of the fuel

flowing in and out of the nozzle placed inside the Fused Silica Receiver is represented by the yellow arrow and the orange arrow respectively.

For the purpose of the experiment, a number of parameters were taken into account such as the nozzle material and the nozzle geometry.

By making use of 3 types of single hole injector nozzles placed consecutively inside the receiver, it was possible to study the cavitation jet.

- Acrylics: Cylindrical, Conical and Hemispherical
- Brass: Cylindrical and Hemispherical
- Aluminum-steel: Conical – Aluminum-steel was chosen for the Conical nozzle to ease the manufacturing process

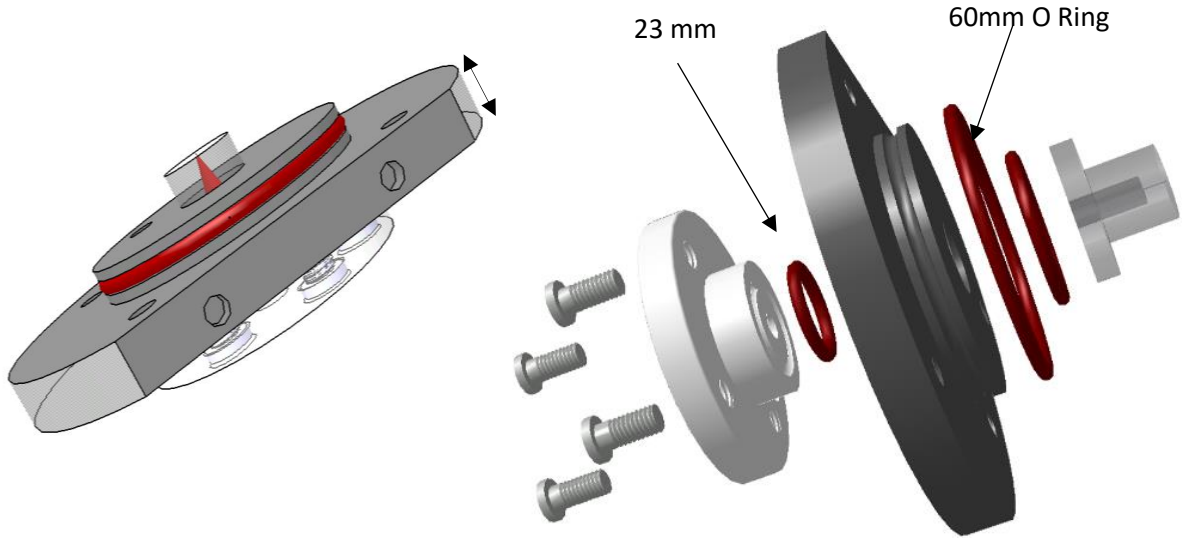

Figure 17 CATIA design of the Exploded view of the injector Unit positioned on top of the Fused Silica Receiver base.

The unit was constrained with the use of 4 M4 screws. To make sure that fluid leakage did not occur, a 2 mm thick O-ring was used for the base considering a 23 mm, a 34 mm and a 60 mm diameter O

Ring respectively. The Conical nozzle inserted inside the injector unit is shown on the left-hand-side of Figure 17. The exploded view of the injector unit, with the Cylindrical nozzle, is shown on the right-hand-side.

The drawing below, generated from CATIA shows the Conical nozzle with all relevant dimensions. Pease refer to Appendix A for the drawing of the Cylindrical and the Hemispherical nozzles.

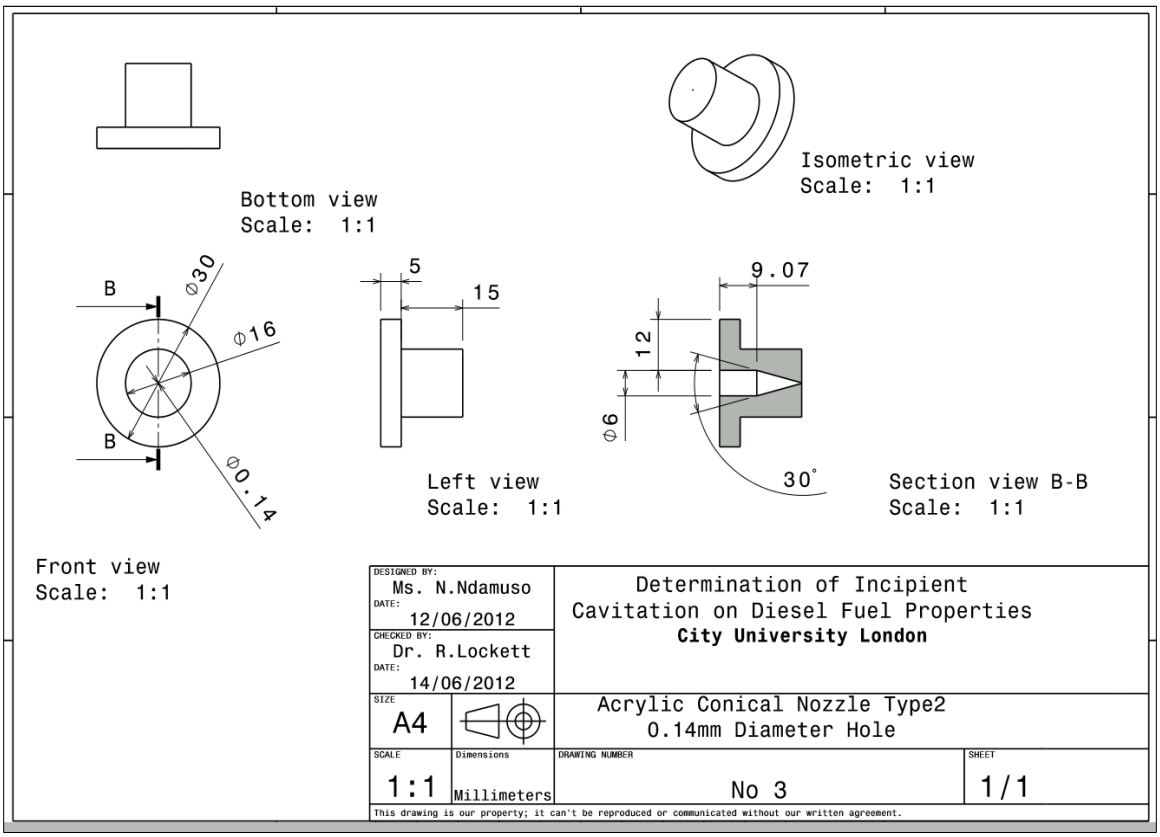

Figure 18 Acrylic Conical nozzle, 14mm hole diameter

The study of stresses taking place in and/or around an engineering device, as tremendous pressures are exerted upon the device, is vital in order to avoid failure. Hence, the tensile stress (stress leading to material expansion), as well as the yielding stress (stresses that causes material plastic deformation

to the point where the material cannot return to its original shape) of the injector nozzle, were estimated using CATIA Structure Analysis.

It was then necessary to test a significant number of nozzles in order to understand the limits of the material used during the experiment. The Acrylic Yield Strength as well as the Ultimate Tensile Strength of Acrylic is generally between 20,000 x 10^6 Pa and 75,000 x 10^6 Pa. Hence prior to the experiment, 600 N and 900 N load were applied to the top of the nozzle using CATIA, in order to investigate the maximum stress that the acrylic material can withstand.

Samples form two batches of Acrylic nozzles were first tested inside the laboratory in order to obtain their corresponding Young's Modulus. The Young's Modulus was then used to obtain the corresponding maximum stresses. Below are CATIA drawings of one of the Conical nozzles from the second batch.

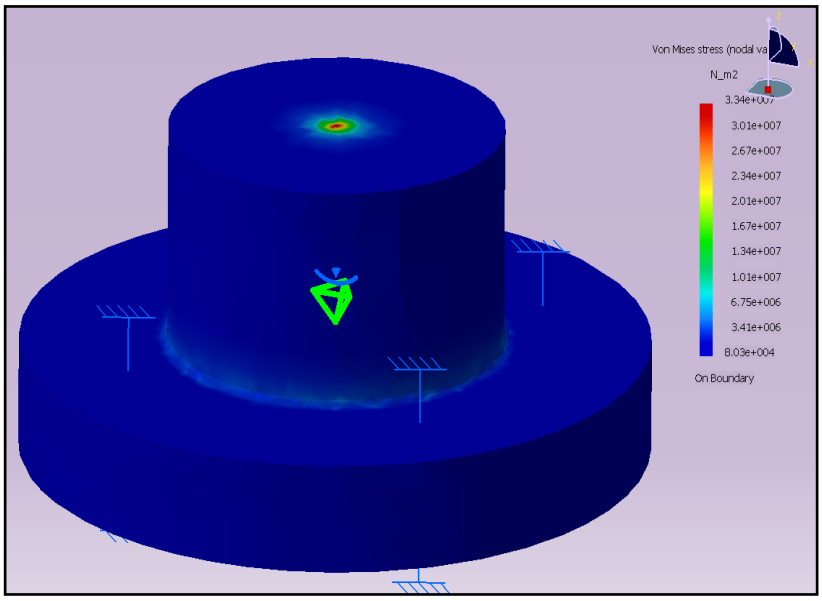

Figure 19 900N load applied onto the New Nozzle Model

The first batch gave rise to higher stresses compared to the second batch – it was first concluded that the cracks formed when using the first batch were mainly due to the fact that the first batch of acrylic material was purchased and left inside the laboratory depot for a period of at least 10 years.

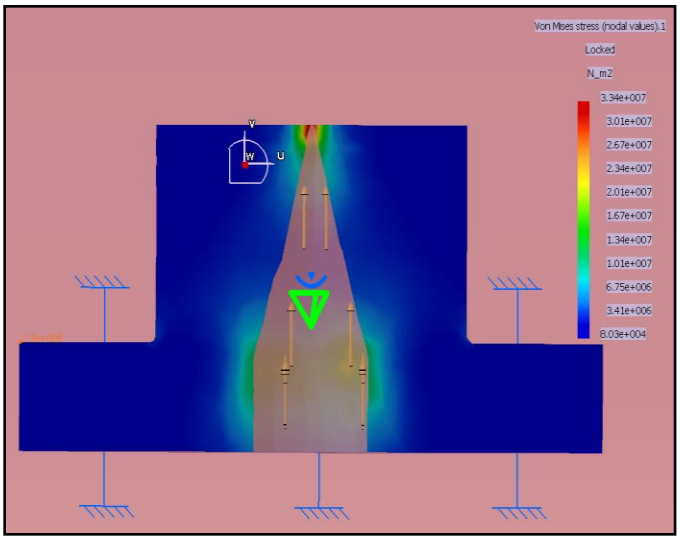

Figure 20 Section view of the 900N load applied onto the New Nozzle Model

Considering a safety factor of 2, the corresponding stress of the tested materials were obtained.

Conical Nozzle	Distributed force (N)	Max Stress (x 10^6 Pa)
First Batch	900	155.6
	600	103.8
Second Batch	900	66.8
	600	44.6

Table 4 CATIA structure analysis data – Acrylic testing maximum stresses

From the table above, the maximum stresses obtained when applying a vertical force of 900N on the nozzle, were 155.6 x 10^6 Pa and 66.8 x 10^6 Pa considering the first batch and the second batch of acrylic nozzles respectively. From the results, the acrylic nozzles maximum stress obtained were

below the material Yield Strength. This meant that the acrylic material made use of during the experiment was not susceptible to fail under stress.

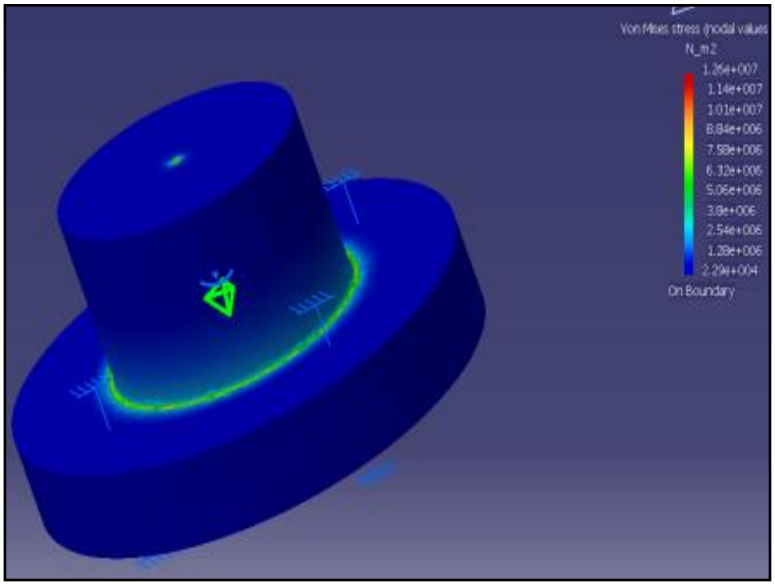

Figure 21 900N load applied onto the New Nozzle Model

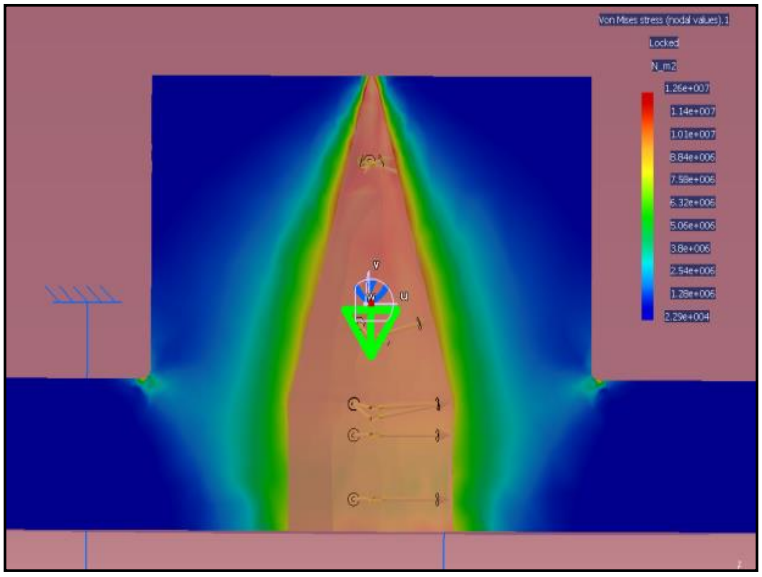

Figure 22 Section view of the 60bar gauge applied onto the New Nozzle Model

Table 5 Shows a decrease in the maximum stress withstood by the acrylic nozzle, from 853 x 10^6 Pa to 12.6 x 10^6 Pa, considering the first batch and the second batch respectively.

From the results, it was concluded that the second batch of nozzles were less susceptible to fail under pressure. Once more, the maximum stress obtained were below the material Yield Strength.

Conical Nozzle	Distributed Pressure (bar)	Mass Stress (x 10^6 Pa)
First Batch	60	853
Second Batch	60	12.6

Table 5 CATIA structure analysis data using Pressure

The stresses obtained when applying a 60bar gauge pressure on the acrylic nozzle are represented in Figure 21, Figure 22 and Table 5.

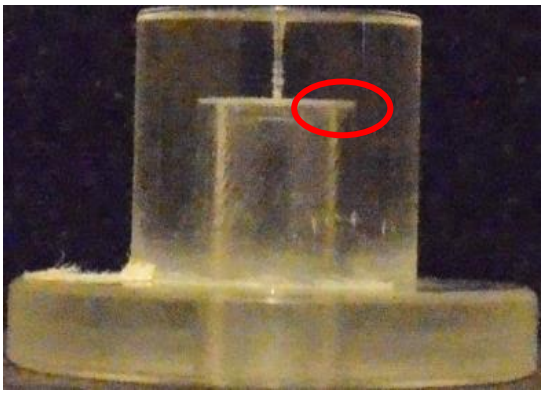

While conducting the experiment, as crack formation was mostly noticed on some of the Cylindrical acrylic nozzles taken from the second batch of nozzles, the use of the Cylindrical acrylic nozzle was discontinued leading to the use of the Brass and Aluminum-steel nozzles.

Figure 23 Crack formed on the Cylindrical 0.25mm acrylic nozzle

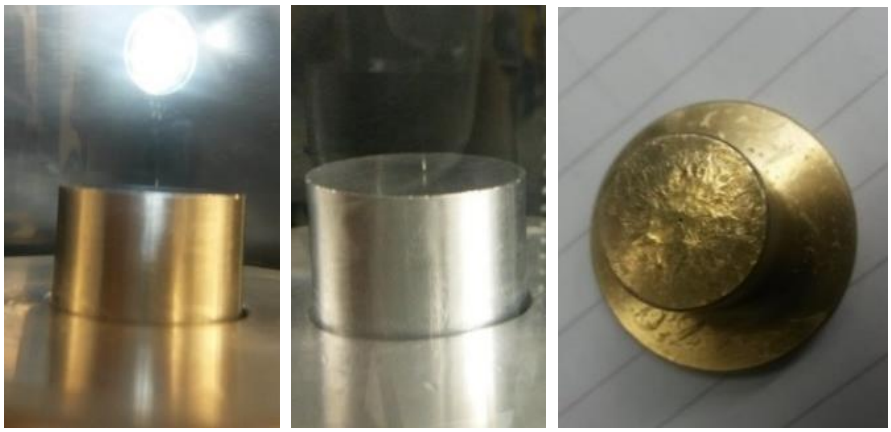

Figure 24 0.25 mm Brass and Aluminum-steel nozzles

As a maximum Upstream Pressure of 80 bar gauge was considered during the experiment, it was not necessary to conduct a structural analysis for the Brass and Aluminum-steel nozzles as they could withstand high levels of pressures and stresses far beyond what was expected during the experiment.

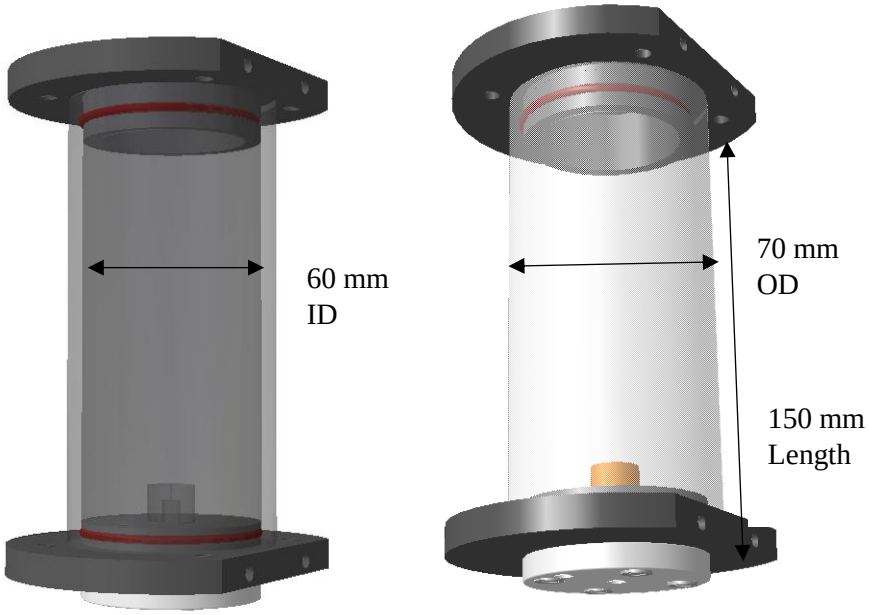

Figure 25 Cylindrical Acrylic and Cylindrical Brass nozzle respectively, inside the 60 mm Inner Diameter (ID) 70 mm Outer Diameter (OD) Fused Silica Receiver

It was however crucial to investigate the structural strength of the Fused Silica Receiver, as high pressures of up to 15 bar gauge downstream of the nozzle where reached during the experiment. Hence, a structural analysis of the Fused Silica Receiver was conducted in order to find out the minimum receiver thickness needed to withstand pressures of up to 15 bar gauge downstream of the nozzle.

Fused Silica Material Properties		Unit
Density	2.203	kg/m3
Poisson's ratio μ	0.16	
Coeff of Expansion	0.550×10^{-6}	$/^0C$
Specific Heat Capacity	703	$Jkg^{-1}K^{-1}$
Shear Modulus	$3{,}100. \times 10^{6}$	Pa
Young's Modulus at 25^0C, E	$72{,}700 \times 10^{6}$	Pa
Yield Stress	52.5×10^{6}	Pa
Safety Factor	2.0	
Allowable stress	26.3×10^{6}	Pa
Internal Pressure, P_{in}	3×10^{6}	Pa
External Pressure, P_{out}	0	Pa

Table 6 Fused Silica Material Properties

The Allowable Stress calculated using the Fused Silica Yield Stress, and the Maximum Internal Pressure were obtained using Equation 20 and Equation 21.

$$Allowable\ Stress = \frac{Yield\ Stress}{Safety\ Factor} \quad \textit{Equation 20}$$

$$Allowable\ Stress = \frac{52.5 \times 10^6}{2} = 26.3\ \times 10^6\ Pa$$

$$P_{in} = 15bar\ \times 101325\ Pa\ \times Safety\ Factor \quad \textit{Equation 21}$$

$$P_{in} = 3\ \times 10^6\ Pa$$

Where P_{in} is the Maximum Internal Pressure.

Lame's Theory, represented by Equation 22 to Equation 24 below, was used to obtain the minimum thickness to be considered for the Fused Silica Receiver – the minimum thickness obtained was to ensure that the material did not fail due to stresses formed as a result of high pressures inside the Fused Silica Receiver.

$$\sigma_z = -\frac{P_i {r_i}^2 - P_0 r_0^2}{r_i^2 - r_0^2}, \quad \textit{Equation 22}$$

$$\sigma_r = -\frac{P_i\left[\left({r_0}/{r}\right)^2 - 1\right] + P_0\left[\left({r_0}/{r_i}\right)^2 - \left({r_0}/{r}\right)^2\right]}{\left({r_0}/{r_i}\right)^2 - 1} \quad \textit{Equation 23}$$

$$\sigma_\theta = \frac{P_i\left[\left({r_0}/{r}\right)^2 + 1\right] + P_0\left[\left({r_0}/{r_i}\right)^2 + \left({r_0}/{r}\right)^2\right]}{\left({r_0}/{r_i}\right)^2 - 1} \quad \textit{Equation 24}$$

Where P_i is the Internal Pressure, P_o is the External Pressure, r_i is the internal radius, r_o is the external radius and r is the radius at the point of interest.

By slowly reducing the Fused Silica Receiver thickness, from 25 mm to 5 mm, the Longitudinal σ_z, the Radial σ_r and the Circumferential σ_θ inner stresses and outer stresses on the Fused Silica Receiver were calculated.

It was concluded that a Fused Silica Receiver thickness of 5 mm was adequate for the purpose of the experiment as the stresses applied to a Fused Silica Receiver of 5 mm thickness were not significant enough to cause any harm to the experiment or to the members of the personnel involved in the laboratory – the Allowable stress was calculated as 26.3 x 10^6 Pa, considering a safety factor of 2.

Using Hooke's Law, the stress/strain relationship obtained due the deformation caused by the changes in pressure inside the Fused Silica Receiver was estimated.

Hence, the longitudinal, the radial and the circumferential strains were obtained using equation 25 to equation 27.

$$\varepsilon_z = \frac{1}{E}[\sigma_z - v(\sigma_z + \sigma_\theta)] \quad \textit{Equation 25}$$

$$\varepsilon_{z\,Inner} = -194.652 \times 10^{-6} m$$

$$\varepsilon_{z\,Outer} = -194.652 \times 10^{-6} m$$

Where ε_z is the Longitudinal strain and E is the Young's Modulus.

$$\varepsilon_r = \frac{1}{E}[\sigma_r - v(\sigma_\theta + \sigma_z)] \quad \textit{Equation 26}$$

$$\varepsilon_{r\ Inner} = -60.338\ \times\ 10^{-6} m$$

$$\varepsilon_{r\ Outer} = -11.831\ \times\ 10^{-6} m$$

Where ε_r is the Longitudinal strain.

$$\varepsilon_\theta = \frac{1}{E}[\sigma_\theta - v(\sigma_z + \sigma_r)] \quad \textit{Equation 27}$$

$$\varepsilon_{\theta\ Inner} = 305.294\ \times\ 10^{-6} m$$

$$\varepsilon_{\theta\ Outer} = 256.791\ \times\ 10^{-6} m$$

Where ε_θ is the Longitudinal strain.

Fused Silica Receiver Stress (x$10^{6)}$ Pa		
Inner Stress	Longitudinal	4.3 – 11.5
	Radial	3
	Circumferential	5.6 – 19.6
Outer Stress	Longitudinal	0
	Radial	0
	Circumferential	4.5 – 16.8

Table 7 Longitudinal, Radial and Circumferential stresses, considering 25 mm to 5 mm decrease in thickness

3.3. Experimental Set-up

The rig consisted of two distinct parts where, the first part comprised the mechanical rig connected to the N_2 bottle from the British Oxygen Company (BOC), located next to the fuel cabinet as showed in Figure 26. And the second part comprised the injector unit as well as the optical settings.

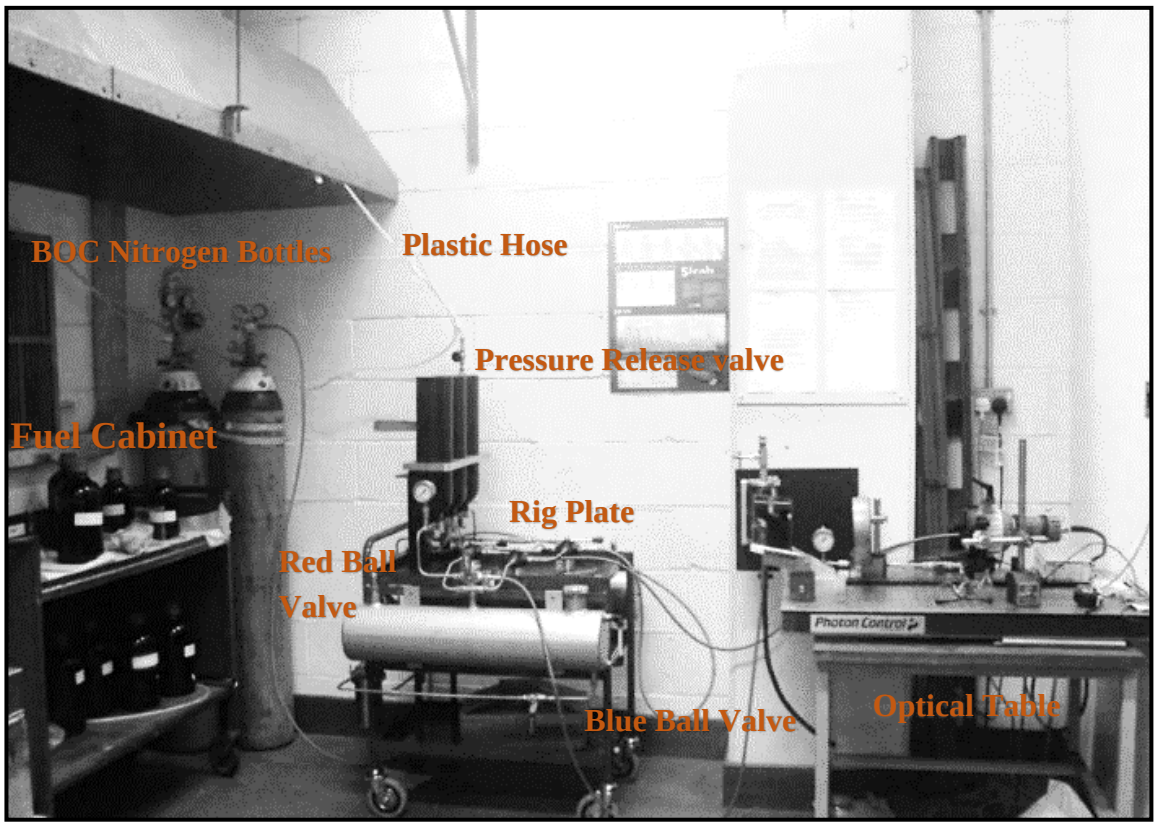

Figure 26 Set up of the mechanical rig inside City University Thermodynamic Laboratory

230 bar compressed Oxygen free bottles were provided by the BOC for the purpose of the incipient cavitation experiment.

Rig Set Up Part One: The mechanical rig, made up of a closed loop continuous flow comprised the black painted extinguisher bottles (or High Pressure Bottles) positioned upside-down, on top of the rig plate – A pressure release valve was installed on top of one of the High Pressure Bottles in order to release the excess N_2 from the bottles to the atmosphere, avoiding cases of over-pressurization.

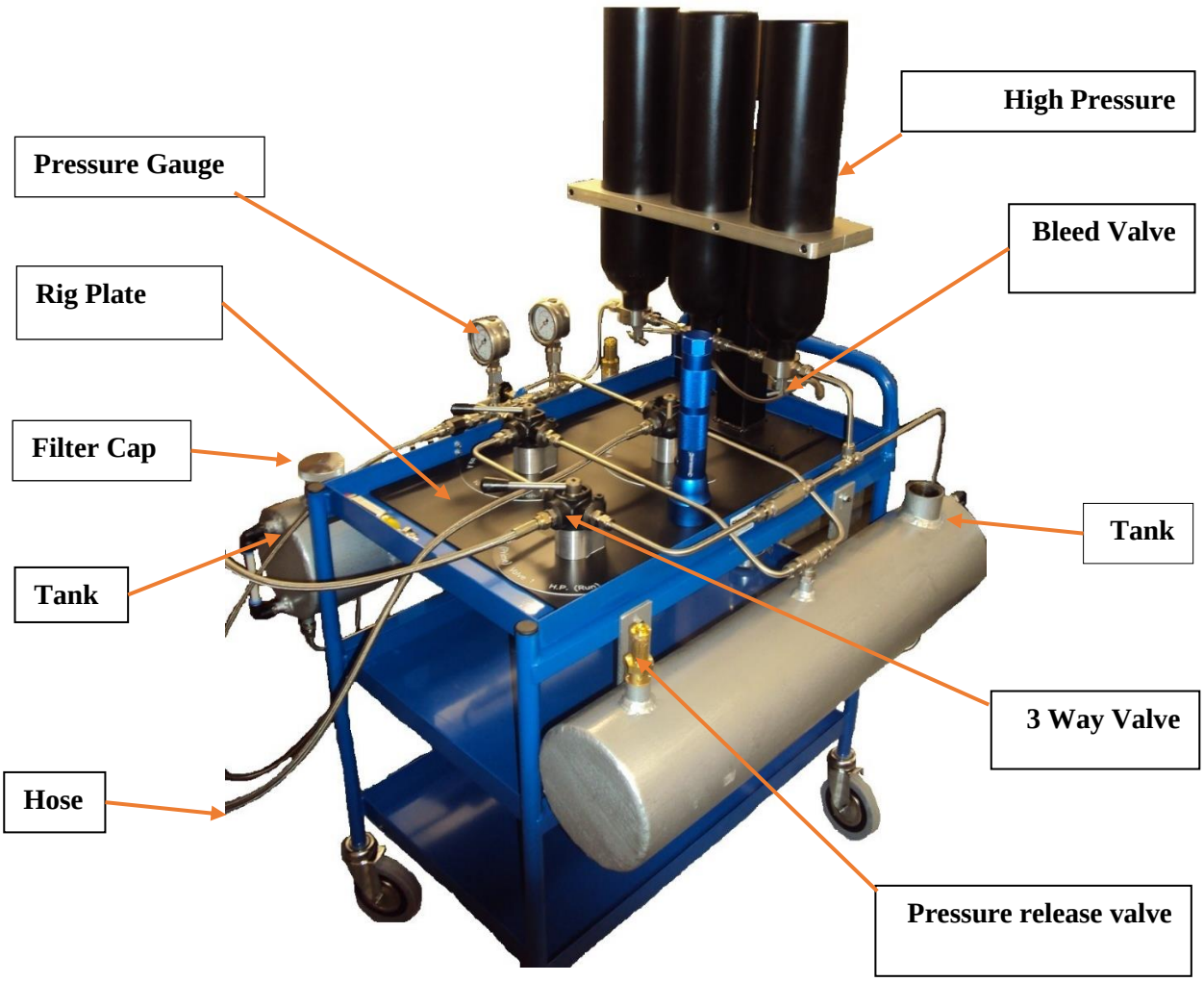

Figure 27 Mechanical Cavitation Rig

The rig likewise comprised 3 Way Vales placed on top of the rig plate and 2 x 10 L grey Fuel tanks (TankA and TankB) on the two sides of the rig plate respectively. The rig was placed in between the N_2 bottle and the optical table located to the right of the Figure 26.

The closed loop system was designed so that the pressure inside the BOC N_2 bottle could move the fuel located in TankA through the 6 mm ID hose, filling up one High Pressure Bottle at a time – The 10 L fuel moved towards the Fused Silica Receiver. From then, the fuel moved through the injector nozzle placed inside the receiver. The fuel flow followed a closed loop, moving back to the second fuel tank (considered as a fuel damp) at the end of the cycle.

Figure 28 Figure 28-1 and Figure 28-2 shows the 3 ways vales located on top of the rig plate connected to the pressure gauges. On Figure 28-3, a 5-micron stainless steel filter used to block fuel impurities can be seen at the back of the rig.

Rig Set Up Part Two: Placed on top of the optical table were the Injector unit (with the nozzle positioned inside the receiver) and the concave lens – on the other side of the lens was the mirror positioned to the same level as the concave lens, used to reflect the light coming from the mirror straight into the injector nozzle. To the right side was positioned the ARRILUX Pocket PAR 200 lamp as well as the camera connected to the Computer Unit.

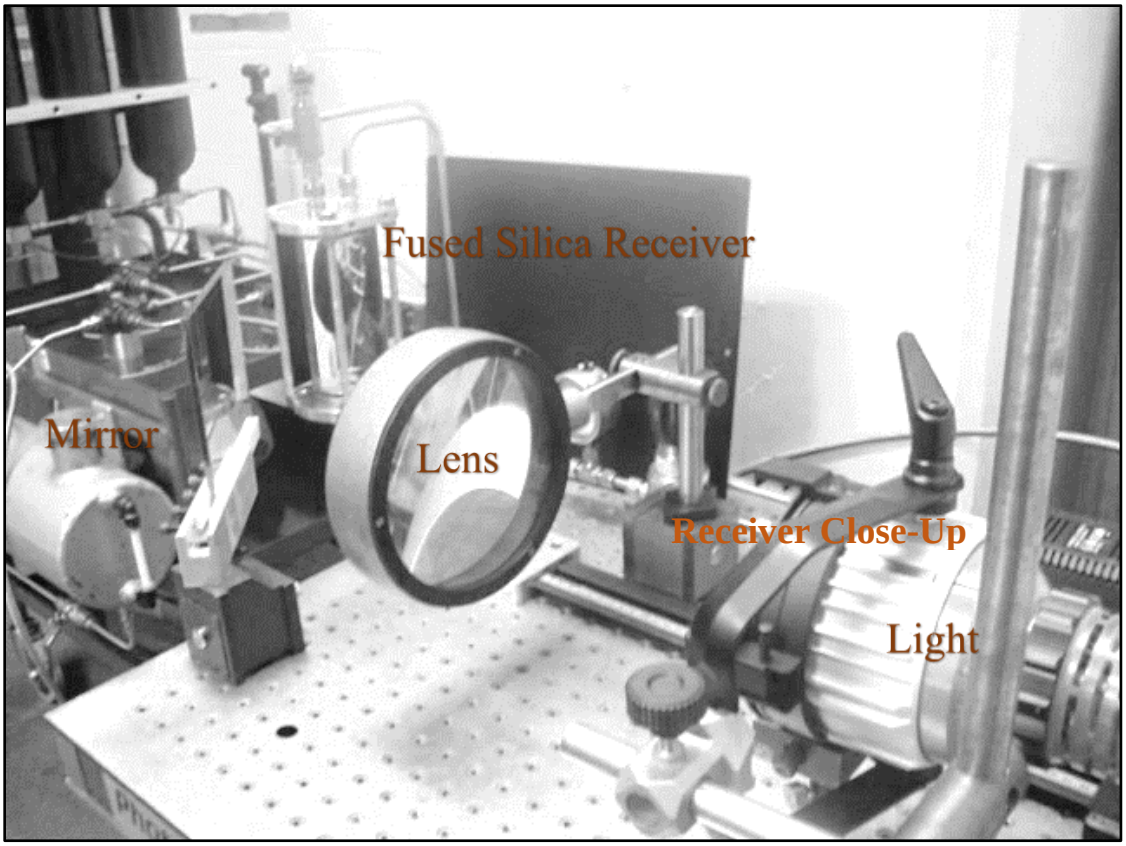

Figure 29 Experimental set up showing the injector unit

The light coming from the lamp travelled through the focused lens, and was reflected by the mirror, shining through the Fused Silica Receiver – the shining light eased up the view of the incipient cavitation formation. Hence, the camera transmitted the image received to the computer for data collection.

A close up of the Conical nozzle placed inside the Fused Silica Receiver is seen from the Figure *30*. Two pressure valves were used to control the pressure of the moving fluid from TankA to the Fused Silica Receiver. The second pressure valve was used in order to regulate the N_2 flow.

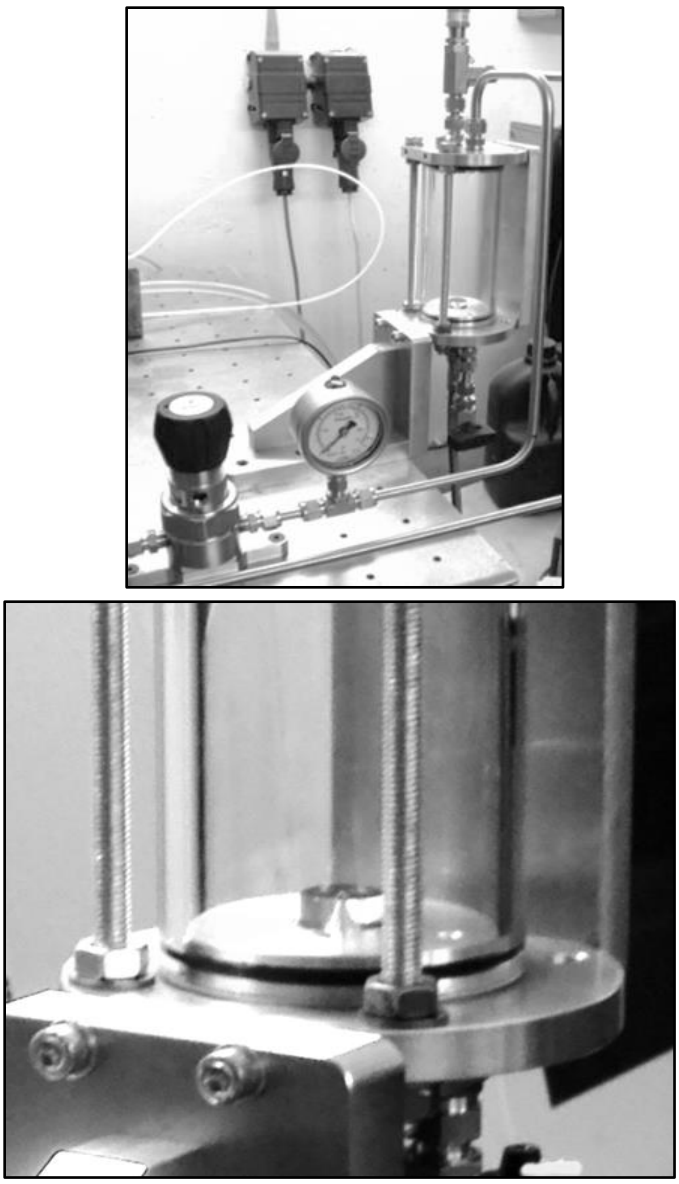

Figure 30 Close Up of Receiver

The length and the width of the cavitated jet varied depending on the pressures upstream and downstream of the nozzle. The length varied from near zero to approximately 100 mm long and the width varied from near zero to approximately 30 mm wide – At the point of onset the length and the width of the jet were reduced to near zero.

3.4. Methodology

16 fuel mixing samples were used for the study of the incipient cavitation jet where at the start of each experiment, the rig was fitted with a new fuel filter – the nylon filter used at first, was replaced with a metallic filter as it did not retain all pollutants.

The fuel mixtures were poured consecutively into the rig – the mixture was based on the Shell Matrix represented in Table 2 and Table 3. In order to reduce the risk of human error, 25 repetitive sets of measurements per fuel per nozzle hole diameter, per geometrical shape and material were conducted; by setting up the Upstream Pressure it was possible to obtain the corresponding Downstream Pressure variation of the jet looking at the threshold pressure at which the mixture cavitated – The Vapour Pressure, the Discharge Coefficient, the Ca and the jet speed are some of the parameters looked into during the experiment. The Upstream Pressure varied from 10 to 80 bar gauge as a function of Downstream Pressure, which reached regions of 15 bar gauge.

Hence the Standard Deviations (STDEV) representing the spread-out of the Downstream Pressures were obtained.

$$P_{DM} = \frac{\sum(P_D)}{n} \quad \textit{Equation 28}$$

$$STDEV = STDEV(P_D)$$

Where P_{DM} is the Downstream Pressure Arithmetic Mean, P_D is the Downstream Pressure and n is the number of runs conducted.

3.5. Operational procedures

At the first instance, it was necessary to turn off all operating machineries. This included the BOC N_2 bottle and Gas Regulator; the Ball Valves, the Bleed valves underneath each of the 3 High Pressure Fuel Bottles and the 3 way valves. Hence the High Pressure Fuel Bottles were filled by pressurizing the fuel Tank. As the 3 way valves were positioned, the pressure on the BOC N_2 Bottle was turned on – 0.5 bar gauge was set as the maximum pressure, this was done using the Gas Regulator.

Before running the rig, the Filler Cap located on the Tank was loosen. Next the 3 way valves$_1$ (only) was positioned. At this stage, the pressure on the BOC N_2 Bottle was set.

The Fuel contained inside the Fused Silica Receiver was drained by placing the Drainage Bottle underneath the Fused Silica Receiver. The pressure was then released and the fuel drained. The fuel was safety poured from the Drainage Bottle into one of the tanks. In order to drain the fuel contained inside the Rig, the main part of the rig was isolated from the Fused Silica Receiver unit. The whole fuel was located in one tank which was then pressurized. The Gas Regulator was set to a maximum of 0.5 bar gauge. At this stage, the tank was filled to the maximum level.

Before replacing the Nozzle, the Fused Silica Receiver was first emptied – Here the 4 M4 bolts located at the base of the Fused Silica Receiver was Unscrewed. The new Injector nozzle was than inserted. Hence, the rig piece and the 4 M4 Screw Bolts were reattached.

Please refer to Appendix A for a detailed explanation of the operational procedures.

3.6. Discharge Coefficient Measurements

The purpose of this part of the thesis was to be able to measure the Cd of the 0.14mm and the 0.25 mm hole Cylindrical, Hemispherical and Conical nozzles, taking into consideration the added, 0%, 0.1%, 1%, 5%, 10%, 15% and 20% n-Octane concentration in pure n-Hexadecane.

One of the ways of measuring the flow characteristics through the nozzle is to compare the mass flow rate discharged from an experimental nozzle to that of an ideal nozzle. In order to comply with the standardized guidelines requirements of the design and the installation of Diesel injectors and control valves, it was important to look at the uncertainty associated with the nozzle hole flow measurement accuracy. Among many, the factors impacting the overall flow measurement techniques are the fluid properties, the liability associated with the flow profiles, and the equations used for the calculation of the Cd. Furthermore, the secondary devices used during the experimental processes may greatly impact the flow measurements uncertainty levels.

The Cd can be impacted when the flow is experiencing choking due to the presence of cavitation bubbles restricting the nozzle hole area, this can be detrimental to some control valves – as the pressures considered are higher than the optimum design pressures and as the flow experiences choking the presence of bubbles can create a buildup of pressures upstream of the device, considerably reducing the flow downstream of the device. [43]

As the valve's downstream operating pressure reaches the vapour pressure of the fluid, the valve experiencing choking conditions may sometimes experience string cavitation. For some valves, such as the butterfly valve, the string cavitation condition is seen favourable as it takes place at a significant distance from the valve. [191]

The mechanisms used in *the present study* can be compared to the mechanism of the injector system subjected to pressures upstream and pressures downstream of the needle lift. It can likewise be compared to the mechanism taking place inside control valves as they experience Upstream Pressures and Downstream Pressures. This very much highlight the importance of *the present study*. Other scientists have established similar comparison while conducting experimental studies. As an

example, Tullis [191] in his book compared the cavitation potential in a valve controlled venturi pipe to the cavitation occurring in a submerged jet. In order to compare the parameters of the Venturi pipe to that of the submerged jet, such as the velocity and the pressure, the author compared the throat diameter of the venturi to the contracted diameter of the jet.

In order to be able to measure the Cd, the mechanical rig system utilized in *the present study* was modified so as to enable the fuel to be poured inside an air-sealed beaker. The air-sealed beaker was positioned at 30 cm below the nozzle exit in order to reduce the effect of gravity on the fuel mixture – gravity can have a greater impact on the heavier fuel in the mixture causing ambiguities in the flow measurements.

Hence, the Bernoulli's equation for Single Phase Incompressible liquid flow through an injector orifice was used to obtain the cavitated flow Cd as it passed through the injector nozzle.

A stop watch was used to obtain the Volumetric Flow rate (Q) of the fuel being poured inside the beaker through a 6mm ID hose. The Q was measured using the sum of Q in milliliter per minutes $^{ml}/_{min}$ divided by the number of times Q was measured (n). The results were then converted into meter cubed per second $^{m^3}/_{s}$, where 1.6667×10^{-8} represents the conversion from $^{ml}/_{min}$ to $^{m^3}/_{s}$. Hence the Q was measured for the 0.14mm and the 0.25mm Cylindrical, Hemispherical and Conical nozzle respectively, this considering the increased n-Octane percentage in n-Hexadecane fuel mixtures.

$$Q_{^{m^3}/_{s}} = \frac{Sum\left(Q_{\,^{ml}/_{min}}\right) \times \left(1.6667 \times 10^{-8}\right)}{n} \quad \textit{Equation 29}$$

Using Equation 30, an error estimate related to the change in the value of Q was calculated at around $\pm\ 10^{-9}\ ^{m^3}/_{s}$ considering the 0.14mm and $\pm\ 10^{-8}\ ^{m^3}/_{s}$ considering the 0.25 mm nozzle.

$$Uncertainty\ Estimate = \frac{\sum STDEV\ \left(Q_{m^3/s}\right)}{n} \quad \textit{Equation 30}$$

Where n is the number of measurements.

The flow velocity, V was obtained by dividing Q by the cross-sectional Area A, of the 0.14mm hole diameter nozzle and the 0.25 mm hole diameter nozzle, using Equation 31.

$$V_{m/s} = \frac{Q_{m^3/s}}{A_{m^2}} \quad \textit{Equation 31}$$

Where the Cross-sectional Area $= \pi r^2$ was obtained considering 0.14 mm and 0.25 mm diameter nozzle hole.

The mass flow rate $\dot{m}$ was further obtained by dividing Q by the density ρ. Where the ρ was obtained for each fuel mixtures taking into account the changes in the n-Octane concentration from 0% to 20%. The ρ varied from $773_{kg/m^3}$ to $751_{kg/m^3}$ with the change in n-Octane concentration.

$$\dot{m}_{\ kg/s} = Q_{m^3/s} \times \rho_{\ kg/m^3} \quad \textit{Equation 32}$$

Next, the pressure drop across constriction was obtained using Equation 33.

$$\Delta P_{Pa} = Pressure_{bar\ Gauge\ delivered} - 1_{bar\ Gauge\ received} \times 100000 \quad \textit{Equation 33}$$

Where 1 bar gauge = 100,000 Pa

Hence, the Single Phase Incompressible Cd was obtained using Equation 34.

$$C_d = \frac{\dot{m}_{\,kg/s}}{A_{m^2} \times SQRT\left(2 \times \rho_{\,kg/m^3} \times \Delta P_{Pa}\right)}, \quad \textit{Equation 34}$$

The error estimate was obtained using Equation 35.

$$\frac{\Delta C_d}{C_d} = \sqrt{\left(\frac{\Delta \dot{m}}{\dot{m}}\right)^2 + \left(\frac{\Delta P_{pa}}{P_{pa}}\right)^2} \quad \textit{Equation 35}$$

Based on Equation 34, as the flow area experiences choking due to cavitation within a controlled valve, a reduction of the mass flow rate leading to the reduction of the Cd could be observed.

This can come at an advantage when considering valves that are designed to operate in choking conditions, providing a means of controlling the mass flow rate, a means of controlling the operation limits of the valve. When choking takes place within an area, cavitation intensity is high on that area as it can be prone to damages and high noise level. During *the present study*, an audible noise of around 10 dB to 40 dB was perceived as cavitation took place.

3.7. Saturated Vapour Pressure, Cavitation Number and Reynolds Number

By regulating the pressure ratio (downstream and upstream of the nozzle), it was possible to control the exit velocity of the jet. The velocity of the fuel jet was obtained using the Bernoulli equation.
By changing the composition of the fuel, it was possible to obtain the Saturated Vapour Pressure of each mixture. Considering the vapour pressure of n-Octane and n-Hexadecane respectively, it was possible to calculate using Raoul's Law, the partial pressure of the fuel mixtures. Hence the total pressure of the fuel mixtures at room temperature was obtained.

Looking at an atmospheric temperature of around 23^0C, and using the vapour pressure data obtained from Antoine's Equation – from Yaws' Handbook of Antoine Coefficients for Vapour Pressure, the Saturated Vapour Pressure of each fuel was obtained.

$$log10\ (P_{Sat(mmHg)} = A - \frac{B}{(T_{[Co]}+C)} \quad \textit{Equation 36}$$

From the Figure 31, it can be seen that n-Octane reached high vapour pressures for the corresponding temperature compared to n-Hexadecane.

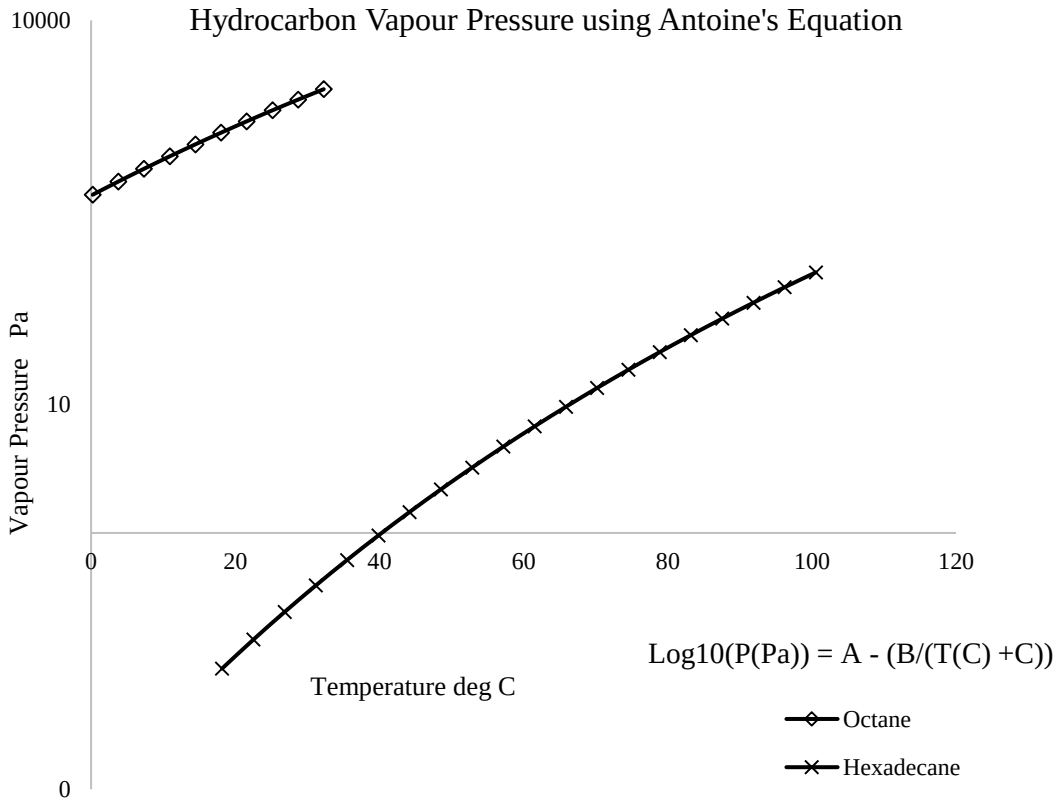

Figure 31 Antoine's Equation used for the Homogeneous of n-Hexadecane-n-Octane mixtures

The vapour pressure of n-Octane and n-Hexadecane at 296K, obtained from Antoine's Vapour Pressure Data was 1771.410 Pa and 0.158 Pa respectively

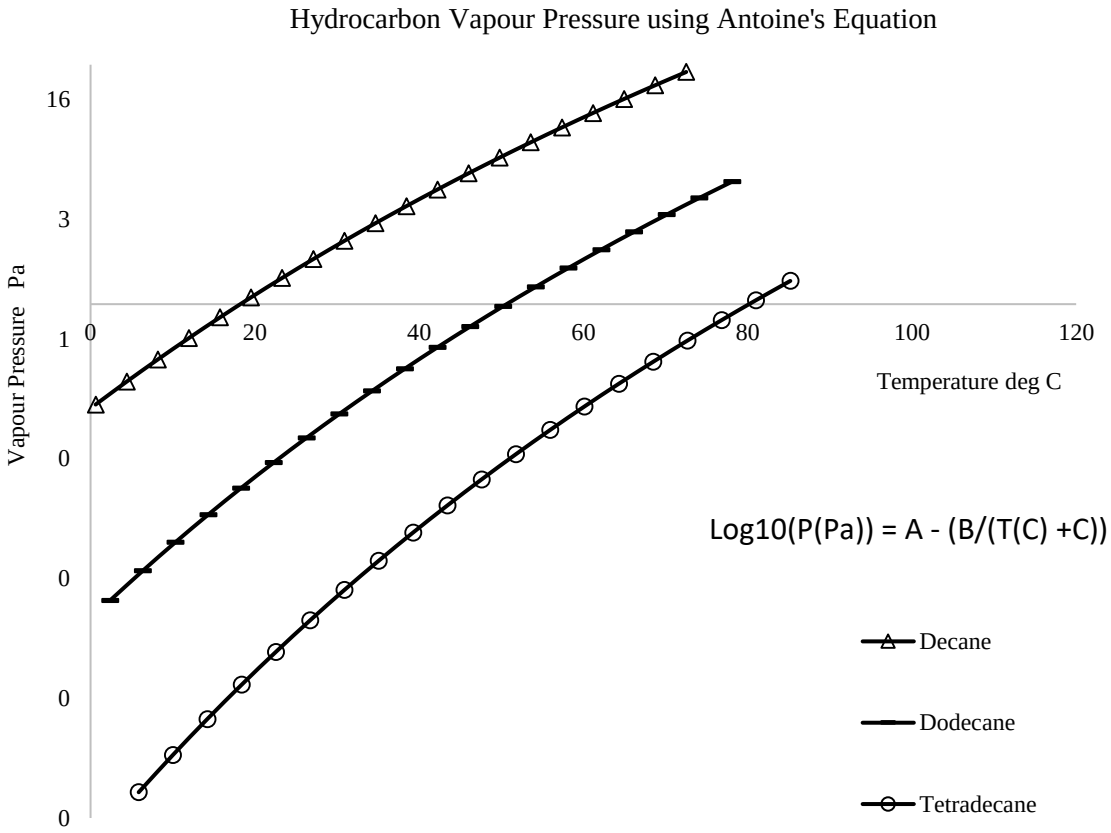

Figure 32 Second set of mixtures: Antoine's Equation – Decane, "n-Dodecane" and N-Tetradecane

As expected, from Figure 32 a considerable increase in the vapour pressure of n-Decane was noted in comparison to the Vapour pressure of n-Dodecane and n-Tetradecane, with the increase of temperature, reaching pressures of up to 20 bar absolute (abs) at 70 ^{0}C – This was expected as n-Decane has a lower density compared to n-Dodecane and n-Tetradecane. n-Decane's Vapour Pressure increased considerably.

	n-Octane	n-Decane	n-Dodecane	n-Tetradecane	n-Hexadecane
Density mg/ ml, kg/m3	703	730	750	764.50	773
Molar mass g/mol	114.144	142.176	170.208	198.240	226.272
Vapour pressure pa @ around 296 K	1771.410	185.907	16.953	1.313	0.158
Vapour pressure pa @ around 348 K	19282.451	3378.856	580.907	95.242	19.269

Table 8 Vapour pressure of n-Octane, n-Decane, n-Dodecane, n-Tetradecane and n-Hexadecane mixtures

Using Raoult's Law of partial pressure, the Saturated Vapour Pressure was obtained considering the mixture to be in equilibrium.

$$p = p_A^* x_A + P_B^* x_B + \ldots \quad \textit{Equation 37}$$

By multiplying the vapour pressure of each fuel with the corresponding mole fraction – the mole fraction was deduced from the molar mass of each fuel, the partial fraction of the fuel was obtained. Hence the total Saturated Vapour Pressure was deduced from the partial fraction of each fuel mixture.

	FUEL9	FUEL10	FUEL11	FUEL12	FUEL13	FUEL14	FUEL15	FUEL16
n-Octane %	0.1	0.5	1	2	5	10	15	20
Volume L	0.01001	0.0501	0.1001	0.2002	0.5005	1.0010	1.502	2.0020
Total Tank Mass kg	0.00704	0.0352	0.0704	0.141	0.352	0.704	1.0556	1.407
Mass Uncertainty kg	0.00000352	0.0000176	0.0000352	0.0000705	0.000176	0.000352	0.000528	0.000703
Mole	0.0000617	0.000309	0.00062	0.00123	0.00309	0.00617	0.00926	0.0123
Mole fraction	0.00180	0.00896	0.0178	0.0349	0.0829	0.153	0.213	0.266
Partial Pressure Pa	3.196	15.865	31.449	61.801	146.819	271.163	377.826	470.328
Partial Pressure Error Pa	1.6E-6	7.8E-6	15.4E-6	30.2E-6	71.8E-6	132.5E-6	184.5E-6	230.4E-6
n-Hexadecane %	99.9	99.5	99	98	95	90	85	80
Volume L	10	10	10	10	10	10	10	10
Total Tank Mass kg	7.73	7.73	7.73	7.73	7.73	7.73	7.73	7.73
Mass Uncertainty kg	0.00386	0.00386	0.00386	0.00386	0.00386	0.00386	0.00386	0.00386
Mole	0.0342	0.0342	0.0342	0.0342	0.0342	0.0342	0.0342	0.0342
Mole fraction	0.998	0.991	0.982	0.965	0.917	0.847	0.787	0.734
Partial Pressure Pa	0.157	0.156	0.155	0.152	0.145	0.134	0.124	0.116
Partial Pressure Error Pa	864.3E-6	858.2E-6	850.4E-6	835.7E-6	794.1E-6	733.5E-6	681.6E-6	635.7E-6

Total Density kg/m3	772.874	772.373	771.746	770.558	767.198	762.285	758.070	754.414
Total Viscosity Ns/m2	0.00347	0.00345	0.00342	0.00337	0.00323	0.00303	0.00285	0.00270
Total Saturated Vapour Pressure Pa	**3.353**	**16.022**	**31.604**	**61.953**	**146.963**	**271.296**	**377.950**	**470.444**
Total Saturated Vapour Pressure Error Pa	864.3E-6	858.3E-6	850.6E-6	836.3E-6	797.4E-6	745.4E-6	706.1E-6	676.1E-6

Table 9 Total Saturated Vapour Pressure of n-Octane and n-Hexadecane mixtures@ 23 deg C.

The saturated vapour pressures obtained during the experiment were comparable to those provided by Shell in Table 1. Referring to Shell's Matrix, the Total Saturated Vapour Pressures at around 343k (~ 70 ^{0}C) of Fuel 6 and Fuel 8 respectively were stated as 740 Pa and 100 Pa.

	FUEL2	**FUEL3**	**FUEL4**	**FUEL5**	**FUEL6**	**FUEL7**	**FUEL8**
n-Octane %	**4**	**1**	**3**				
Volume L	0.4	0.1	0.3				
Total Tank Mass mg	0.281	0.07	0.211				
Mole	2.464	0.616	1.848				
Mole fraction	0.0631	0.0139	0.0519				
Partial Pressure Pa @ 296 K	111.762	24.653	91.934				
Partial Pressure Pa @ 348 K	1216.567	268.357	1000.731				
n-Decane %	**15**	**41**		**22**	**15**		
Volume L	1.5	4.1		2.2	1.5		
Total Tank Mass kg	1.095	2.993		1.606	1.095		
Mole	7.702	21.051		11.296	7.702		
Mole fraction	0.197	0.476		0.290	0.174		
Partial Pressure Pa @ 296 K	36.669	88.435		53.939	32.419		
Partial Pressure Pa @ 348 K	666.452	1607.308		980.335	589.212		
n-Dodecane %	**10**	**28**		**10**	**75**		**4**
Volume L	1	2.8		1	7.5		0.4
Total Tank Mass kg	0.75	2.1		0.75	5.625		0.3
Mole	4.406	12.338		4.41	33.048		1.763
Mole fraction	0.113	0.279		0.1132	0.748		0.0454
Partial Pressure Pa @ 296 K	1.913	4.726		1.919	12.685		0.77
Partial Pressure Pa @ 348 K	65.554	161.955		65.747	434.674		26.399
n-Tetradecane %	**5**		**14**			**29**	**96**
Volume L	0.5		1.4			2.9	9.6
Total Tank Mass kg	0.382		1.0703			2.217	7.339
Mole	1.928		5.399			11.184	37.022
Mole fraction	0.0494		0.152			0.316	0.955
Partial Pressure Pa @ 296 K	0.0648		0.199			0.414	1.253
Partial Pressure Pa @ 348 K	4.703		14.444			30.056	90.914
n-Hexadecane %	**66**	**30**	**83**	**68**	**10**	**71**	
Volume L	6.6	3	8.3	6.8	1	7.1	
Mass kg	5.102	2.319	6.416	5.256	0.77	5.488	
Mole	22.547	10.249	28.355	23.23	3.42	24.255	
Mole fraction	0.577	0.232	0.796	0.597	0.077	0.684	
Partial Pressure Pa @ 296 K	0.0911	0.0365	0.1256	0.0941	0.0122	0.108	
Partial Pressure Pa @ 348 K	11.127	4.463	15.347	11.498	1.49	13.188	
Total Saturated Vapour Pressure Pa @ 296 K	**150.499**	**117.851**	**92.258**	**55.952**	**45.116**	**0.522**	**2.0237**
Total Saturated Vapour Pressure Pa @ 348 K	1964.403	2042.0834	1030.522	1057.579	1025.38	43.244	117.313
Total Saturated Vapour Pressure Error Pa	1.2E-3	1.1E-3	999.9E-6	1.0E-3	999.0E-6	866.0E-6	1.1E-3

Table 10 Total saturated pressure of n-Octane, n-Decane, n-Dodecane, n-Tetradecane and n-Hexadecane mixtures.

Considering the Antione's Equations at 348 K, in *the present study* the corresponding Saturated Vapour Pressures were obtained as 1025.38 Pa and 117.31 Pa for Fuel 6 and Fuel 8 respectively. Comparing the results obtained with those from the Shell's Matrix, a slight increase in the Saturated Vapour Pressure was noted as the temperature was increased from 343K (from Shell's Matrix) to 348 K. Hence the accuracy of the results obtained from the experiment was acceptable for the purpose of *the present study*.

In order to relate the flow conditions with the cavitation intensity, the Ca was calculated; the Ca is a dimensionless number used to represent the degree of development of cavitation in flow calculations; it represents the potential of the flow to cavitate – At the incipient stage, the $Ca_{Critical}$ denotes the point where cavitation starts due to changes in the static pressure. It is mostly a function of the device constriction and determines the losses associated with the device being subjected to the flow.

To obtain the $Ca_{Critical}$ equation, the Mole fraction of n-Hexadecane and n-Octane were first obtained. The total mass inside the Tank was obtained using Equation 38.

$$Total\ Mass_{Tank} = Vol \times \rho \quad \textit{Equation 38}$$

The Mole was obtained using Equation 39.

$$Mole = \frac{Total\ Mass_{Tank}}{Molar\ Mass\ M} \quad \textit{Equation 39}$$

Hence the Mole Fractions of n-Octane and n-Hexadecane were calculated using Equation 40 and Equation 41.

$$Mole\ Fraction_{Octane} = \frac{Mole_{\ Octane}}{Mole_{\ Octane} + Mole_{\ Hexadecane}} \quad \textit{Equation 40}$$

$$Mole\ Fraction_{\ Hexadecane} = \frac{Mole_{\ Hexadecane}}{Mole_{\ Octane} + Mole_{\ Hexadecane}} \quad \textit{Equation 41}$$

The varying densities of the n-Hexadecane-n-Octane mixtures were obtained using Equation 42.

$$\rho_{Mixture} = (Mole\ Fraction_{Octane} \times \rho_{Octane}) + (Mole\ Fraction_{Hexadecane} \times \rho_{Hexadecane}), \quad \textit{Equation 42}$$

From the uncertainty ΔC ±0.05%, of the hydrocarbon fuel measurement, the uncertainties of the mass of each measured fuel before mixture was calculated.

Hence the error in the mole fraction was obtained using Equation 43.

$$\frac{\Delta Mole\ Fraction_{Octane}}{Mole\ Fraction_{Octane}} = \sqrt{\left(\frac{\Delta Mole_{\ Octane}}{Mole_{\ Octane}}\right)^2 + \left(\frac{\Delta Mole_{\ Octane}}{Mole_{\ Octane}}\right)^2 + \left(\frac{\Delta Mole_{\ Hexadecane}}{Mole_{\ Hexadecane}}\right)^2} \quad \textit{Equation 43}$$

By multiplying the n-Octane Vapour Pressure and n-Hexadecane Vapour Pressure respectively (Obtained from the Antoine Coefficients at 296 K vapour pressure) by the Mole Fraction, the Partial Vapour Pressure was obtained. Hence the results obtained for the Partial Vapour Pressure of n-Octane were added to the results obtained for the Partial Vapour Pressure of n-Hexadecane to calculate the total Saturated Vapour Pressure.

The total Saturated Vapour Pressure Errors were therefore calculated using Equation 44.

$$\Delta P_{TSV\,\alpha} = \sqrt{\left(\Delta P_{P_A}\right)^2 + \left(\Delta P_{P_B}\right)^2 + \left(\Delta P_{P_C}\right)^2 + \cdots + \left(\Delta P_{P_Z}\right)^2} \quad \textit{Equation 44}$$

The $Ca_{Critical}$ was obtained from Equation 45 using the Upstream pressure, the Downstream Pressure as well as the total Saturated Vapour Pressure. This is due to the fact that the Upstream and Downstream Pressure ratios were used to obtain the onset of cavitation.

$$Ca_{Critical} = \frac{P_{Up} - P_{Down}}{P_{Up} - P_{TSV}} \quad \textit{Equation 45}$$

The error associated with the critical cavitation number was obtained using Equation 46.

$$\frac{\Delta Ca_{Critical}}{Ca_{Critical}} = \sqrt{2x\left(\frac{\Delta P_{Up}}{P_{Up}}\right)^2 + \left(\frac{\Delta P_{Down}}{P_{Down}}\right)^2 + \left(\frac{\Delta P_{TSV}}{P_{TSV}}\right)^2} \quad \textit{Equation 46}$$

The $Ca_{FullyDevp}$ on the other hand represents the cavitation number at the fully development stage of the cavitation. It was obtained from Equation 47, using the Upstream pressure, the total Saturated Vapour Pressure and the dynamic pressure.

$$Ca_{FullyDevlt} = \frac{P_{up} - P_{TSV}}{{}^{1}/_{2}\,\rho V^2} \quad \textit{Equation 47}$$

The error associated with the Fully developed cavitation number was obtained using Equation 48.

$$\frac{\Delta Ca_{FullyDevlt}}{Ca_{FullyDevlt}} = \sqrt{\left(\frac{\Delta P_{Up}}{P_{Up}}\right)^2 + \left(\frac{\Delta P_{TSV}}{P_{TSV}}\right)^2 + \left(\frac{\Delta V}{V}\right)^2} \textit{Equation 48}$$

Considering the Viscosity of n-Hexadecane and n-Octane at 20 ^{0}C as 0,003474 N·s/m² and 0,000542 N·s/m² respectively, the Viscosity of the n-Hexadecane- n-Octane mixture was obtained using Equation 49.

$$\mu_{Mixture} = (Mole\ Fraction_{Octane} \times \mu_{Octane}) + (Mole\ Fraction_{Hexadecane} \times \mu_{Hexadecane}) \quad \textit{Equation 49}$$

Considering a varying cavitated jet length of 5 cm to 10 cm and the varying Fully Developed Cavitation Downstream Pressures, the corresponding Re were obtained using Equation 50.

$$Re = \frac{\rho \times V \times L}{\mu} \quad \textit{Equation 50}$$

Blank Page

CHAPTER IV. EFFECT OF INCIPIENT CAVITATION ON n-HEXADECANE BASED FUEL JET – RESULTS AND DISCUSSIONS

During *the present study*, the jet cavitation was formed due to the reduction of pressures caused by the presence of strong eddies. Cavitation occurred within the turbulent eddies formed in the jet mixing/diffusion zone [32] due to turbulence decay formation. This in turn caused the fluid to expand and the surface tension between the layers of the local fuel to increase, causing the pressure to drop considerably.

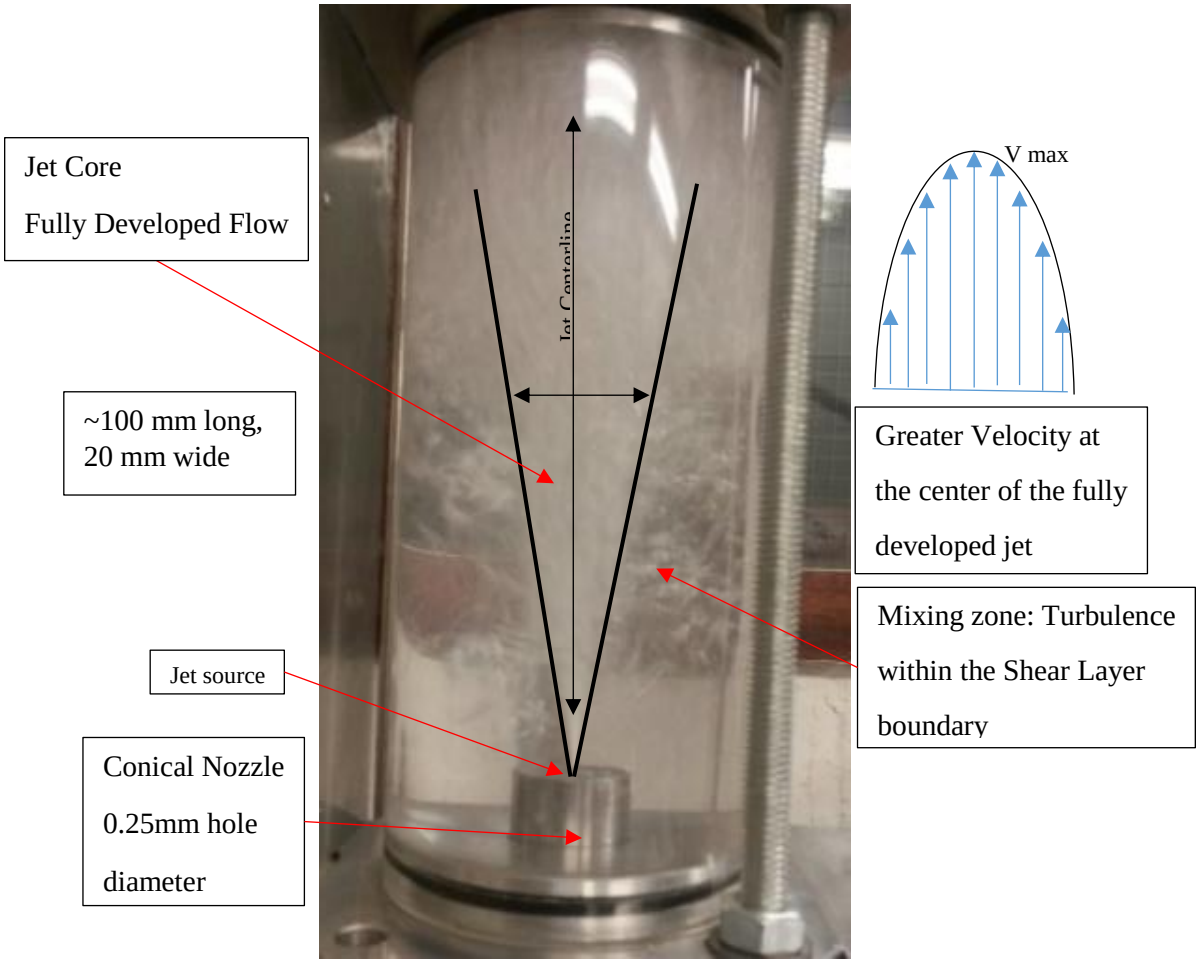

Figure 33 Turbulent Cavitated Jet Profile, 0.25 mm Conical Nozzle, 61 bar Upstream

The increase in the size of the bubble tend to increase the velocity of the bubble, however due to the instability of those bubbles, they tend to split into smaller bubbles. [189] – Similarly, in *the present study,* an increase in the flow velocity downstream of all tested nozzles was visually inspected as cavitation took place. [31]

The surface roughness tends to impact the cavitation as well as the level of turbulence occurring inside the flow. A turbulent effect can lead to a decrease in the Ca. Impurities in the fuel can also affect the Ca as collusions occurring between the solid particles (impurities) and the fuel particles can lead to the breakup of a greater number of bubbles. Hence, the impurities and fuel particles collusion can increase in the propensity of the fuel to cavitate.

The changes in the nozzle geometry did impact the jet as stronger jets were noted when considering the Conical nozzles. Due to the increase of the nozzle hole diameter from 0.14 mm to 0.25 mm, the overall length and the overall width of the jet increased. Hence more bubbles were present in the core of the jet [28] for the same upstream and Downstream Pressures. Please refer to Figure 34.

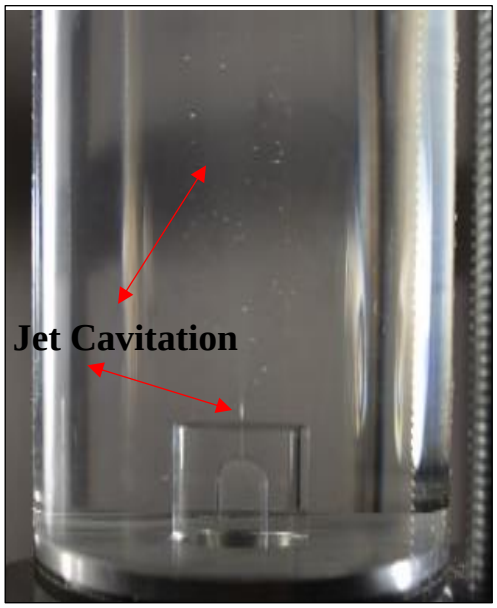

By making use of the Cylindrical, the Hemispherical and the Conical single hole injector nozzles consecutively placed inside a 60mm inner diameter Fused Silica Receiver, it was possible to study the cavitated jet.

Figure 34 n-Hexadecane based cavitated jet – 0.25mm hole Cylindrical Nozzle.

While investigating cavitation taking place outside of the nozzle tip [163, 166], a second type of cavitation was observed between the layers of the jet and the stagnant fuel inside the receiver.

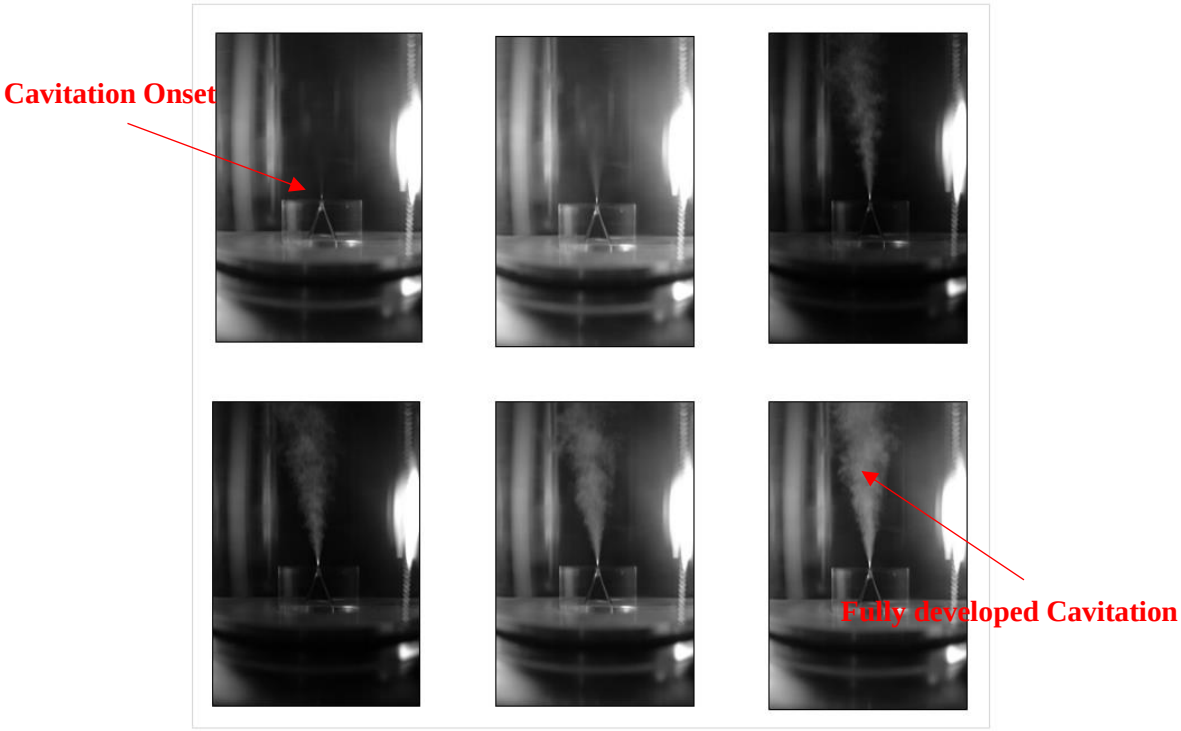

Figure 35 Decrease in Cavitation Downstream Pressure for a fixed Upstream Pressure – 0.25mm hole Conical Nozzle.

The Incipient Cavitation Jet Profile is represented in Figure 35, this considering the 0.25 mm diameter hole Conical Nozzle at 31 bar abs Upstream of the nozzle. A change in Downstream Pressure from 11 bar abs to 1 bar abs (considering a decrement of 2 bar abs from the onset of cavitation to the fully cavitated jet) was considered.

The geometric cavitation (which increased as the Downstream Pressure reduced) was observed as a white spot [39, 162], of a "foamy like" appearance. In all tested nozzles, the small bubbles formed were at first observed as a white solid spot just outside of each nozzle respectively. Hence the presence of

the white spot denoted the start of the cavitation. The white spot increased in strength as the fully developed stage of the jet was reached.

Because incipient cavitation was associated with the flow outside of the nozzle, the use of metal nozzles was considered for the experiment instead of the use of acrylic nozzles – the same phenomenon was observed by Xing *et al.* [173] who discovered that the core vortex of the jet was lifted vertically due to cavitation and that cavitation was observed outside of the nozzle as a result. Similarly to *the present study*, the authors observed a trail of bubbles caused by the presence of eddies formed due to the increase in the jet turbulence as it reached the fully developed stage.

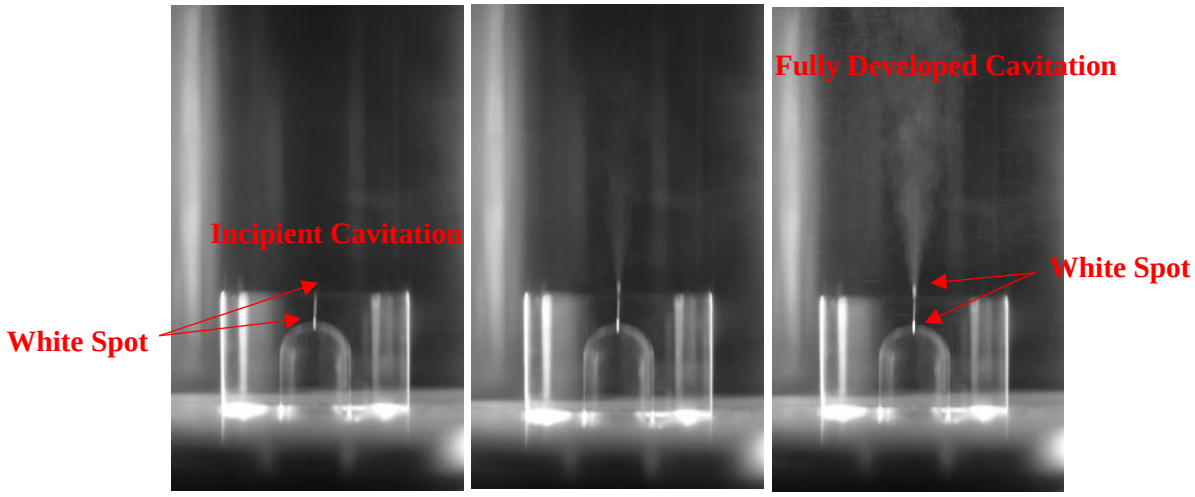

Figure 36 Decrease in Cavitation Downstream Pressure for a fixed Upstream Pressure – 0.14mm hole Hemispherical Nozzle.

The cavitation process timeframe, including the formation, the growth and the collapse of bubbles often took place within few seconds.

When comparing the results obtained for all Cylindrical and Hemispherical tested nozzles, the presence or the absence of the white spot inside the nozzles did not impact the final results. This was

verified by measuring the desinent cavitation number, as each set of measurement was repeated 25 times in order to make sure that hysteresis did not impact the results obtained.

The desinent cavitation number represent the point of cessation of cavitation and can be explained as followed: as it known, larger bubbles are inclined to cavitate before smaller bubbles. The process can lead to an increase in the number of bubbles experiencing cavitation and hence the process can lead to a further reduction in pressure. With the increase in the reduction in pressure, an increase in the number of smaller bubbles collapsing takes place. Hence the pressure at which cavitation starts may differ from the pressure at which cavitation stops. In *the present study*, the desinent cavitation results were similar to the incipient cavitation results as smaller bubbles cavitation were observed before larger bubbles were detected.

Although the inaudible noise emitted at the start of the incipient cavitation officially represents the start of cavitation and often takes place prior to the audible and visible part of the cavitation is perceived, the selected starting point of cavitation in *the present study* (incipient cavitation starting point was set as cavitation was visibly perceived) was appropriate for the purpose of the experiment.

4.1. Effect of Fuel Parameters on Cavitation

This section contains the results obtained from the Cylindrical, Hemispherical and Conical 0.14 and 0.25 mm nozzles for the different percentage mixtures of n-Octane, n-Decane, n-Dodecane, n-Tetradecane and n-Hexadecane fuels – A linear fitting was added to the cavitation onset pressure ratio measurements as during the experiment, the changes in the Downstream pressures varied proportionally to the changes in the Downstream pressures.

This section additionally contains a consistency check done 3 years after the experiment was first performed.

The section furthermore shows graphs of the volumetric flow rate changes due to changes in n-Octane concentration and Upstream Pressure as well as graphs of Critical Cavitation Number ($Ca_{Critical}$) and the Fully Developed Cavitation Number ($Ca_{FullyDevlt}$).

4.1.1. Pressure Measurements – Fuel Mixture of n-Octane in n-Hexadecane

Represented in this section are the results obtained from the Cylindrical, Hemispherical and Conical 0.14 mm nozzles, this considering the mixture of n-Octane in n-Hexadecane fuels.

Two important facts are to be considered when analysing the Pressure Onset graphs represented in this section. Each point on the graph is a representation of the onset of cavitation, represented by:

- The changes in Upstream Pressures due to the corresponding changes in the Downstream Pressures looking at the graphs from the bottom position to the top position.
- The changes in the Downstream Pressures due to changes in the n-Octane concentration looking at the graphs from the left side to the right side.

Because n-Octane has a higher Saturated vapor Pressure than n-Hexadecane for example, adding n-Octane in the fuel mixture increase its overall Saturated Vapour Pressure – a mixture with a higher Saturated Vapour Pressure will have a greater molecular kinetic energy compared to a mixture with a lower Saturated Vapour Pressure. The greater the molecular kinetic energy the greater the impact between molecules, hence the greater the chances of bubble formation, growth and collapse leading to cavitation formation.

The uncertainty of the Downstream Pressure varied between 0.05 bar abs and 0.35 bar abs depending on the different nozzle parameters considered during the experiment. Please refer to Equation 50. The error bars represent the variations in the values obtained for the pressure measurements. The change in the Upstream Pressure (Y Direction) were negligible compared to the changes in the Downstream Pressure (X Direction) measurements.

$$Uncertainty\ Estimate = {\sum STDEV\ (\ bar\ abs)}/{n} \quad \textit{Equation 51}$$

Where n was the number of Upstream Pressure measurement considering parameters such as the nozzle geometry, the material as well as the hole diameter.

Cylindrical

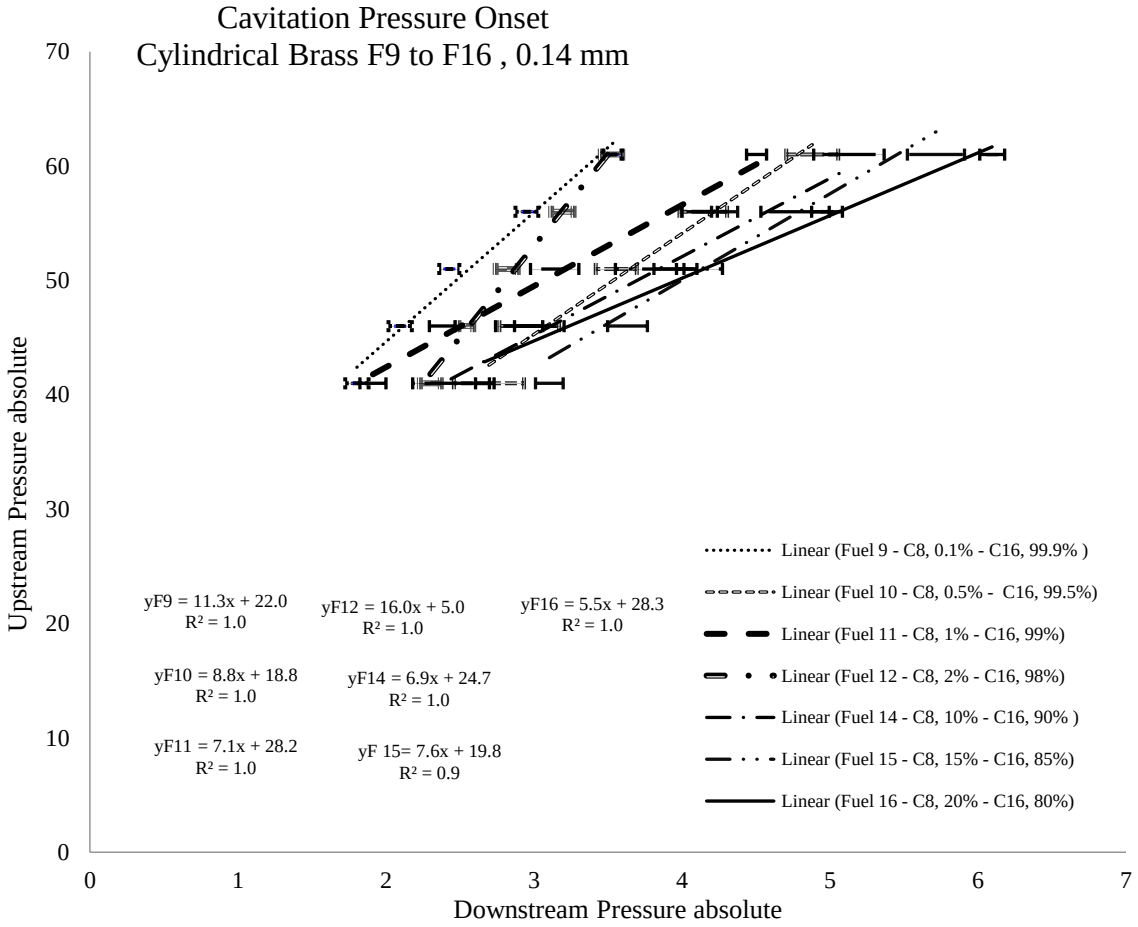

Figure 37 Cavitation Pressure Onset Cylindrical 0.14mm: n-Hexadecane- n-Octane

Changes in Upstream Pressures due to changes in Downstream Pressures – Looking at each fuel individually, an increase in the Upstream Pressure was noted with the increase of the Downstream Pressure

Changes in Downstream Pressure due to changes in Fuel concentration: As seen from Figure 37, considering the 0.14 mm Cylindrical Brass nozzle and testing Fuel 9, Fuel 13 and Fuel 16 respectively, at 61 bar Upstream pressure, the corresponding Downstream pressures were obtained as 3.53 bar, 3.63 bar and 6.09 bar respectively for the Cylindrical nozzle. The Downstream Pressure

increased with the increase in the n-Octane concentration. This can be seen from the noticeable shift of the pressure ratios to the right-hand-side of the graph.

Hemispherical

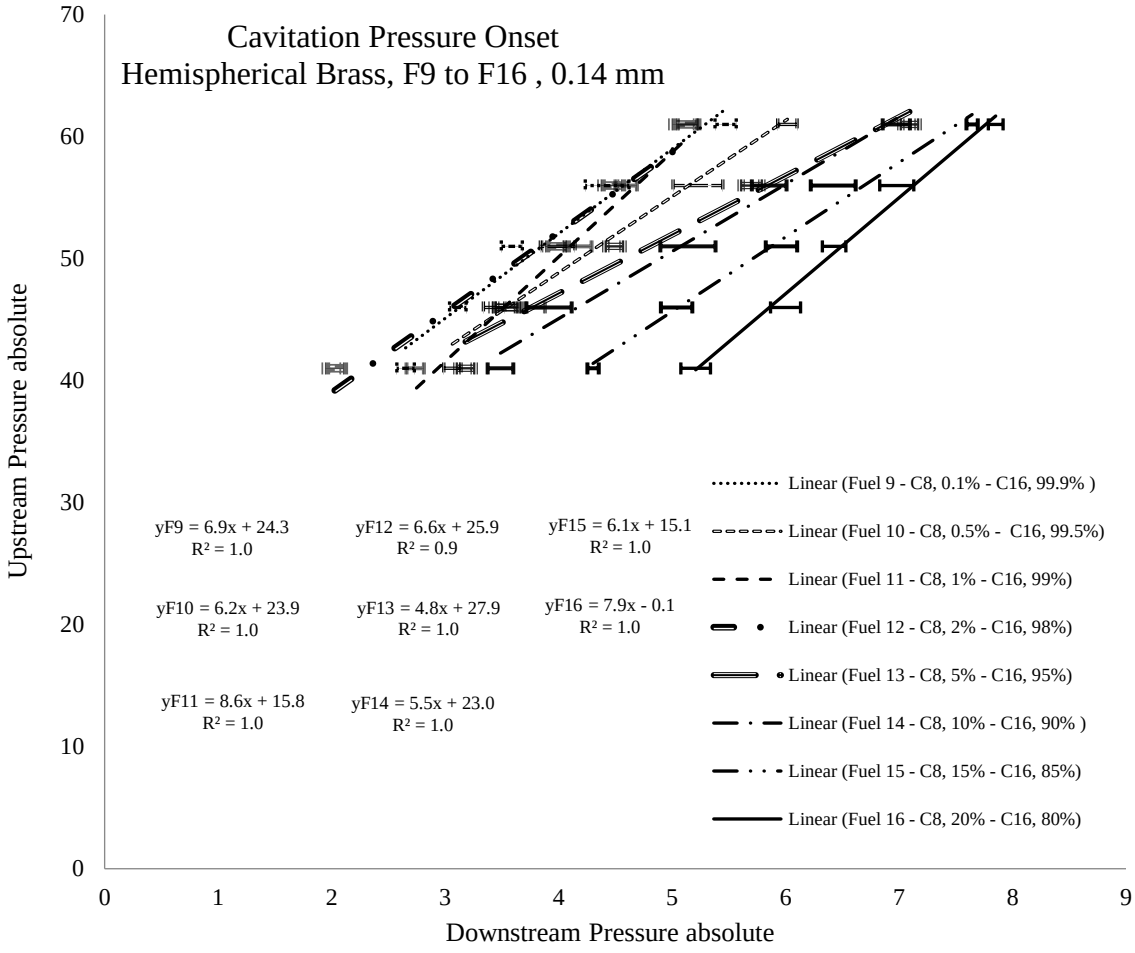

Figure 38 Cavitation Pressure Onset Hemispherical 0.14mm: n-Hexadecane- n-Octane

Changes in Upstream Pressures due to changes in Downstream Pressures: The increase in the Upstream Pressure due to the increase in Downstream Pressure was represented.

Changes in Downstream Pressure due to changes in Fuel concentration – From the results obtained from the Hemispherical nozzle, a noticeable shift of the pressure ratios to the right-hand-side of the

graph was also observed. As seen from Figure 38, considering the 0.14 mm Hemispherical Brass nozzle and testing Fuel 9, Fuel 13 and Fuel 16 respectively, at 61 bar Upstream Pressure, the corresponding Downstream Pressures were 5.47 bar, 7.09 bar and 7.89 bar respectively.

Conical

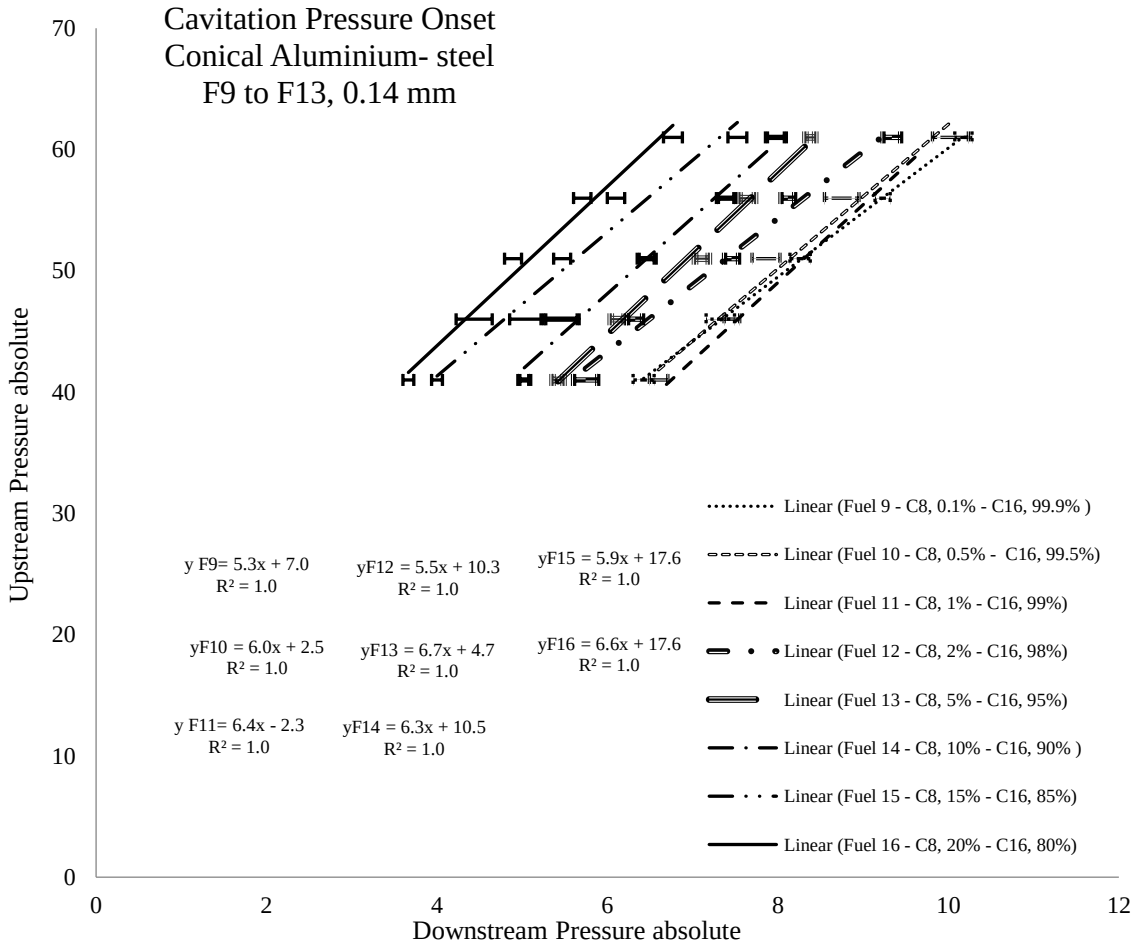

Figure 39 Cavitation Pressure Onset Conical 0.14mm: n-Hexadecane- n-Octane

Changes in Upstream Pressures due to the changes in Downstream Pressures: The increase in the Upstream Pressure due to the increase in Downstream Pressure was likewise represented for the Conical nozzle.

Changes in Downstream Pressure due to changes in Fuel concentration: When considering the Conical nozzle on the other hand, the shift of the pressure ratios appeared to be towards the left-hand-side of the graph. This could be explained by the fact that the flow inside the Hemispherical and Cylindrical nozzles followed a similar geometrical pattern as it flew in and out of the nozzle. Hence, a different flow pattern was noticed inside the Conical nozzle due to the geometrical differences between the 3 nozzles. As seen from Figure 39, considering the 0.14 mm Aluminum-steel nozzle and testing Fuel 9, Fuel 13 and Fuel 16 respectively, at 61 bar Upstream pressure, the corresponding Downstream Pressures were 10.18 bar, 8.38 bar and 6.74 bar respectively.

From the Figure 37 to Figure 39, it can be seen that, the change in the Upstream Pressure was linear to the change in the Downstream Pressure. This was because the change of the Fused Silica Receiver's inside pressure required a proportional change in the Upstream Pressure and Downstream Pressure in order to obtain that onset of cavitation.

The lowest values of incipient cavitation pressures ratio were observed on the Cylindrical nozzle. The results were explained by the fact that the flow through the Cylindrical nozzle hole encountered a 90 degrees angle disturbance while travelling from the Upstream of the nozzle hole to the Downstream of the Nozzle hole.

When considering the Hemispherical nozzle, the disturbance to the flow was reduced as the angle of disturbance slightly increased, increasing in turn the incipient cavitation pressure measurements. When looking at the Conical nozzle, the angle of disturbance was further increased from 90 degrees to 135 degrees. As the flow was directed toward the nozzle hole, the diameter of the fluid stream reduced considerably, leading to an increase in the fluid velocity from the Upstream of the nozzle hole to the Downstream of the nozzle hole.

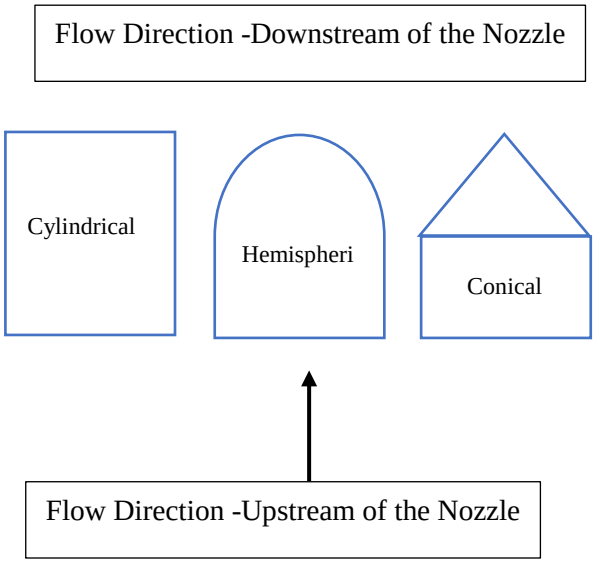

Figure 40 Nozzle Flow Direction of the Cylindrical, Hemispherical and Conical Nozzles

4.1.2. Pressures Measurements – Fuel mixture of n-Octane, n- Decane, n-Dodecane, n-Tetradecane and n-Hexadecane

Represented in this section are the results obtained from the Cylindrical, Hemispherical and Conical 0.14 mm and 0.25 mm nozzles respectively, this considering the varying concentrations of n-Octane, n-Decane, n-Dodecane, n-Tetradecane and n-Hexadecane fuels.

Cylindrical

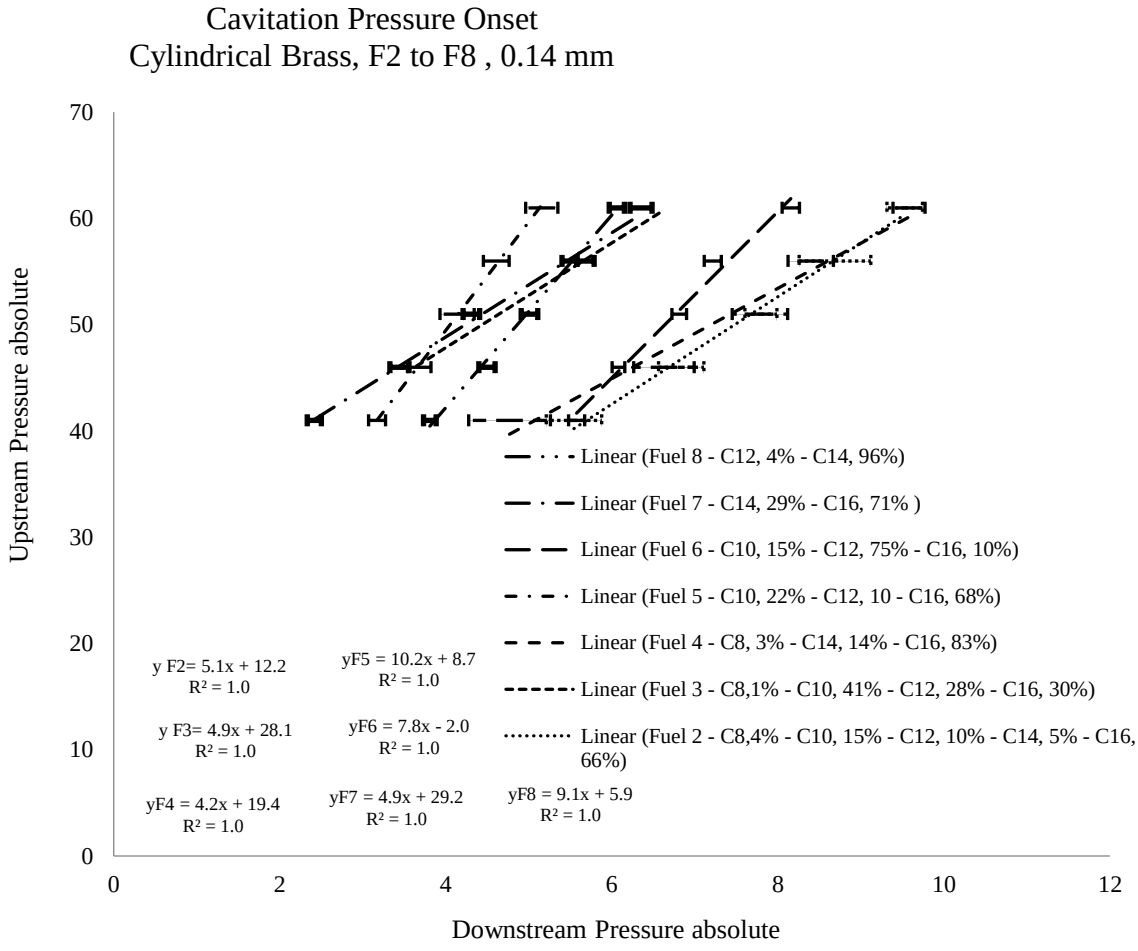

Figure 41 Cavitation Pressure Onset Cylindrical 0.14mm: F2 to F8

Looking at Figure 41, considering the 0.14mm Cylindrical nozzle, and testing Fuel 7 and Fuel 5, the lowest values of the pressure ratio were observed at the onset of cavitation.

As compared to the Cylindrical nozzle in Figure 41, when looking at Figure 42, considering the 0.14mm Hemispherical nozzle and testing Fuel 7 and Fuel 8 the lowest values of the pressure ratios were once more observed at the onset of cavitation.

Hemispherical

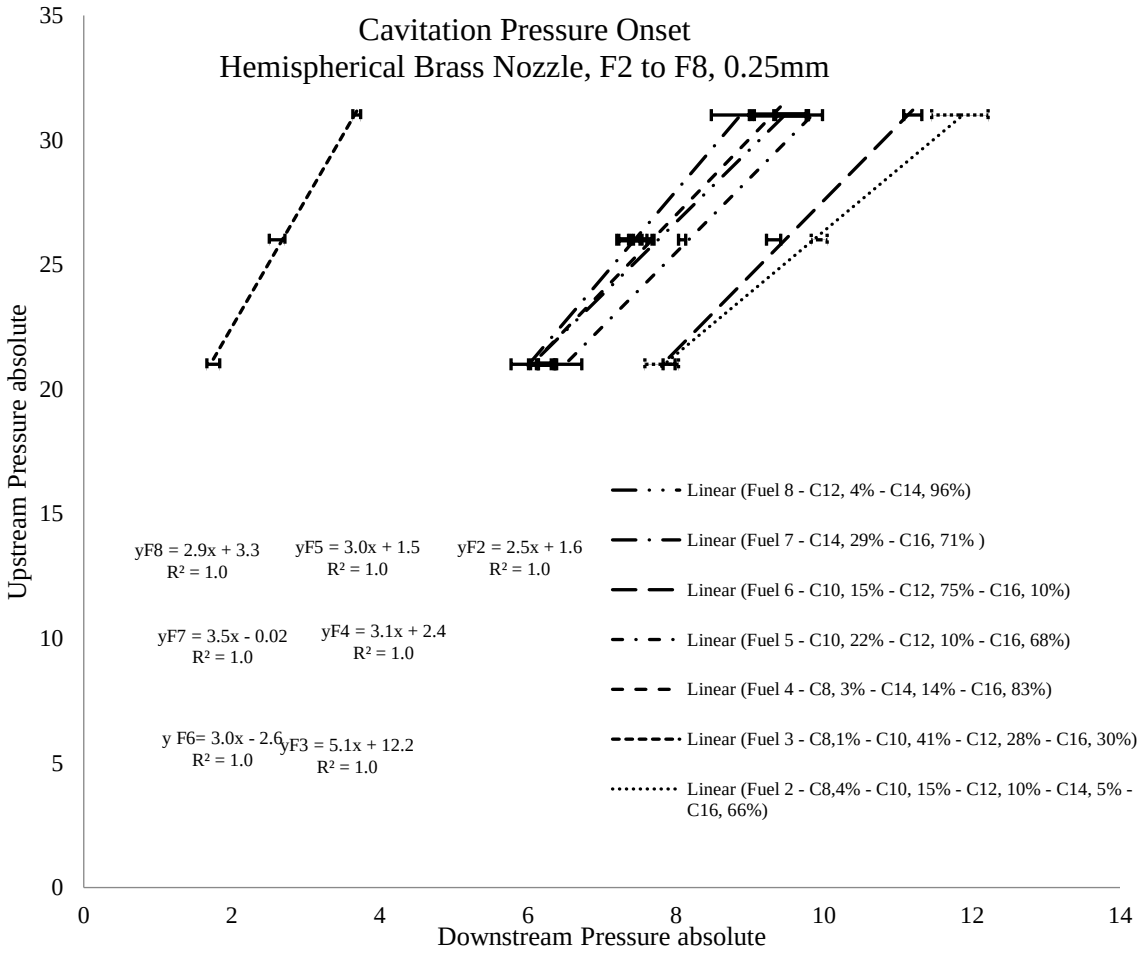

Figure 42 Cavitation Pressure Onset Hemispherical 0.25mm: F2 to F8

A discrepancy was noted on the results obtained for Fuel 3 as the nozzle did not fully cavitate; this could have happened due to nozzle hole restriction. The pressure ratios obtained from Fuel 2 were observed at the right-hand-side of the graph. As expected, looking at Figure 43, the opposite behaviour was observed for the Conical nozzle. When considering the 0.14 mm Conical Nozzle, Fuel 7 was seen on the far right-hand-side of the graph and Fuel 6 on the far left-hand-side of the graph. This indicated that Fuel 6 was not easily prone to cavitation.

Conical

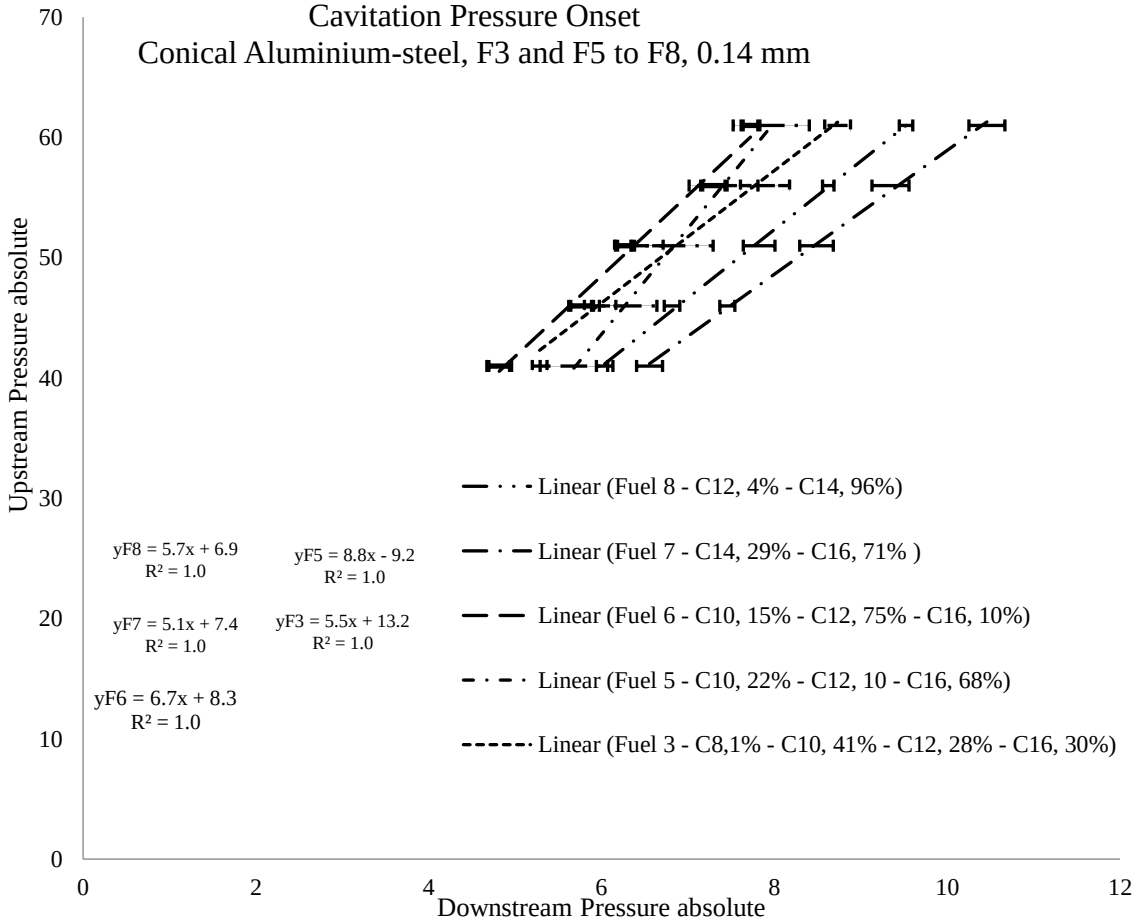

Figure 43 Cavitation Pressure Onset Conical 0.14mm: F2 to F8

Referring back to the n-Octane- n-Hexadecane mixtures, an increase in the n-Octane concentration led to an increase in the Saturated Vapour Pressure and led to the move of the Cylindrical and n-Hemispherical plotted graphs from the left-hand-side of the graph to the right-hand-side of the graph. Based on Shell's matrix in Table 3, Fuel 7 had the lowest Saturated Vapour Pressure in comparison to Fuel 2 and Fuel 3 which had the highest Saturated Vapour Pressure. The results obtained in Figure 41 to Figure 43 observed a similar pattern – Observing each figure from the left-hand-side of the graph to the right-hand-side of the graph, an increase in Saturated Vapour Pressure was noted for the

Cylindrical nozzle as well as for the Hemispherical nozzle. Once more, the reverse phenomenon was observed when considering the Conical nozzle.

4.1.3 Pressures Measurements – Consistency Check

A consistency check was done in September 2015 which reproduced the experimental settings of the incipient cavitation experiment done in Jan 2012, using the n-Hexadecane-n-Octane mixture. Below are the graphs obtained from the Cylindrical Brass 0.14mm nozzle and the Conical Aluminum-steel 0.14mm as well as the Conical Aluminum-steel 0.25mm nozzle.

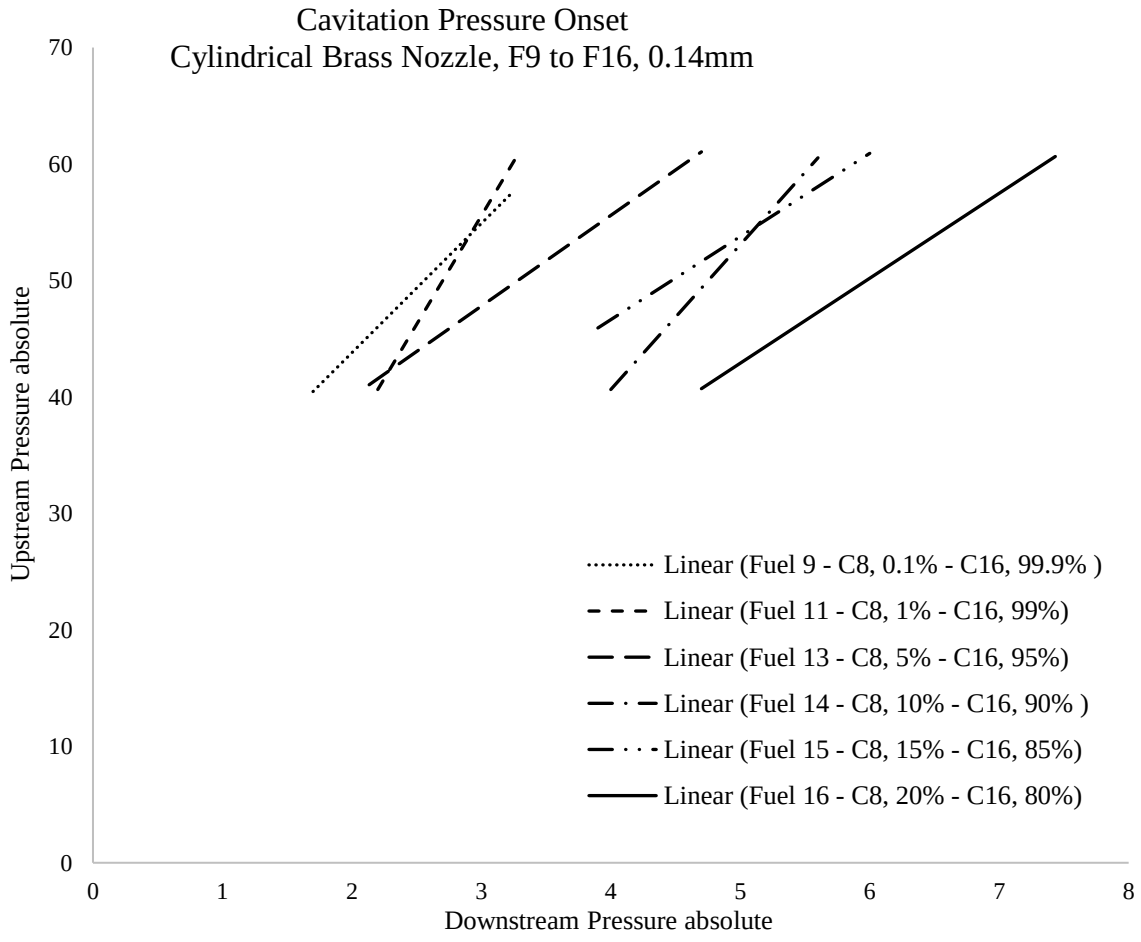

Figure 44 Cavitation Pressure Onset Cylindrical 0.14mm: n-Hexadecane-n-Octane$_2$

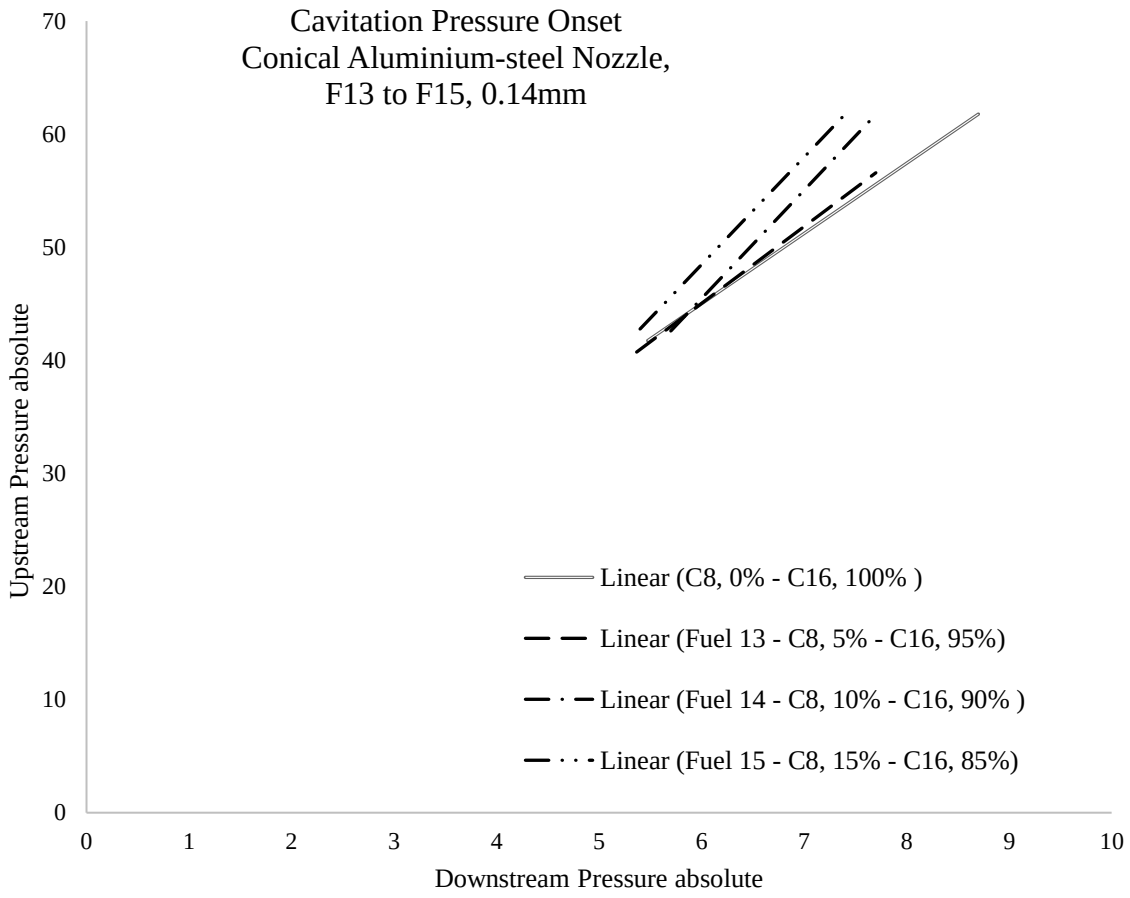

Figure 45 Cavitation Pressure Onset Conical 0.14mm: n-Hexadecane- n-Octane$_2$

As expected, a consistency in the results was observed – an increase in the Upstream Pressure due to the increase in the Downstream Pressure was noticed as well as an increase in the Upstream Pressure due to the increase in the n-Octane concentration when considering the Cylindrical nozzle.

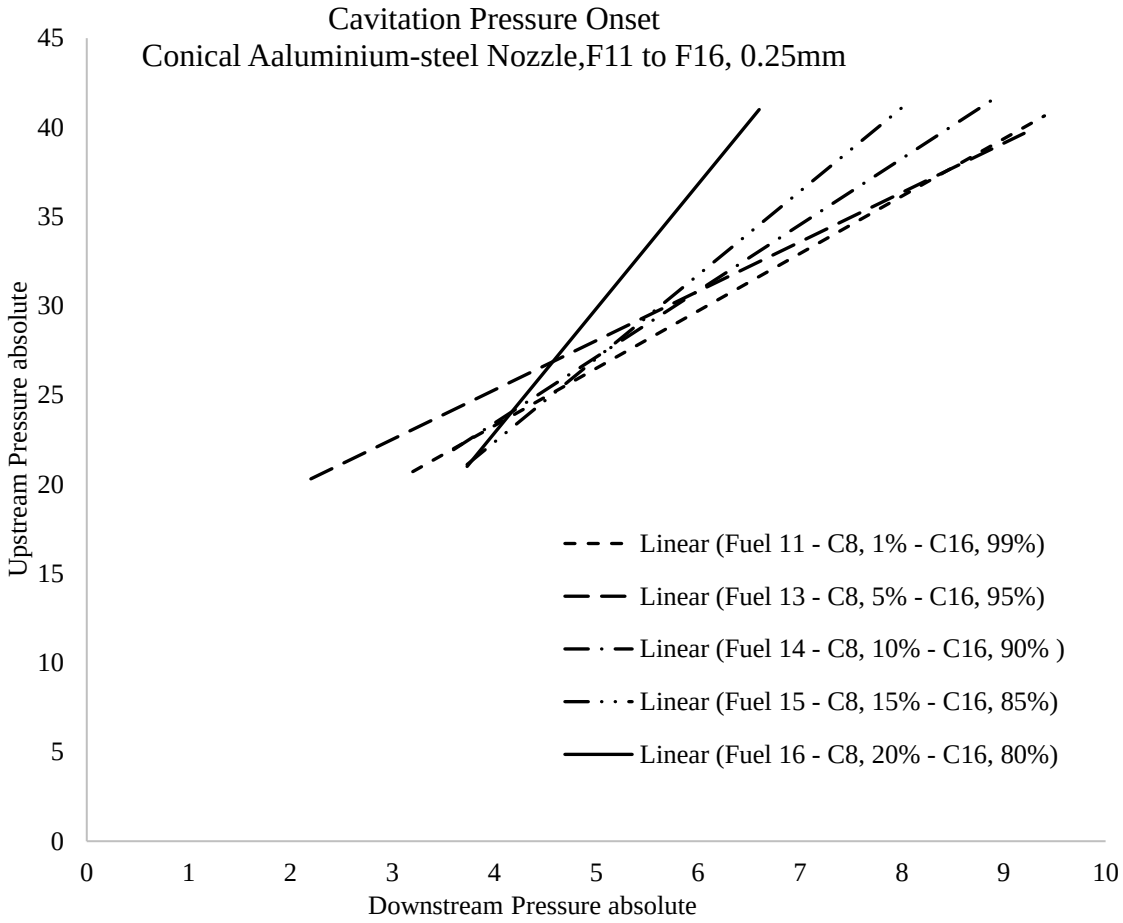

Figure 46 Cavitation Pressure Onset Conical 0.25mm: n-Hexadecane-n-Octane$_2$

The check indicated as previously observed in 2012, that the propensity of the fuel to cavitate increased with the increase in the n-Octane percentage in n-Hexadecane when considering the Cylindrical and the Hemispherical nozzles. The reversed phenomenon was once more observed for all Conical nozzles.

4.1.4. Discharge Coefficient Results

Two sets of graphs were plotted in this section. The first set of graphs represents the changes in the Volumetric Flow Rate Q due to the changes in the n-Octane concentration and the Upstream Pressure. The second set represents the change in the Cd due to the changes in the n-Octane concentration and the Upstream Pressure.

The Volumetric Flow rate error bars were obtained using Equation 30. The Octane percentage error bars were small compared to those of Q on the Y direction. The errors in the Y direction were obtained using Equation 19 where each hydrocarbon fuel had an error estimate of ± 0.05%.

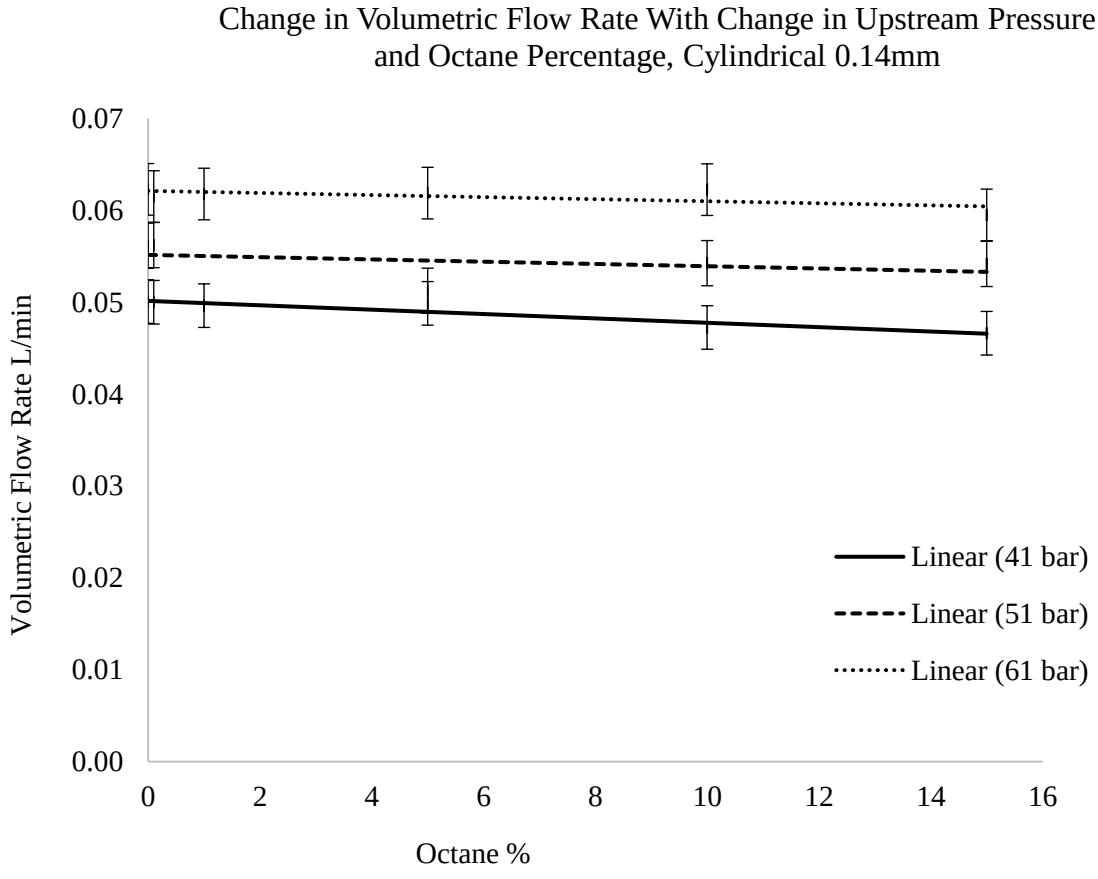

Figure 47 Decrease in Volumetric Flow Rate due to increase in n-Octane percentage and Pressure, 0.14 mm nozzle Cylindrical

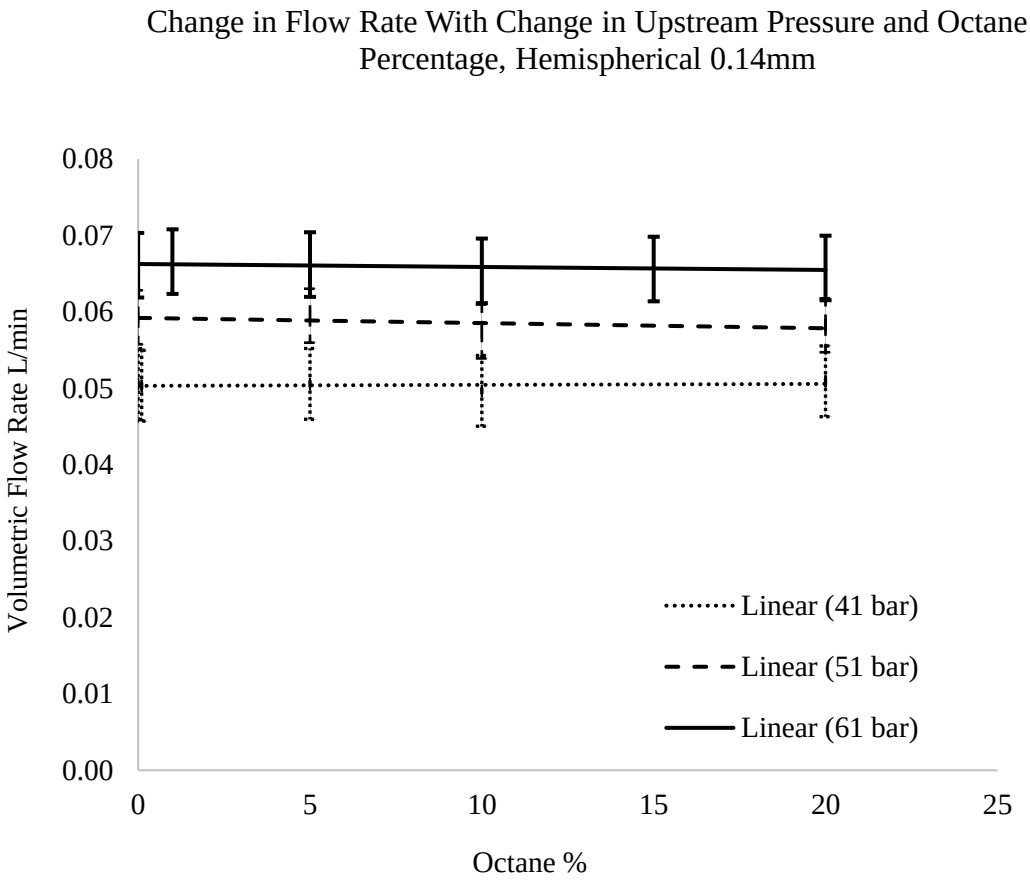

Figure 48 Decrease in Volumetric Flow Rate due to increase in n-Octane percentage and Pressure, 0.14 mm nozzle Hemispherical

Q increased due to the increase in Upstream Pressure from 41 bar abs to 61 bar abs. This was as expected as, by increasing the pressure applied to the fuel, a greater fuel quantity travelled through the nozzle hole per second.

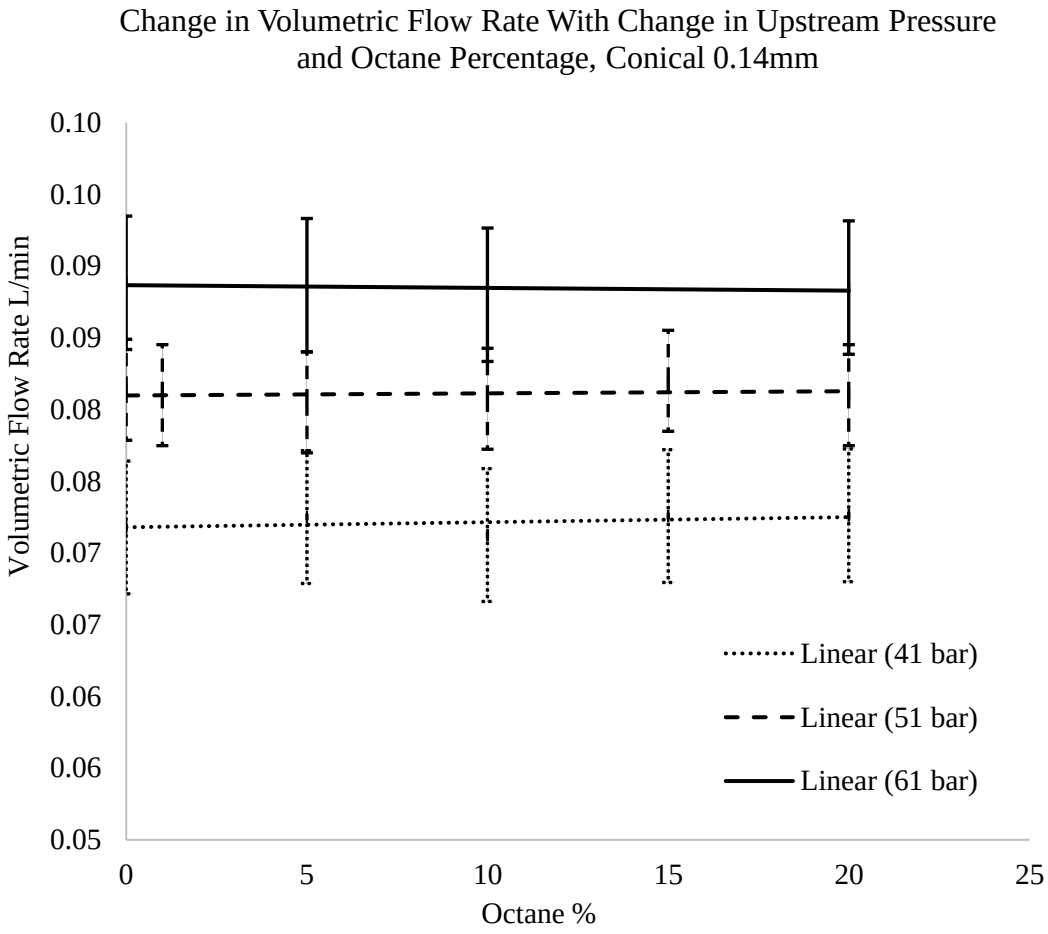

Figure 49 Decrease in Flow Velocity due to increase in n-Octane percentage and Pressure, 0.14 mm nozzle Cylindrical

The slight decrease in Q was noticed for all the data due to the increase in n-Octane concentration – As the n-Hexadecane was mixed with an increasing concentration of n-Octane, the fuel mixture density decreased. Hence, the increase in n-Octane concentration led to the increase of the cavitation occurring inside the fuel, which in turn led to a slight decrease in the flow rate.

A second set of graphs was plotted to highlight the changes in the Cd due to the changes in the n-Octane concentration and the changes in the Upstream Pressure.

The errors associated with the Cd were obtained using Equation 35. The Octane percentage error were small compared to those of the Cd on the y direction. They were obtained using Equation 19 where each hydrocarbon fuel had an error estimate of ± 0.05%.

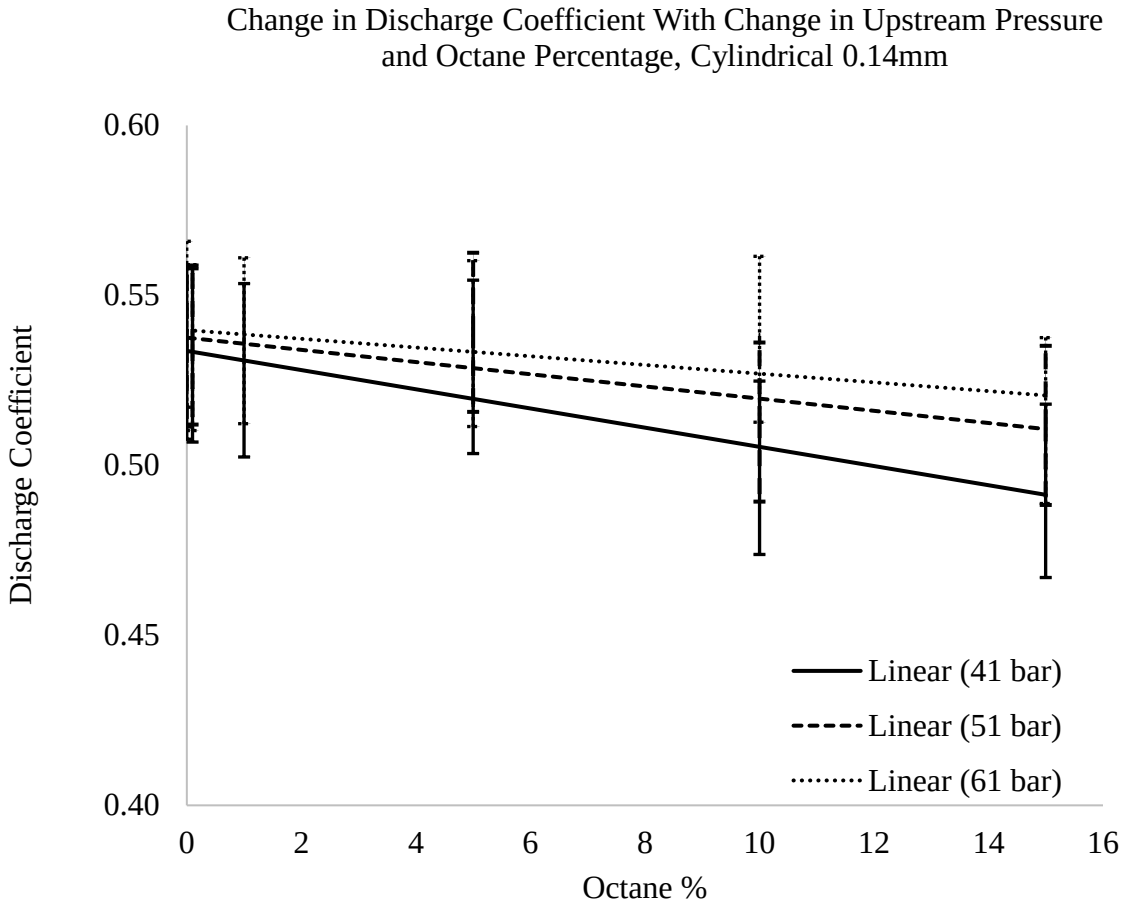

Figure 50 Decrease in Cd due to the increase in n-Octane concentration and Pressure, Cylindrical 0.14mm

Using a cross-sectional area of 4.9 x 10^{-8} m^2, the 0.25 mm Conical nozzle was found to have the highest value of Cd of 0.845, followed by the Hemispherical nozzle which had a Cd of 0.774.

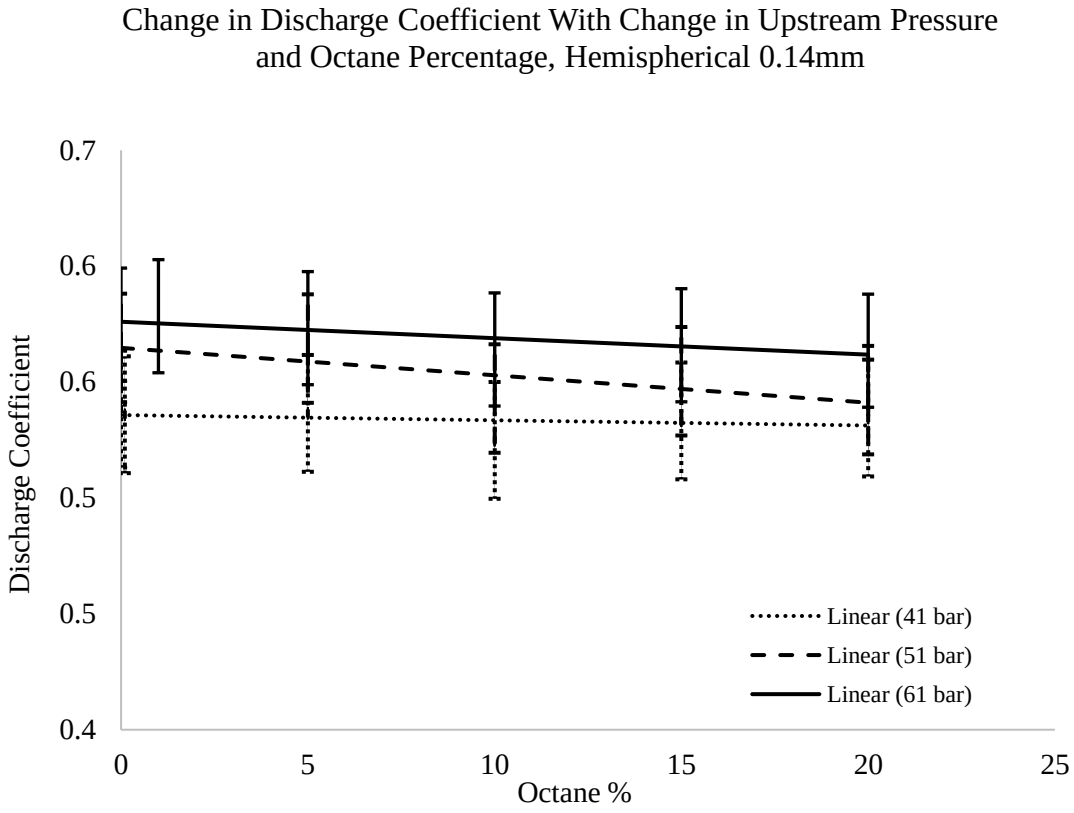

Figure 51 Decrease in Cd with the change in n-Octane and Pressure, Cylindrical 0.25 mm nozzle

The 0.14 mm hole nozzle was seen to have a lower Cd in general compared to the 0.25 mm hole nozzle, i.e. A Cylindrical Nozzle Cd variation of 0.481 to 0.542 was noted for the 0.14 mm and, a Cylindrical nozzle Cd variation of 0.701 to 0.751 was noted for the 0.25 mm. This seems to indicate that the values obtained from the 0.25 mm hole nozzles where much more comparable to the ideal Cd of the flow through the injector nozzle which is equal to 1.

Toward the end of the experiment, a considerable decrease in the flow rate was noticed as the 0.14mm Cylindrical nozzle had difficulty cavitating due to the fact that bubbles were trapped inside the hole of the nozzle leading to a nozzle hole blockage. This occurred when collecting readings for the 20%

n-Octane concentrated fuel – Hence, the data obtained when considering the 0.14 mm Cylindrical nozzle hole at 20% n-Octane concentration were too low to be considered.

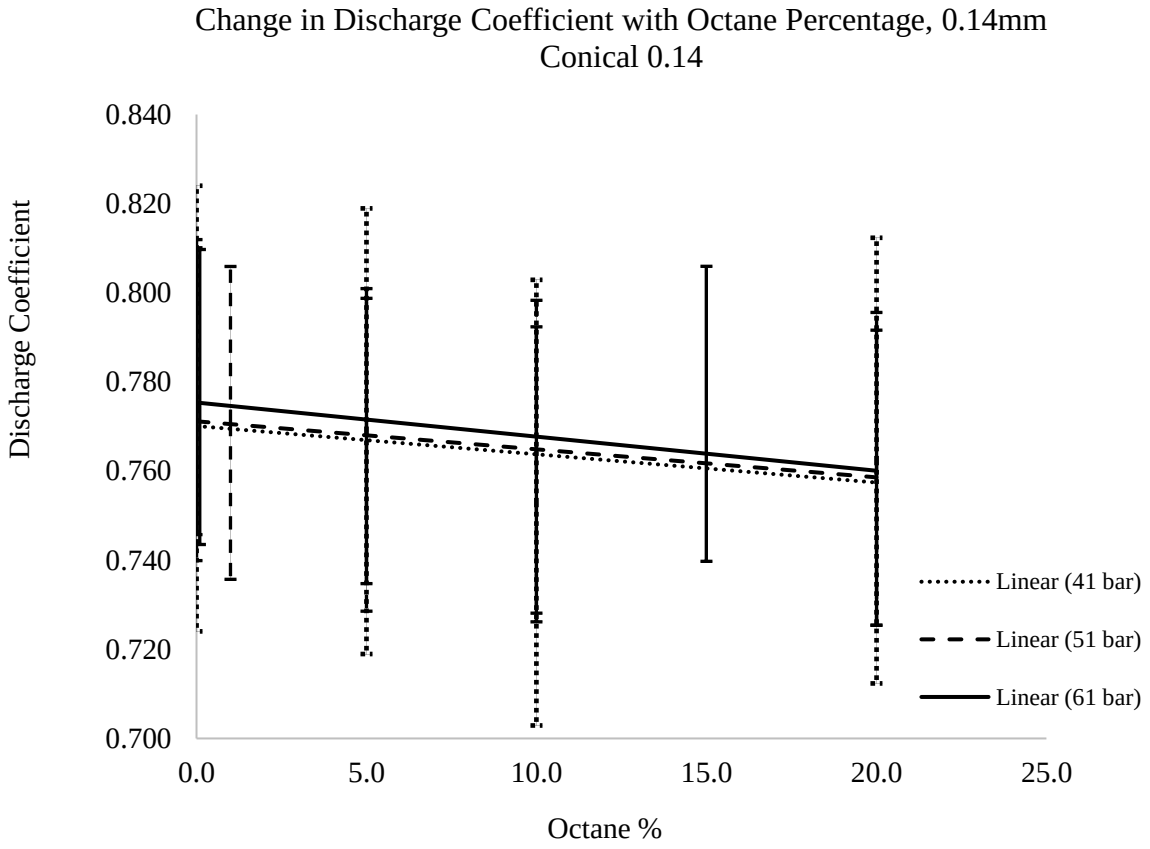

Figure 52 Decrease in Cd due to the increase in n-Octane concentration and Pressure, Conical 0.25mm

In their work, Dingle and Lai [153] also obtained Cd varying between 0.8 and 0.88 at 101 bar. Typical injector nozzles are designed with Cd varying between 0.6 and 0.9. In *the present study*, for all tested fuels, the Cd was seen to reduce due to turbulence [24,46] occurring inside the receiver as the fuel was prone to cavitation.

4.1.5. Incipient Cavitation Dependency on Saturated Vapour Pressure and Surface Tension

From the results obtained in *the present study*, it can be deduced that the increase in the Saturated Vapour Pressure of the fuel led to the increase in the propensity of the fuel to cavitate. Incipient cavitation is very much dependent on the Saturated Vapour Pressure of the fluid.

Comparing the results obtained from Shell's Matrix to those obtained during the experiment at City University laboratory, the figures below displayed a similar pattern.

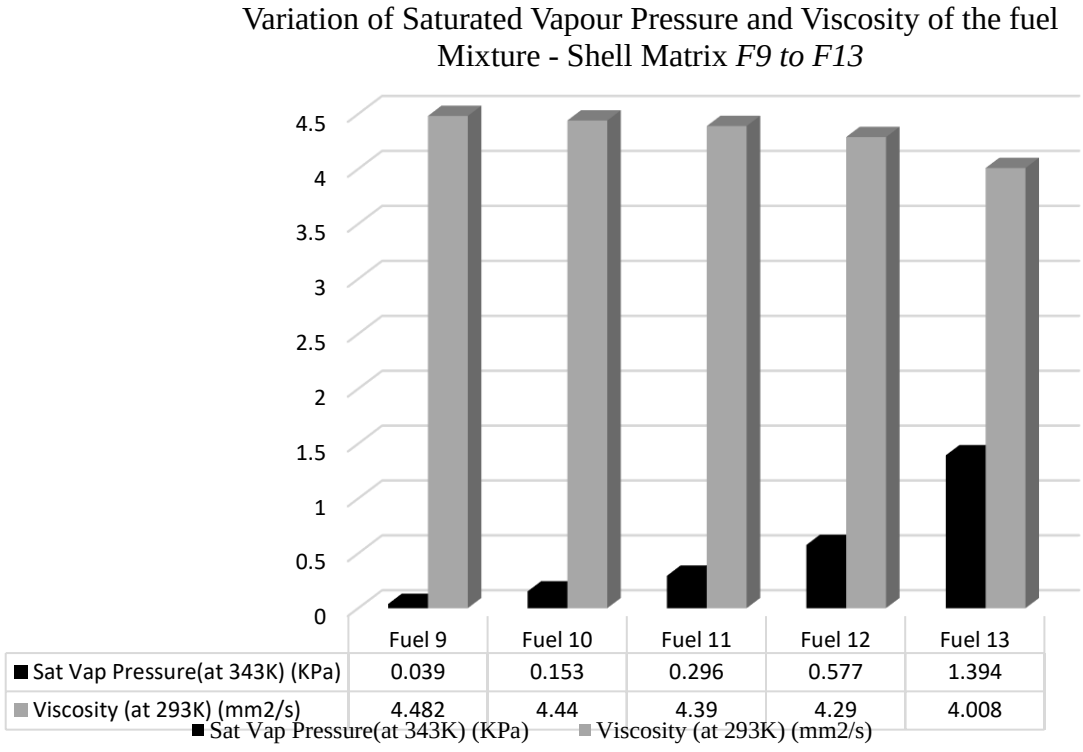

Figure 53 Comparison of the changes of Saturated Vapour Pressure to the Changes of Viscosity of the fuel mixture – Shell Matrix *F9 to F13*

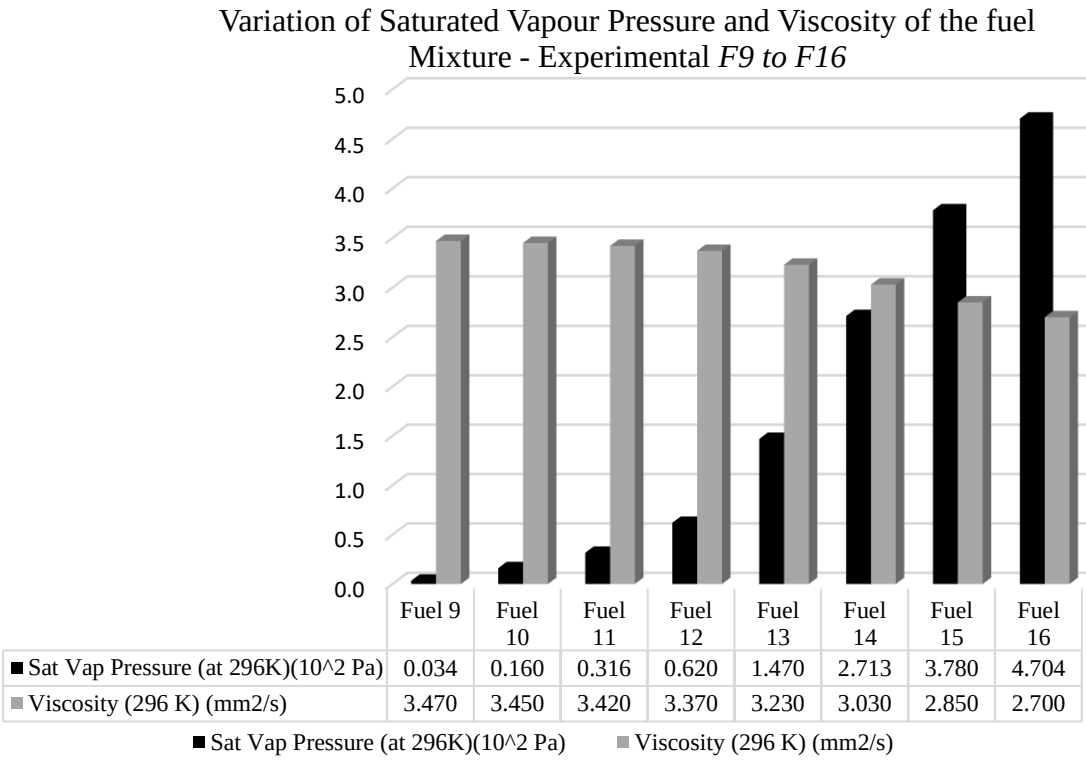

Figure 54 Comparison of the changes of Saturated Vapour Pressure to the Changes of Viscosity of the fuel mixture – Experimental *F9 to F16*

Looking at Figure 53 and Figure 54, a decrease in the viscosity of the mixture was noted as the Saturated Vapour Pressure increased. Likewise, Price *et al.* [4] came to the same conclusions while working on the impact of cavitation on hydrocarbons. The authors found out that cavitation was not easily induced in liquids with higher viscosity compared to those with lower viscosity due to the stronger existing forces between them and their ability to resist the flow.

Looking at the second set of fuels mixtures (Fuel 8 to Fuel 2), an increase in the propensity of the fuel to cavitate was noted with the decrease in the viscosity of the fuel. The results are shown in in

Figure 55 and Figure 56. The results obtained from Shell Matrix were similar to those obtained from the experiment.

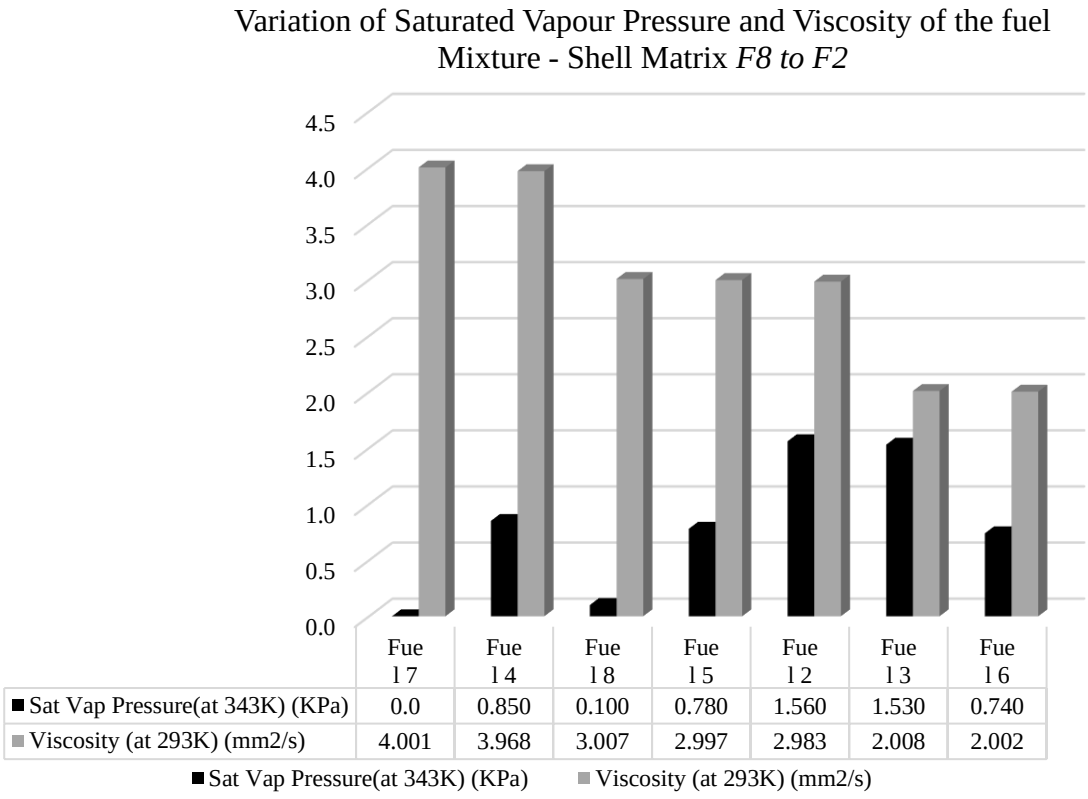

Figure 55 Comparison of the changes of Saturated Vapour Pressure to the Changes of Viscosity of the fuel mixture – Shell Matrix *F8 to F2*

As shown from Figures 41 to Figure 43, Fuel 7 and Fuel 8 did not cavitate as much as Fuel 2 and Fuel 3. This was once more observed in Figure 55 as a low Saturated Vapour Pressure was obtained for Fuel 7 and for Fuel 8, and a higher Saturated Vapour Pressure was obtained for Fuel 2 and for Fuel 3. Referring to Table 3, Fuel 7 and Fuel 8 were made up of 0% n-Octane. Hence this explained the low values of Saturated Vapour Pressures obtained for the two mixtures. The high value of Saturated Vapour Pressure obtained for Fuel 2 was justified by the fact that Fuel 2 mixture had the

highest concentration of n-Octane, 4%. Although Fuel 3 was only made up of 1% Octane, it had the highest concentration of n-Decane, 41%. This justified its high Saturated Vapour Pressure value compared to the other mixtures.

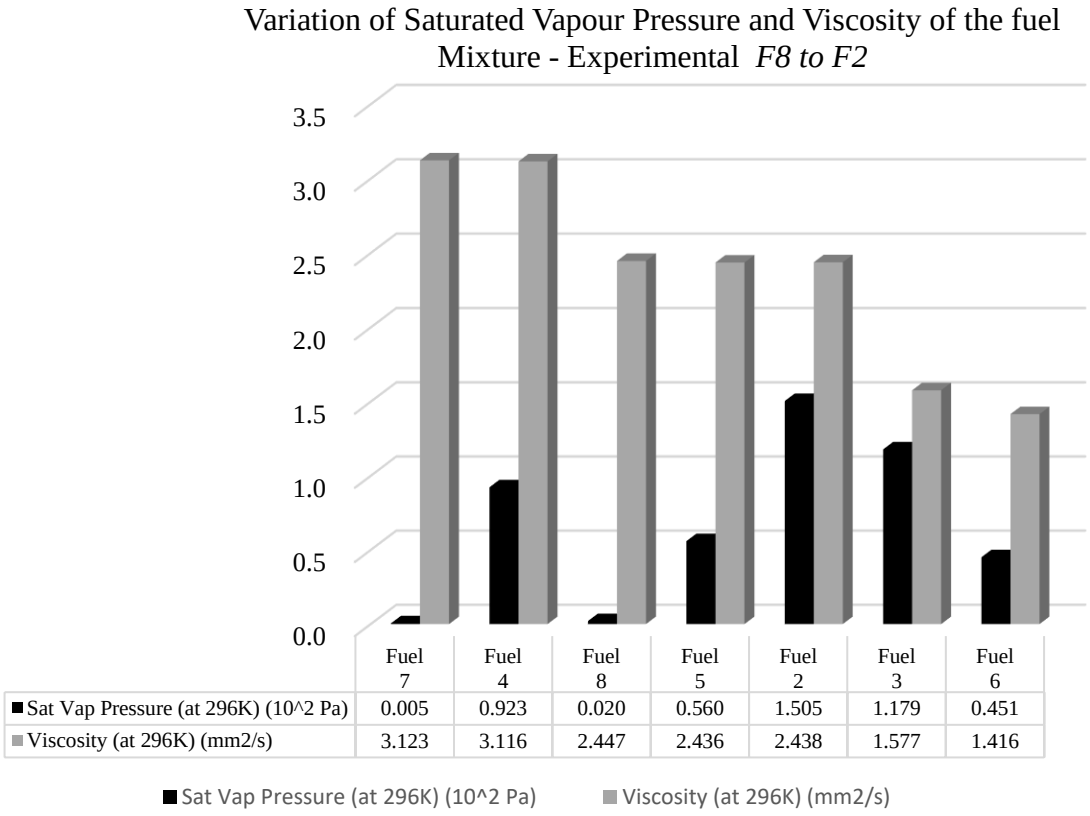

Figure 56 Comparison of the changes of Saturated Vapour Pressure to the Changes of Viscosity of the fuel mixture – Experimental *F8 to F2*

In comparison to Fuel 4 which had 3% n-Octane and 0% Decane, Fuel 5 had 0% n-Octane and 22% Decane. This explained why the Saturated Vapour Pressure of Fuel 4 was higher than that of Fuel 5. Even though Fuel 6 had a lower percentage of Decane, 15%, in comparison to Fuel 5, 22%, it was made up of 75% dodecane. Hence this justified why Fuel 5 had approximately the same Saturated

Vapour Pressure as Fuel 6, i.e. From Shell Matrix, the Saturated Vapour Pressures were obtained as 0.78 kPa and 0.74 kPa for Fuel 5 and Fuel 6 respectively. Refer to Table 2 and Table 3.

Contrary to the viscosity which was mostly affeccted by the total fuel volume – The viscosity was affected by the percentage of the greatest fuel mixture constituent's volume, i.e. n-Hexadecane and n-Tetradecane. The Saturated Vapur Pressure was very much affected by the concentration of n-Octane in the mixture.

When looking at Figure 53 to Figure 56, the decrease in viscosity can be compared to the decrease of the heaviest fuel mixture constituent. As an example, Fuel 7, Fuel 4, Fuel 8 and Fuel 5 had 100%, 97%, 96% and 68% respectively of n-Hexadecane and n-Tetradecane mixture. This explaines the decrease in the viscosity of the different mixtures.. More work is still needed in the area in order to undestand the full impact of viscosity on the incipient cavitaiton phenomena

The incipient cavitation is very much dependent on the Saturated Vapour Pressure as it is dependent on the cavitation bubble number and the cavitation bubble intensity. The Ca decreases with the increase in the Saturated Vapour Pressure – The Ca expresses how likely the fuel will cavitate, the lower the Ca the more likely the fuel will cavitate. It represents the difference between the local pressure and the vapour pressure. As the collapse of bubbles is reliant on the balance between the internal pressures inside the bubble and the external pressures outside of the bubble, a growth in the external pressure will alter the point of onset of cavitation as more forces are required to counteract the added pressure in order to form the bubble.

The key results showed in these graphs were that, the fuel was prone to cavitation as Saturated Vapour Pressure increased as well as that, the changes occurring in the Cylindrical and Hemispherical nozzles

were opposite to the changes occurring in the Conical nozzle. This was as expected as the results obtained in Chapter 4.1 to Chapter 4.3 showed a difference in the flow behavior when considering the Cylindrical nozzle, the Hemispherical nozzle and the Conical nozzle respectively.

The Critical Cavitation errors varied between ± 0.9 and ± 0.3 as the concentration of Octane increased. The errors were obtained using Equation 45. The linear fitting was added to show how the Critical Cavitation Number varied due to the change in the Saturated Vapour Pressure as the concentration of n-Octane increased.

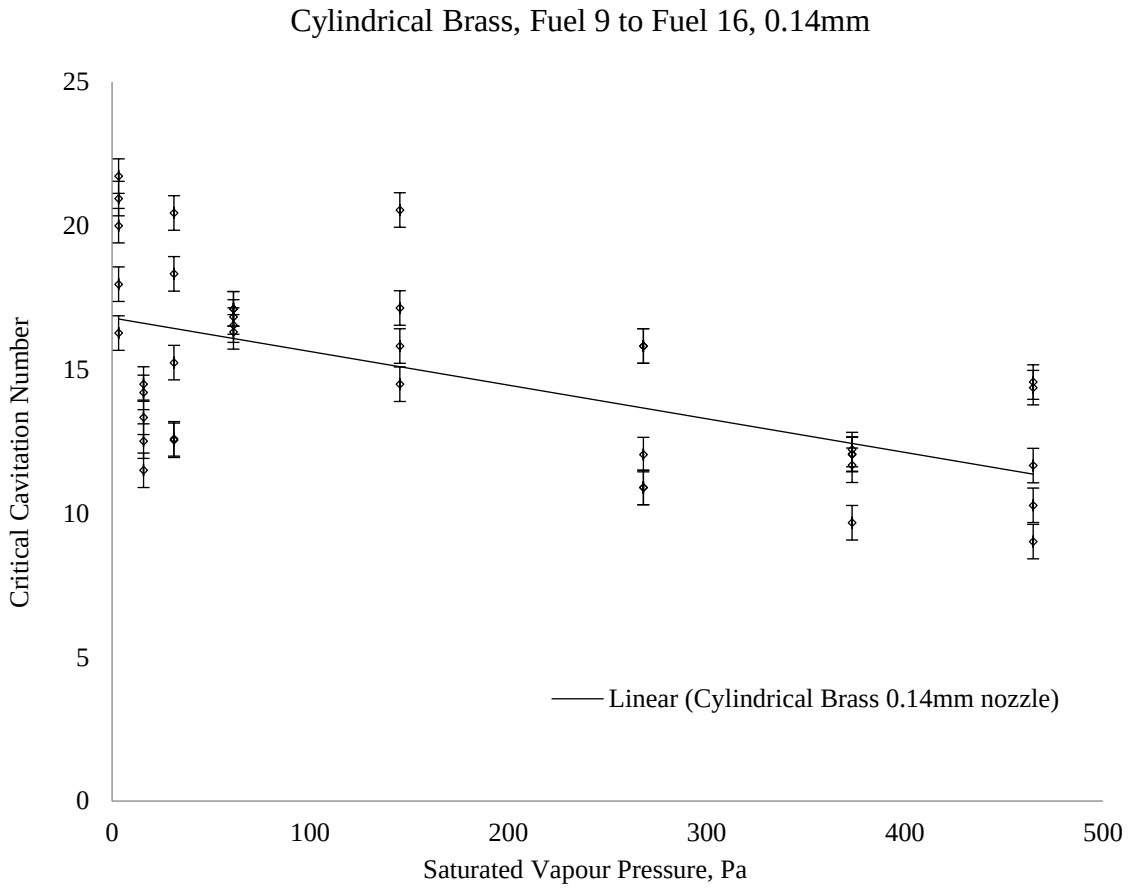

Figure 57 Ca variation due to Saturated Vapour Pressure, 0.14 mm Cylindrical, F9 to F16

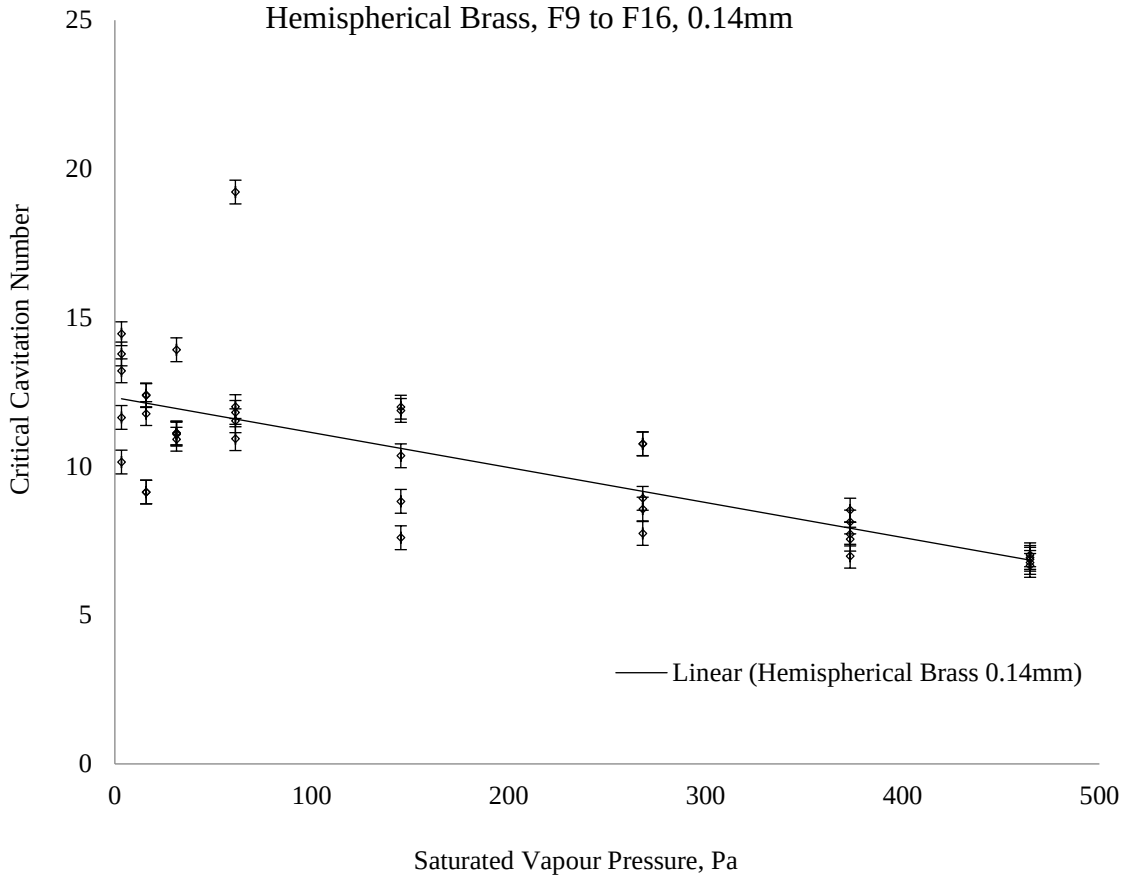

Figure 58 Ca variation due to Saturated Vapour Pressure, 0.14 mm Hemispherical, F9 to F16

The increase in the percentage of n-Octane led to an increase of the saturated vapour pressure. As known, the higher the vapour pressure the lower the impact of cavitation bubble collapse. This meant that a fuel richer in n-Octane not only was easily prone to cavitation, but also was better at moderating the aftershocks resulting from the collapse of bubbles.

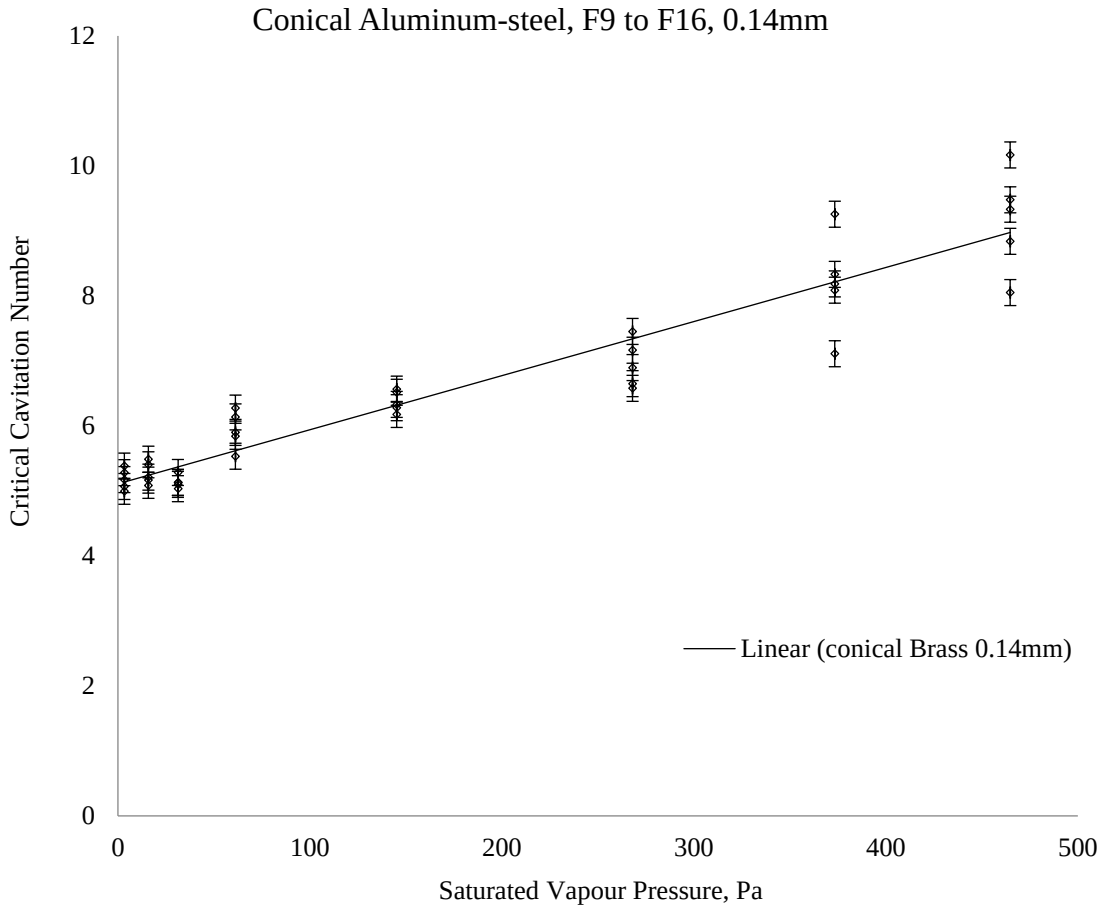

Figure 59 Ca variation due to Saturated Vapour Pressure, 0.14 mm nozzle Conical, F9 to F16

Incipient cavitation is also dependent on the surface tension. [37] In *the present study*, the wall boundaries between the stagnant fuel inside the Fused Silica Receiver and the flowing jet through the stagnant fuel, acted as two solid surfaces experiencing high surface tensions. The surface tensions between the two layers tend to decrease with the decrease in the viscosity of the fuel as a lesser viscous fuel will be made up of weaker chemical bonds make it easier for its molecules to detach and form bubbles.

Furthermore, considering the decrease in the surface tension of the stagnant fuel to be proportional to the decrease in the viscosity of the fuel, it is possible to assume that the strength of the cavitated jet will vary proportionally to the change in the fuel viscosity. [186]

As previously stated, due to the geometry of the Conical nozzle which affected to flow pattern, the flow in the Conical nozzle experienced choking, leading to an increase in the Ca as the saturated pressure increased – This meant that the Conical nozzle's propensity to cavitate decreased with the increase in saturated vapour pressure.

This also explained the high velocities observed in the Conical nozzles as the nozzle hole was reduced due to choking in comparison to the Cylindrical and Hemispherical nozzles – for the 0.14mm Conical nozzle for example, the flow velocity varied between 73.660 m/s ± 0.001 m/s and 78.670 m/s ± 0.001 m/s at 41 bar abs, compared to the Cylindrical nozzle where it varied between 50.506 m/s ± 0.001 m/s and 54.243 m/s ± 0.001 m/s at 41 bar abs.

4.1.6. Critical Cavitation Number and Fully Developed Cavitation Number Comparison considering n-Hexadecane-n-Octane Fuel mixture

A comparison was made between the $Ca_{Critical}$ taking place at the onset of cavitation and the $Ca_{FullyDevlt}$, in order to highlight the differences between the 2 states of the jet flow. This helped to understand the impact that changing parameters such as, the physical properties of the fuel and the nozzle's geometrical properties and material, has on cavitation.

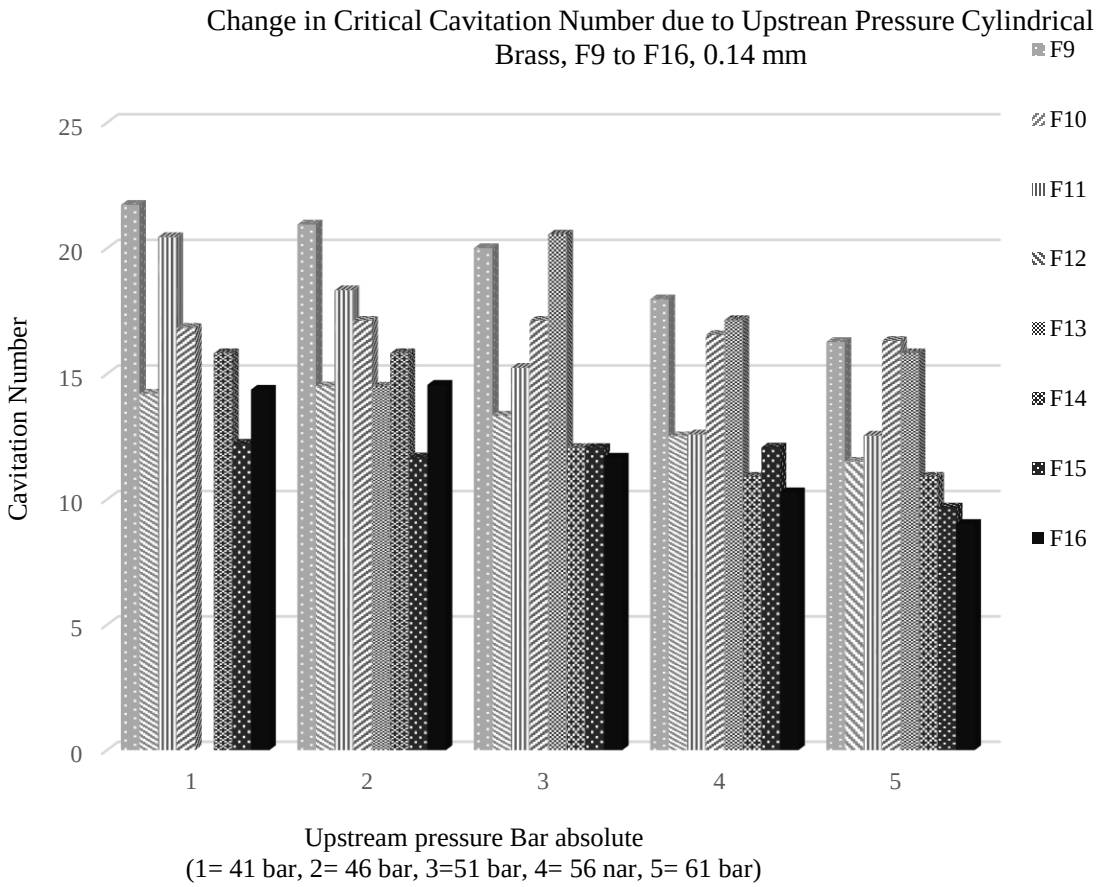

Figure 60 Critical Cavitation Number as a function of Fuel Composition, Cylindrical 0.14mm

From Figure 60, it can be observed that a decrease in the $Ca_{Critical}$ was noted as the Upstream Pressure increased. As an example, considering the 0.14 mm Cylindrical Nozzle and testing Fuel 9 at 41 bar abs for a $P_{Sat\ Vap}$ of 3.35 Pa ± 0.01 Pa (Please refer to Table 9 for detail), a $Ca_{Critical}$ of 21.73 ± 0.01 at 41bar abs was obtained. The $Ca_{Critical}$ decreased to 20.95 ± 0.01 at 46 bar abs. The $Ca_{Critical}$ decrease even further to 16.27 ± 0.01 Pa at 61 bar.

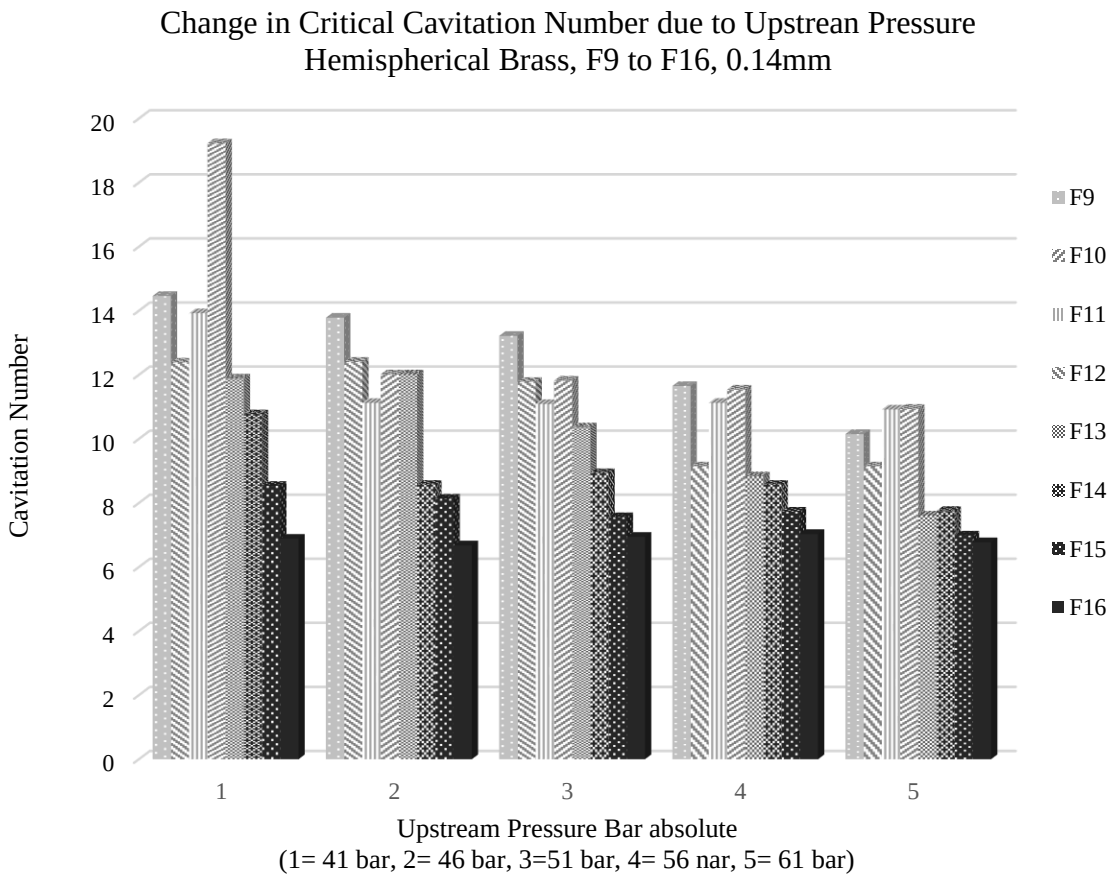

Figure 61 Critical Cavitation Number as a function of Fuel Composition, Hemispherical 0.14mm

Looking at Figure 62 below, the lower values of the $Ca_{Critical}$ were obtained when considering the Conical Nozzle compared to when considering the Cylindrical and the Hemispherical nozzles respectively.

This can be explained by the fact that, although the flow inside the Conical nozzle behaved as though a flow plug with the $Ca_{Critical}$ increasing with the increase in the n-Octane concentration, the geometry of the Conical nozzle allowed for an increase in the velocity of the jet.

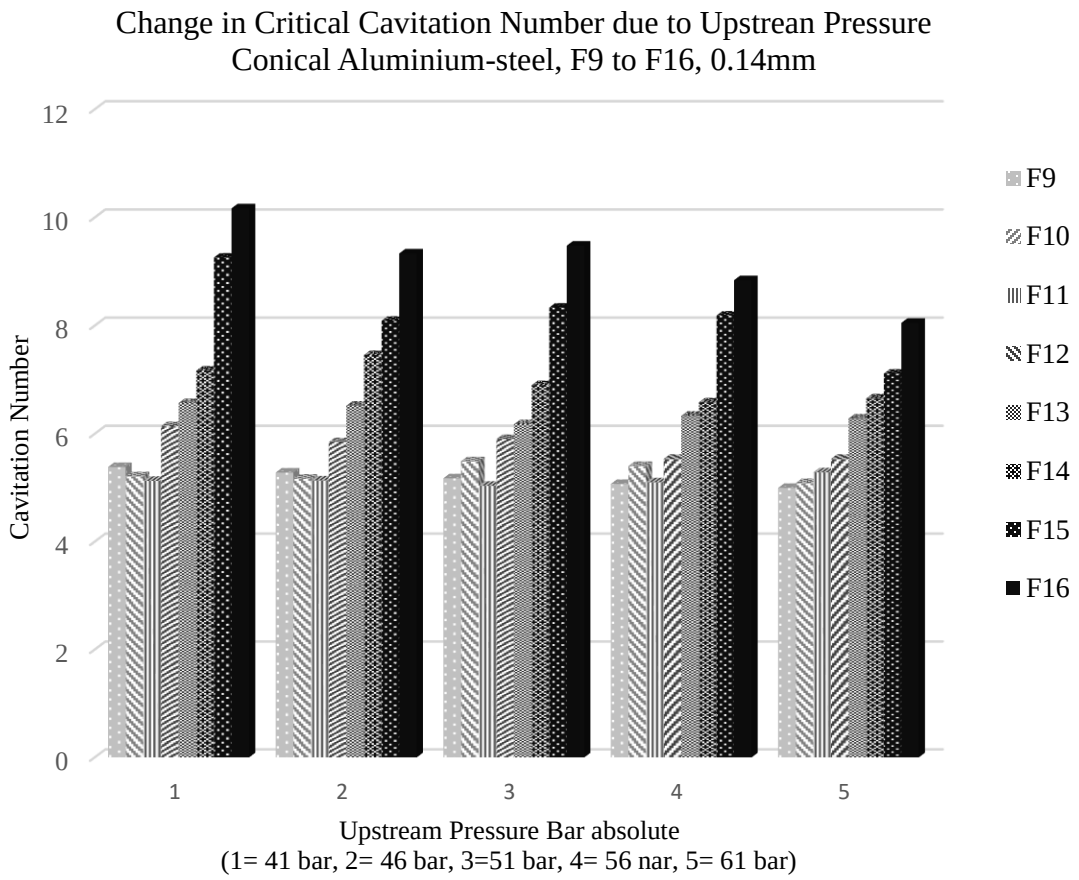

Figure 62 Critical Cavitation Number as a function of Fuel Composition, Conical 0.14mm

In comparison to the Cylindrical nozzle and the Hemispherical nozzle, the Conical nozzle was easily subjected to cavitation because of its geometrical shape which helped to speed up the flow going through the nozzle. The increase in the flow velocity led to an increase in the jet turbulence within the Fused Silica Receiver which in turn led to an increase in the cavitation bubble formation, collusion and collapse.

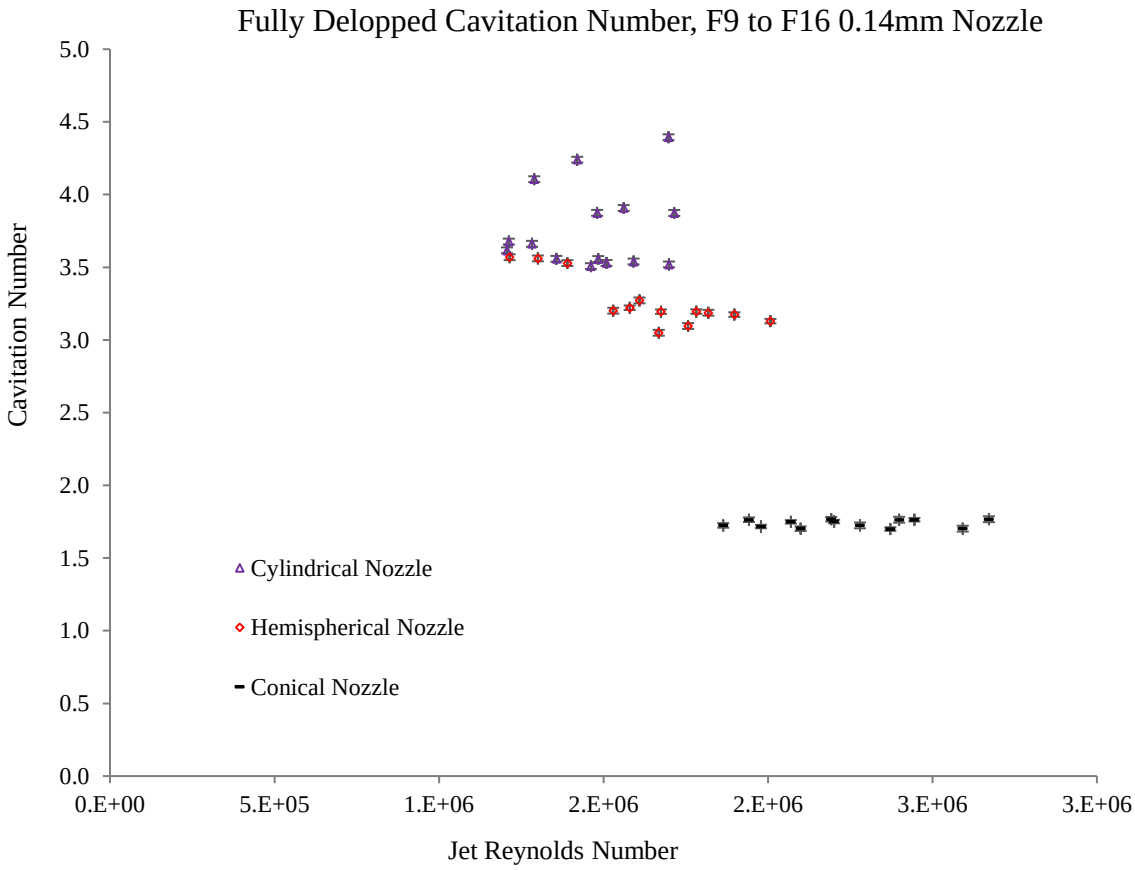

Figure 63 Fully Developed Cavitation Number as a function of Jet's Reynolds Number 0.14mm

A decrease in the $Ca_{Critical}$ was observed as the Re increased, this considering the Cylindrical as well as the Hemispherical Nozzle. This was as expected as the Re increased with the increase in the flow turbulence – an increase in the Re was noted with the increase in the n-Octane concentration. The reverse phenomenon was observed for the Conical Nozzle. [192]

As the experiment was conducted at the university, preliminary results obtained during the first stage of the experiment were published. The results demonstrated the variation of the Critical Cavitation

Number as a function of the Jet's Re considering the 0.14mm hole nozzle. [183] The results presented in Figure 63 and Figure 64 were in agreement with the preliminary results published when the experiment first took place.

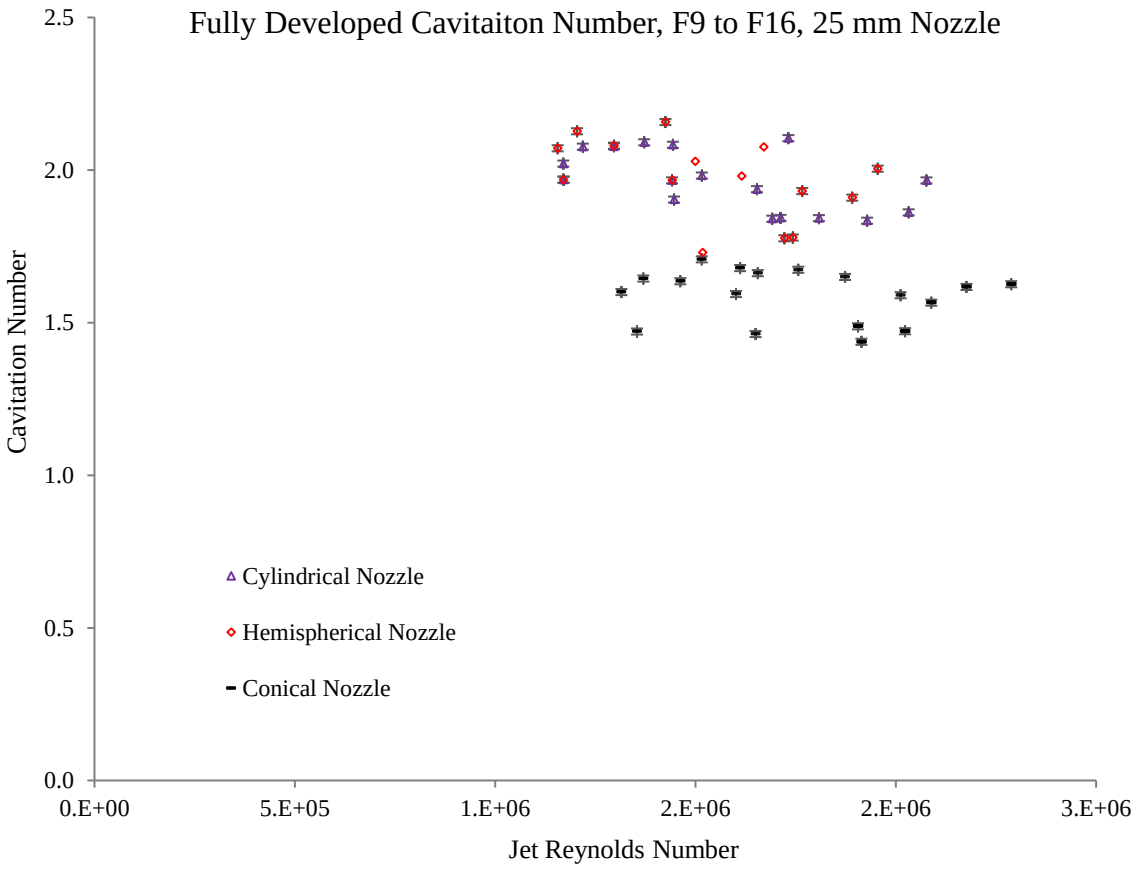

Figure 64 Fully Developed Cavitation Number as a function of Jet's Reynolds Number 0.25mm

As expected, high values of the $Ca_{Critical}$ were noted in comparison to the values obtained for the $Ca_{FullyDevp}$. As a higher value of Ca often denotes a non-cavitating flow, the higher value of the $Ca_{Critical}$ obtained in *the present study*, was justified as this denoted the start of cavitation, the point of onset [193].

Hence, higher Re were obtained from the fully developed cavitated flow. i.e. the Hemispherical $Ca_{Critical}$ varied from 5 to 15 whereas the Hemispherical $Ca_{FullyDevp}$ varied from 3 to 3.6.

The value obtained for the $Ca_{FullyDevp}$ was within the range of a typical fully developed cavitation flow inside real life ICE injectors where the Ca ranges between 0.5 and 5. [184]

Using Equation 47, the errors associated with the $Ca_{FullyDevp}$ were obtained. The errors varied from ± 0.02 to ± 0.01 as the n-Octane concentration increased.

4.2. Summary

Using the fuel matrix provided by Shell, the parametric study was conducted inside City University Laboratory where experimental data were collected for a total of 16 paraffin based fuel mixtures, tested with the use of a purposely built mechanical rig.

Hence, this part of the thesis focused of the various ways of controlling the cavitation phenomena occurring inside the fuel injector and the pump spill control valves. The control of cavitation was done by varying the physical parameters of the fuel as well as the nozzle's geometrical parameters as well as by varying the nozzle's material.

The experiment was set up as to enable the Upstream and the Downstream Pressure ratios to be measured. The study was first conducted using Acrylic – the CATIA software was used to analyze the first set of acrylic nozzles. The selection of the transparent material was considered appropriate as it was first thought that a visual access to the jet flowing inside the injector will be required. However, it was surprisingly observed that incipient cavitation started at the top of the nozzle. Moreover, crack formation was noticed on some of the acrylic nozzles. Hence a switch from Acrylic nozzles to metal nozzles was proposed. 25 runs were conducted for each fuel mixture – ensuring accuracy of the results. From this, the Upstream to Downstream Pressure ratio was obtained

considering a STDEV of the 25 measurements. As expected, for all data, an increase in the Upstream Pressure due to the increase in the Downstream Pressure was noted. To check the consistency of the results obtained, the same experiment was repeated after 2 years, this considering only the n-Hexadecane-n-Octane mixture. The results confirmed once more the increase of the propensity of the fuel to cavitate with the increase in the n-Octane concentration when considering the Cylindrical and the Hemispherical nozzle respectively. The reversed phenomenon was again observed when considering the Conical nozzle due to geometrical differences between the three types of nozzles leading to a difference in their boundary layers.

Using the Bernoulli's equation for Single Phase Incompressible liquid through the nozzle, it was possible to obtain the Cd, the Q and the V of the Hexadecane-n-Octane mixtures flowing through the nozzle. For all data, a decrease in the Cd was observed with the increase in the n-Octane concentration – the Cd values obtained from the experiment ranged between 0.5 and 0.8 and were comparable to the typical Diesel Injectors Cd values which vary between 0.5 and 0.9. Based on the work done by Chemloul [46], the Cd decreases due to increase in turbulence. This explained the decrease in the Cd observed *in the present study* with the increase in cavitation turbulence. When measuring Q, human error was taken into consideration by calculating the Standard Deviation of the experimental measurements. The deviation varied between ± 0.003 L/min to ± 0.01 L/min and did not have a major impact on the results.

Using Antoine's Equation and Rault's law, the total Saturated Vapour Pressure was obtained considering the partial saturated pressure of each mixtures. As expected, the total Saturated Vapour Pressure increased with the increase in n-Octane concentration. The results were compared to those obtained from Shell matrix in order to confirm their accuracy.

The viscosity of the mixture was seen to be affeccted by the total fuel volume, the Saturated Vapur Pressure on the other end was affected by the n-Octane concentration in the mixture. Both phenomena impacted the cavitaiton of the fuel although more is needed to understand the full impact of viscosity on cavitation.

The Critical Cavitation Number ($Ca_{Critical}$) and the Fully Developed Cavitation Number ($Ca_{FullyDevlt}$) were calculated. The values obtained were within the appropriate range; the $Ca_{FullyDevp}$ varied between 0.5 and 5. It was once more observed that the Cylindrical and the Hemispherical behaved similarly in comparison to the Conical nozzle as the flow inside the Conical nozzle behaved as though a flow plug as it experienced choking due to nozzle geometry.

Blank Page

CHAPTER V. HIGH PRESSURE SUSTAINED HYDRODYNAMIC CAVITATION OF DIESEL AND BIODIESEL FUELS – EXPERIMENTAL INVESTIGATION

5.1. Introduction

Allowing the fuel located in the spill control valve of the ICE injection system, to cavitate over a certain period of time often leads to the formation of harmful pollutants. With the use of the common rail system a big improvement has been noted in the reduction of pollutants generated from the engine combustion and the traffic congestion.

Hence, the use of the common rail system is said to have revolutionized the DI technology, leading to a decrease in the popularity of the IDI – As the fuel is injected inside the combustion chamber, high pressures reaching over 2000 bar can be observed inside the rails.

The majority of common rail system's industries has made use of a somewhat similar common rail operating system, this from when it was first invented. The operating system has remained mainly unchanged and is made up of comparable unit systems; on the hydraulic side, the common rail injectors are connected to the high pressure fuel rail with the high pressure fuel pipes. On the electronic side, the injectors are connected to the ECU with the use of engine wires. The ECU then supplies a precise voltage which depends on the amount of fuel needed to be injected, to the actuator – The high pressure pump is made up of two outlet ports, where the first port is connected to the pump solenoid spill valve which controls the fuel injection mechanism and the second port is connected to the main injector.

Scientists such as Price *et al.* [4] have concluded that the fuel flowing through the spill ports and the valves of the injector and the pump is subjected to cavitation which, is said to be responsible for the

degradation and the ageing of the fuel. The authors have furthermore concluded that fuel degradation takes place at a faster rate when considering high pressures and can impact the spray structure and atomization.

Hence it can be said that while the use of the common rail systems has led to the reduction of pollutants, it has not suppressed the problem in hand – Inside the control spill valve injector system, hydrodynamic cavitation as well as ultrasound cavitation can be observed leading to acoustic cavitation formed as a sonochemical reaction of the fuel components takes place [4] – The occurrence of ultrasound cavitation does impact the chemical composition of the fuel.

Hence Sonochemistry, which is the study of acoustic cavitation formed as a result of the ultrasound effect (the ultrasound effect takes place inside the liquid as a result of in chemical activities increase within the fluid mixture), can be used in order to study the sonochemical reaction of the fuel components.

As the fuel is subjected to high temperatures and high pressures, the chemical activities taking place within it are directly caused by the wavelength of the ultrasonic sound waves being longer than the atom's bond length.

The presence of sound waves passing through the fluid will cause the contraction and the expansion of the fluid which in turn will promotes the formation, the growth and the collapse of bubbles – As the bubbles experience in turn, a contraction and an expansion, some will collapse due to overexpansion leading to the presence of localized hot spots as heating and cooling phenomenon takes place simultaneously. In some cases, the collapse of a bubble can trigger a chain reaction leading to complex dynamic bubble collapse. [4]

The formation of primary radical reactions and secondary radical reactions takes place due to the dissociation of vapour located inside the bubbles, as they collapse due to ultrasound cavitation – the formation of stable species often lead to the formation of more species. [4, 194-195]

The simultaneous changes in the chemical composition and the changes in the physical phases taking place as the cavitated bubbles collapse, has a detrimental impact on the injector system as well as on the spray atomization processes as it is often considered irreversible.

As the use of highly pressurized injectors is increasingly on demand, manufactures are finding themselves under tights pressures requirements to respect the guidelines set by emission regulation companies in order to produce vehicles with increased combustion efficiency as well as better spray atomization.

Therefore, this part of the thesis, looked into the effect of the sustained induced hydrodynamic cavitation formation on the Diesel and the Biodiesel fuels, using a recirculating continuous rig that mimic the flow in and around the injector and the pump spill control valves systems. This part of the thesis looked at the impact of hydrodynamic cavitation as well as the effect of the internal energy compression of the fuel, taking place simultaneously inside the ICE. The study was done in order to understand the extent of pollutant formation inside the ICE due to cavitation, independently of the effect of internal energy compression.

The Laser Power Transmissivity, β as well as on the Attenuation Coefficient, α of the fuel were calculated to determine how quickly the laser penetrated the cavitated commercial fuel, RME biofuel and the GTL paraffin fuel.

.

The experiment was done for a period of 30 hours, leaving the fuel to cavitate inside the 1650 bar continuous flow Rig for 10 hours every day using a low carbon Steel Delphi HB X 6965489 single

hole Cylindrical sac nozzle. A heavy fuel will often give rise to a higher value of α in comparison to a lighter fuel as the laser beam quickly weakens as it passes through it.

The impact of the changes caused by the temperature on the fuel was separated from the impact of the changes caused by cavitation alone using a Water Bath system were the fuel was placed inside a purposely modified tea urn at 60 ^{0}C for a period of 30 hours, leaving the fuel to likewise heat for 10 hours per day – In order to make sure that both experiments started at the same temperature, 60 ^{0}C was considered for the Water Bath system as the pressurized fuel was directed to the Common Rail diesel system at a temperature of 60 ^{0}C before being subjected to cavitation.

5.2. Fuel composition, Purity and Source

The experiment tested three different fuels, the Commercial Diesel fuel (Fuel A), the biofuel Rape Methyl Ester (RME) and the Gas To Liquid (GTL) fuel provided by Shell – GTL is made up from the conversion of hydrocarbon gases such as natural gas.

An old stock (Aged Fuel A) of approximately one year obtained from the City University Thermodynamics oil store was first tested. As it run out, a new diesel fuel (New Fuel A) was purchased for the purpose of the experiment. The RME and the GTL were likewise delivered by Shell. in a 25 L container steel drum, with a Net Weight of 22kg and 124.8kg respectively at 15 ^{0}C. The Minimum Flash Point was noted as 173 ^{0}C and 94 ^{0}C for the RME and the GTL respectively. All data can be obtained from the Bio Diesel Fame Safety Data Sheet and the GTL Gasoil Safety Data Sheet for domestic and commercial heating and lighting equipment.

5.3. Schematic Model Rig design

Similar to the design of the incipient cavitation rig used in the first part of *the present study*, a detailed engineering drawing of the recirculating rig was done using the CAD software prior to the experiment. This was done in order to obtain an accurate overview of the experimental set up.

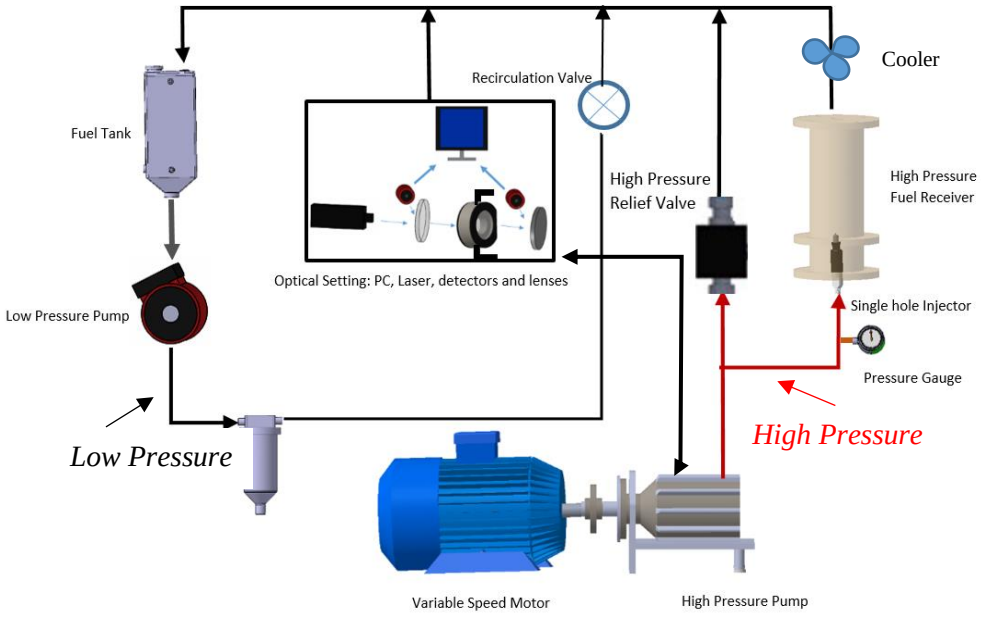

Figure 65 Design of the Continuous Rig and Optical Settings

In order to obtain the optical measurements, a portion of the fuel was redirected to the optical settings through the Bottom of the Optical Cell as it leaved the HPP.

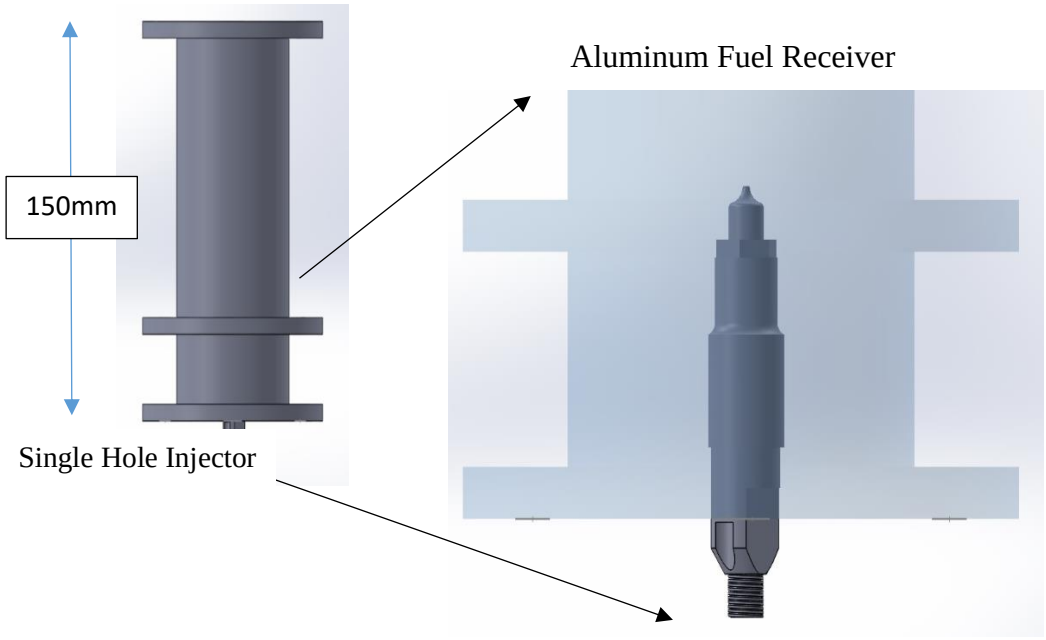

Figure 66 Close-up of the Single Hole 0.213 mm hole Delphi Injector inside the 150 mm long Aluminum Fuel receiver

Below is a close-up of the optical setting comprising the laser, detectors, Neutral Density Filter and Aluminum mirror, the Optical Cell and PC.

Fused Silica Windows of diameter of the optical Cylinder, thickness and wideness of 50 mm, 3 mm and 10 mm respectively were considered when designing the Optical Cell. The stainless steel cylinder had a diameter, thickness and wideness of 80 mm, 30 mm and 20 mm respectively.

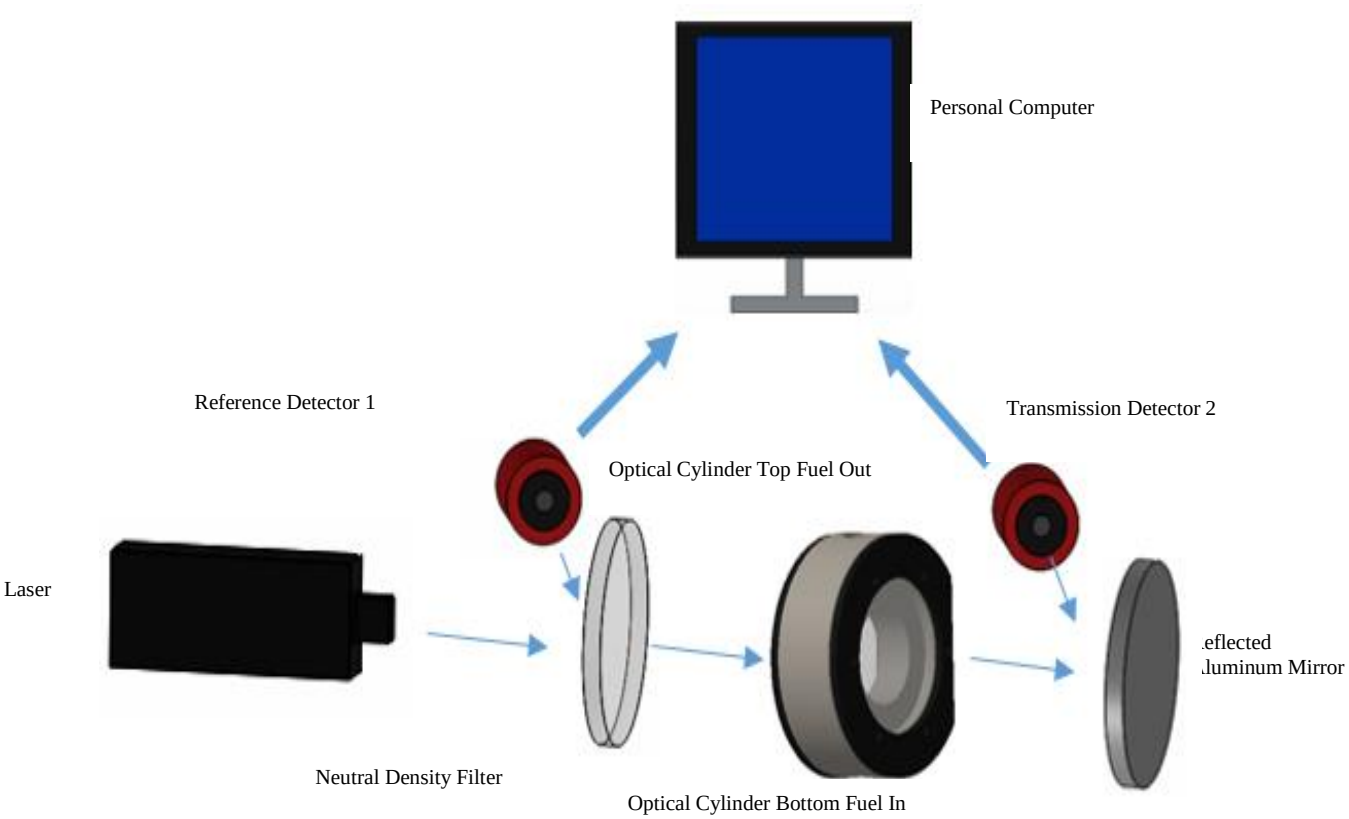

Figure 67 Close-up of the Optical Setting

5.4. Experimental Analysis and Methodology

The Rig System built for the study of the Sustained Hydrodynamic Cavitation was designed based on the design of an existing cavitation rig inside City University Laboratory.

The rig set up consisted of two distinct parts; the continuous flow rig as well as the optical setting.

5.4.1. Rig Set Up Part One

The Continuous Flow Rig was made up of a 3.5 L Tank, a Low Pressure Pump (LPP), a fixed displacement HPP, a 5 μm nylon fuel Filter, a cooler, a variable motor and a 0.4 mm hole Injector. The rig was flushed prior to the experiment in order to remove all sources of impurity contained inside it. The fuel located inside the 3.5 L tank was initially filtered and delivered to the HHP. The temperature, being set previous to the fuel entering the HHP, was recorder between 40^0C and 45^0C. The pressurized fuel was than directed to the Common Rail diesel system and hence it was directed to the injector system– The Common Rail diesel system is designed so that the fuel coming from the HPP is carefully separated and distributed to the individual injectors.

Figure 68 Continuous Flow Rig

The fuel leaving the HHP had an average controlled temperature of around 60 ^{0}C. A rise in temperature was noted as the fuel flew pass the Injector, reaching up to 110 ^{0}C – The raise of temperature was noted due to boiling of the fuel induced as cavitation formation took place as the pressure was set to1650 bar. The use of a cooler was necessary in order to cool down the fuel which was then returned to the tank at a temperature of 40 ^{0}C – this was vital in order to avoid the constant increase in the temperature of the recirculated fuel as the fuel was left to cavitate.

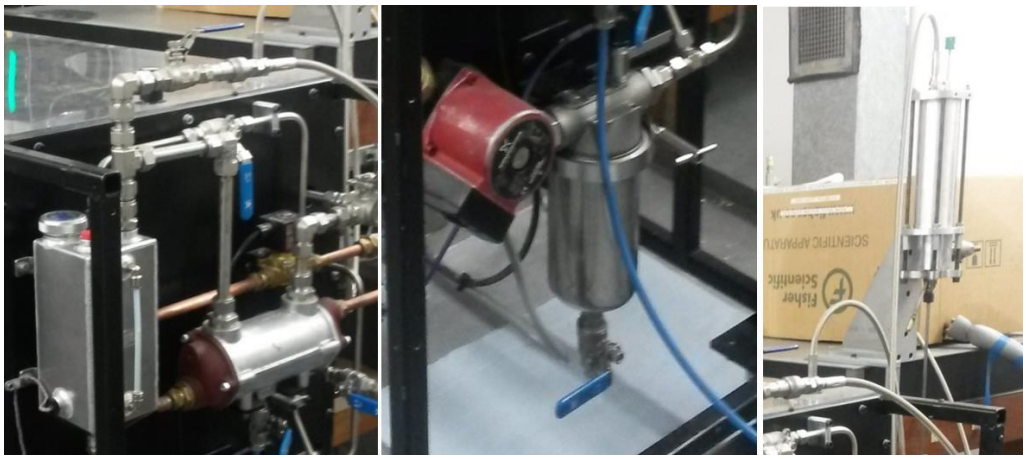

Figure 69 Close-up of the Continuous Flow Rig showing the Tank, the LPP, filter and the Injector placed inside the Aluminum Fuel Receiver.

The fuel filter was replaced after each fuel mixture experiment was performed in the aim to maintain consistent results.

Figure 70 Needless 0.213 mm hole diameter, low carbon Steel Delphi HB X 6965489

In order to avoid cases of pressurized fuel being returned to the pressure pump due to the presence of the needle inside the injector, the injector needle was removed assuring a continuous fuel flow throughout the system.

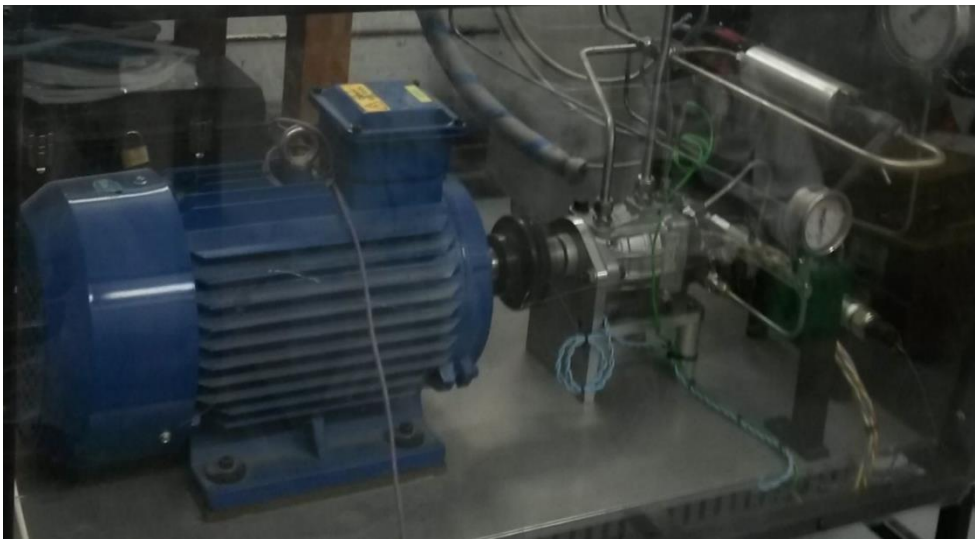

Figure 71 Variable Speed Motor connected to the HPP

Cavitation was induced by controlling the speed of the 1600 rpm variable motor, considering a fine or a coarse adjustment. Being able to physically control the Injection pressure meant that a fix pressure could be set for the purpose of the experiment. A tachometer was used to read the pressure

being set. The cylinder was prefilled with fuel prior to conducting the experiment allowing the pressurized jet to flow through a receiver filled with fuel at atmospheric pressure.

By means of linear extrapolation the actual Volume Flow Rate ($Q_{1650bar}$) of the 0.213 mm nozzle at 1650 bar pressure was derived from the Volume Flow Rate of the same nozzle at 1000 bar pressure ($Q_{1000bar}$) as well as at 1350 bar pressure ($Q_{1350bar}$). (Zeeshan Fatmi, Private Communication, September 2016).

Circulating fuel Volume Flow rate		
Diesel Density ρ_f	832	Kg/m3
Nozzle Hole Diameter D	0.000213	m
Cross Sectional Area	0.0000000356	m2
Coeff Of Discharge C_d	0.8	
Delivery Pressure P_D	165000000	Pa
Received Pressure P_R	100000	Pa
Bernoulli Velocity V_B	629.598	m/s
Mass Flow Rate	0.0187	Kg/s
Theoretical Volume Flow Rate Q_T	1.0759	L/min
Actual Volume Flow Rate $Q_{1650bar}$	~ 1.129 ± 0.001	L/min

Table 11 Calculation of the Volume Flow Rate

The Bernoulli Velocity was obtained in order to obtain the theoretical Volume Flow Rate Q_T using Equation 51

$$V_B = \sqrt{\frac{2(P_D - P_R)}{\rho_f}} \quad \textit{Equation 52}$$

$$V_B = \sqrt{\frac{2(1650 \times 10^5 - 1 \times 10^5)}{832}}$$

$$V_B = 629.598 \ {}^{m}/_{S}$$

Hence the theoretical value of Q_T was obtained using Equation 52.

$$Q = C_d \times V_B \times Area, \quad \textit{Equation 53}$$

$$Q_T = 0.8 \times 629.598 \times 0.0000000356$$

$$Q_T = 1.0759 \ {}^{L}/_{min}$$

Using linear extrapolation, $Q_{1650bar}$ was obtained by considering the mean value of $Q_{1000bar}$ of 0.909 L/min and 0.885 L/min as well as the mean value of $Q_{1350bar}$ of 1.058 L/min and 1.035 L/min, directly measured from the laboratory. Hence, $Q_{1650bar}$ was calculated as 1.129 L/min.

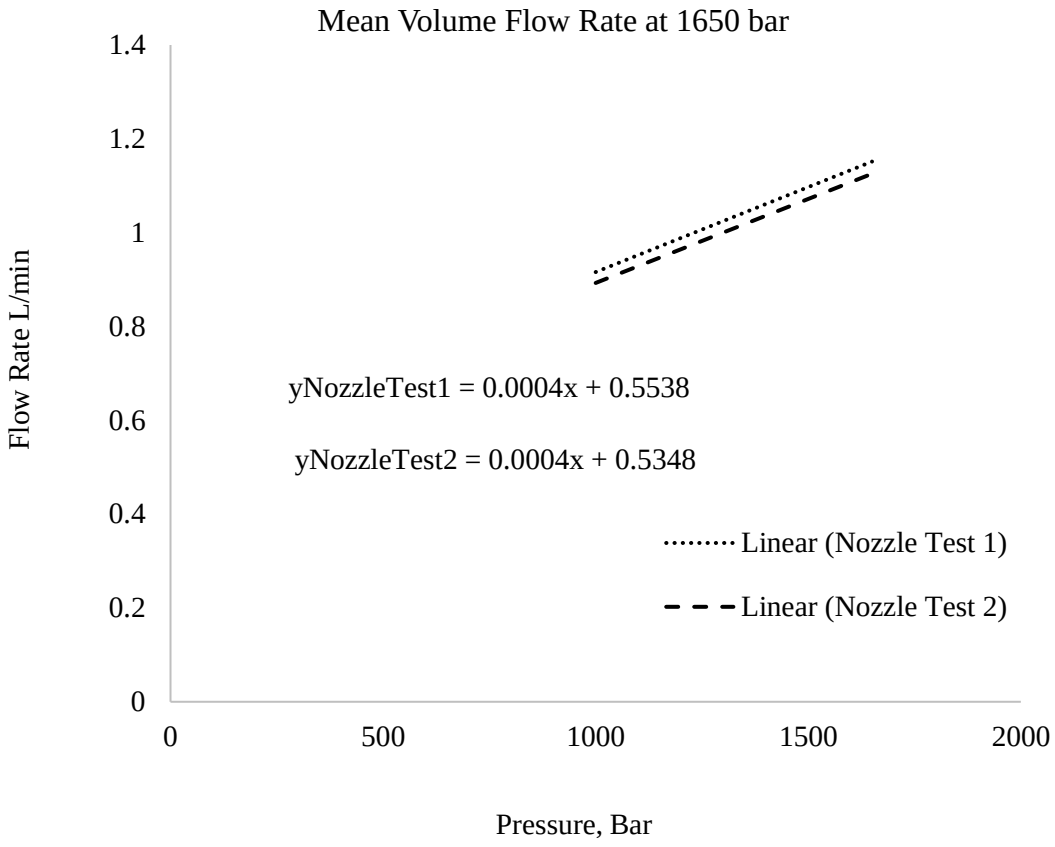

Figure 72 Determination of the Actual Mean Volumetric Flow Rate at 1650 bar pressure

5.4.2. Rig Set Up Part Two: Optical Set Up

The first step was to setup the PC Link software, the second steps consisted of properly connecting the laser and detectors to the PC. (Refer to Figure 67).

5.4.2.1. The PC Link Software

The PC Link Software obtained from Laser Point Company, was installed onto the PC where the laserPoint detector head was connected to the interface unit – The PC Link was connected to a USB

port used to convert signals received onto the PC into a laser Power/Energy reading. The temporal variation of the power transmitted and the power reflected by the laser beam was obtained from the detectors. Hence the temporal variation was displayed on the Visual interface of the PC Link software.

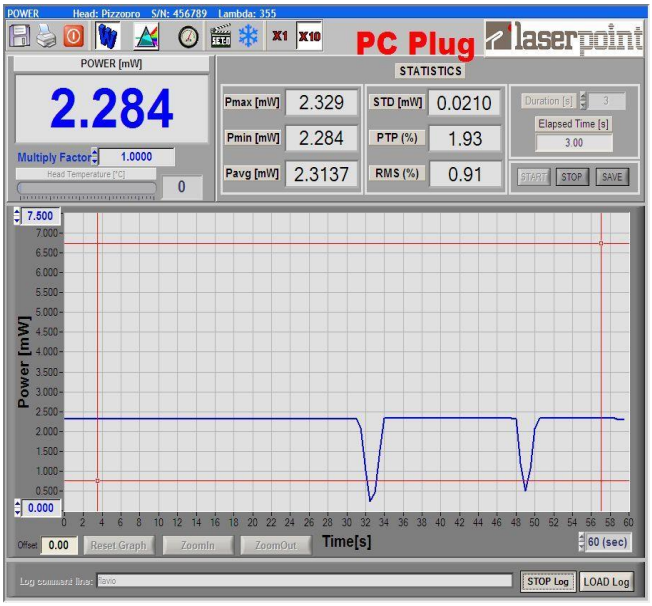

Figure 73 PC Link Software Interface [196]

The average value of the transmitted power and the reflected power measured during the last acquisition interval, Pavg (W) was obtained considering the maximum power obtained during the last acquisition interval, Pmax (W), as well as the minimum power, Pmin (W) obtained during the last acquisition interval.

Pavg Transmitted was divided by Pavg Reflected in order to obtain the Power transmission of the laser beam – A decrease in the transmissivity indicated that the laser was losing its ability to easily penetrate the fuel.

ZeroHrsFuelADay4_08-04-13_1 - Notepad

le Edit Format View Help

02BBF Vis 090347

on Apr 08 15:25:03 2013

Date	Time	Pmax (mW)	Pmin (mW)	Pavg (mW)	PTP	STD	RMS
Apr 08 2013	15:26:19	0.0	-0.0	0.00	200.00	0.002	1337.9
Apr 08 2013	15:27:19	0.0	0.0	0.00	100.00	0.003	331.66
Apr 08 2013	15:28:19	1.7	0.0	0.64	100.00	0.768	119.39
Apr 08 2013	15:29:19	1.6	1.5	1.57	4.35	0.019	1.23
Apr 08 2013	15:30:19	1.5	1.5	1.53	1.94	0.008	0.51
Apr 08 2013	15:31:19	1.5	1.5	1.51	1.96	0.007	0.44
Apr 08 2013	15:32:19	1.5	1.5	1.51	2.63	0.007	0.44
Apr 08 2013	15:33:19	1.5	1.5	1.50	1.99	0.011	0.70
Apr 08 2013	15:34:19	1.5	1.5	1.49	1.99	0.011	0.71
Apr 08 2013	15:35:19	1.5	1.5	1.49	1.99	0.011	0.71

Figure 74 Example of PC Link Software Power Intensity Results output

5.4.2.2. Laser and Detectors

Here a standard positioning of the laser used in the study of spectral scattering and absorption was considered. The carefully calculated distances [3] allowed for the reading of the laser beam intensities measurements.

The 405nm laser shined through the 1 cm thick fuel as it flew through the Optical Cell. Detector 1 and Detector 2 were used to record the laser beam intensity as it penetrated the fuel. Hence, the measurements were collected using a Personal Computer (PC). At this point the fuel was redirected to the tank passing through the Top of the Optical Cell. The High Pressure Relief Valve connected to the tank, was set to 1800 bar and placed downstream of the HPP in case an emergency was to occur where the pressure will be released to avoid bursting of the injector placed inside the fuel receiver.

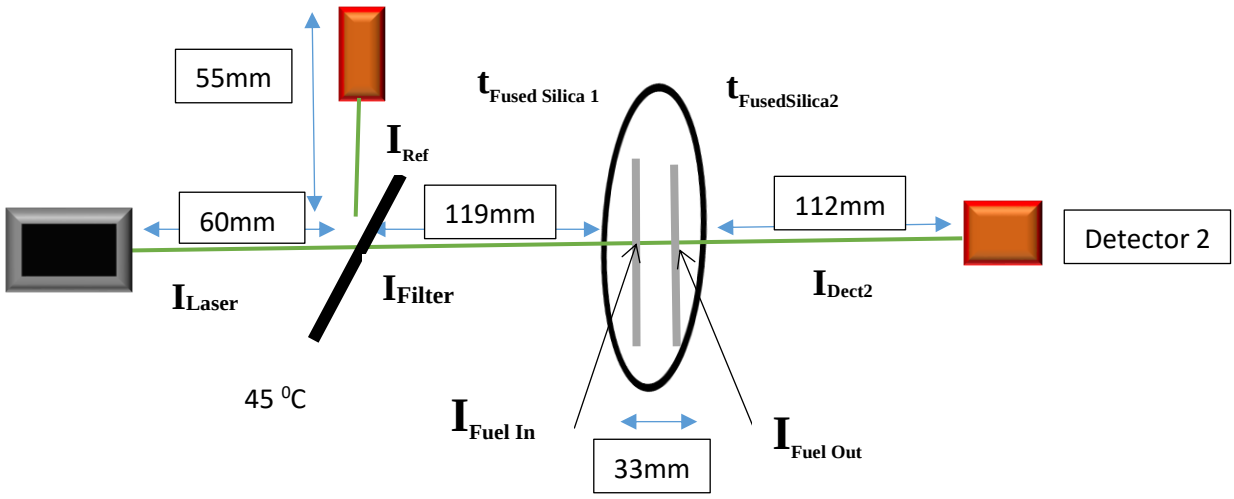

Figure 75 Optical Set-up

I_{Laser} Full laser bean intensity

I_{Filter} - Part of intensity I_{Laser} transmitted through Filter

I_{Ref} - Part of Intensity I_{Laser} reflected by the beam Filter

$t_{Fused\ Silica1}$ Fused Silica window transmissivity through the Optical Cell Window1

$t_{Fused\ Silica2}$ Fused Silica window transmissivity through the Optical Cell Window2

$I_{Fuel\ In}$ Intensity as laser enters the fuel

$I_{Fuel\ Out}$ Intensity as laser prepares to leave the fuel

I_{Dect2} Intensity to the second detector

Using the Beer-Lambert Law which represents the relationship between the properties of the medium through which the beam is moving and how fast the beam is being attenuated, it was possible to calculate α. The Beer-Lambert Law was made use of when setting up the optical equipment.

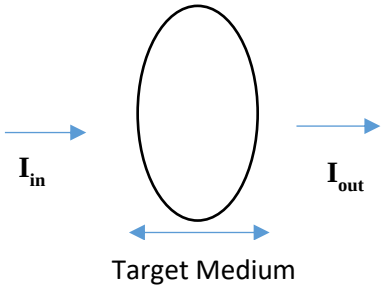

Figure 76 Intensity in and out of the medium

α denotes the capacity of one medium to gradually decrease the intensity of the other medium going through it – α consist of the scattered as well as the absorption coefficient.

The laser beam can experience one or both phenomena where, the intensity of the light is reduced due to absorption and scattering. The use of detectors helped to determine the impact of the intensity of the light due to absorption and/or scattering. As the absorption coefficient is used for measuring how fast the laser beam intensity lessens as a result of absorption, the absorption taking place in the Neutral Density Filter as well as the Optical Cell were considered to have an impact on the overall intensity of the laser beam.

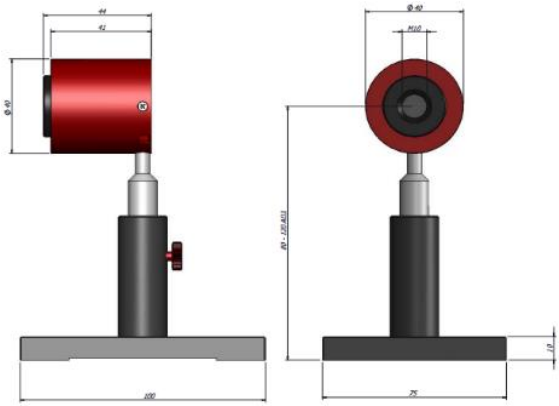

Figure 77 Detectors used during the experiment

The detectors comprised sensitive thermopile sensors for Low Power laser which can detect power as low as 10μW and energy of up to 2mJ.

In *the present study*, α was used to obtain the impact of absorption and scattering considering a narrowed beam were the detectors read the reflected as well as the transmitted laser intensity – α is used to predict the amount of attenuation that will take place per path length.

$$\propto = \propto_{absorbed} + \alpha_{Scattered} \quad \textit{Equation 54}$$

Where $\propto_{absorbed} \gg \alpha_{Scattered}$,

Hence,

$$\alpha = \propto_{absorbed} \quad \textit{Equation 55}$$

The total transmitted beam intensity I_{Out} through a medium equals the beam Intensity I_{in} multiplying by the natural logarithm of the Attenuation Coefficient α and the path length (l).

$$I_{Out}(l) = I_{in} e^{-\alpha l} \quad \textit{Equation 56}$$

The transmittance Tr was obtained using Equation 56.

$$Tr = \frac{I_{Out}}{I_{In}} = e^{-\alpha l} \quad \textit{Equation 57}$$

The self-normalised signal was plotted using equation 57. The self-normalized signal is considered as the true scale of the change in the signal and is used for comparing the relative variation of the results obtained from a matching starting point.

$$Self - Normalised\ intensity = \frac{\frac{I}{I_0}(t)}{\frac{I}{I_0}(t0)}, \quad \textit{Equation 58}$$

The Spectral Attenuation Coefficient α(t), was obtained using Equation58.

$$\alpha_{(t)} = -\frac{ln\frac{I_{In(L)}}{I_{Out(L)}}(t)}{l} \quad \textit{Equation 59}$$

As the $\propto_{Scattered}$ value was considered to be extremely small, the total α was equalled to the Absorption Coefficient, $\propto_{absorbed}$ only.

Care must be considered when calculating α as a change in the chemical as well as a change in the physical features of the mediums may easily affect the linearity of the Beer-Lambert law – an uneven medium thickness concentration may lead to a deviation of the absorptivity coefficients when considering high concentrations regions because of the electrostatic interactions occurring between molecules that are closely packed to each other. However, using the maximum absorption band, this considering a nonmonochromatic radiation, the deviations can be reduced.

5.5. Operational Procedures

The rig, was purposely built inside City University laboratory where Fuel A, RME and GTL hydrocarbon fuels were tested. Consideration was given to all aspects of the health and safety regulations to be observed when conducting experiments using highly pressurized devices.

To start with, all operating machineries were turned off enabling the rig to be drained. Here the valve to the LPP was closed, the pipeline connected to the filter was removed, the HPP was drained as well as the rest of the fuel left inside the filter. 2.5L of fuel was drained from the cooling unit. At this stage, the injector cylinder was drained as well as the high pressure piping and pump along with the fuel contained inside the common rail. 3.5 L of 95% n-Hexadecane was used to flush the rig where an injection temperature of 40 ^{0}C and a pressure of 300 bar were set. The procedure took around 30 minutes to be completed. The rig was filled starting with the pipping system and the filter. At this stage, the HPP was turned on to a maximum of 20 bar to fill the injection cylinder. The Flushing procedures were repeated for a second time. Hence the rig was ready to be filled.

The PC Link 2 Software was turned on in order to run the rig. Following a set of directions, the pressure controls and the emergency controls were set. The LPP was turned on, making sure that all emergency stops were lifted. Hence the start button was pressed on and the operating key was released. The next step was to power the 405 nm laser. At this stage, a note of the temperature reading at the inlet of the HPP was required before turning the HPP on.

Please refer to Appendix B for a detailed explanation of the operational procedures.

5.6. Experimental Equipment Calibration

An optical equipment calibration took place prior to the experiment. The optical calibration was conducted in order to consider the impact of the Neutral Density Filter and the Optical Cell on the final Attenuation Coefficient. The heating test calibration on the other hand, was conducted in order to consider the impact of the high temperatures occurring inside the rig as the fuel undergoes recirculated sustained hydrodynamic cavitation.

5.6.1. Optical Equipment calibration setup and Methodology

It was deemed unnecessary to completely recalibrate the optical equipment as this was previously done by researchers at City University while completing a similar experimental procedure [27] – although the previous experiment made use of different parameters (different rig, fuels, nozzle, pressures, etc.) the optical set up reminded the same.

Hence the optical calibration employed considered two cases where the first case took into account the full laser beam power and the second case considered the beam going pass a Neutral Density Filter.

Hence, the Reference pPower and Transmitted Power through the detectors were obtained.

Case 1 The Full Beam Power was considered without the use of the Optical Cell and without the use of the Neutral Density Filter. The average Reflected Power was set to zero. Hence the average Transmitted Power was obtained as 14.507 mW.

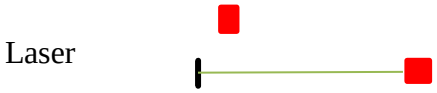

Figure 78 Laser Full Beam Power Arrangement

Case 2 The Neutral Density Filter was considered without the use of the Optical Cell

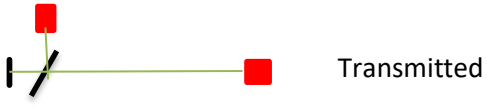

Figure 79 Laser Beam Power Arrangement with Neutral Density Filter

The transmitted intensity was obtained as 13.00143 mW while the reference was obtained as 1.429 mW. Hence the transmissivity was obtained as 9.101 mW. The transmittance percentage, which reflected the total beam power intensity, coming from the Neutral Density Filter was obtained as 89.62% this considering the percentage loss from the transmitted beam intensity in case1, 14.507 mW and case2, 13.0014 mW. This meant that 10.38% where absorbed by the Neutral Density Filter placed at 45 degree angle and was recorded into detector 1.

5.6.2. Heating Test Calibration setup and Methodology

As the fuel recirculated inside the Continuous Flow rig, it was subjected to high temperature levels which in turn impacted the fuel's chemical properties. Hence a heating calibration test was done to determine the effect of heating the fuel as it is subjected to cavitation.

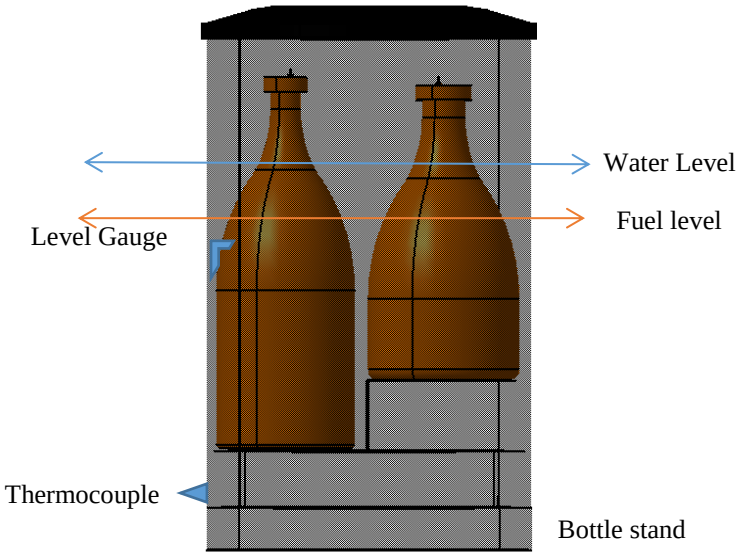

Figure 80 The Water Bath Setting using a Modified Tea Urn (Design not to scale)

The heating calibration was done using a modified Tea Urn – the Urn was modified as to accommodate two bottles of fuel of 2.5 L and 1L respectively.

The modified Tea Urn calibration test was done following all safety precautions in order to avoid incidents occurring while heating the fuel at 60^0C.As such, a thermocouple as well as a Level Gauge were used to carefully control the temperature level and the water level respectively.
A 1mm tube, attached on the top of each bottle's cap allowed the fuel to breath, avoiding cases of sudden bottle burst due to temperature build up.

At the start of the experiment, setting the LPP at 0.5 bar gauge and making sure the HPP was not running in order to avoid inducing cavitation, each fuel sample (new samples were considered for each heating calibration test) was placed inside the rig to collect the Pre-Heating average Reference and Pre-Heating average Transition Power measurements. Hence the samples were poured inside the bottles and then successively placed inside the Urn. The fuel samples were heated for 30 hours, 10 hours over 3 days – the heating tests were conducted for 3 of the 4 tested fuels: The New Fuel A, the GTL and the GTL+RME. Approximately 30 minutes were needed for the water temperature and the tea urn temperature to reach 60^0C.

At the end of each 10 hours, the fuel samples were placed aside and allowed to cool down reaching room temperatures. The fuel was then place back inside the rig the following day in order to collect the Post-Heating average Reference and Post-Heating average Transition Power measurements. The percentage change in the transmissivity of the fuel helped to determine the changes caused by heating

alone and was compared to the percentage change in the transmissivity of the fuel due cavitation and heating.

5.7. Spectral Attenuation Coefficient Calculation

In order to obtain the Intensity of the beam going in and out of the fuel $I_{In\ Fuel}$ and $I_{Out\ Fuel}$, it was necessary to calculate the Intensity of the laser beam through the Neutral Density Filter and the Optical Cell Window$_1$ and the Optical Cell Window$_2$. The transmissivity of the Neutral Density Filter was obtained considering the intensity through the laser I_{Laser} and the intensity reflected by the Neutral Density Filter Iref.

Hence, using equations previously derived by researchers at City University, it was possible to obtain the value of α, considering the Fuel A, GTL and RME.

α was then calculated using Equation 59.

$$\alpha\ (t) = \frac{ln\frac{a}{b}}{l} \quad \textit{Equation 60}$$

Where

$$a = t_{FusedSilica1} \times t_{FusedSilica1} \left(\frac{1-r_{fuel}}{r_{fuel}}\right) r_{mirror}\, I_{Ref} \quad \textit{Equation 61}$$

And

$$b = I_{Dect2} \quad \textit{Equation 62}$$

Hence α was obtained using Equation 62 [3] when considering Fuel A.

$$\alpha_{(t)} = \frac{ln\frac{7.63\, I_{Ref}}{I_{T2}}(t)}{1.03}$$ *Equation 63*

Equation 63 [3] was used when considering GTL and RME fuels

$$\alpha_{(t)} = \frac{ln\frac{8.76\, I_{Ref}}{I_{T2}}(t)}{1.03}$$ *Equation 64*

Blank Page

CHAPTER VI. HIGH PRESSURE SUSTAINED HYDRODYNAMIC CAVITATION OF DIESEL AND BIODIESEL FUELS – RESULTS AND DISCUSSIONS

In order to mimic the activities taking place inside the fuel combustion system, the rig was built to promote the formation of cavitation due to constant recirculation of the fuel. The system was designed so that one side of the rig was subjected to high pressures (pump, injectors, common rail system) and the other side was subjected to the low pressures (low pressure pump, fuel tank), in the aim to tackle the cavitation phenomenon occurring inside Diesel injection systems such as injectors and pumps spill control valves.

The results of the normalised Transmission Signal (which represent how easily a material can be penetrated by the laser) along with the results of the normalised spectral Attenuation Coefficient (which represents how much the laser deteriorate as it penetrates the material) obtained from the 30 hours' cavitation experiment, were represented in this chapter.
The results of the 30 hours' heating tests were likewise presented highlighting the effect of cavitation as well as the effect of heating.

6.1. Commercial Diesel (Fuel A), Gas to liquids (GTL) and Rapeseed Methyl Ester (RME) fuel investigation at 1650 bar

Before and after the 30 hours' cavitation experiment took place, each fuel was poured into the rig where the reference power and transmission power were obtained.

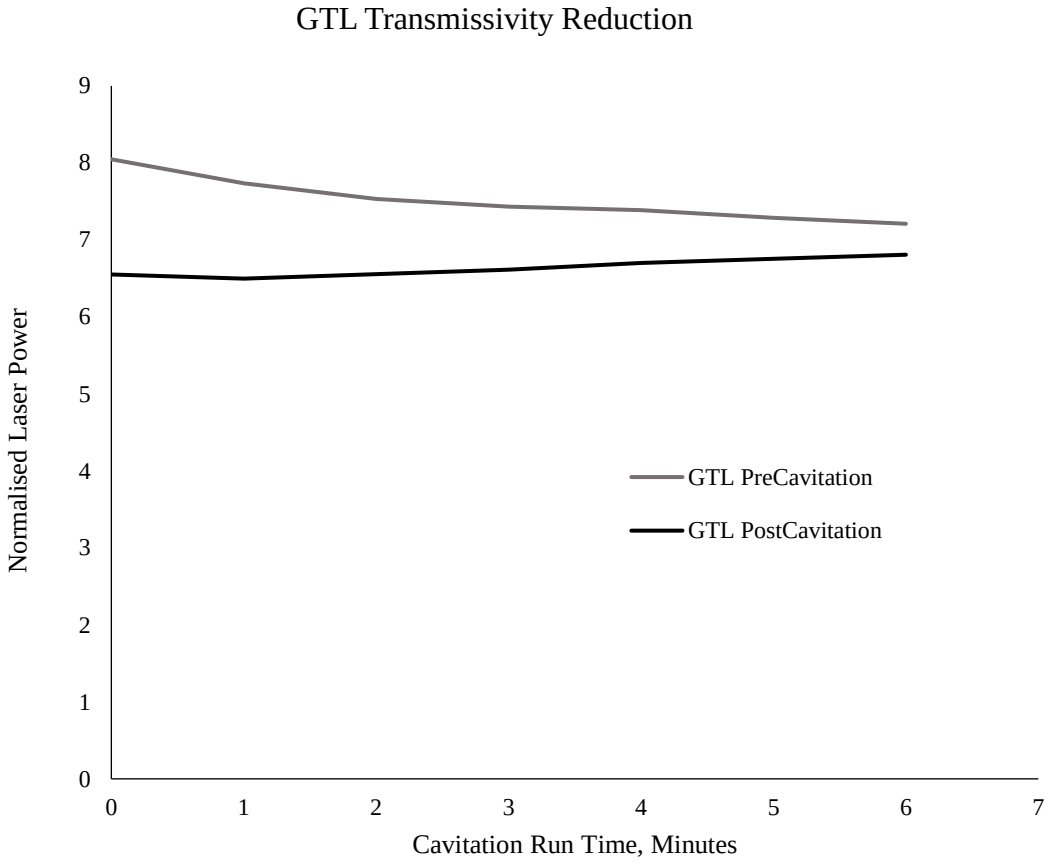

Figure 81 Average laser Power plotted against time, before and after cavitation

Plotted above is the normalised laser power intensity of the GTL obtained before and after the start of the experiment. The results were obtained by dividing the transmission power over the reference power for a 6 minutes' period.

Considering the GTL fuel, as expected a decrease in the laser intensity was noted from 8.046 before cavitation to 6.55 after cavitation at around 10 seconds after testing.

6.1.1. Normalized and Self-Normalized Transmissivity Signal

Each of the Normalised/Self-normalised graphs plotted in this section was made up of three distinct curves, (please refer to Figure 82), representing the sustained hydrodynamic cavitation experiment taking place over three distinct days.

The laser power reference and transmission readings obtained from the PC Link software were averaged from 1 minutes to 15 minutes in order to obtain an average of the effect of temperature that varies due to cooling, on the laser power transmission as it passed through the fuel.

All graphs showed a decrease in the transmission intensity where the average reference power intensity results varied from a maximum to a minimum value.

When considering the Aged Fuel A, the average Reference Power intensity varied from 1.849 ± 0.001mW to 1.550 ± 0.001mW respectively. The Average Transmitted Power intensity on the other hand varied from 3.612 ± 0.001mW to 2.639 ± 0.001mW respectively. For the New Fuel A, the average Reference Power intensity varied from 1.732 ± 0.001mW to 1.573 ± 0.001mW respectively and the Transmitted Power intensity varied from 2.701 ± 0.001mW to 3.446 ± 0.001mW respectively.

Averaged Intensity Day1 to Day3 ± 0.01mW	**Aged Fuel A**	**New Fuel A**	**GTL**	**GTL+RME**
Reference power intensity	1.849	1.732	1.559	1.659
Maximum and Minimum	1.550	1.573	1.719	1.500
Transmitted power intensity	3.612	3.446	12.672	6.150
Maximum and Minimum	2.639	2.701	11.401	4.321

Table 12 Average Intensity of Diesel and Biodiesel fuels tested

Looking at Figure 82 below, as expected the normalised laser Transmission Power signal decreased with time as the laser beam transmitted through the fuel experienced a decrease in strength due to cavitation. The normalised laser Transmission Power signal decreases due to the high temperatures obtained as a result of bubble collapse as well as, as a result of recirculation leading to the emergence of carbonaceous materials [4, 194-195] as sonochemistry takes place which in turn affected the purity of the fuel – a high Transmission Signal show how easily a material can be penetrated by the laser. The deposits formed can be compared to soot particles obtained from a diesel fuel flame.

Lockett *et al.* [194], making use of the same cavitation rig used in *the present study*, and considering equivalent pressure and temperature conditions, found out that the normalised laser Transmission Power decreased with time as cavitation took place. The authors discovered that the changes observed in the fuel composition were not dependant on the Upstream Pressure but were dependent on the volumetric flow rate as an increase in the volumetric flow rate led to an increase in the number of bubbles subjected to cavitation. The authors concluded that the degradation of the fuel took place inside the receiver downstream of the nozzle and hence they concluded that as the bubble collapse took place inside the receiver the change in the fuel composition was due to an ultrasound induced cavitation. Henceforth, based on those conclusions it seemed plausible to compare the results obtained from *the present study* to those obtained from studies conducted by researches such as Jeshani [3] who made use of a 550bar pressure and a volumetric flow rate of 4L/min considering a 5-hole asymmetric nozzle recirculating rig in his study of sustained hydrodynamic cavitation. In *the present study*, a volumetric flow rate of 1 L/min was obtained considering a single asymmetric nozzle.

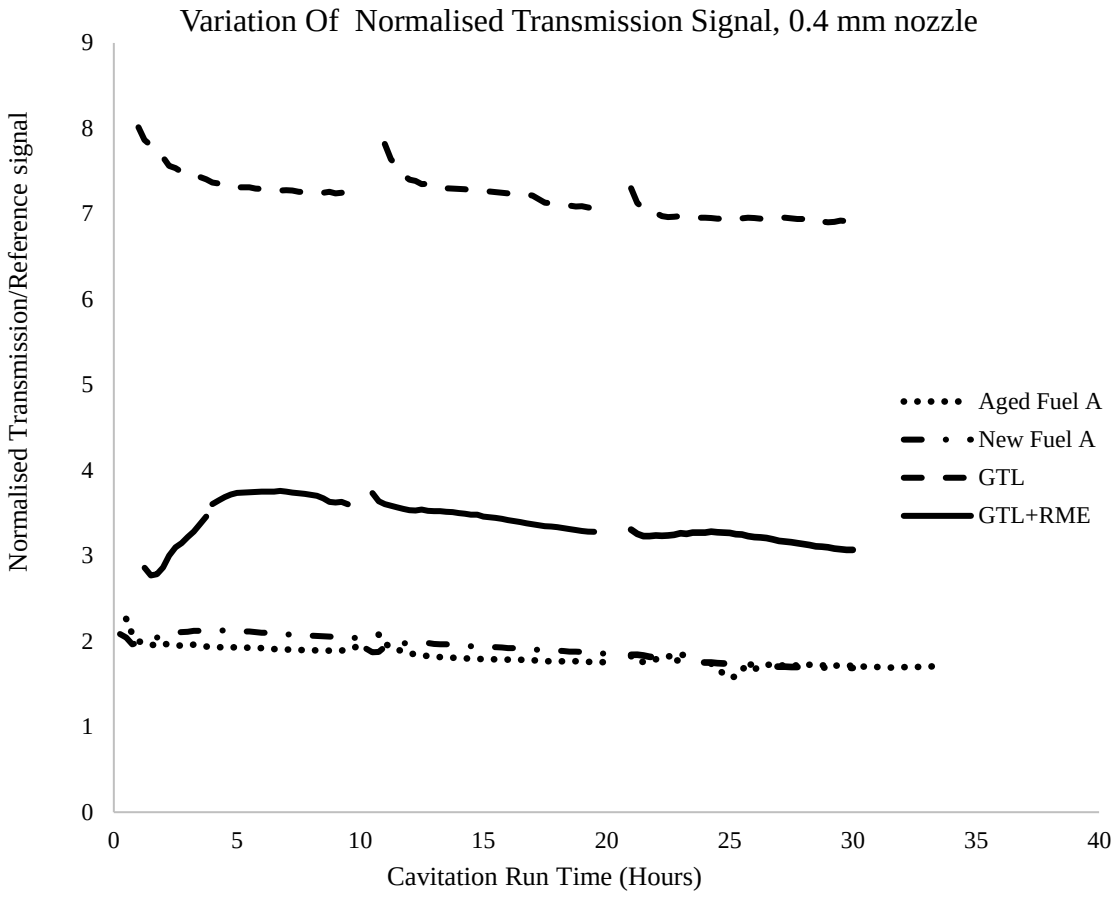

Figure 82 Normalised Transmission Signal of all tested fuels

Looking at the four graphs of Figure 82, they followed the same pattern. The four graphs are each subdivided into three different sections representing the 3 days during which the cavitation experiment took place. Looking at day two of the GTL for example, the first part of the curve represents the set of results obtained as the rig was turned on at the beginning of the experiment – during this period, the temperature was stabilized leading to a slight decrease in the laser Transmission Signal. The middle part of the curve contains more accurate results information collected for a longer period of time. The third part represents the results obtained as the different components of the rig (the pump, the laser, etc.) were turned off before the PC Link software was

turned off – the PC will still be emitting results for a few seconds at this point. The results obtained during the third part of the experiment depended on the amount of time taken by the laboratory personnel conducting the experiment to shut down the system at the start of the experiment. A this point, the Normalised Transmission Signal of the GTL decreased as the temperature of the rig was stabilised. A similar pattern was noted for the New Fuel A and the Aged Fuel A. Researchers at City University obtained similar results when looking at the changes in the Normalised Laser Transmission of Diesel mixed with paraffin based fuels. [3]

Similar to Lockett *et al.* [194] who discovered that the fuel was altered chemically as sustained hydrodynamic cavitation took place, a higher absorption rate was obtained for the Aged Fuel A in comparison to the New Fuel A.

The Aged Commercial Diesel fuel reached the lowest Normalised Transmission Signal as it was greatly affected by cavitation in comparison to the other 3 fuels. As expected, the aged fuel had the highest percentage reduction in Normalised Transmission Signal over the 3 days period as the laser intensity was considerably reduced due to cavitation. The Aged Fuel A was visually inspected at the end of the experiment – the fuel was darkened in comparison to the start of the experiment as well as in comparison to the other 3 fuels. The percentage reduction of the Normalised Transmission Signal over the 3 days period was noted as 31.452% ± 0.001% for the Aged Fuel A and 20.626% ± 0.001% for the New Fuel A respectively. Apart from the difference in the chemical composition of the fuels, the difference in percentages between the Aged Fuel A and the New Fuel A was due to the fact that the Aged Fuel A was left inside the laboratory for a number of years before the experiment, therefore contented impurities before the experiment.

The self-normalised signal was plotted using Equation 58.

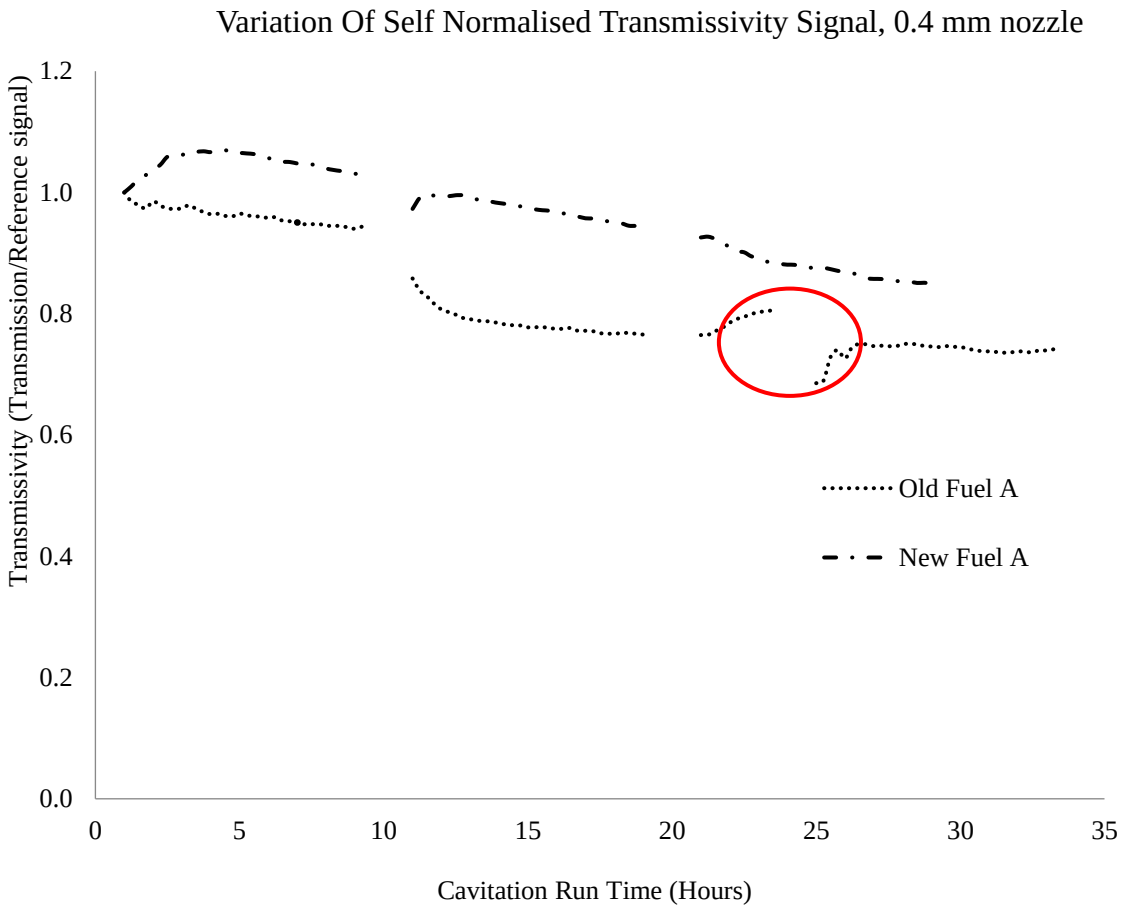

Figure 83 Self-Normalised Transmission Signal of commercial Diesel Fuel

At the beginning of day 3, as seen on Figure 83, there was a power interruption which explains the gape shown on day 3, considering the Aged Fuel A – Circled in red, the gap shows the discontinuity encountered as an electrical interruption led to the complete loss of power causing a sudden increase of the transmitted signal. The experiment was restarted soon after; the rest of the results were not impacted. Only results taken after the electrical interruption were taken into account for the purpose of the experiment.

At the end of the 3 days, the paraffin based GTL fuel was visually transparent compared to the commercial Diesel fuels because of the increase in pollutant in the latter as the fuel was left to cavitate as well as because of the difference in the chemical composition of the GTL paraffin based fuel and the commercial Diesel fuels. This explained the greater value of the Normalised Transmission Signal percentage increase of the commercial Diesel fuels. in comparison to the GTL paraffin of 13.876% ± 0.001%.

As expected, adding 20% of the RME to the GTL fuel at the start of the experiment, decreased the Normalised Transmission Signal from a maximum of 8.0135 ± 0.0001 for the GTL fuel to a maximum of 3.924 ± 0.001 for the GTL+RME fuel.

Researchers have also discovered that the percentage decrease of the Normalised Transmission Signal of paraffin based fuels was negligible in comparison to the percentage decrease of the Normalised Transmission Signal of the commercial Diesel fuels. [3] Moreover, while conducting a similar experiment making use of the same rig as in *the present study*, and testing a paraffin blend Diesel fuel, Lockett *et al.* [194] similarly discovered a decrease in the Transmission Signal of the GTL paraffin fuel at the start of the experiment as a percentage of the biofuel RME was added to the mix. This was due to the difference in the chemical composition of the GTL paraffin based fuel and the RME biofuel.

Variation Of Self-Normalised GTL+RME Signal

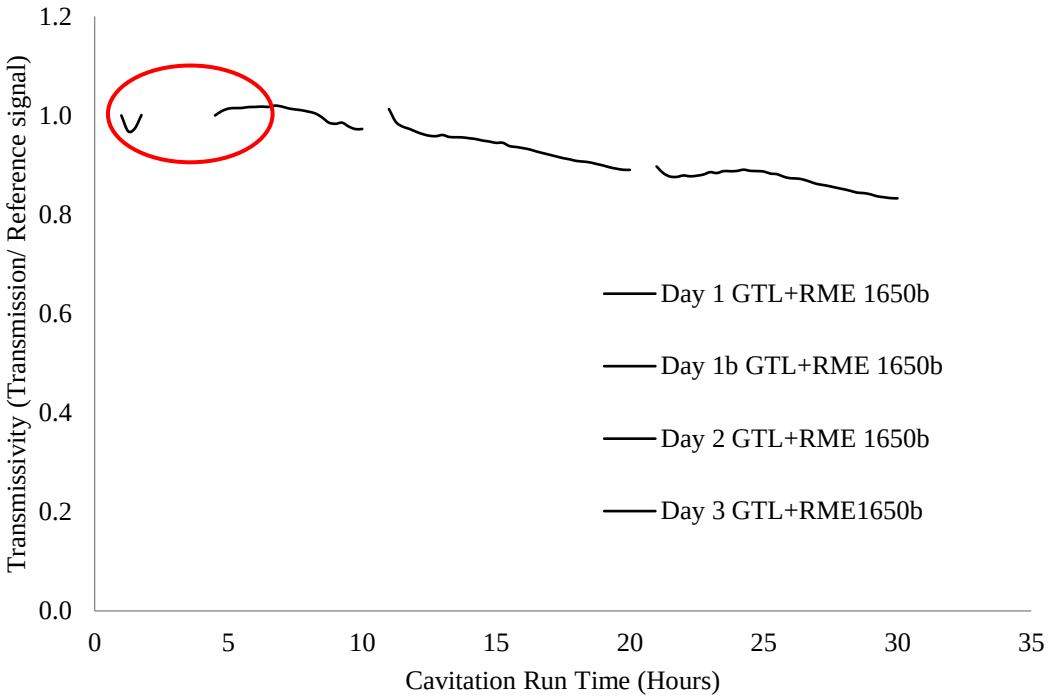

Figure 84 Self-Normalised Transmission Signal of GTL+RME

As showed in Figure 84, the electrical interruption occurred on the first day while testing the GTL+RME fuel. A beginning of the experiment before the electrical interruption, the signal increased. As the experiment was restarted the signal was seen to decrease. Only results taken after the electrical interruption were taken into account for the purpose of the experiment.

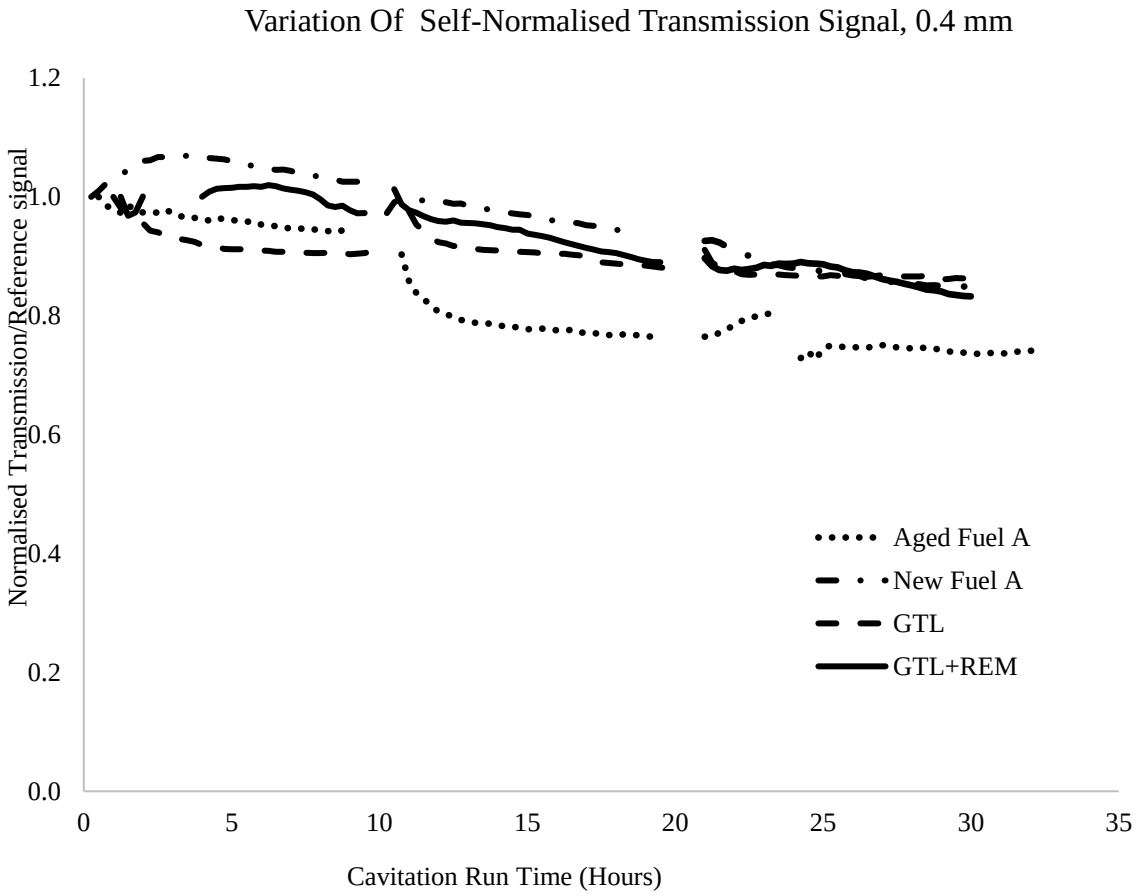

Figure 85 Self-Normalised Transmission Signal of all tested fuels

From Figure 85, the results show a linear decrease in Transmission Signals for all tested fuels.

Over the 3 days period however, the decrease in the Normalized Transmission Signal, as observed in Figure 85 above when considering the GTL+RME was in disagreement with a number of literature reviews where an increase in the Normalised Transmission Signal was noted stating that the fuel was easily penetrated by the laser over time – When comparing the Normalised Transmission Power of GTL and GTL+RME obtained in *the present study*, the increase in the rate of decrease of the two fuels noted over the 3 days period (from 13.876% for GTL and 26.341% for GTL+RME) led to the

conclusion that when adding 20% RME to the GTL fuel, the signal transmission greatly reduced as the capacity of the fuel to penetrated by the laser decreased.

However, Fröhlich *et al.* [198] while investigating the effect of ultrasound cavitation on RME discovered the existence of tocopherols antioxidants in RME solutions. Hence, scientists at Shell while conducting research on the subject concluded that the destruction of those antioxidant, responsible for the absorption properties of the RME, was the root cause of the increase in the Normalized Transmission laser power of the RME over time. As he conducted research on sustained hydrodynamic cavitation, Jeshani [3] also discovered that the Normalized Transmission power increased when adding the biofuel RME to the paraffin based fuel GTL, as the Fatty acid contained in the fuel impacted the oxidation process taking place in the biofuel. This meant that the fuel was easily penetrated by the laser. The author concluded that among plausible solutions to the problem was the add antioxidants to the mix.

The difference in temperatures considered during the sustained cavitation experiment conducted by the author in comparison to *the present study* may have impacted the behaviour of the GTL+RME mixture. Or else, looking at Figure 85, it can be seen that the GTL+RME signal was increasing right until the electrical interruption. This may have caused a reverse in the signal received from the software. Further investigations need to be conducted to fully understand the changing behaviour of the fuel.

6.1.2. Spectral Attenuation Coefficient Results

Based on the optical set up as described in Chapter 4 and using Equation 58 and Equation 5.7–3, the Attenuation Coefficient of each tested fuel was calculated. The minimum and the maximum Attenuation Coefficient of each tested fuel were obtained: Aged Fuel A, 1.177 cm^{-1} ± 0.001 cm^{-1} and

1.526 cm^{-1} ± 0.001 cm^{-1} respectively; New Fuel A, 1.275 cm^{-1} ± 0.001 cm^{-1} and 1.461 ± 0.001 cm^{-1} respectively; GTL 0.0862 cm^{-1} ± 0.0001 cm^{-1} and 0.229 cm^{-1} ± 0.001 cm^{-1} respectively and GTL+RME 0.819 cm^{-1} ± 0.001 cm^{-1} and 1.0154 cm^{-1} ± 0.0001 cm^{-1} respectively.

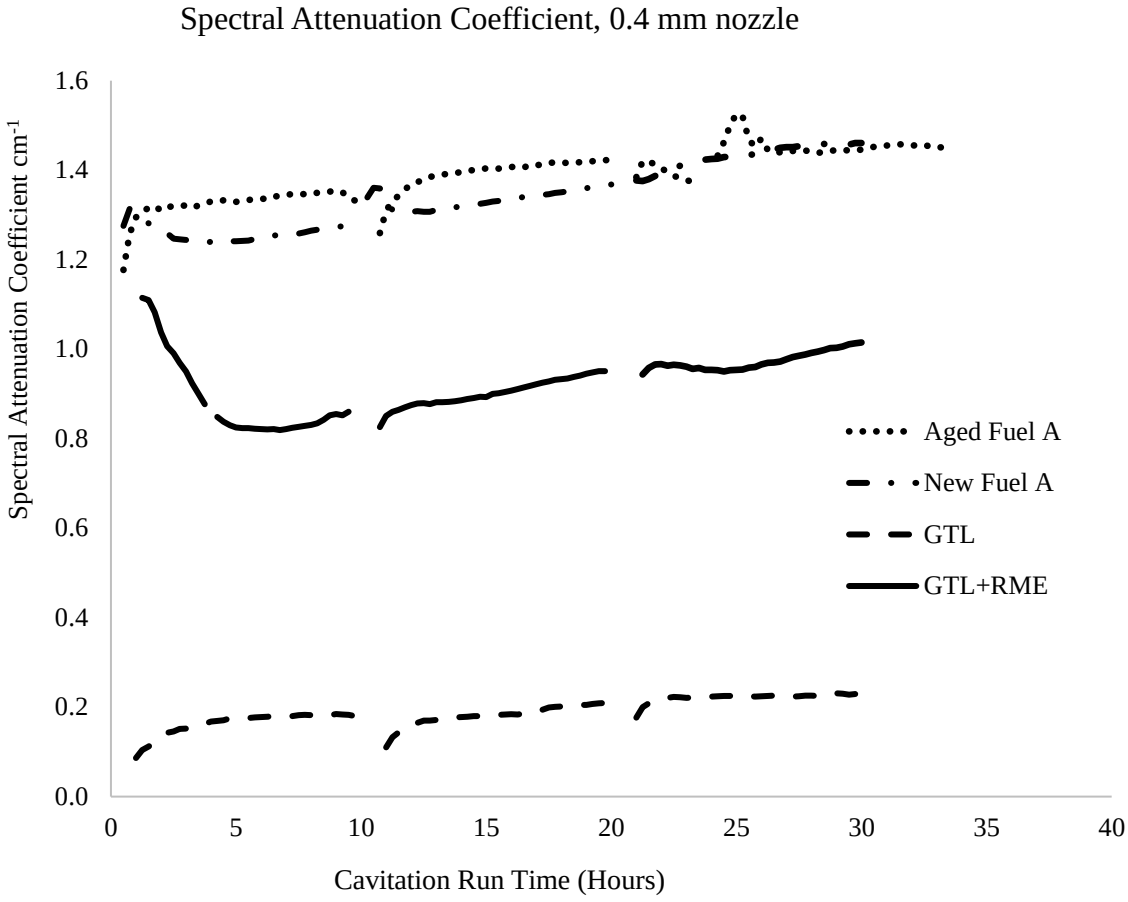

Figure 86 Spectral Attenuation Coefficient Signal of all tested fuels

As observed from Figure 86, the Attenuation Coefficient of the Aged Fuel A is seen to increase at a slightly greater rate than the New Fuel A. This showed that the laser capability to penetrate the fuel reduced at a faster rate in the Aged Fuel A compared to the New Fuel A. The percentage increase of the Attenuation Coefficient was noted as 21.199% ± 0.001 % and 18.0783% ± 0.001 % for Aged Fuel

A and the New Fuel A respectively. This could have been due to the age difference between the 2 fuels leading to a difference in the chemical changes occurring inside each of the fuels as a result of cavitation, as well as due to the impurities inside the fuel prior to cavitation leading to the Aged Fuel A being more prone to cavitation in comparison to the New Fuel A over a long period of time. The GTL fuel had the lowest Attenuation Coefficient at the start of the experiment as expected as it contained less pollutants compared to GTL+RME and the commercial Diesel fuels.

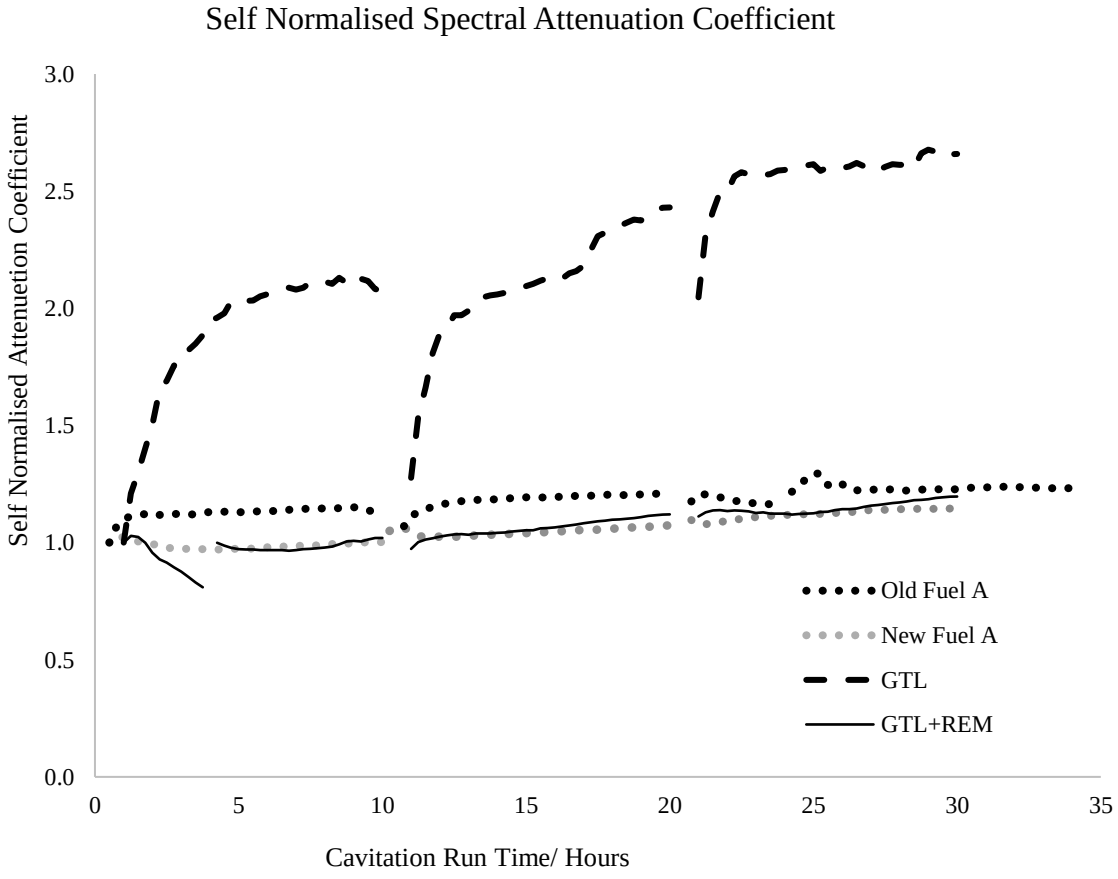

Figure 87 Self-Normalised Attenuation Coefficient

However, as showed in Figure 87, the GTL fuel showed a high increase in Attenuation Coefficient compared to the other four fuels as it was subjected to cavitation over the 3 days period. This meant the laser deteriorated faster when penetrating the GTL fuel in comparison to GTL+RME and the commercial Diesel fuels.

Based on the literature [3], a decrease in Spectral Attenuation Coefficient of the GTL+RME should be noted in comparison to the Spectral Attenuation Coefficient of GTL alone, as adding a percentage of the biofuel RME to the mix means that the absorbing capability of the biofuel antioxidants decrease as cavitation takes place for a long period of time. Hence, as expected, when comparing the Attenuation Coefficient of the GTL to the Attenuation Coefficient of GTL+RME, a decreased in its rate of change was observed.

Even though there was an increase in the Attenuation Coefficient of the GTL+RME biofuel blend, 23.964% ± 0.001% (right until the electrical interruption, the Attenuation Coefficient of the GTL+RME was decreasing) the Attenuation Coefficient percentage increase decreased with the added 20% RME in GTL – this led to the conclusion that the laser was less attenuated as it penetrated the GTL+RME fuel compared to when it penetrated the GTL only. In accordance with literature reviews, this meant that more absorbing species were destroyed when adding 20% biofuel RME to the GTL paraffin fuel as it was subjected to a 3 days' cavitation period

Hence, adding the biofuel RME to the GTL paraffin fuel reduced the propensity of the paraffin fuel to cavitate.

6.2. Cavitation and Heating Test Results Comparison - 30 hours

A comparison of the results obtained from the 30 hours' discontinuous cavitation to the results obtained from the 30 hours discontinuous heating tests of the fuel was necessary in order to study the impact that cavitation alone had on the fuel – as the rig was subjected to high temperatures when cavitating, it was necessary to separate the impact of cavitation to the impact of high temperatures occurring during cavitation.

No heating test was done for the Aged Fuel A. All the other fuels were tested using the modified tea urn water bath at 60^0C.

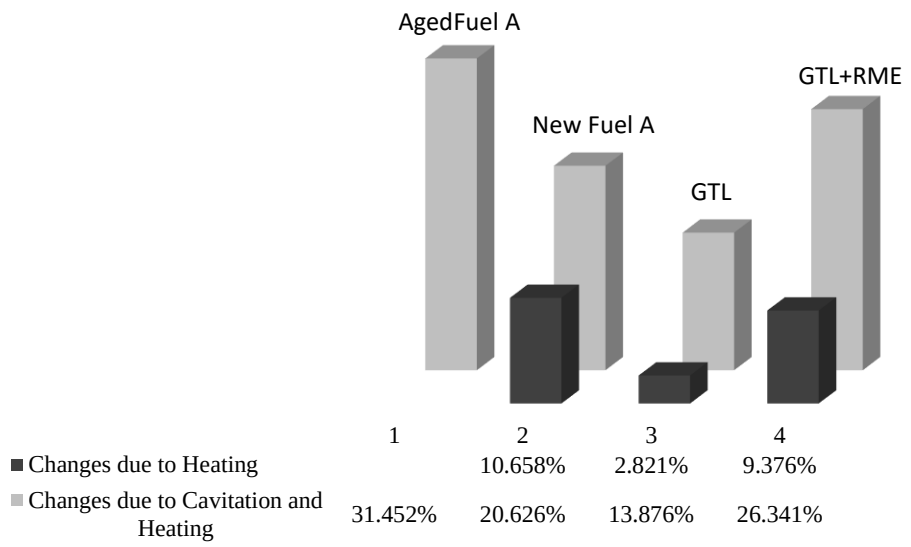

Figure 88 Cavitation and heating testing Transmission Reduction

As an example, a 20.626% ± 0.01 % decrease of the Normalized Transmission due to cavitation and heating was noted for the New Fuel A compared to a 10.658% ± 0.001 % decrease in the Normalized Transmission noted due to heating alone. Subtracting the two results, the decrease in the Normalized Transmission due to cavitation alone was calculated as 9.968% ± 0.001 % for the New Fuel A, 11.0554% ± 0.001 % for the GTL and 16.965% ± 0.001 % for the GTL+RME. In their study of the sustained hydrodynamic cavitation, Lockett and Jeshani [188] when separating the impact of cavitation to the impact of heating found out that, the effect of cavitation and heating on the fuel was greater in comparison to the effect of heating alone.

Equally, the results obtained in Figure 88, showed that cavitation and heating had a greater impact on the fuel in comparison to heating alone. The percentages changes obtained from the heating test was calculated using the 0 Hours reference and the 0 Hours transition before the heating began and, the 30 Hours reference and the 30 Hours transition after heating results were obtained from the PC link software – the reference power and the transition power were then used to obtain the average transmitted power. Hence the average transmitted power obtained before the heating test began, was used in conjunction with the average transmitted power obtained after the heating test ended, in order to obtain the percentage of change due to heating.

The results obtained here are in agreement with the study conducted by Jeshani [3], where he was able to compare the effect of cavitation and heating. The author concluded that the increase in the Attenuation Coefficient was due to the formation of chemical reaction taking place inside the fuel, leading to the formation of polycyclic aromatic hydrocarbons (PAH). The author made use of a two-dimensional Gas Chromatography (GC X GC) analysis of the fuel subjected to cavitation and discovered that cavitation led to the formation of soot particles while heating on the other hand did

not. The results obtained in *the present study* were likewise in agreement with Price *et al.* [4] who discovered that the changes in the fuel composition taking place while considering high temperatures, as cavitation bubble collapse was observed, led to the formation of carbonaceous particles.

6.3. Summary

The study of the high pressure sustained hydrodynamic cavitation was conducted inside City University Thermodynamics Laboratory with the use of a purposely built recirculation common rail rig which mimicked the flow inside the injector spill valve and the pump spill valve systems.

Using the Beer-Lambert Law, the Normalised and Self-Normalised Transmission Signal which decreased with time for all tested fuels, as well as the Spectral Attenuation Coefficient and the Self-Normalised Attenuation Coefficient which behaved contrary to the Transmission Signals, were presented considering the 30 hours' cavitation experiment and the 30 hours' heating tests – As during cavitation, the fuel was likewise subjected to high temperatures, the experiment focused on the effect of cavitation and heating taking place inside the rig.

Using a combination of the commercial Diesel fuel, the GTL and the biofuel RME, it was possible to study the changes occurring inside the fuel as a result of the high pressure sustained cavitation. An increase in the percentage reduction of the normalised transmission power of the GTL and the GTL+RME was noted. The aged commercial Diesel fuel had the lowest Normalised Transmission Signal 2.639 ± 0.01%, and the highest percentage reduction of the Normalised Transmission Signal, 31.452% ± 0.01%. When comparing the Attenuation Coefficients of all tested fuels, the GTL fuel was seen to display the greatest percentage increase, 121.257%. This meant that for the GTL fuel, the

laser light was attenuated at a faster rate over the 3 days' period in comparison to the other tested fuels. This was as excepted as the fuel ability to absorb the laser light increased as the fuel was left to cavitate. Due to the presence of impurities contaminating the fuel making it harder for the laser to go through it.

Using the modified tea urn, the heating test was conducted for the New Fuel A, the GTL and the GTL+RME fuel. No tests were conducted for the Aged Fuel A. It was concluded as expected that the combined effect of cavitation and heating on the fuel, was greater than the effect of heating alone.

Based on the literature reviews [3,188] the study concluded that the changes in the Transmission Signals were due to the sustained hydrodynamic cavitation which took place inside the receiver. This meant that cavitation took place downstream of the nozzle – As the fuel was heated at 60 degrees (also considered as the temperature at which the fuel entered the injector), its transmission signal was not impacted. The Transmission signal was greatly impacted once the fuel was located inside the receiver downstream of the nozzle.

Due to the sonochemical reaction taking place within the fuel (the effect of ultrasound generating acoustic cavitation responsible for the change in the chemical composition of the fuel), the tested fuels when visually inspected were seen to have experienced degradation. The presence of harmful pollutants was noticeable.

Blank Page

CHAPTER VII. CONCLUSIONS

7.1. Overview

The main question here was: “How to find ways of controlling the cavitation phenomena occurring inside the FIE from the incipient stage, to the fully developed stage, to leaving the fuel to cavitate for a sustained period of time”. Hence, the present work presents a novel method of controlling the cavitation phenomena as there exists a gap to be filled, as scientists are still not able to fully control the cavitation phenomena occurring inside the injector valves – Scientists are yet to demonstrate the interactions between the vapour and the liquid flow, as well as the main causes responsible for the mechanisms impacting the flow.

By changing the fuel composition, the geometrical parameters and the material of the nozzles, as well as by changing the operating conditions of the fuels, this study made use of two distinct rigs purposely designed to understand the cavitation phenomena.

7.1.1. Effect of Incipient Cavitation on n-Hexadecane Based Fuel Jet

The study was first conducted using a mechanical rig capable of reaching sustaining pressures of up to 80 bar upstream of the nozzle and 15 bar downstream of the nozzle, making use of the Cylindrical, Hemispherical and Conical single hole injector nozzles consecutively placed inside a 60 mm inner diameter Fused Silica Receiver – Acrylic nozzles were first considered due to the fact that they provided a better visual access to the high speed jet flowing inside the injector. As geometric cavitation was observed outside of the nozzle and as crack formation was noticed on some of the acrylic nozzles, a switch from acrylic nozzles to the metal nozzles was needed.

The effects of cavitation were observed between the high speed jet boundary layers and the stagnant fuel inside the receiver due to the presence of the shear flow within the turbulent jet mixing/diffusion zone, leading to the jet experiencing friction while travelling through the stagnant liquid. The fully developed cavitated jet increased in length and in width as the Downstream Pressure decreased for the fixed Upstream Pressure. The mechanism considered was compared to the mechanism inside the injector system subjected to pressures upstream and downstream of the needle lift. It was also compared to the mechanism taking place inside control valves facing pressures upstream and downstream of the valve – *The Present Study* can be applied Hydraulic pumps, discharge control valves and noise energy dissipation.

Henceforth the parametric study looked at, the impact of incipient cavitation as the jet travelled through the injector nozzle and flew into a stationary liquid, as well as the impact of the incipient cavitation due to the change in the fuel composition of the alkane hydrocarbon fuels. The study was conducted by manually manipulating the Back Pressure to counteract the fixed Upstream Pressure and hence blocking the jet flowing through the nozzle in order to obtain the onset of cavitation – The study made use of the fuel matrix provided by Shell Global Solutions where 16 paraffin based fuel mixing samples were poured consecutively into the rig considering the Acrylic, Brass and Aluminum-steel nozzles.

The fuel mixtures were made up of an increased n-Octane percentage in n-Hexadecane based fuel as well as of mixtures of n-Octane, n-Decane, n-Dodecane and n-Tetradecane in n-Hexadecane.

When measuring the onset pressure, the Upstream Pressure varied from 10 to 80 bar gauges as a function of Downstream Pressure. The Standard Deviation representing the spread-out of the Downstream Pressures was taken into consideration as 25 repetitive sets of measurements per fuel per nozzle hole diameter, geometrical shape and material were performed reducing the risk of human

error and hence ensuring the accuracy of the results. An increase in Upstream Pressure due to the increase in Downstream Pressure was noted for each tested fuel.

As expected, the change in the fuel composition affected the changes in the onset of cavitation. It was discovered that the increase in the Saturated Vapour Pressure of the fuel increased the propensity of the fuel to cavitate when considering the Cylindrical and the Hemispherical nozzles. The Conical nozzle behaved contrary to the other two types of nozzles. A consistency check of the results was conducted approximately two years after the first incipient cavitation experiment was completed, considering the n-Hexadecane-n-Octane mixture. The test confirmed the increase in the Upstream Pressure due to the increase in the Downstream Pressure as well as the increase in the Upstream Pressure due to the increase in the n-Octane concentration while testing the Cylindrical and the Hemispherical nozzles. The reverse phenomenon was once more observed for the Conical nozzle.

Using Antoine's Equation and Rault's law, the total Saturated Vapour Pressure increased with the increase in the n-Octane concentration. The results were compared to those obtained from Shell matrix to confirm their accuracy. The flow in the Cylindrical and the Hemispherical nozzles behaved differently to the flow in the Conical nozzles.

Using Bernoulli's equation for Single Phase Incompressible liquid through the nozzle, the Volumetric Flow Rate was obtained enabling the calculation of the Discharge Coefficient, the Cavitation Number and Reynolds Number for the n-Hexadecane-n-Octane mixture to be completed. When measuring the flow rate, human error did not impact the results as it was considered negligible. The Discharge Coefficients of the 0.14mm and the Discharge Coefficients of the 0.25 mm hole Cylindrical, Hemispherical and Conical nozzles were calculated, taking into consideration the added, 0%, 0.1%, 1%, 5%, 10%, 15% and 20% n-Octane concentration into pure n-Hexadecane. The Discharge

Coefficient decreased with the increase in n-Octane concentration and were comparable to the typical Discharge Coefficient of Diesel Injectors which varies between 0.6 and 0.9.

The Discharge Coefficient can be affected by choking of the flow due to the presence of cavitation bubbles restricting the nozzle hole area. This was observed as the Cavitation Number of the Conical nozzle increased as the Saturated Vapour Pressure increased –This meant that the Conical nozzle's propensity to cavitate decreased with the increase in Saturated Vapour Pressure. This also confirmed the high velocities observed in the Conical nozzles as compared to those observed in the Cylindrical nozzles and in the Hemispherical nozzles as the Conical nozzle hole was reduced due to choking. A decrease in the Cavitation Number with the increase in the Saturated Vapour Pressure was observed in the Cylindrical nozzles and the Hemispherical nozzles as turbulence impacted the flow. It was concluded that the viscosity was affeccted by the total volume of the fuel whereas the Saturated Vapour Pressure was affected by the percentage of n-Octane in the fuel mixture.

The changes in the nozzle geometry did impact the jet as stronger jets were noted when varying the diameter of the nozzle hole from 0.14 mm to 0.25 mm – the overall length and width of the jet increased as more bubbles were present in the core of the jet considering the same Upstream and Downstream Pressures.

The Critical Cavitation Number was compared to the Fully Developed Cavitation Number. Lower values of Critical Cavitation Number were obtained for the Conical nozzle as it highly cavitated compared to the Cylindrical nozzle and the Hemispherical nozzle respectively.

As a higher value of Cavitation Number often denotes a non-cavitating flow, the higher value of Critical Cavitation Number obtained at the start of cavitation was justified. The Fully Developed Cavitation Number varied between 0.5 and 5 and were within the appropriate ranges. It was once

more observed that the Cylindrical nozzles and Hemispherical nozzles behaved similarly in comparison to the Conical nozzle.

It can be concluded that the overall stability of the jet is very much dependent on the nozzle geometrical parameters as well as the physical and the chemical properties of the fuel as these determine the flow characteristics.

7.1.2. High Pressure Sustained Hydrodynamic Cavitation of Diesel and Biodiesel Fuels

With the aim of controlling the fuel emissions pollutions generated by the ICE system, this part of the thesis focused on the control of the sustained hydrodynamics cavitation as well as on the control of the internal energy compression of the Diesel and Biodiesel fuel flows taking place simultaneously inside injectors spill valves and high-pressure pumps spill valves. A 1650 bar, 3.5 L High Pressure Recirculating Continuous Flow Rig, made up of mechanical and electrical components was used to test the commercial Diesel, the Gas to Liquids and the Rapeseed Methyl Ester fuels. The tests looked at the resulting effects of leaving the fuels to cavitate for 30 hours, 10 hours per day, using a needless (to unsure continuous flow) low carbon Steel Delphi HB X 6965489 single hole Cylindrical sac nozzle. A 405 nm laser beam was shined through each fuel giving readings of the resulting effects of subjecting the fuel to cavitation, versus the resulting effects of heating the fuels overnight inside a modified Water Bath tea urn at 60 degrees Celsius for the equivalent period of time.

As the fuel was subjected to reoccurring cavitation inside the rig, a change in the fuel composition took place due to ultrasound cavitation occurring in the receiver; because of the highly complex mechanism found in most hydrocarbon fuels, the formation of new elements inside the fuel at high temperatures can lead to the deterioration of the Fuel Injection Equipment.

In order to mimic what happens inside the injector and the pump spill control valves, the experimental set up enabled one side of the rig to be subjected to high pressures – considering the pump, the injector and the common rail system, and the other side to be subjected to the low pressures – considering the Low Pressure Pump and the fuel tank. As the highly pressurized fuel was release into the low pressure side, going through the valves, the fuel cavitated. As the bubbles were formed, some remind trapped inside the injection system with the valves constantly subjected to cavitation.

From the Bernoulli's equation for Single Phase Incompressible liquid flow through an injector orifice, the Volume Flow Rate was calculated.

Using the Beer-Lambert Law, a linear decrease in the Normalised Transmission Signals and in the Self-Normalised Transmission Signals was noted for all tested fuels. An increase in the Spectral Attenuation Coefficient and in the Self-Normalised Attenuation Coefficient was noted when subjecting the fuel to 30 hours' cavitation. The laser power reference and transmission readings were averaged from 1 minutes to 15 minutes as the effect of temperature variation due to cooling was considered.

The decrease in the Normalised Transmission Signals and the Self-Normalised Transmission Signals were explained based on the changes in the chemical composition of the fuel as high pressures and high temperatures took place inside the receiver due to cavitation bubble collapse – It was concluded that the changes in the Transmission Signals were the results of the sustained hydrodynamic cavitation which promoted the changes in the chemical composition of the fuel as well as the degradation of the fuel as sonochemical reactions took place due to bubble collapse.

The Commercial Aged Diesel fuel had the lowest Normalised Transmission Signal. The Gas to Liquids fuel, transparent compared to the commercial Diesel fuel, had the highest normalised

transmission signals. Contrary to literature, a decrease in the Normalized Transmission Signal of the Gas to Liquids and the Rapeseed Methyl Ester fuel mixture was noticed.

The Gas to Liquids fuel displayed the greatest percentage increase in the Attenuation Coefficient as the attenuation took place at faster rate in comparison to the other fuels. A faster reduction of the ability of the laser to penetrate the fuel was noted in the Commercial Aged Diesel fuel in comparison to the new Fuel. The age difference as well as the impurities inside the fuel and/or the chemical changes taking place inside the fuel were affecting the results.

A decreased in the absorbing species inside the fuel mixture was noted as 20% Rapeseed Methyl Ester was added to the Gas to Liquids fuel. Hence the laser was less attenuated as it penetrated the Rapeseed Methyl Ester and Gas to Liquids fuel mixture, compared to when it penetrated the Gas to Liquids fuel alone.

A heating test was conducted for all fuels but the Commercial Aged Diesel fuel using a Modified Commercial Tea Urn water bath at 60^0C to separate the impact of temperature to the impact of cavitation to determine the effect of heating the fuel alone.

It was determined that the effect of subjecting to fuel to cavitation and heating was greater than the effect of subjecting the fuel to heating alone.

A comprehensive risk assessment which involved following all safety precautions i.e. protective wear and visible laboratory safety warning signs, were cautiously followed in order to avoid incidents occurring while conducting the cavitation tests and the heating tests. The assessment was conducted at the start of the experiment and underlined the risks associated with the use of the Diesel and Biodiesel fuels at high temperatures and at high pressures.

The overall sets of results obtained during *the present study* were beneficial to experimentalists as well as modelers working on Internal Combustion Engines Cavitation Research. The study can be

considered as a big step forward toward a better understanding of the cavitation phenomena taking place inside the Internal Combustion Engine, mainly inside injectors and pumps spill control valevs, as it must be acknowledged that more is still needed to be done on the subject of cavitation in Fuel Injection Systems.

7.2. Recommendations for Future Work

For the incipient cavitation experiment, the use of an electronically controlled rig could have reduced the amount of time taken to conduct the experiment – the first experimental measurements took two years to be completed as a set of 25 measurements were taken into consideration for each change of pressure in order to reduce the likelihood of human and mechanical errors. Moreover, making use of different working fluids could have given rise to a better understanding of the cavitation phenomenon occurring inside the receiver.

More work needs to be done to fully investigate the existing differences in the flow pattern at the onset of cavitation as well as at the fully developed stage – From the results obtained it can be concluded that the cavitation phenomena occurring between the jet and the stagnant fuel is dependent on the changes in the composition of the fuel. Hence a quantitative analysis, looking precisely at how much the jet is affected by the fuel composition, can be useful as it can lead to a better understanding of the cavitated turbulent jet flow occurring inside the receiver. A thorough study of the impact of the chemical composition changes occurring inside the fuel as well as a study of the chemical reaction occurring inside the bubble can provide a better understanding of the impact that the increase in the n-Octane concentration has on the propensity of the fuel to cavitate.

An analysis of the cavitated bubbles using an empirical method to quantify the number of bubbles inside the receiver is needed. The analysis will also look at the stability and the evolution of the bubbles and the monitoring of the bubbles' size distribution. Moreover, a study of the noise level and the bubble oscillation frequency will help to determine the strength of the cavitation bubble collapse and hence this will help to finding out the damages that can be caused to the neighborhood of the jet as cavitation takes place inside devises such as control valves. Furthermore, a closer look at the Conical nozzle behaving as a plug is needed in order to find out if the flow pattern is repetitive and if it can be controlled.

A comprehensive study of the shear flow phenomena looking at the impact of the shear tension on cavitation, making use of spectrometric flow visualization techniques to carefully observe the area between the jet and the stagnant fuel, is required. Hence, a comparison of the results obtained for the cavitating shear flow to the results obtained for the non-cavitating shear flow will have to be completed, looking at parameter such as the exit velocity distribution, the Cavitation number and the Reynolds number in order to provide a better understanding of cavitation on the jet.

For the sustained hydrodynamic cavitation experiment, by considering higher pressures and higher temperatures for example, as nowadays the common rail can reach pressures higher than 2000 bar, and by conducting not only an experimental analysis but also a chemical analysis of the fuels, an array of data can be obtained which will thoroughly demonstrate the changes taking place on the chemical composition of the Diesel and Biofuels as they undergo sustained hydrodynamic cavitation – Due to time constraint experienced while conducting the experiment, it was not possible to conduct a chemical analysis of the fuel after it experienced cavitation and heating respectively.

By changing the material as well as the geometrical features of the nozzle (shape and hole nozzle) as only one type of nozzle was used in this study, a broad range of data can be collected, given researchers a solid leg to stand on. Furthermore, by modifying the rig, allowing for a discontinued flow and hence by considering the impact of the needle inside the nozzle, modelers could mimic the flow taking place inside the injector. This will enable them to study what happen to the flow – entrainment for example, can take place as part of the fuel travels in the opposite direction back into the nozzle.

Further the experiments need to be conducted for a longer period of time, for more than 3 days on the Paraffin based Gas to Liquids and the Fatty Acid Rapeseed Methyl Ester in order to properly study the effect of sustained hydrodynamic cavitation on the paraffin based fuels and on the Biodiesel fuels at varying pressures, not only at 1650 bar. This will help to obtain a broader range of data in order to fully understand the behavior of the paraffin fuel as sustained cavitation takes place.

Blank Page

PUBLICATION

Lockett R., Ndamuso N. and Price, R., "*Cavitation Inception in Immersed Jet Shear Flows*." In Journal of Physics: Conference Series (Vol. 656, No. 1, p. 012090). IOP Publishing. (2015).

REFERENCES

[1] Hirschel E.H. ed., Numerical Flow Simulation II: CNRS-DFG Collaborative Research Programme Results 1998–2000 (Vol. 75), Springer Science & Business Media, pp.181, (2013).

[2] Bonnick A., "*Automotive computer controlled systems"*. Routledge, (2007).

[3] Jeshani M., "*The Optical Characterisation of Cavitation Flow in Diesel Fuel Injection Equipment*" [online], Available: http://openaccess.city.ac.uk/3414/, (2013).

[4] Price R., Blazina D., Smith G. and Davies T., "*Understanding the impact of cavitation on hydrocarbons in the middle distillate range*", *Fuel,156*, pp.30-39, (2015).

[5] Oda T. and Yasuda Y., "*Experimental Investigation on Structure of Cavitating Flow and Velocity Field inside a 2-D Hole Nozzle",* In Proc. ICLASS, vol. 2003, (2003).

[6] Andriotis A. "*Investigation of Cavitation inside Multi-hole Injectors for large Diesel Engines and its Effect on the Near nozzle Spray Structure*" City University London, School of Engineering and Mathematical Sciences, Doctoral Dissertation, (2009).

[7] Schmidt D., Rutland C., Corradini M., Roosen P. and Genge O., "*Cavitation in Two-Dimensional Asymmetric Nozzles*", No. 1999-01-0518, SAE Technical Paper, (1999).

[8] Schmidt D., "*Cavitation in Diesel Fuel Injector Nozzles*", Mechanical Engineering, University of Wisconsin-Madison, Doctoral Dissertation, (1997).

[9] Echouchene F., Belmabrouk H., Penven L. and Buffat M., "*Analysis of the cavitation in Diesel Injectors*", International Renewable Energy Congress November, pp. 5-7, (2009).

[10] Martynov S, Mason D., Heikal M., Sazhin S. and Gorokhovski[2] M., "*Modelling of Cavitation Flow in a Nozzle and Its Effect on Spray Development*", International Heat Transfer Conference 13, Begel House Inc., (2006).

[11] Karrholm F., Weller H. and Nordin N., "*Modelling Injector Flow Including Cavitation Effects for Diesel Applications*", ASME/JSME 2007 5th joint fluids engineering conference, American Society of Mechanical Engineers, pp. 465-474, (2007).

[12] Giannadakis E. "*Modelling of Cavitation in Automotive Fuel Injector Nozzles*", Imperial College London, Doctoral Dissertation, (2005).

[13] Martynov S., "*Numerical Simulation of the Cavitation Process in Diesel Fuel Injectors*", University of Brighton, Doctoral Dissertation, (2005).

[14] Schmidt D., Rutland C. and. Corradini M., "*A Numerical Study of Cavitating Flow through Various Nozzle Shapes*" Paper no. 971597, SAE Technical Paper, (1997).

[15] Beaudoin J., Cadot O., Aider J., Gosse K., Paranthoe¨n P., Hamelin B., Tissier M., Allano D., Mutabazi I., Gonzales M. and Wesfreid J. "*Cavitation as a complementary tool for automotive aerodynamics*" Experiments in Fluids 37, no. 5, pp.763-768, (2004).

[16] Noltingk B. and Neppiras E., "*Cavitation produced by Ultrasonics*", Proceedings of the Physical Society. Section B, Volume 63, Number 9, pp. 674, (1950).

[17] Jose J., Mmbaga J., Hayes R. and Xu Z., "*Modeling Cavitation in a High-Intensity Agitation Cell*", The Canadian Journal of Chemical Engineering 89, no. 5, pp.1154-1164, (2011).

[18] Brennen C., "*Cavitation and Bubble Dynamics*", Cambridge University Press, (2013).

[19] Soh W., "*An energy approach to cavitation bubbles near compliant surfaces*", Applied mathematical modelling 16, no. 5, pp. 263-268, (1992).

[20] Hauke G., Fuster D. and Dopazo C., "*Dynamics of a single cavitating and reacting bubble*", American Physical Society, Physical Review E 75, (2007).

[21] Arcoumanis C., Gavaises M., Abdul-Wahab E. and Moser V.,"*Modelling of Advanced High-Pressure Fuel Injection Systems for Passenger Car Diesel Engines*" SAE Technical Paper No. 1999-01-0910, (1999).

[22] Arcoumanis, C., Gavaises, M., and French, B., "*Effect of Fuel Injection Processes on the Structure of Diesel Sprays*," Paper no 970799, SAE Technical Paper, (1997).

[23] Giannadakis E., Gavaises M. and Arcoumanis C., "*Modelling of cavitation in diesel injector nozzles*", Journal of Fluid Mechanic, vol. 616, pp. 153–193, (2008).

[24] Giannadakis E., Gavaises M., Roth H. and Arcoumanis C., "*Cavitation Modelling in Single-Hole Diesel Injector Based on Eulerian-Lagrangian Approach*" In Proc. THIESEL International Conference on Thermo-and Fluid Dynamic Processes in Diesel Engines. Valencia, Spain, (2004).

[25] Mitroglou N., Arcoumanis C., Mori K., Motoyama Y., "*Mixture distribution in a multi-valve twin-spark ignition engine equipped with high-pressure multi-hole injectors*" Journal of Physics: Conference Series, vol. 45, no. 1, p. 46. IOP Publishing, (2006).

[26] Arcoumanis, C., Gavaises, M., Nouri, J., Abdul-Wahab, E. et *al.*, "*Analysis of the Flow in the Nozzle of a Vertical Multi-Hole Diesel Engine Injector*", Paper no 980811, SAE Technical, (1998).

[27] Berckmuller M., Tait N., Lockett R., Greenhalgh D., Ishii K., Urata Y., Umiyama H., Yoshida K., "*In-Cylinder Crank Angle Resolved Imaging of Fuel Concentration in a firing Spark-Ignition- Engine Using Planar LIFs*", No. CONF-940711, The Combustion Institute, Pittsburgh, United States, (1994).

[28] Yan Y., Gashi S., Nouri J., Lockett R. and Arcoumanis, "*Investigation of spray characteristics in a spray-guided DISI engine using PLIF and LDV*", Journal of Physics: Conference Series, Vol. 85, No. 1, p. 012036, IOP Publishing, (2007).

[29] Lockett R., Richter J. and Greenhalgh D., "T*he characterisation of a diesel spray using combined laser induced fluorescence and laser sheet dropsizing*" Lasers and Electro-Optics Europe, CLEO/Europe. Conference, pp. 148-148, IEEE. (1998).

[30] Yang M., Xiao S., Kang C., Wang Y., "*Effect of Geometrical Parameters on Submerged Cavitation Jet Discharged from profiled Central-body Nozzle*", Chinese Journal of Mechanical Engineering, Volume 26, Issue 3, pp. 476-482, (2013).

[31] Iyer C. and Ceccio S., "*The influence of developed cavitation on the flow of a turbulent shear layer*", Physics of Fluids (1994-present) 14, no. 10, pp. 3414-3431, (2002).

[32] O'Hern T., "*An experimental investigation of turbulent shear flow cavitation*", Journal of fluid mechanics 215, pp. 365-391, (1990).

[33] Yang S., Siow Y., Teo C. and Hanjalic K., "*A KIVA code with Reynolds-stress model for engine flow Simulation*", Energy 30, no 2, pp. 427–445, (2005).

[34] Su H., Mosbach S., Kraft M., Bhave A., Kook S. and Bae C., "*Two-stage Fuel Direct Injection in a Diesel Fuelled HCCI Engine*", Society of Automotive Engineers of Japan, DOI: 10.4271/2007-01-1880, (2007).

[35] Bae C., Yu J., Kang J., Kong J., Cuenca R. and Lee K., "*The Influence of Injector Parameters on Diesel Spray*", THIESEL 2002 Conference on Thermo- and Fluid-Dynamic Processes in Diesel Engines, (2002).

[36] Jing-Chuan H., "*Conditions for incipient cavitation formation*", Applied Mathematics and Mechanics, Applied Mathematics and Mechanics 10, no. 2, pp. 163-166, (1989).

[37] Falcucci G., Jannelli E., Ubertini S. and Succi S., *"Direct numerical evidence of stress-induced cavitation*". Journal of Fluid Mechanics 728, pp.362-375, (2013).

[38] Mansoor M., Uddin J., Marston J., Vakarelski I. and Thoroddsen S., "*The onset of cavitation during the collision of a sphere with a wetted surface*", Experiments in fluids 55, no. 1, no 1-7, (2014).

[39] Sou A., Biçer B. and Tomiyama A., "*Numerical simulation of incipient cavitation flow in a nozzle of fuel injector*". Computers & Fluids 103, pp.42-48, (2014).

[40] Fang Z., Kang Y, Wang X., Li1 D., Hu Y. and Huang M., "*Numerical and experimental investigation on flow field characteristics of organ pipe nozzle*", IOP Conference Series: Earth and Environmental Science, vol. 22, no. 5, p. 052020. IOP Publishing, (2014).

[41] Straka W., Meyer R., Fontaine A. and Welz, J., "*Cavitation inception in quiescent and co-flow nozzle jets*", Journal of Hydrodynamics, Ser. B 22, no 5, 813-819, (2010).

[42] Gavaises, M., Papoulias, D., Andriotis, A., Giannadakis, E. and Theodorakakos, A., 2007. Link between cavitation development and erosion damage in diesel injector nozzles (No. 2007-01-0246). SAE Technical Paper.

[43] ASTM G32-09, "*Standard Test Method for Cavitation Erosion Using Vibratory Apparatus*" ASTM International, (2009).

[44] Chahine G., Conn A., Johnson V. and Frederick G., "*Cleaning and Cutting with Self-resonating Pulsed Water Jets*", Proceedings of the second US water jet conference, pp.195-207, (1983).

[45] Wright M., Epps B., Dropkin A. and Truscott T., "*Cavitation of a submerged jet*", Experiments in fluids 54, no. 6, pp. 1-21., (2013).

[46] Chemloul N., "*Experimental Study of Cavitation and Hydraulic Flip Effects on Liquid Jet Characteristics into Crossflows*", Journal of Applied Fluid Mechanics 5, no.4, pp. 33-34, (2012)

[47] Reid B., Gavaises M., Mitroglou N., Hargrave, G., Garner C., Long, E., McDavid, R., "*On the Formation of string cavitation inside fuel injectors*" Experiments in fluids 55, no. 1, pp. 1-8, (2014).

[48] Andriotis A. and Gavaises M., "*Influence of Vortex Flow and Cavitation on Near Nozzle Diesel Spray Dispersion Angle*", Atomization and Sprays 19, no. 3, pp. 247–261 (2009).

[49] Boretti A., Jin S., Zakis G., Brear M., Attard W., Watson H., Carlisle H. and Bryce W., "*Experimental and Numerical Study of an Air Assisted cavitation for a D.I.S.I. Engine*", No. 2007-01-1415. SAE Technical Paper, (2007).

[50] Nishimura A., and Assanis D., "*A Model for Primary Diesel Fuel Atomization Based on Cavitation Bubble Collapse Energy*", Eight International Conference on Liquid Atomization and Spray Systems, (2000).

[51] Dabiri S., Sirignano W, and Joseph D., "*Cavitation in an orifice flows*", University of California, Irvine, California 92697-3975, Physics of Fluids (1994-present) 19.7: 072112., (2007).

[52] Giannadakis, E., Papoulias, D., Gavaises, M., Arcoumanis, C., Soteriou, C., & Tang, W. (2007). "*Evaluation of the predictive capability of diesel nozzle cavitation models*", No. 2007-01-0245. SAE Technical Paper, (2007).

[53] Andriotis A., Papoulias D., Mitroglou. N., Theodorakakos A. and Gavaises M., "*Characterization of string cavitation in large-scale Diesel nozzles with tapered holes*", American Institute of Physics. Physics of Fluids 21, 052107, (2009).

[54] Wang J., Joseph D. and Funada T., "*Viscous potential flow analysis of stress induced cavitation in an aperture flow*", Journal of Atomization and Sprays, pp.763-776, (2004).

[55] Tian L. "*Variable orifice nozzle*" U.S. Patent 7,938,337, issued May 10, (2011).

[56] Rissman J. and Kennan H., "*The Government's Role in Energy Technology Innovation Advanced Diesel Internal Combustion Engines*", Case Studies, American Energy Innovation Council.

[57] Safgönül B., Ergeneman M., Arslan H. E., Soruşbay C., "*Internal Combustion Engines*" – MAK 493E Combustion in CI-Engines, Istanbul Technical University, pp.188-204, (1999).

[58] Van Horn Armstrong, L.; Diesel Engine; [online] Available: http://www.britannica.com/EBchecked/topic/162716/diesel-engine/45712/Subsequent-developments-and-applications

[59] Kügler T., "*Nozzle holders*", Diesel Engine Management, Springer Fachmedien Wiesbaden, pp. 162-167, (2014).

[60] Lafayette, C.; Diesel Engine; [online] Available: http://www.britannica.com/EBchecked/topic/162716/diesel-engine/45712/Subsequent-developments-and-applications

[61] Crua C., "*Combustion Processes in a Diesel Engine*", School of Engineering, University of Brighton, Ricardo Consulting Engineers, PhD. Dissertation (2002).

[62] Khair, M.K., Jääskeläinen, H.; "*Combustion in Diesel Engines*"; [online] Available: https://www.dieselnet.com/tech/diesel_comb.php

[63] Rumsey J., Eckerle W., Stanton D., Farrell L., "*Off-Highway Heavy Vehicle Diesel Efficiency Improvement and Emissions Reduction*", Advanced Combustion Engine R&D FY Progress Report 311 V.1, Cummins Incorporated, (2005).

[64] [61] Schumacher L. and Gerpen J., "*Research Needs Resulting from Experiences of Fueling of Diesel Engines With Biodiesel*", Liquid Fuels and Industrial Products from Renewable Resources-Proceedings of the Third Liquid Fuel Conference, pp. 207-216, (1996).

[65] Zawadzki A., Shrestha D., He B., "*Biodiesel Blend Level Detection Using Ultraviolet Spectra*" Transactions of the ASABE 50, no. 4, pp. 1349-1353, (2007).

[66] Biodis Engineering Swiss, Biodiesel Process [online] Available: http://www.biodis-swiss.com/biodieselen.htm

[67] Bioenergy: Refueling the Future, The First Generation [online] Available: http://refuelingthefuture.yolasite.com/first-generation-biofuels.php

[68] Caprotti R, Breakspear A., Graupner Olaf, Thomas Klaua and Oliver Kohnen, "*Diesel Injector Deposits Potential in Future Fueling Systems*" SAE Technical Paper Series No. 2006-01-3359, (2006).

[69] Trasatti S., "*1799–1999: Alessandro Volta's 'Electric Pile': Two hundred years, but it doesn't seem like it*", Journal of electroanalytical chemistry 460, no 1, pp.1-4, (1999).

[70] Michelet H., "*L'inventeur Isaac de Rivaz: 1752-1828*", Vol. 2, Editions Saint-Augustin, (1965).

[71] Guarnieri M., "*When cars went electric, part one [historical]*", Industrial Electronics Magazine, IEEE 5, no 1, pp.61-62, (2011).

[72] LaFontaine B., "*Great Inventors and Inventions*", Dove Publication, Inc, pp.23, (1997).

[73] Surhone L., Tennoe M., Henssonow S., "*Alphonse Beau de Rochas*", Betascript Publishing, (2011).

[74] Volti R., "*Cars and Culture: The Life Story of a Technology*", Greenwood Publishing Group, pp. 3-4, (2006).

[75] Bird A., Daimler G., "*Gottlieb Daimler: inventor of the motor engine*", Weidenfeld & Nicolson (1962).

[76] Russell J., Cohn R., "*Gottlieb Daimler*", Book on Demand, 2012

[77] Linde A., "*Preston Tucker & Others: Tales of Brilliant Automotive Innovations*", pp. 150, (2011)

[78] Scalr D., "*Auto Repair for Dummies",* 2nd Edition, Wiley Publishing, pp. 134, (2011).

[79] Kiijarvi J., "*Diesel Fuel Injection System Simulation*", Helsinki University of Technology, Finland, PhD. Dissertation, 2003

[80] How Cars Work, The Workings of a Car Explained [online], Available: http://www.driving-test-success.com/how-cars-work.htm

[81] Thurston R., "*A History of the Growth of the Steam-engine, Parts 1-2*", (1878).

[82] Kras S., "*The Steam Engine*", Chelsea House Publisher, (2004)

[83] Moon J., "*Rudolf Diesel and the diesel engine*", Priory Press, (1974).

[84] Lepage J., "*German Military Vehicles of World War II: An Illustrated Guide to Cars*", McFarland and Company Inc., pp.104, (2007).

[85] Challen B., Baranescu R., "Diesel Engine Reference Book", Second Edition, pp.5, (1999).

[86] Erjavec J., Thompson R., "*Automotive Technology: A Systems Approach*", Cengage Learning, (2014).

[87] Zellat M., Abouri D., Conte T., "*Advanced modeling of DI Diesel Engines: Investigations on Combustion, High EGR level and multiple-injection Application to DI Diesel Combustion Optimization*" CD-adapco Group.

[88] Zhao, H., "*Advanced Direct Injection Combustion Engine Technologies and Development*" Volume2: Diesel Engines, Vol. 2. Elsevier, pp.120, (2009).

[89] Tuan T., Okada H., Tsukamoto T., Ohe K. and Iwasawa K., "*Effect of Rounding-off Nozzle Hole Inlet on Fuel Injection and Combustion Characteristics under High-Temperature and High-Pressure*" Marine Engineering 42, no. 2, pp.288-294, (2007).

[90] Abu-Gharbieh R., "*Laser sheet imaging and image analysis for combustion research",* Doctoral Dissertation, Chalmers University of Technology, (2001).

[91] The Lubrizol Corporation, "*Fundamentals of Compression-Ignition Engines (Part 1)"* [online] Available: http://www.hddeo.com/Fundamentals-of-Compression-Ignition-Engines-Part-1.html, (2015).

[92] Lane, B., "*Car emissions*"; [online] Available: http://www.nextgreencar.com/caremissions.php, (2015).

[93] Ganesan V., "*Internal Combustion Engines*", Tata McGraw-Hill Limited, 4th Edition, pp.324, (2012).

[94] Kobori S., Kamimoto T. and Aradi A., "*A study of ignition delay of diesel fuel sprays*", International Journal of Engine Research 1, no1, pp. 29-39, (2000).

[95] Hussain J., Palaniradja K., Alagumurthi N. and Manimaran R., "*Effect of exhaust gas recirculation (EGR) on performance and emission characteristics of a three cylinder direct injection compression ignition engine*", Alexandria Engineering Journal 51, no 4, 241-247. (2012).

[96] Dingle P., Lai M., "*Diesel Common Rail and Advanced Fuel Injection Systems*", Warrendale, PA: Society of Automotive Engineers, 138, Chap2, (2005).

[97] Tamilporai P., Chandrasekaran S. and Jancirani J., "*Design Of An Aftercooler For A Turbo Charged Diesel Engine*", no. 2004-28-0041, SAE Technical Paper, (2004).

[98] [96] Zhang L., "*A study of pilot injection in a DI diesel engine*", no.1999-01-3493, SAE Technical Paper, (1999).

[99] [97] Diesel combustion chambers; [online] Available: http://www.cdxetextbook.com/engines/comp/cylHeads/dieselcombustion.html

[100] [98] Macdonald D., "*The influence of inherent injector characteristics on high speed, multievent, fuel delivery*", INOV8 Technologies Plc CERC Chalmers, Combustion Engine Research Center Annual Report, (2000).

[101] Majewski W., Jääskeläinen H., "*What is Diesel Fuel*", [online], Available: http://www.dieselnet.com/tech/fuel_diesel.php

[102] Basics of Refining and Processing Additional Light Sweet Crude Oil [online] Available: http://www.sec.gov/Archives/edgar/data/1035002/000119312514065039/d680806dex9901.htm

[103] Statistical Data Set, Fuel Consumption (ENV01), Department for Transport, Transport energy and environment statistics, [online] Available: https://www.gov.uk/government/statistical-data-sets/env01-fuel-consumption, (2013).

[104] Chan J., "*Explanatory Memorandum to The Passenger Car, fuel consumption and CO_2 emissions information, amendment, Regulations 2013*", The Department for Transport, Environment Strategy, [online] Available: http://www.legislation.gov.uk/uksi/2013/65/pdfs/uksiem_20130065_en.pdf

[105] Euro Emissions Standards, Progressively tighter exhaust emissions limits to improve air quality and health, [online] Available: https://www.theaa.com/motoring_advice/fuels-and-environment/euro-emissions-standards.html

[106] Rumsey J., Eckerle W., Stanton D. and Farrell L., "*V.1Off-Highway Heavy Vehicle Diesel Efficiency Improvement and Emissions Reduction*", Cummins Inc., DOE Technology. FY Progress Report, (2004).

[107] Policy paper 2010 to 2015 government policy: Transport emissions, [online] Available: https://www.gov.uk/government/publications/2010-to-2015-government-policy-transport-emissions/2010-to-2015-government-policy-transport-emissions

[108] Clark R., Evans J. and Virrels I., "*An Evaluation of Shell GTL Diesel – The Environmental Benefits*", 8th Diesel Engine Emissions Reduction Workshop, An Evaluation of Shell GTL Diesel-the Environmental Benefits." Presentation at 8th, (2002).

[109] Busch R., "*Advanced Diesel Common Rail Injection System for Future Emission Legislation Roger Busch Common Rail System Engineering for PC Diesel Systems*" Robert Bosch GmbH 10th Diesel Emission Reduction Conference, pp. 1-27, (2004).

[110] Hervé G., Yves, D. and Agneta F., "*Biofuels and World Agricultural Markets: Outlook for 2020 and 2050*", INTECH Open Access Publisher, (2011).

[111] DECC, UK., "*Planning our electric future: A White Paper for secure, affordable and low-carbon electricity*", (2011).

[112] Oil and Gas, *Offshore Energy Strategic Environmental Assessment (SEA): An overview of the SEA process* [online] Available: https://www.gov.uk/guidance/offshore-energy-strategic-environmental-assessment-sea-an-overview-of-the-sea-process

[113] Petroleum and other liquids, United Kindon, [online] Available: http://www.eia.gov/beta/international/analysis.cfm?iso=GBR

[114] Lee S., Huh K., Kim Y. and Lee J., "*Analysis of in-cylinder fuel−air mixture distribution in a heavy duty CNG engine*", International Journal of Automotive Technology, Vol. 2, no. 3, pp. 93-101, (2001).

[115] Demirbas A., "*Importance of biodiesel as transportation fuel*", Energy policy 35, no 9, pp. 4661-4670, (2007).

[116] Hossain A., Salleh A., Boyce A., Chowdhury P. and Naqiuddin M., "*Biodiesel fuel production from algae as renewable energy*". American journal of biochemistry and biotechnology 4, no. 3 pp. 250-254, (2008).

[117] Emadi A., Lee Y. and Rajashekara K., "*Power electronics and motor drives in electric, hybrid electric, and plug-in hybrid electric vehicles*". Industrial Electronics, IEEE Transactions 55, no.6, pp. 2237-2245, (2008).

[118] Air Pollution; [online] Available: http://www.edu.dudley.gov.uk/roadsafety/pollution.htm

[119] Environmental Protection Agency "*Control of Air Pollution from Motor Vehicles: Tier 3 Motor Vehicle Emission and Fuel Standards Proposed Rule*", Federal register, Vol. 78, No. 98, Part II, 40 CFR Parts 79, 80, 85, (2013).

[120] Patz J., Campbell-Lendrum D., Holloway T. and Foley J., "*Impact of regional climate change on human health*", Nature 438 no.7066, pp.310-317, (2005).

[121] Diesel Distributor Fuel-injection Pumps – Robert Bosch GmbH, Postfach 300220, D-70442 Stuttgart. Automotive Equipment Business Sector, Department for Automotive Services, Technical Publications (KH/PDI2), (1999).

[122] World Health Organization; Available:
http://www.euro.who.int/mediacentre/PR/2004/20040617_1

[123] Uchida M. and Kai S., "*Air-fuel ratio control system*", Patent No. 4,913,122. Washington, DC: U.S. Patent and Trademark Office, (1990).

[124] "*Heavy Duty Vehicle Efficiency. Why Transport and Why HDV?*" Energy Technologies Institute, Holywell Building, Loughborough. UK.

[125] Kong S., Senecal1 P. and Reitz R., "*Spray Modeling in Diesel and Direct-Injection Gasoline Engines*" Oil & Gas Science and Technology, Rev. IFP, Vol. 54, No. 2, pp. 197-204, (1999).

[126] Karrholm F., "*Numerical Modelling of Diesel Spray Injection, Turbulence Interaction and Combustion*", Thermodynamic and Fluid Dynamics, Chalmers University of Technology, Sweden. Chap2, (2008).

[127] Habchi C., Verhoeven D., Huynh Huu C., Lambert L., Vanhemelryck J. and Baritaud T., "*Modeling Atomization and Break up in High−pressure Diesel Sprays*" Paper no. 970881. SAE Technical Paper, (1997).

[128] Kuo, K., "*Recent advances in spray combustion: Spray atomization and drop burning phenomena*" (Vol. 1). AIAA. (1996)

[129] Car encyclopedia, Fuel Injector [online], Available: http://repairpal.com/fuel-injector

[130] ProFlow Injection Technologies, Types of Fuel Injectors [online] Available:
http://www.proflowtech.com/types-of-fuel-injectors/

[131] Macdonald D., "*The characterisation of high pressure injection*", INOV8 Technologies PLC

[132] Giannadakis E. and Gavaises M., Theodorakakos A., "*The Influence of Variable Fuel Properties in High-Pressure Diesel Injectors*", Paper no. 2009-01-0832. SAE Technical Paper, (2009).

[133] Wakuri Y., Fujii M., Amitani T. and Tsuneya R., "*Studies on the penetration of fuel spray in a diesel engine*", Bulletin of JSME 3, no.9, pp.123-130, (1960).

[134] Mollenhauer K. and Tschöke H., "*Handbook of diesel engines*". Springer Science & Business Media, pp.147, (2010).

[135] "MotorBoating and Sailling", Magazine No. 3, Vol. 179, pp.38,)1997.(

[136] Nunney M., "*Light and Heavy Vehicle Technology*", Elsevier Ltd., Fourth Edition, pp.158, (2007).

[137] Zhao H., "*Advanced Direct Injection Combustion Engine Technologies and Development*" Volume2: Diesel Engines, Vol. 2. Elsevier, pp.61-67, (2009).

[138] Nagata K., "*State-of-Art technologies for Diesel Common Rail system*", no. 2004-28-0068, SAE Technical Paper, (2004).

[139] Zhao H., "*Advanced Direct Injection Combustion Engine Technologies and Development*" Volume2: Diesel Engines, Vol. 2. Elsevier, pp.75-77, (2009).

[140] Common Rail Fuel Injection, [online] Available: https://www.dieselnet.com/tech/diesel_fi_common-rail.php

[141] Reif K., "*Diesel Engine Management: Systems and Components*", Springer Fachmedien Wiesbaden, pp.64, (2014).

[142] Diesel Fuel Injectors Common Rail – Common Rail System [online], Available: http://www.densoautoparts.com.au/products/diesel-fuel-injectors/commonrail.aspx

[143] Lechner A.; (May 2013); "*Advantages of Servo-Driven Hydraulics for Large Injection Machines*"; Plastics Technology Plastics Technology 59, no. 5, pp. 40-44, (2013).

[144] Reif K., "*Diesel Engine Management: Systems and Components*", Springer Fachmedien Wiesbaden, pp.178, (2014).

[145] Saxena, S., '*Automobile Engineering*". Laxmi Publications, pp.32, (2009).

[146] Bell J., "*Modern Diesel Technology: Electricity and Electronics*". Cengage Learning, (2013)

[147] Giannadakis E., Papoulias D., Theodorakakos A. and Gavaises M., "*Simulation of cavitation in outward-opening piezo-type pintle injector nozzles*", Proceedings of the Institution of Mechanical Engineers, Part D: Journal of Automobile Engineering 222, no. 10, pp. 1895-1910, (2008).

[148] Lee J., Min K., Kang K., Bae C., Giannadakis E., M Gavaises and Arcoumanis C., "*Effect of piezo-driven and solenoid-driven needle opening of common-rail diesel injectors on internal nozzle*

flow and spray development", International Journal of Engine Research, Vol. 7, no 6, pp. 489-502, (2006).

[149] Nunney M., "*Light and Heavy Vehicle Technology*", Elsevier Ltd., Fourth Edition, pp.219, (2007).

[150] Standards catalogue, Fuel Systems http://www.iso.org/iso/iso_catalogue/catalogue_ics/catalogue_ics_browse.htm?ICS1=43&ICS2=060&ICS3=40

[151] Crolla D., "*Encyclopedia of Automotive Engineering*". John Wiley & Sons, Chap13, (2015).

[152] Zhao H., "*Advanced Direct Injection Combustion Engine Technologies and Development*" Volume2: Diesel Engines, Vol. 2. Elsevier, pp.86-87, (2009).

[153] Dingle P., Lai M., "*Diesel Common Rail and Advanced Fuel Injection Systems*", Warrendale, PA: Society of Automotive Engineers, 138, chap5, (2005).

[154] Fuel System – Injection Nozzles, pp. FU12 [online] Available: http://www.toyota4wd.dk/Teknik/1PZ-1HZ-1HDT/5-FU.pdf

[155] Akagawa H., Miyamoto T., Harada A., Sasaki S., Shimazaki N., Hashizume T. and Tsujimura K., "*Approaches to solve problems of the premixed lean diesel combustion*" (No. 1999-01-0183). SAE Technical Paper, (1999).

[156] Marsh E. and Waldron C., "*Some Characteristics of Sprays Obtained from Pintle-type Injection Nozzles.*", (1933).

[157] Diesel Fuel Injector Nozzles [online], Available: https://www.dieselnet.com/tech/engine_fi_nozzle.php

[158] Kornfeld M. and Suvorov L., "*On the destructive action of cavitation*", Journal of Applied Physics 15, no.6, pp.495-506, (1944).

[159] Parsons C. and Cook S., "*Investigations into The Causes of Corrosion or Erosion of Propellers*", Journal of the American Society for Naval Engineers 31, no2, pp.536-541, (1919).

[160] Samson, A.G., Technical Information, "*Cavitation in Control Valves*" Samson AG, Frankfurt, Germany. (2003).

[161] Gavaises M., Papoulias D., Giannadakis E., Andriotis A., Mitroglou N. and Theodorakakos A., "*Comparison of cavitation formation and development in Diesel VCO nozzles with cylindrical and converging tapered holes*", THIESEL 2008 Conference on Thermo-and fluid dynamics processes in Diesel Engines, Valencia, Spain, (2008).

[162] Ganippa L., Bark G., Andersson S. and Chomiak J., "*Cavitation: a contributory factor in the transition from symmetric to asymmetric jets in cross-flow nozzles*". Experiments in Fluids, 36(4), pp.627-634, (2004).

[163] Chaves H., Knapp M., Kubitzek A., Obermeier F. and Schneider T., "*Experimental study of cavitation in the nozzle hole of diesel injectors using transparent nozzles*" No. 950290, SAE technical paper, (1995).

[164] Parkin B. and Holl J., "*Incipient-Cavitation Scaling Experiments for Hemispherical and 1.5-Caliber Ogive-Nosed Bodies*", No. S7958, California Institute of Technology Pasadena Hydrodynamics Lab, (1953).

[165] Befrui B., Corbinelli G., Hoffmann G., Andrews J. and Sankhalpara S., "*Cavitation and Hydraulic Flip in the Outward-Opening GDi Injector Valve-Group*", Paper no. 2009-01-1483, SAE Technical Paper, (2009).

[166] Bergwerk, W., "*Flow pattern in diesel nozzle spray holes*", Proceedings of the Institution of Mechanical Engineers, 173(1), pp.655-660, (1959).

[167] Liao Z., Li J., Chen D., Deng X., Tang C. and Zhang F. "*The Theory and Experimental Study of the Self-Excited Oscillation Pulsed Jet Nozzle (Pipeline Pulsed Flow Generator)*", Chinese Journal of Mechanical Engineering (English Edition) 16, no. 4, pp. 379-383, (2013).

[168] Chahine G., Johnson Jr., Lindenmuth, W., and Frederick, G., "*The use of self-resonating cavitating water jets for underwater sound generation*" The Journal of the Acoustical Society of America 77, no. 1, pp. 113-126, (1985).

[169] Chadwell C., Dingle P., "*Effect of Diesel and Water Co-injection with Real-Time Control on Diesel Engine Performance and Emissions*", SAE Int. World congress, Detroid, (2008).

[170] Cerutti S., Knio O and Katz J., "*Computational study of jet cavitation inception using phase analysis*". In 2000 ASME Fluids Engineering Division Summer Meeting, Boston, MA, (2000).

[171] Katz J. and O'hern T.J., "*Cavitation in large scale shear flows*", Journal of fluids engineering, 108(3), pp.373-376, (1986).

[172] Gopalan S., Katz J. and Knio O., "*The flow structure in the near field of jets and its effect on cavitation inception".* Journal of fluid mechanics, *398*, pp.1-43, (1999)

[173] Xing T. and Frankel S., "*Effect of cavitation on vortex dynamics in a submerged laminar jet*". AIAA journal, 40(11), pp.2266-2276, (2002).

[174] Choi J., Hsiao C., Chahine G. and Ceccio S., "*Growth, oscillation and collapse of vortex cavitation bubbles*". Journal of Fluid Mechanics, *624*, pp.255-279. (2009).

[175] Hutli E., Nedeljkovic M. and Ilic V., "*Visualization of Submerged Cavitating Jet: Part One –The Phenomenon, Time-Synchronization, Photo Objectives and Sono-Luminescence*", 16th Australasian Fluid Mechanics Conference (AFMC), pp. 876-880, (2007).

[176] Hutli E., Nedeljkovic M. and Ilic V., "*Visualization of Submerged Cavitating Jet: Part Two – Influences of Hydrodynamic Conditions, Nozzle Geometry and Visualization System Arrangement*", 16th Australasian Fluid Mechanics Conference (AFMC), pp. 881-886. School of Engineering, (2007).

[177] Schmidt D. and Corradini M., "*The internal flow of diesel fuel injector nozzles: a review*". International Journal of Engine Research, 2(1), pp.1-22. (2001).

[178] Weiguo S., "*Thermodynamics of alkane solutions*", [Online], Available: http://ir.canterbury.ac.nz/handle/10092/7727, (1988).

[179] Brereton R., "*Dissipation of Nitrogen Gas Ejected from Orienting Mechanism of Orbiting Satellites*", (2012).

[180] Battino R., Rettich T. and Tominaga T., "*The Solubility of Nitrogen and Air in Liquids*", Journal of Physical and Chemical Reference, Data 13, no2, pp. 563-600, (1984).

[181] Thomsen E. and Gjaldbaek J., "*The solubility of hydrogen, nitrogen, oxygen and ethane in normal hydrocarbons*", Acta chem. scand, 17(1), pp.127-133, (1963).

[182] Wakefield D. and Marsh K., "*Viscosities of nonelectrolyte liquid mixtures. I. n-Hexadecane + n-Octane*", International Journal of Thermophysics, vol.8, no 6, pp.649-662, (1987).

[183] Tanaka Y., Hosokawa H., Kubota H. and Makita T., "*Viscosity and density of binary mixtures of cyclohexane with n-Octane, n-dodecane, and n-Hexadecane under high pressures*", International Journal of Thermophysics, vol.12, no 2, pp.245-264, (1991).

[184] De Lorenzi L., Fermeglia M. and Torriano G., *"Density and Viscosities of 1,1,1-Trichloroethane plus Paraffins and plus Cycloparafins at 298.15 K",* Journal of Chemical Engineering, 39, no. 3, 483-487, (1994).

[185] Lacher J. and Hunt R.; "*Vapour Pressures of Binary Liquid Mixtures*", Journal of American Chemical Society 63, no 6, pp. 1752–1756, (1941).

[186] Kay W., Hoffman R. and Davies O., "*Vapor-liquid equilibrium relations of binary systems n-butane-n-pentane and n-butane-n-hexane",* Journal of Chemical and Engineering Data, 20, no 3, 333-338, (1975).

[187] Maurice G., Djeridi H. and Barre S., "*Experimental investigation of a cavitating backward-facing step flow*", IOP Conference Series: Earth and Environmental Science, vol. 22, no. 5, p. 052008. IOP Publishing, (2014).

[188] Lockett R. and Jeshani M., "*An experimental investigation into the effect of hydrodynamic cavitation on diesel*", International Journal of Engine Research vol 14, no. 6, pp. 606-621. (2013).

[189] Motion of Bubbles and Bubble characteristics, [online], Available: http://www.seas.ucla.edu/stenstro/Bubble.pdf.

[190] Franc J. and Michel J., "*Fundamentals of cavitation",* (Vol. 76). Springer Science & Business Media, (2006).

[191] Tullis J., "*Cavitation guide for control valves", (*No. NUREG/CR--6031). Nuclear Regulatory Commission, Washington, DC (United States). Div. of Engineering; Tullis Engineering Consultants, Logan, UT (United States), (1993).

[192] Lockett R., Ndamuso N. and Price, R., "*Cavitation Inception in Immersed Jet Shear Flows*." In Journal of Physics: Conference Series (Vol. 656, No. 1, p. 012090). IOP Publishing, (2015).

[193] D'Agostino L. and Salvetti M. eds., "*Fluid dynamics of cavitation and cavitating turbopumps*", Springer Science & Business Media, pp. 1-8, (2008).

[194] Lockett R., Fatmi, Z., Kuti, O. and Price, R., "*An Optical Characterization of the Effect of High-Pressure Hydrodynamic Cavitation on Diesel"* (No. 2016-01-0841). SAE Technical Paper, (2016).

[195] Lockett R., Fatmi Z., Kuti O. and Price R., "*An Investigation into the Effect of Hydrodynamic Cavitation on Diesel using Optical Extinction*". In Journal of Physics: Conference Series (Vol. 656, No. 1, p. 012091). IOP Publishing, (2015).

[196] Lockett R., Liverani L., Thaker D., Jeshani M. and Tait N.P., "*The characterization of diesel nozzle flow using high speed imaging of elastic light scattering",* Fuel, 106, pp.605-616, (2013).

[197] Laserpoint Innovating with Photonics [online], Available: http://www.laserpoint.eu/en

[198] Fröhlich A. and Schober S., "*The influence of tocopherols on the oxidation stability of methyl esters*", Journal of the American Oil Chemists' Society, 84(6), pp.579-585, (2007).

Blank Page

APPENDIX A

A.1. Effect of Incipient Cavitation on n-Hexadecane Based Fuel Jet – Operational Procedures

In the first instance, ahead of filling out the High Pressure Fuel Bottles, a series of operations were required; below are the different steps followed in order to operate the rig.

A.1.1. All operating machineries were turned off

Below is the list of all rig parts needed to be turned off:

- The BOC N_2 bottle and Gas Regulator; the Blue Ball $Valve_A$ and Blue Ball $Valve_B$ used as the fuel flew to and from the $Tank_A$ or the $Tank_B$ – this comprises the Blue Ball Valve at the bottom of the Filter as well as the Red Ball valve connecting the High Pressure Fuel Bottles to the Fused Silica Receiver; the Bleed valves underneath each of the 3 High Pressure Fuel Bottles.
- The 3 way valves were placed in an off switch position – 3 way $valve_1$, 3 way valves, 3 way $valve_3$; leading to the Black Pressure Release Valve at the top of High Pressure Fuel $Bottles_1$ – the Plastic Hose on top of the High Pressure Fuel Bottles1 was used to extract pressure avoiding cases of over-pressurization.
- The Pressure Regulator – Placed downstream of the Fused Silica Receiver was also turned off. Hence the Filler Cap_A on the $Tank_A$ and the Filler Cap_B on the Tank B were loosened, following by the emptying of the 1 L Bottle used to collect the excess fuel from the bottom of the High Pressure Fuel Bottles.

Care was taken to make sure that the Black Valve underneath the Fused Silica Receiver remained closed as well as the M6 Screw on top of the Fused Silica Receiver remained bolted – Hence, the Fused Silica Receiver was filled up with fuel to avoid bubble formation.

A.1.2. Filling High Pressure Fuel Bottles

Fuel located inside the $Tank_A$

As the mechanical rig was a closed-loop system, at the start of the experiment, the fuel could be poured in either of the $Tank_A$ of $Tank_B$.

At the start, the $Filler\ Cap_B$ was loosen and the $Pressure\ Release\ Valve_B$ on $Tank_B$ was open. Hence, the $Tank_A$ was pressurize by closing the $Filler\ Cap_A$ as well as the $Pressure\ Release\ Valve_A$ situated on top of the $Tank_A$.

Next, the $Blue\ Ball\ Valve_A$ situated underneath the $Tank_A$ was opened, making sure that the Red Back Pressure Valve was also opened – This was done to enable the fuel to flow from the $Tank_A$ to the Filter to the High Pressure Fuel Bottles.

The 3 way valves were positioned so that, $3\ way\ valve_1$ was set to Low Pressure (Prime), $3\ way\ valve_2$ to $Tank_A$ and $3\ way\ valve_3$ to $Tank_B$.

As the pressure on BOC N_2 Bottle was turned on – the pressure was set to a maximum of 0.5 bar gauge using the Gas Regulator – The Pressure from N_2 Bottle was not to exceed the Filter maximum working pressure in order to avoid a sudden burst of gas.

At this stage, the rig was ready to be filled up. The High Pressure Fuel Bottles were filled up by opening the $Bleed\ Valve_1$ situated at the bottom of the $High\ Pressure\ Fuel\ Bottles_1$ – this was located far right when standing face to $3\ way\ valve_1$.

It was important to keep an eye on the Bleed $valve_1$ closing it as soon as the High Pressure Fuel $Bottle_1$ was filled to avoid spillage; the procedure was then repeated using High Pressure Fuel $Bottle_2$ and High Pressure Fuel $Bottle_3$.

The Red Back Pressure Valve was then closed making sure that the 3 way $valve_1$ (only) was on the off switch position.

The last step was to make sure, that the Blue Ball $Valve_A$ underneath the$Tank_A$ was closed and, that the pressure inside the $Tank_A$ was released by opening the Pressure Release Valve and loosening the Filler Cap_A situated on top of the $Tank_A$.

A.1.3. Running the rig

Before running the rig, a second check was done on the ball valves in order to make sure that the valves were still turned off. Hence, the Filler Cap_B on the $Tank_B$ was loosen and the Pressure Release Valve was opened. The procedure was repeated for the $Tank_A$ when needed.

Next the 3 way $valve_1$ (only) was positioned to High Pressure (Run) in preparation for data measurement, making sure that 3 way $valve_2$ was set to the $Tank_A$ and that 3 way $valve_3$ was set to the to $Tank_B$.

The pressure on the BOC N_2 Bottle was then set, by setting the Gas Regulator between 5 and 10 bar gauge. Hence the Red Ball Valve was slowly opened (allowing the fuel to flow from the High Pressure Fuel Bottles to the Fused Silica Receiver) first up to a small amount, until the maximum opening was reached – It was vital to keep an eye on the Receiver being filled to avoid cases of spillage.

An adjustment of the pressure readings on the N_2 Bottle was made when required – Hence the Upstream Pressure was set to the highest value needed for the experiment in order to get the

corresponding Downstream Pressure leading to incipient cavitation. In order to decrease the Upstream Pressure, the Nitrogen Regulator was turned anticlockwise to a small amount hence the N_2 inside the High Pressure Fuel Bottles was released by a corresponding amount helping to obtain the required Upstream Pressure.

For cases where the gas appears inside the Fused Silica Receiver, the Red Ball Valve was closed off immediately – N_2 going through could burse the Fused Silica Receiver as the High Pressure Fuel Bottles were emptied of fuel.

N_2 was released by opening the valve connected to the High Pressure Fuel $Bottles_1$ – here care was taken to make sure that the Plastic Hose on top of the High Pressure Fuel $Bottles_1$ was connected to an extract fan to avoid breathing contaminated air.

A.1.4. Draining

- **Fuel contained inside the Fused Silica Receiver**

The different steps followed were: Placing the Drainage Bottle underneath the Fused Silica Receiver, Inserting the Black Hose (connected to the base of the Fused Silica Receiver) inside the Drainage Bottle; Opening the plastic valve at the base of the Fused Silica Receiver; Loosening the Ceiling Bolt on the upper plate of the Fused Silica Receiver – in order to release the pressure and drain the fuel; Closing off the Plastic Valve and tightening the Ceiling Bolt on top of the Fused Silica Receiver and safely pouring the fuel contained in the Drainage Bottle into one of the tanks ($Tank_A$ or $Tank_B$) – Following that, the Drainage Bottle was stored in a safe place for later use.

- **Fuel contained inside the Rig**

The different steps followed were: Isolating the main part of the rig from the Fused Silica Receiver unit – making sure that the Fused Silica Receiver was emptied – disconnecting the Hose to the 3 way

valve$_3$ as well as disconnecting the Hose at the base of the Fused Silica Receiver and hence connecting it to 3 way valve$_3$.

Next, making sure that the whole fuel contained inside the rig was located in one tank. Afterward, pressurizing the Tank$_A$, and hence following the filling procedure to make sure that the complete fuel flew inside the High Pressure Fuel Bottles.

Running the rig following the running procedures, making sure that the whole fuel was located in the Tank$_B$.

Setting the pressure on the BOC N_2 Bottle – the Gas Regulator was set to a maximum of 0.5 bar gauge and hence slowly the Red Blade Valve (allowing the fuel to flow from the High Pressure Fuel Bottles to the Tank$_B$), was opened first up to a small amount, until it was fully opened – this was done while keeping an eye on the Tank$_B$ as it was being filled.

Hence, the Red Ball Valve which connected the Filter to the High Pressure Fuel Bottles was turned off. As the tank get filled to the maximum level, BOC N_2 Bottle was turned off and the 6 mm plastic hose was connected to the Filter on one end as it was inserted into a 2.5 L Drainage Bottle on the other end.

Next, the Filter Blue Ball Valve was opened and the filling Procedure was followed, considering the located fuel in the Tank$_B$. Hence, the Blue Ball Valve$_B$ was opened to enable the fuel to flow from the Tank$_B$ to the Filter.

The BOC N_2 Bottle was set to a very small amount – keeping an eye on the fuel flowing into the 2.5 L drainage bottle until the Tank$_B$ was fully emptied.

Last, the Blue Ball Valve$_B$ was closing off – Which enable the fuel to flow from the Tank$_B$ to the Filter – and hence the N_2 Bottle was switched off.

A.1.5. Receiver Nozzle Replacement

The different steps followed were: Emptying the Fused Silica Receiver by following the Draining Procedure; Placing the laboratory wipe paper on the floor underneath the Fused Silica Receiver – this was a precaution measure in case of spillage; Unscrewing the 4 M4 bolts located at the base of the Fused Silica Receiver – making sure to do this diagonally to avoid being faced with a build-up of pressure on one side of the Fused Silica Receiver base; Safely storing the 4 Screw Bolts and the rig piece attached to the Fused Silica Receiver.

Removing the Injector Nozzle – if need be; Inserting the new Injector Nozzle needed for the experiment – making sure to clean the nozzle with ethanol to clear the hole entry of the nozzle.

Last, reattaching the rig piece and the 4 M4 Screw Bolts – Once more doing this diagonally to avoid pressure build-up; Checking that the Ceiling Bolt on the upper plate of the Receiver and the valve underneath the Fused Silica Receiver were both closed.

A.2. Incipient Cavitation Rig

An additional Six pictures were taken to point out the components of the incipient cavitation rig.

Figure A 2 - 1 Incipient cavitation rig

From Figure A.2-1, the N_2 bottles, the fuel tanks as well as the injector units are represented.

A.3. Acrylic Nozzles

Below is a sample of the Acrylic nozzles used during the experiment.

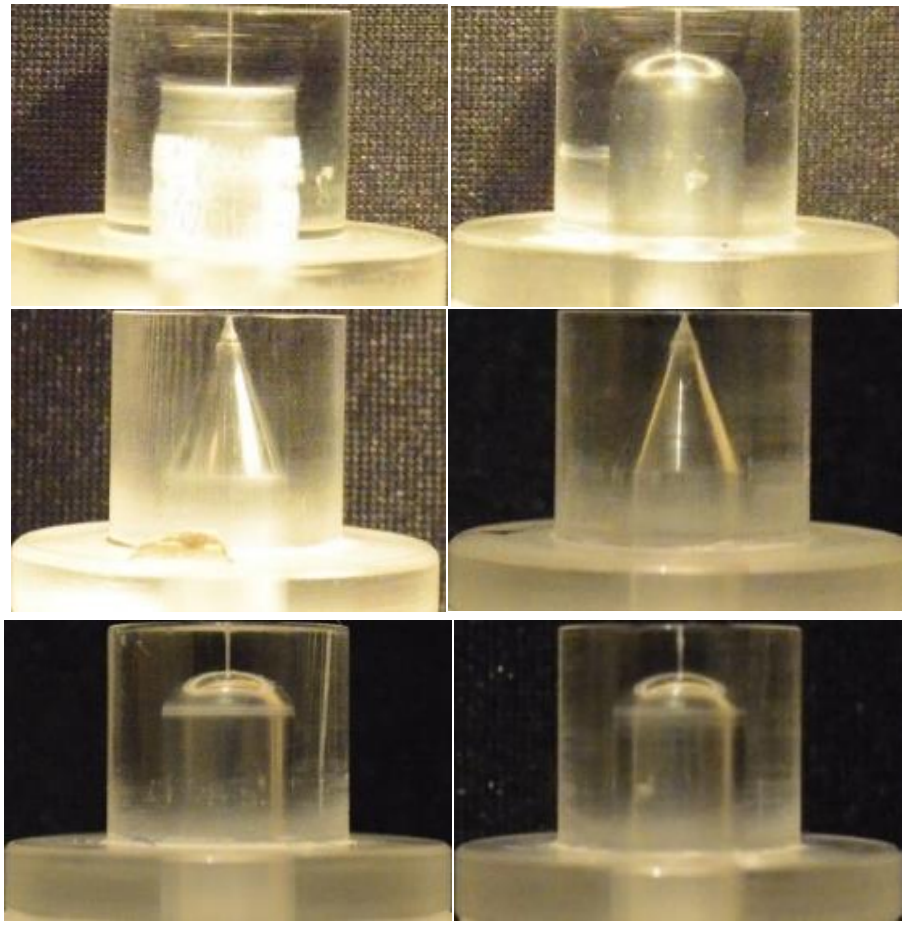

Figure A 3 - 1 0.14 mm Cylindrical, Hemispherical and Conical Nozzles

The pictures of the acrylic nozzles, from the first batch of nozzles, were taken a month into the experiment. The first picture, of the Cylindrical nozzle, shows the extent of the damages caused to the nozzle as the experiment made use of high pressures.

A.4. Saturated Vapour Pressure

The Total Saturated Vapour Pressure was obtained Using the Antoine's Coefficients.

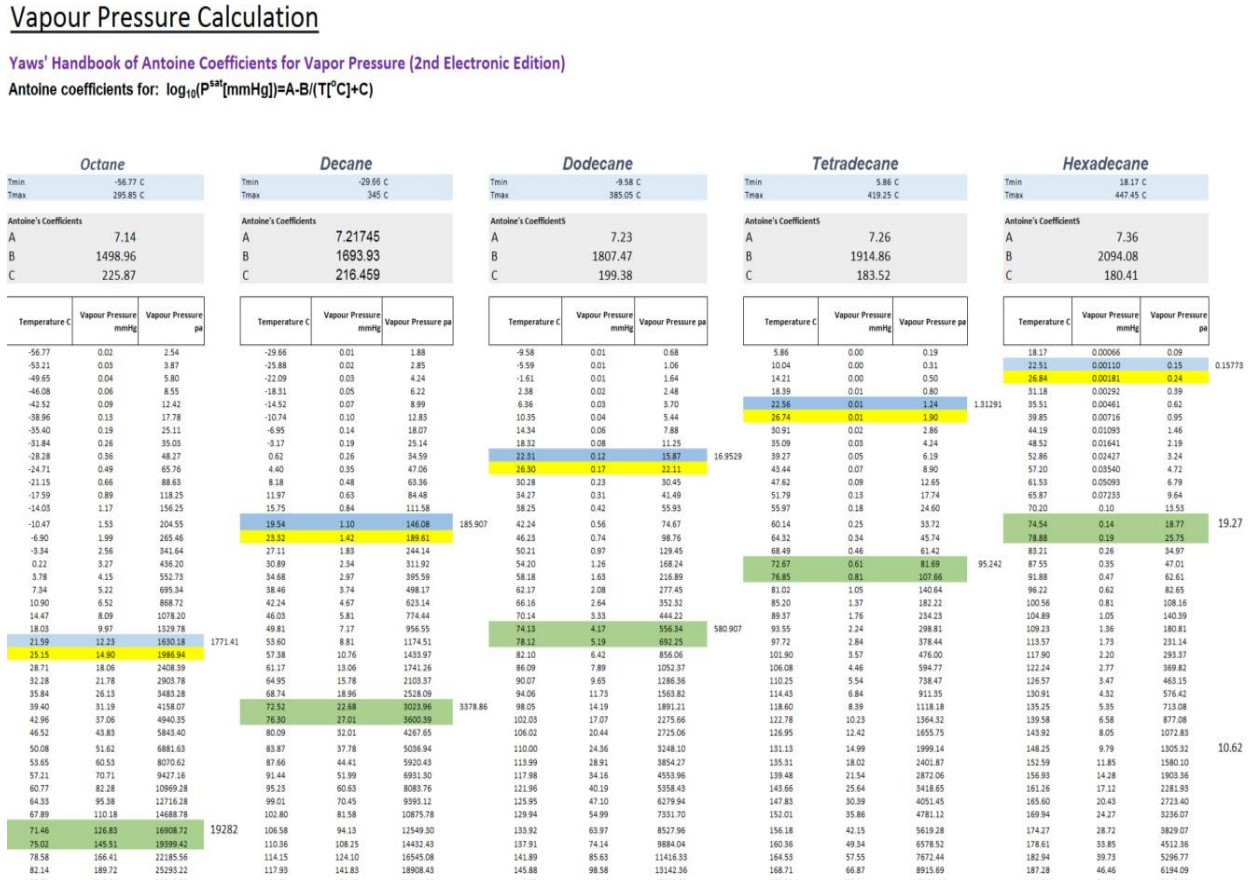

Vapour Pressure Calculation

Yaws' Handbook of Antoine Coefficients for Vapor Pressure (2nd Electronic Edition)

Antoine coefficients for: $\log_{10}(P^{sat}[mmHg])=A-B/(T[^{\circ}C]+C)$

Octane		Decane		Dodecane		Tetradecane		Hexadecane	
Tmin	-56.77 C	Tmin	-29.66 C	Tmin	-9.58 C	Tmin	5.86 C	Tmin	18.17 C
Tmax	295.85 C	Tmax	345 C	Tmax	385.05 C	Tmax	419.25 C	Tmax	447.45 C
Antoine's Coefficients		Antoine's Coefficients		Antoine's Coefficients		Antoine's Coefficients		Antoine's Coefficients	
A	7.14	A	7.21745	A	7.23	A	7.26	A	7.36
B	1498.96	B	1693.93	B	1807.47	B	1914.86	B	2094.08
C	225.87	C	216.459	C	199.38	C	183.52	C	180.41

Temperature C	Vapour Pressure mmHg	Vapour Pressure pa		Temperature C	Vapour Pressure mmHg	Vapour Pressure pa		Temperature C	Vapour Pressure mmHg	Vapour Pressure pa		Temperature C	Vapour Pressure mmHg	Vapour Pressure pa		Temperature C	Vapour Pressure mmHg	Vapour Pressure pa	
-56.77	0.02	2.54		-29.66	0.01	1.88		-9.58	0.01	0.68		5.86	0.00	0.19		18.17	0.00066	0.09	
-53.21	0.03	3.87		-25.88	0.02	2.85		-5.59	0.01	1.06		10.04	0.00	0.31		22.51	0.00110	0.15	0.15773
-49.65	0.04	5.80		-22.09	0.03	4.24		-1.61	0.01	1.64		14.21	0.00	0.50		26.84	0.00181	0.24	
-46.08	0.06	8.55		-18.31	0.05	6.22		2.38	0.02	2.48		18.39	0.01	0.80		31.18	0.00292	0.39	
-42.52	0.09	12.42		-14.52	0.07	8.99		6.36	0.03	3.70		22.56	0.01	1.24	1.31291	35.51	0.00461	0.62	
-38.96	0.13	17.78		-10.74	0.10	12.83		10.35	0.04	5.44		26.74	0.01	1.90		39.85	0.00716	0.95	
-35.40	0.19	25.11		-6.95	0.14	18.07		14.34	0.06	7.88		30.91	0.02	2.86		44.19	0.01093	1.46	
-31.84	0.26	35.03		-3.17	0.19	25.14		18.32	0.08	11.25		35.09	0.03	4.24		48.52	0.01641	2.19	
-28.28	0.36	48.27		0.62	0.26	34.59		22.31	0.12	15.87	16.9529	39.27	0.05	6.19		52.86	0.02427	3.24	
-24.71	0.49	65.76		4.40	0.35	47.06		26.30	0.17	22.11		43.44	0.07	8.90		57.20	0.03540	4.72	
-21.15	0.66	88.63		8.18	0.48	63.36		30.28	0.23	30.45		47.62	0.09	12.65		61.53	0.05093	6.79	
-17.59	0.89	118.25		11.97	0.63	84.48		34.27	0.31	41.49		51.79	0.13	17.74		65.87	0.07233	9.64	
-14.03	1.17	156.25		15.75	0.84	111.58		38.25	0.42	55.93		55.97	0.18	24.60		70.20	0.10	13.53	
-10.47	1.53	204.55		19.54	1.10	146.08	185.907	42.24	0.56	74.67		60.14	0.25	33.72		74.54	0.14	18.77	19.27
-6.90	1.99	265.46		23.32	1.42	189.61		46.23	0.74	98.76		64.32	0.34	45.74		78.88	0.19	25.75	
-3.34	2.56	341.64		27.11	1.83	244.14		50.21	0.97	129.45		68.49	0.46	61.42		83.21	0.26	34.97	
0.22	3.27	436.20		30.89	2.34	311.92		54.20	1.26	168.24		72.67	0.61	81.69	95.242	87.55	0.35	47.01	
3.78	4.15	552.73		34.68	2.97	395.59		58.18	1.63	216.89		76.85	0.81	107.66		91.88	0.47	62.61	
7.34	5.22	695.34		38.46	3.74	498.17		62.17	2.08	277.45		81.02	1.05	140.64		96.22	0.62	82.65	
10.90	6.52	868.72		42.24	4.67	623.14		66.16	2.64	352.32		85.20	1.37	182.22		100.56	0.81	108.16	
14.47	8.09	1078.20		46.03	5.81	774.44		70.14	3.33	444.22		89.37	1.76	234.23		104.89	1.05	140.39	
18.03	9.97	1329.78		49.81	7.17	956.55		74.13	4.17	556.34	580.907	93.55	2.24	298.81		109.23	1.36	180.81	
21.59	12.23	1630.18	1771.41	53.60	8.81	1174.51		78.12	5.19	692.25		97.72	2.84	378.44		113.57	1.73	231.14	
25.15	14.90	1986.94		57.38	10.76	1435.97		82.10	6.42	856.06		101.90	3.57	476.00		117.90	2.20	293.37	
28.71	18.06	2408.39		61.17	13.06	1741.26		86.09	7.89	1052.37		106.08	4.46	594.77		122.24	2.77	369.82	
32.28	21.78	2903.78		64.95	15.78	2103.37		90.07	9.65	1286.36		110.25	5.54	738.47		126.57	3.47	463.15	
35.84	26.13	3483.28		68.74	18.96	2528.09		94.06	11.73	1563.82		114.43	6.84	911.35		130.91	4.32	576.42	
39.40	31.19	4158.07		72.52	22.68	3023.96	3378.86	98.05	14.19	1891.21		118.60	8.39	1118.18		135.25	5.35	713.08	
42.96	37.06	4940.35		76.30	27.01	3600.39		102.03	17.07	2275.66		122.78	10.23	1364.32		139.58	6.58	877.08	
46.52	43.83	5843.40		80.09	32.01	4267.65		106.02	20.44	2725.06		126.95	12.42	1655.75		143.92	8.05	1072.83	
50.08	51.62	6881.63		83.87	37.78	5036.94		110.00	24.36	3248.10		131.13	14.99	1999.14		148.25	9.79	1305.32	10.62
53.65	60.53	8070.62		87.66	44.41	5920.43		113.99	28.91	3854.27		135.31	18.02	2401.87		152.59	11.85	1580.10	
57.21	70.71	9427.16		91.44	51.99	6931.30		117.98	34.16	4553.96		139.48	21.54	2872.06		156.93	14.28	1903.36	
60.77	82.28	10969.28		95.23	60.63	8083.76		121.96	40.19	5358.43		143.66	25.64	3418.65		161.26	17.12	2281.93	
64.33	95.38	12716.28		99.01	70.45	9393.12		125.95	47.10	6279.94		147.83	30.39	4051.45		165.60	20.43	2723.40	
67.89	110.18	14688.78		102.80	81.58	10875.78		129.94	54.99	7331.70		152.01	35.86	4781.12		169.94	24.27	3236.07	
71.46	126.83	16908.72	19282	106.58	94.13	12549.30		133.92	63.97	8527.96		156.18	42.15	5619.28		174.27	28.72	3829.07	
75.02	145.51	19399.42		110.36	108.25	14432.43		137.91	74.14	9884.04		160.36	49.34	6578.52		178.61	33.85	4512.36	
78.58	166.41	22185.56		114.15	124.10	16545.08		141.89	85.63	11416.33		164.53	57.55	7672.44		182.94	39.73	5296.77	
82.14	189.72	25293.22		117.93	141.83	18908.43		145.88	98.58	13142.36		168.71	66.87	8915.69		187.28	46.46	6194.09	

Figure A 4 - 1 Yaw's Handbook of Antoine Coefficients for Vapour Pressure

The Total Saturated Vapour Pressure was obtained considering the vapour pressures of n-Octane, n-Decane, "n-Dodecane" n-Tetradecane and n-Hexadecane respectively. The vapour pressure at 296 K and 70 ^{0}C respectively were obtained using interpolation. From Figure A.3 a decrease in the vapour pressure is observer with n-Octane having the highest vapour pressure.

A.5. CATIA Drawing

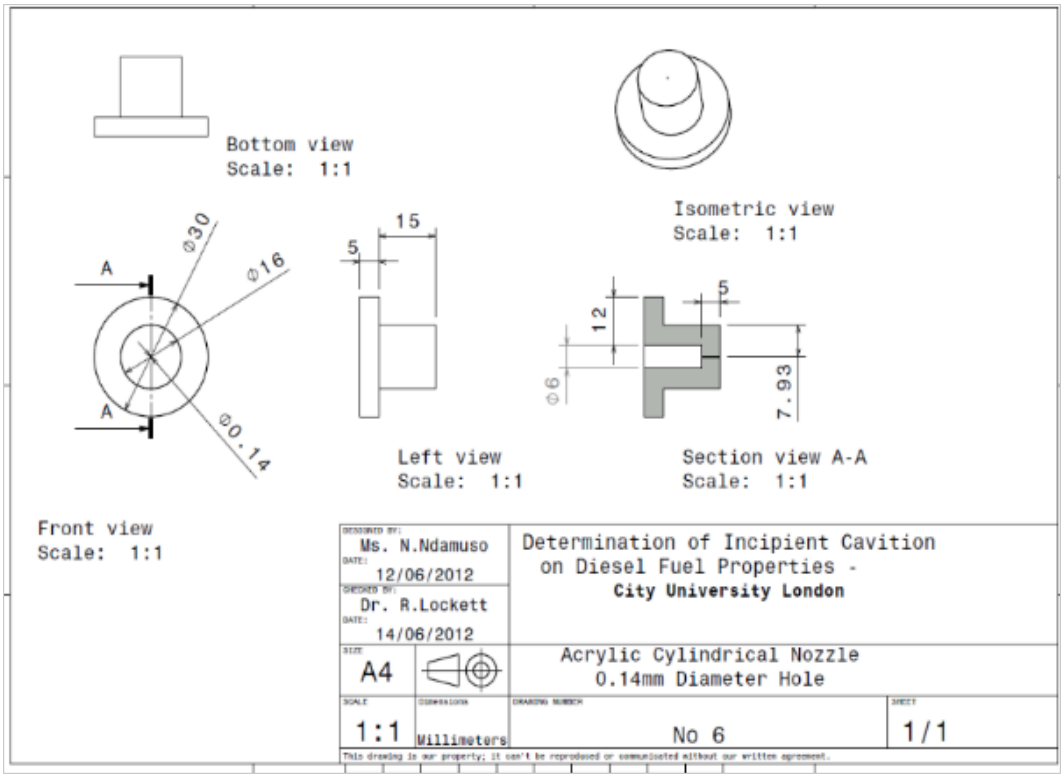

Figure A.5 – 1. Cylindrical nozzle, 14mm hole diameter – 5 mm nozzle depth

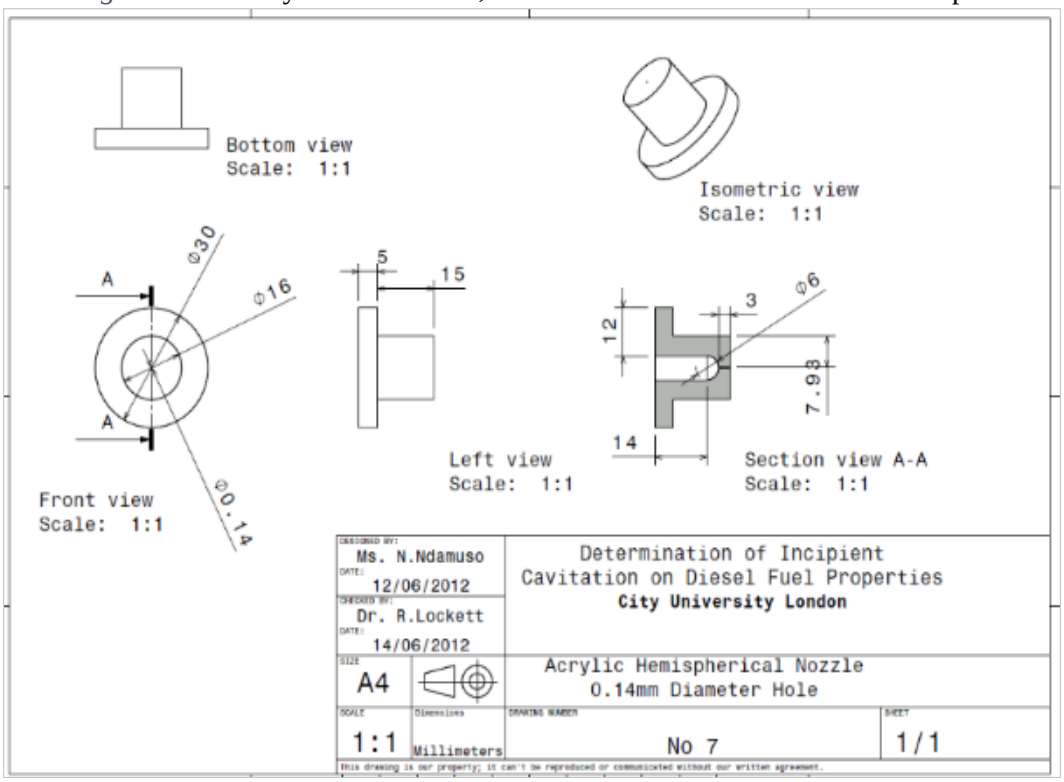

Figure A.5 – 2 Acrylic Hemispherical nozzle, 14mm hole diameter – 3mm nozzle depth

A.6. Discharge Coefficient Results

Below are, the volumetric flow rate as well as the discharge coefficient measurement for the 0.25 mm nozzle hole diameter.

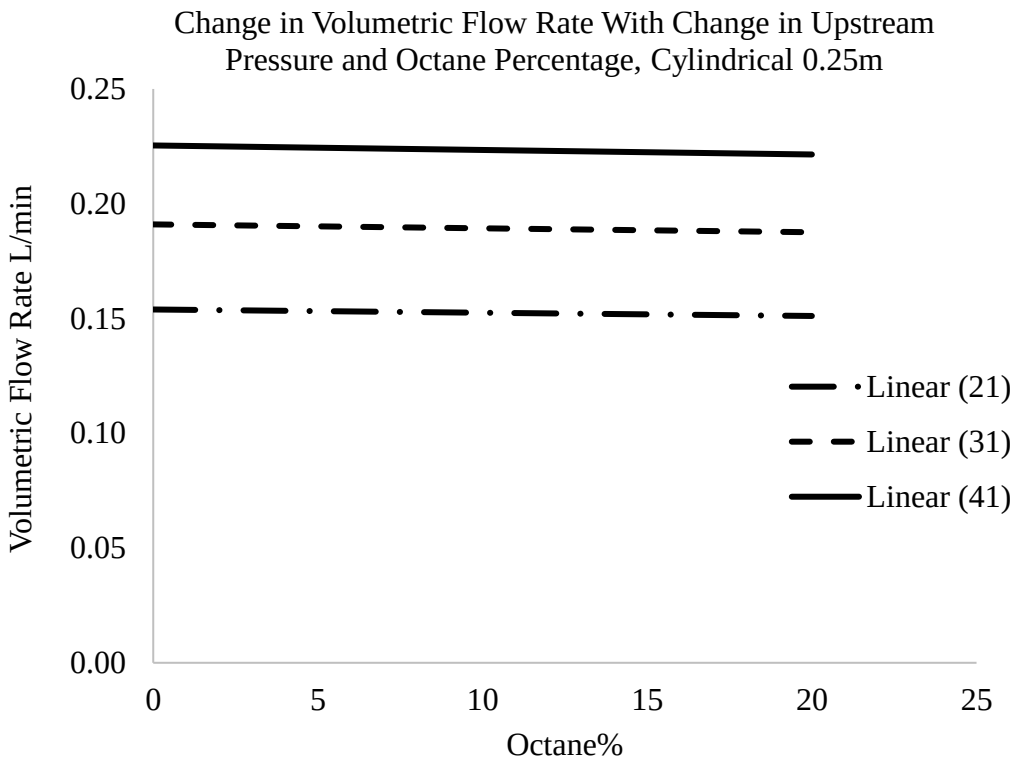

Figure A 6 - 1 Volumetric Flow Rate Cylindrical 0.25m

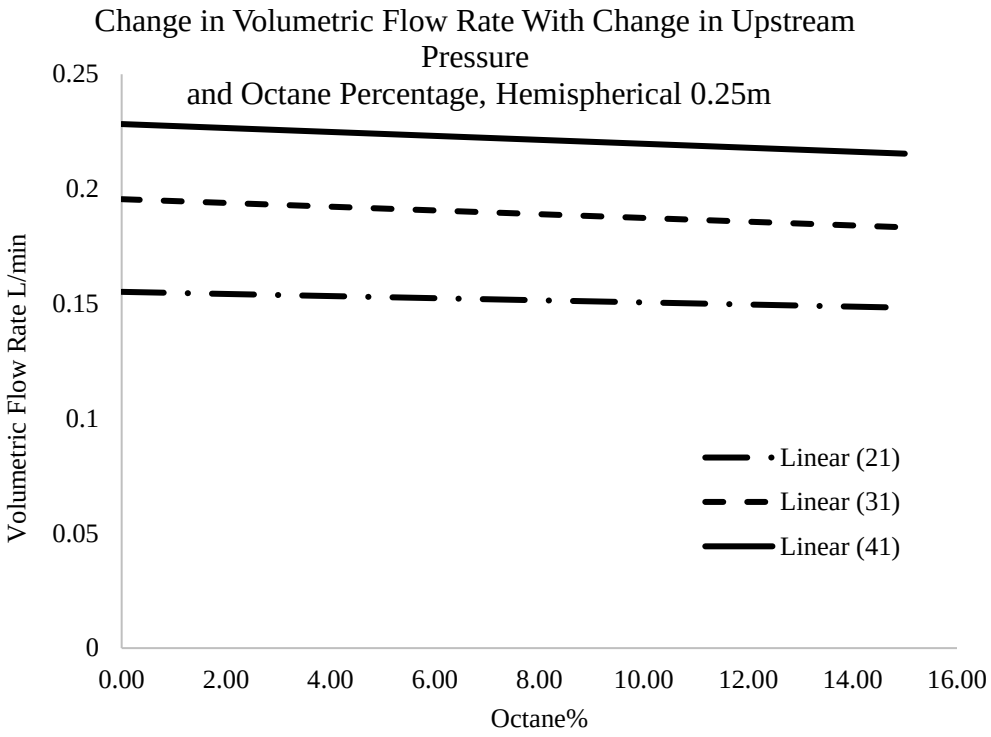

Figure A 6 - 2 Volumetric Flow Rate Hemispherical 0.25m

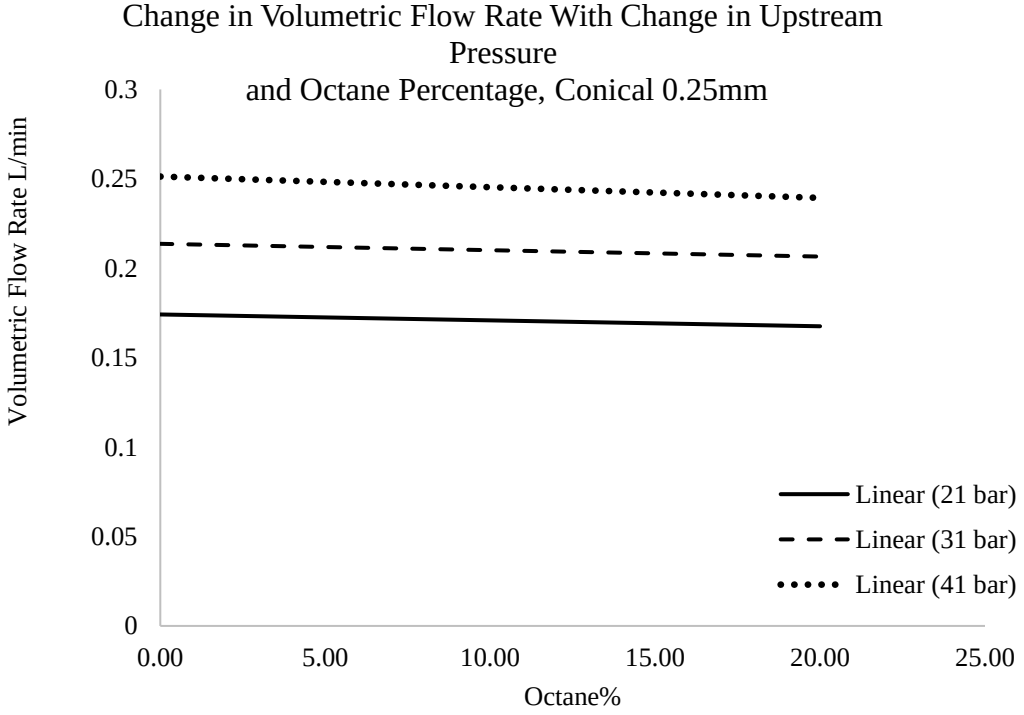

Figure A 6 - 3 Volumetric Flow Rate Conical 0.25m

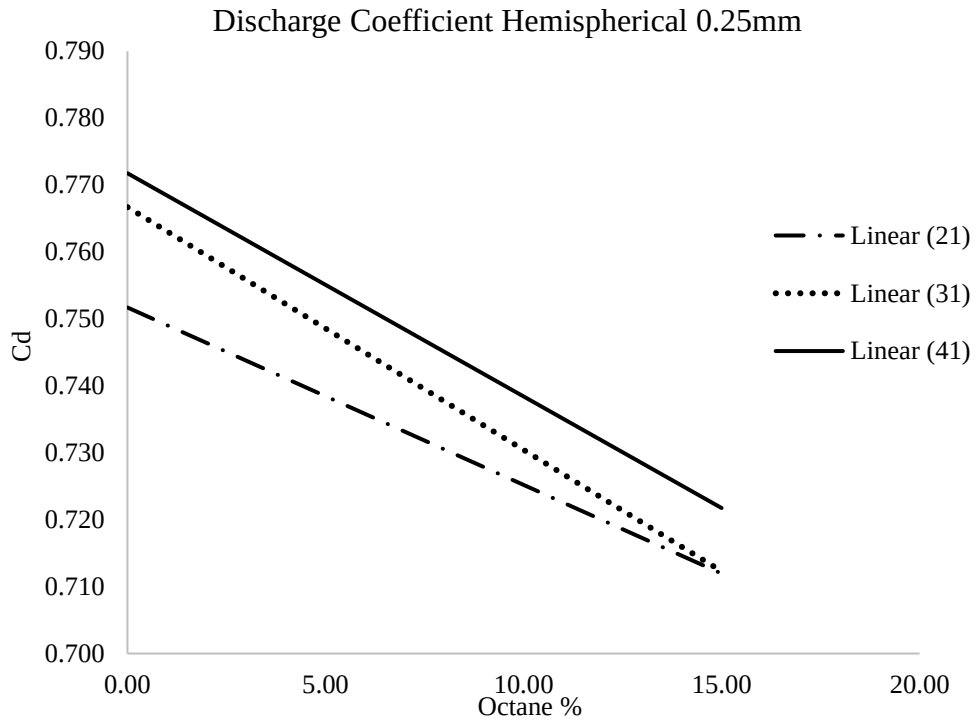

Figure A 6 - 4 Discharge Coefficient Hemispherical 0.25m

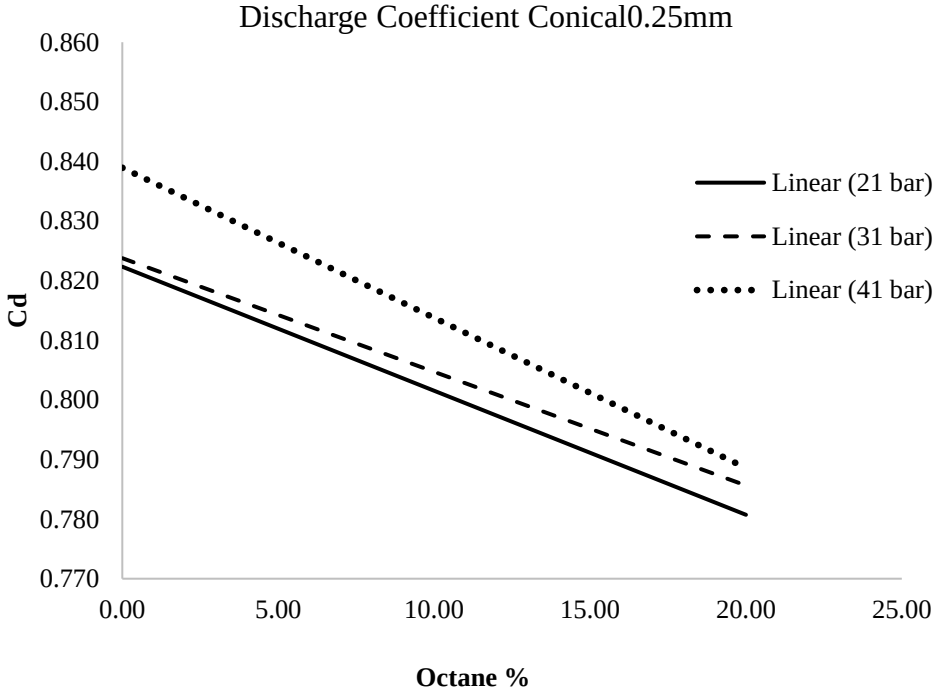

Figure A 6 - 5 Discharge Coefficient Conical 0.25m

A.7. Cavitation Onset Pressure

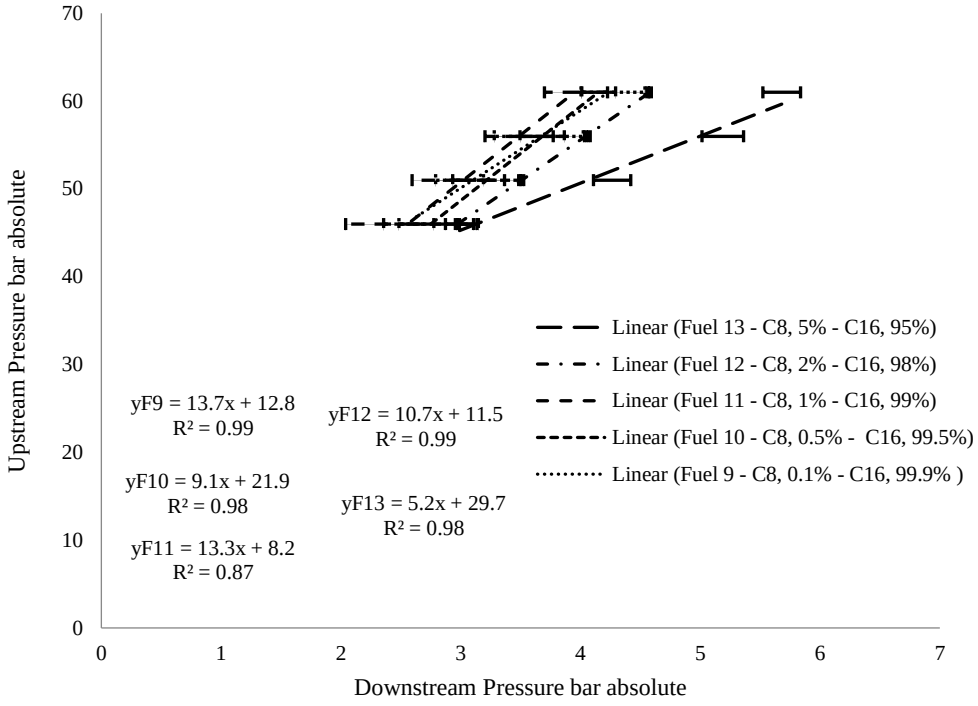

Figure A.7. 1 Cavitation Pressure Onset Cylindrical Acrylic 0.14mm: *n*-Hexadecane- *n*-Octane

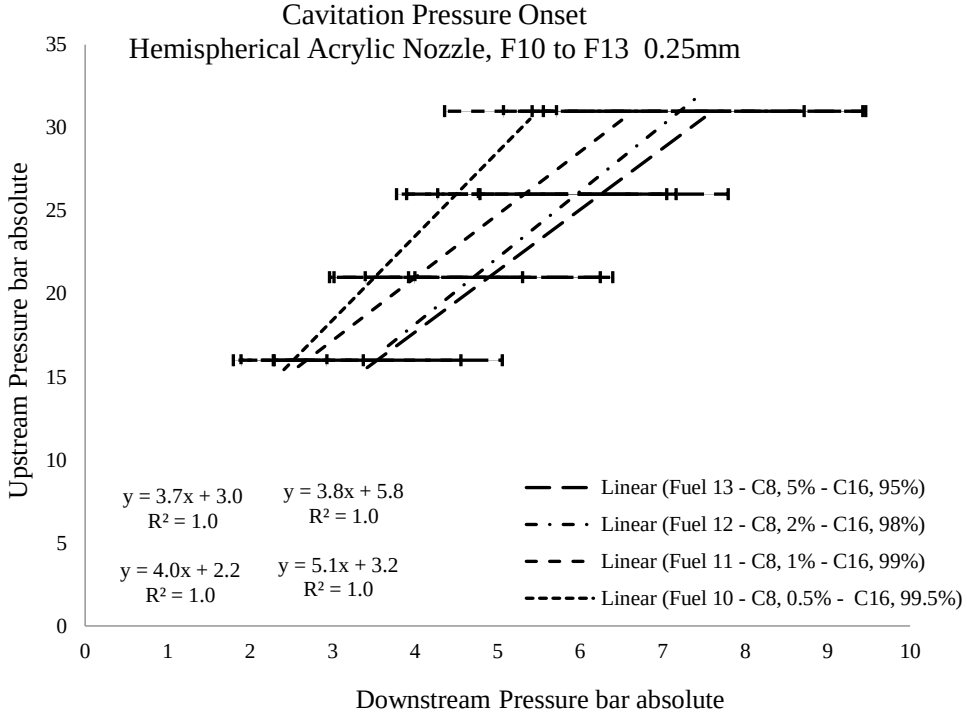

Figure A.7. 2 Cavitation Pressure Onset Hemispherical Acrylic 0.0.25mm: *n*-Hexadecane- *n*-Octane

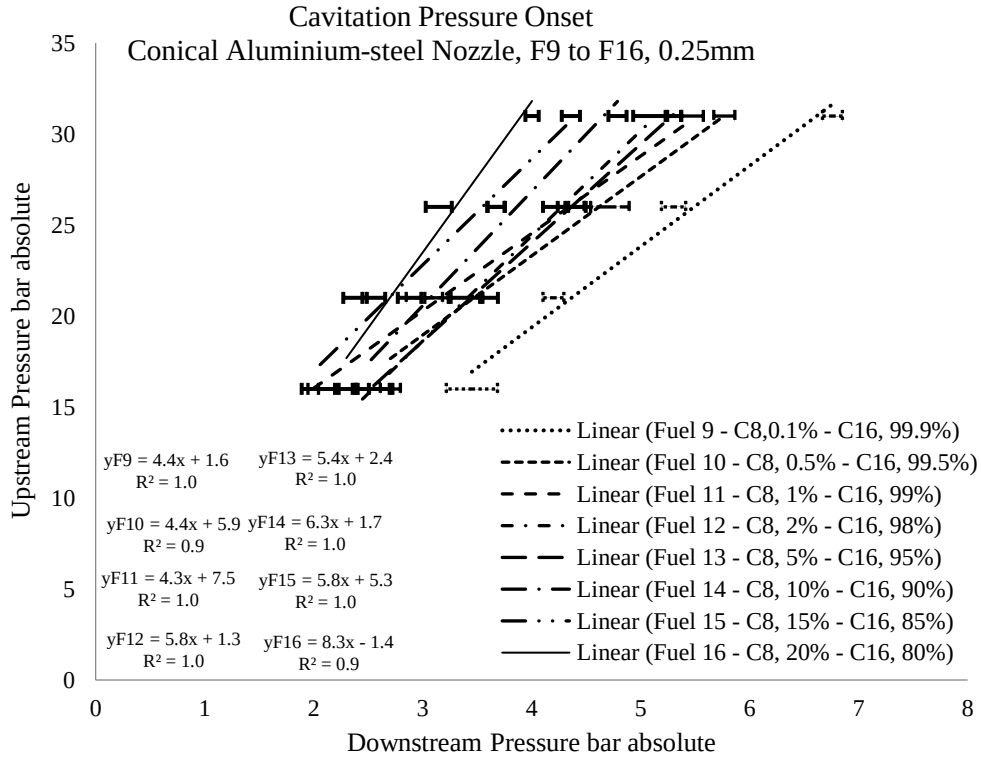

Figure A.7. 3 Cavitation Pressure Onset Conical Aluminium 0.0.25mm: *n*-Hexadecane- *n*-Octane

Changes in Upstream Pressures due to the changes in Downstream Pressures an increase in the Upstream Pressure was noted with the increase of Downstream Pressure

Changes in Downstream Pressure due to changes in Fuel concentration: As seen from Figure A.6.1 and Figure A.6.2, the Downstream pressure increased with the increase in the n-Octane concentration. The reverse was noted for the Conical nozzle in Figure A.6.3.

A.8. Cavitation dependency on Saturated Vapour Pressure

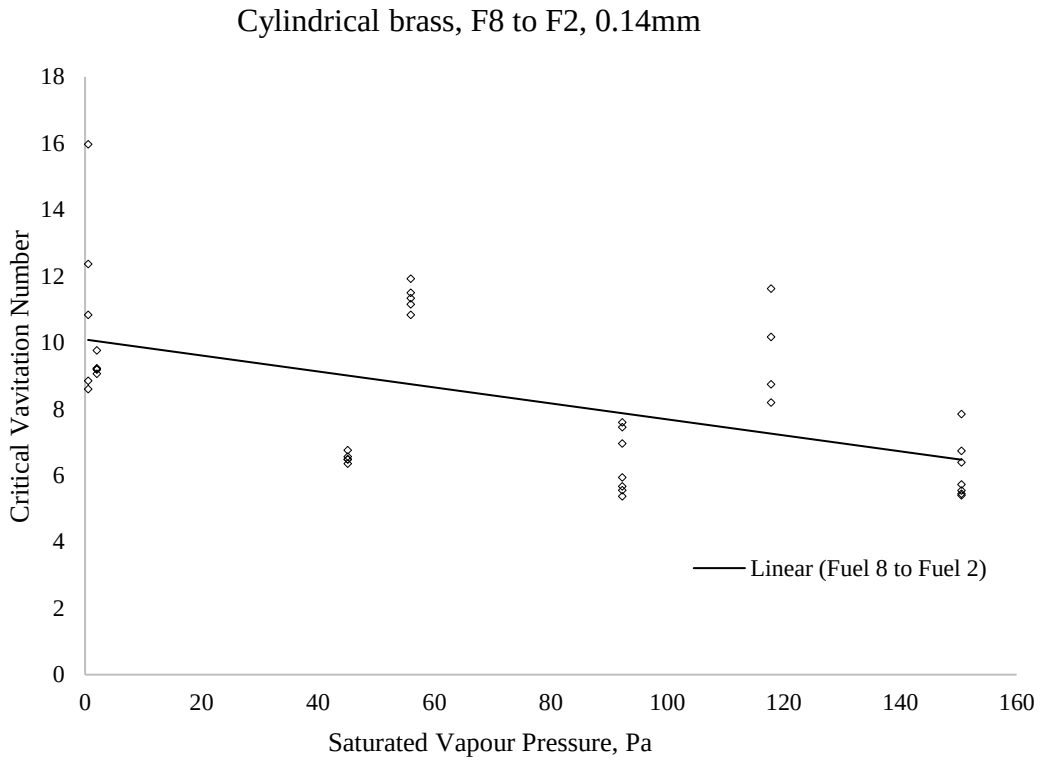

Figure A 8 - 1 Ca variation due to Sat Vap Pressure, 0.14 mm nozzle Cylindrical, F8 to F2

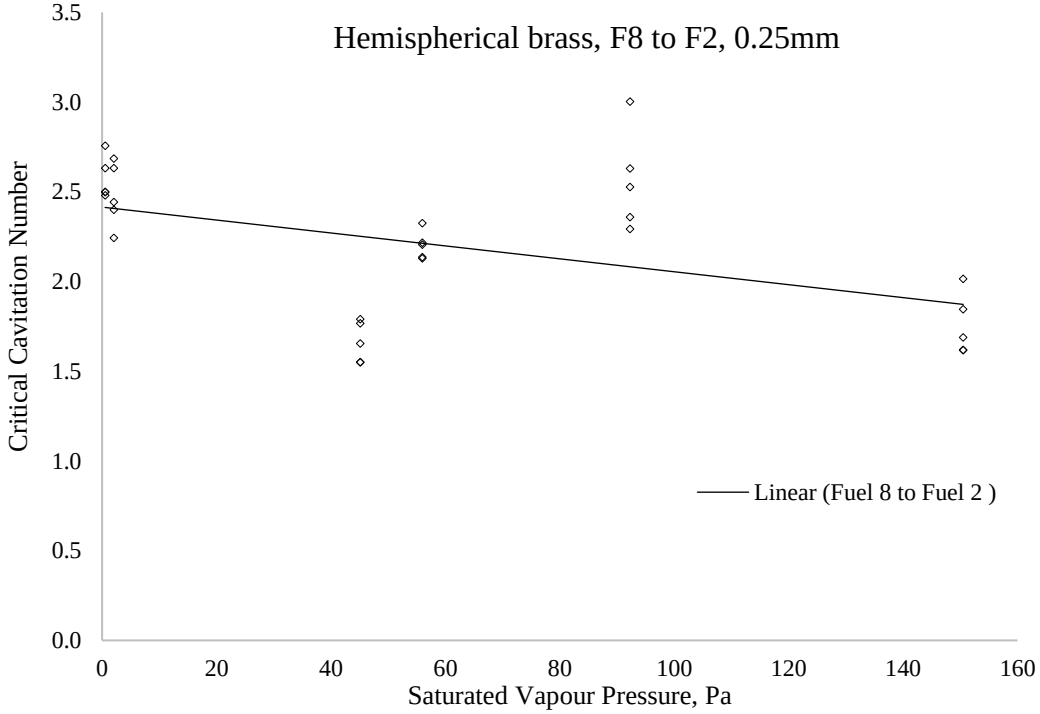

Figure A 8 - 2 Ca variation due to Saturated Vapour Pressure, 0.25 mm nozzle Hemispherical, F8 to F2f2

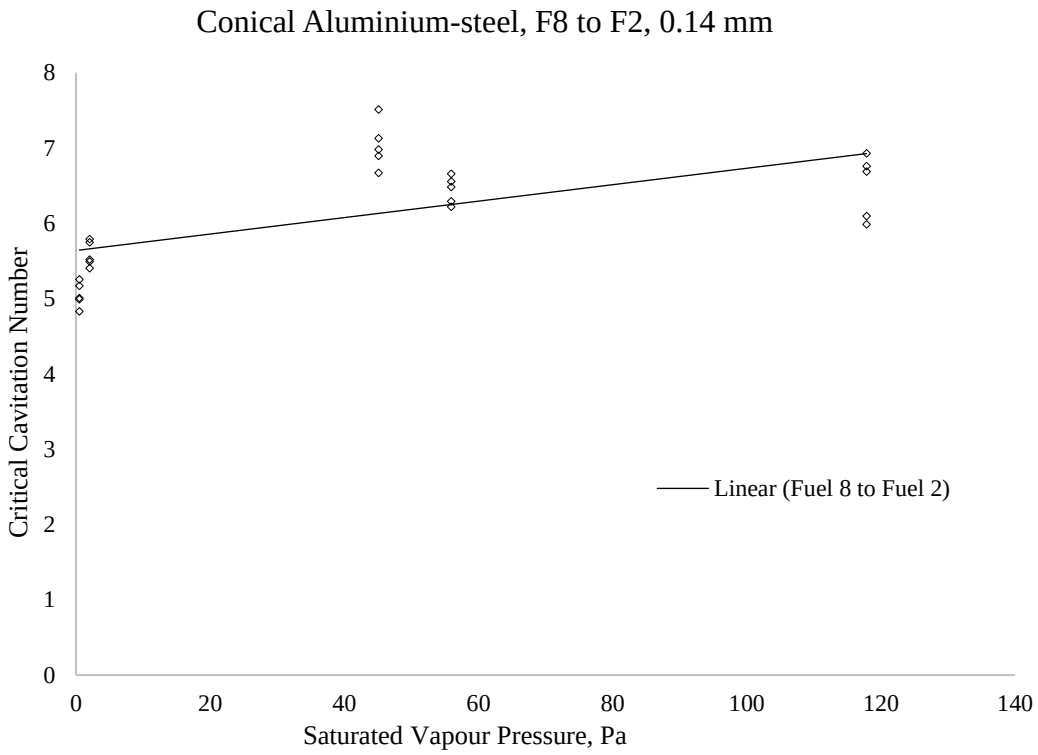

Figure A 8 - 3 Ca variation due to Saturated Vapour increase, 0.14 mm nozzle Conical, F8 to F2

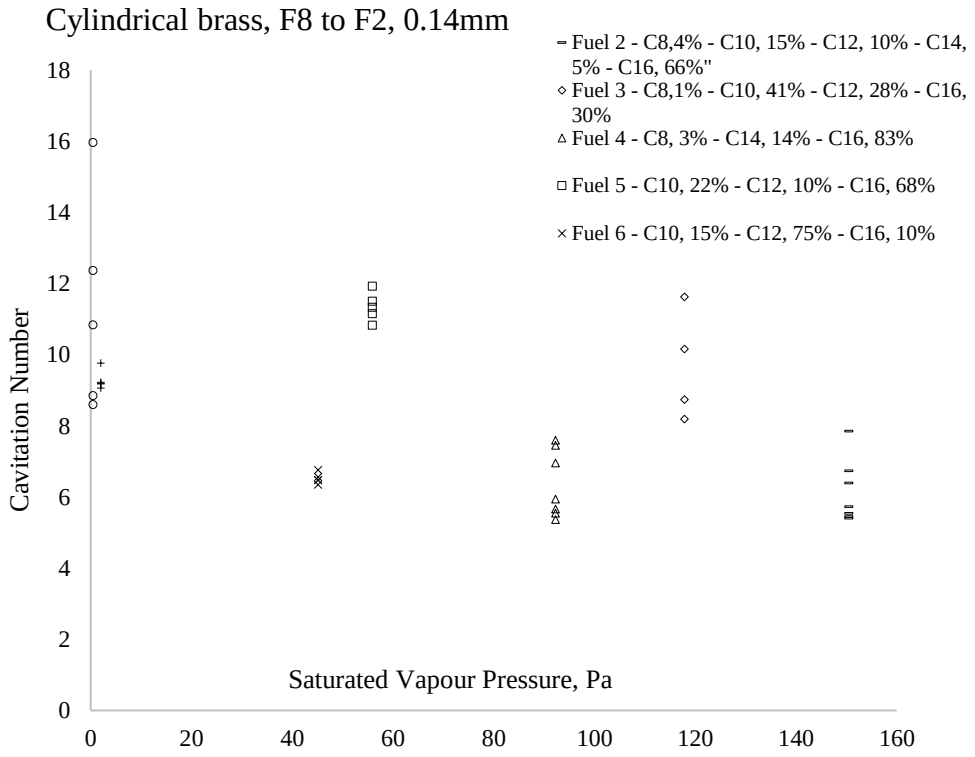

Figure A 8 - 4 Ca variation due to Saturated Vapour increase, 0.25 mm nozzle Cylindrical, F8 to F2

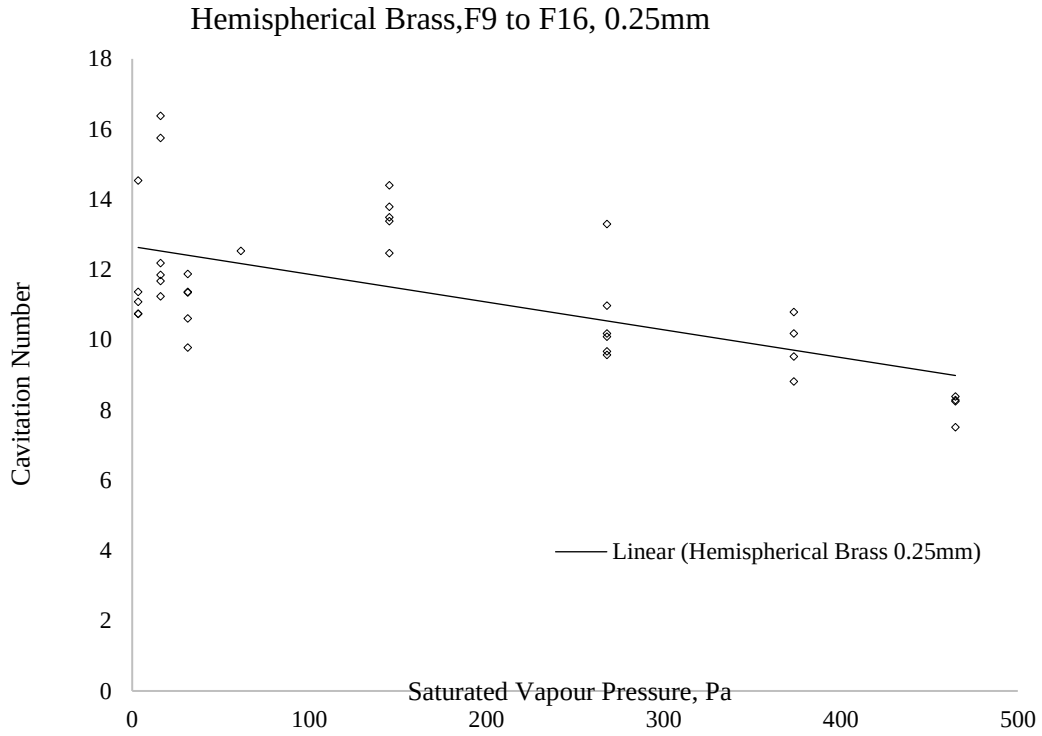

Figure A 8 - 5 Ca variation due to Saturated Vapour increase, 0.14 mm nozzle Hemispherical, F9 to F16

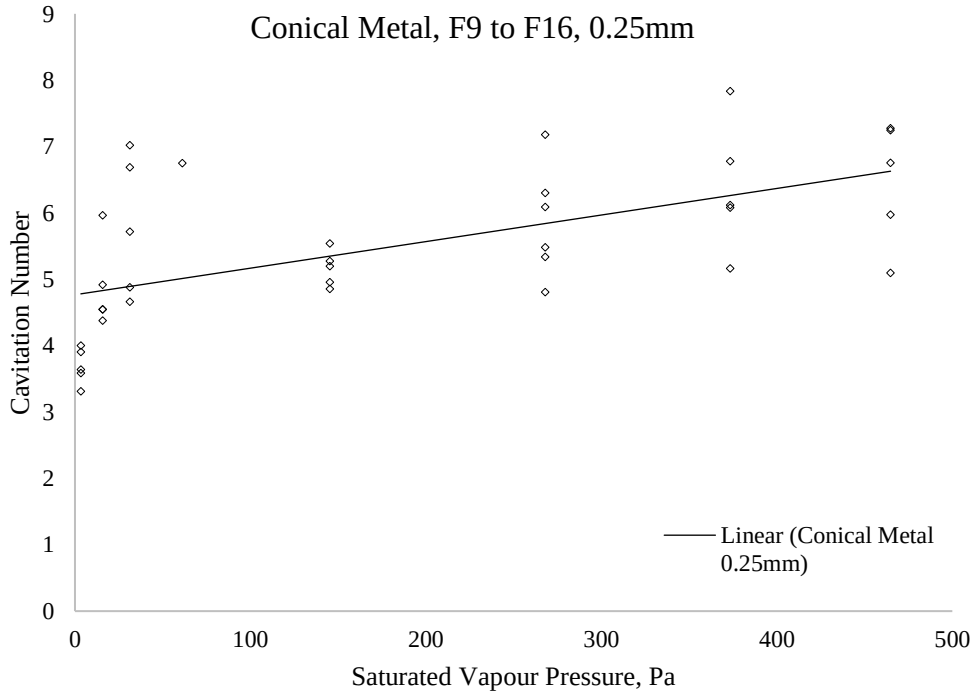

Figure A 8 - 6 Ca variation due to Saturated Vapour increase, 0.25 mm nozzle Conical, F9 to F16

The cavitation behaved has expected for the Cylindrical, Hemispherical and Conical nozzles respectively.

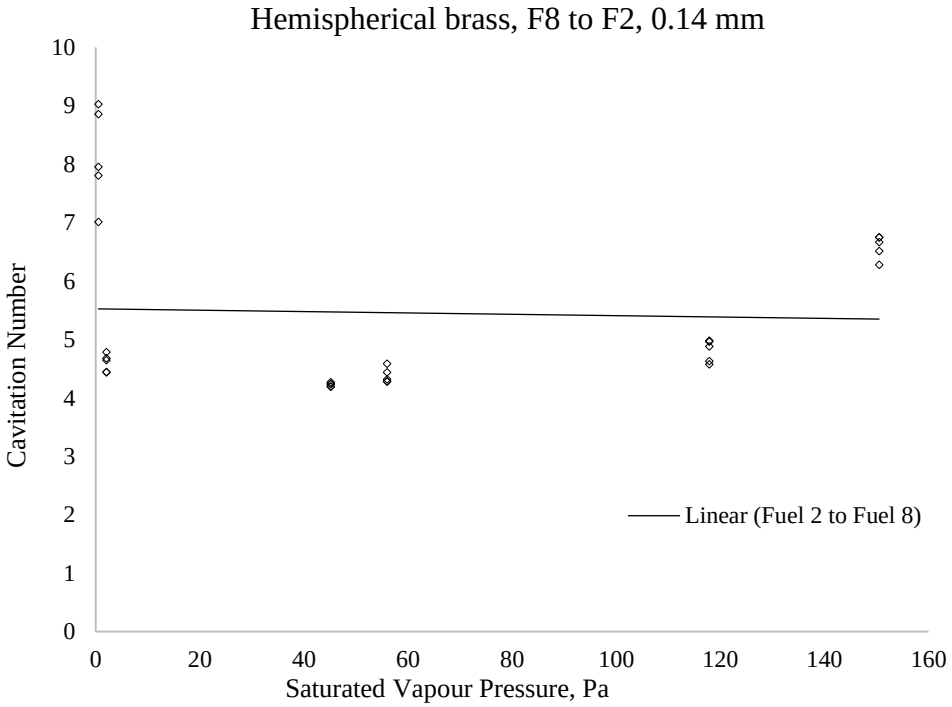

Figure A 8 - 7 Ca variation due to Saturated Vapour increase, 0.14 mm nozzle Hemispherical, F8 to F2

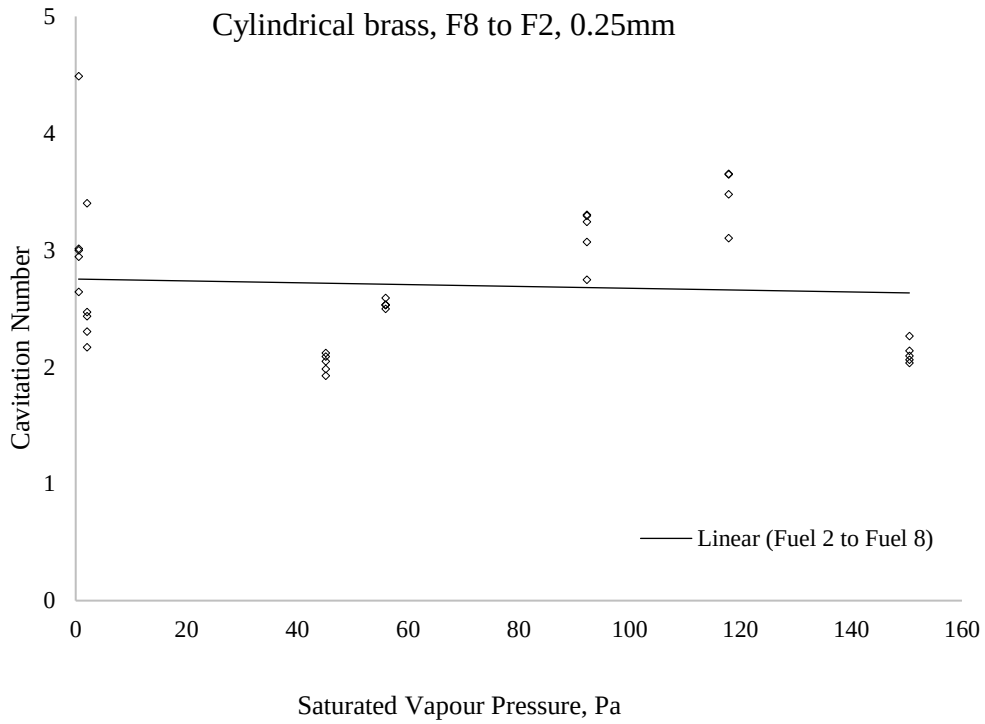

Figure A 8 - 8 Ca variation due to Saturated Vapour increase, 0.25 mm nozzle Cylindrical, F8 to F2

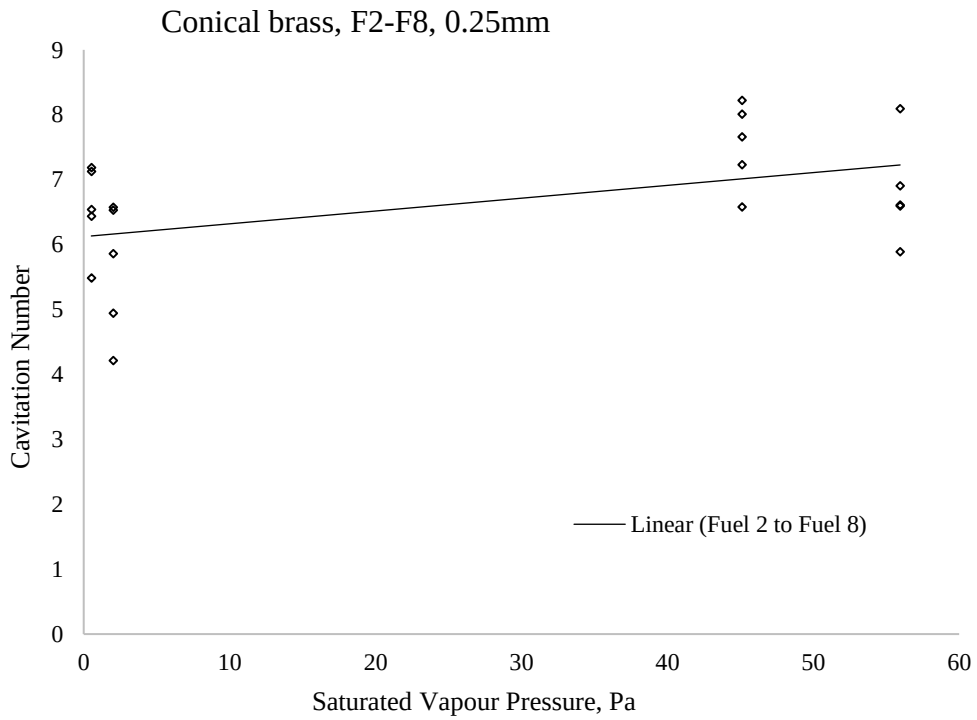

Figure A 8 - 9 Ca variation due to Saturated Vapour increase, 0.25 mm nozzle Conical, F9 to F16

A.9. Cavitation Jet Flow

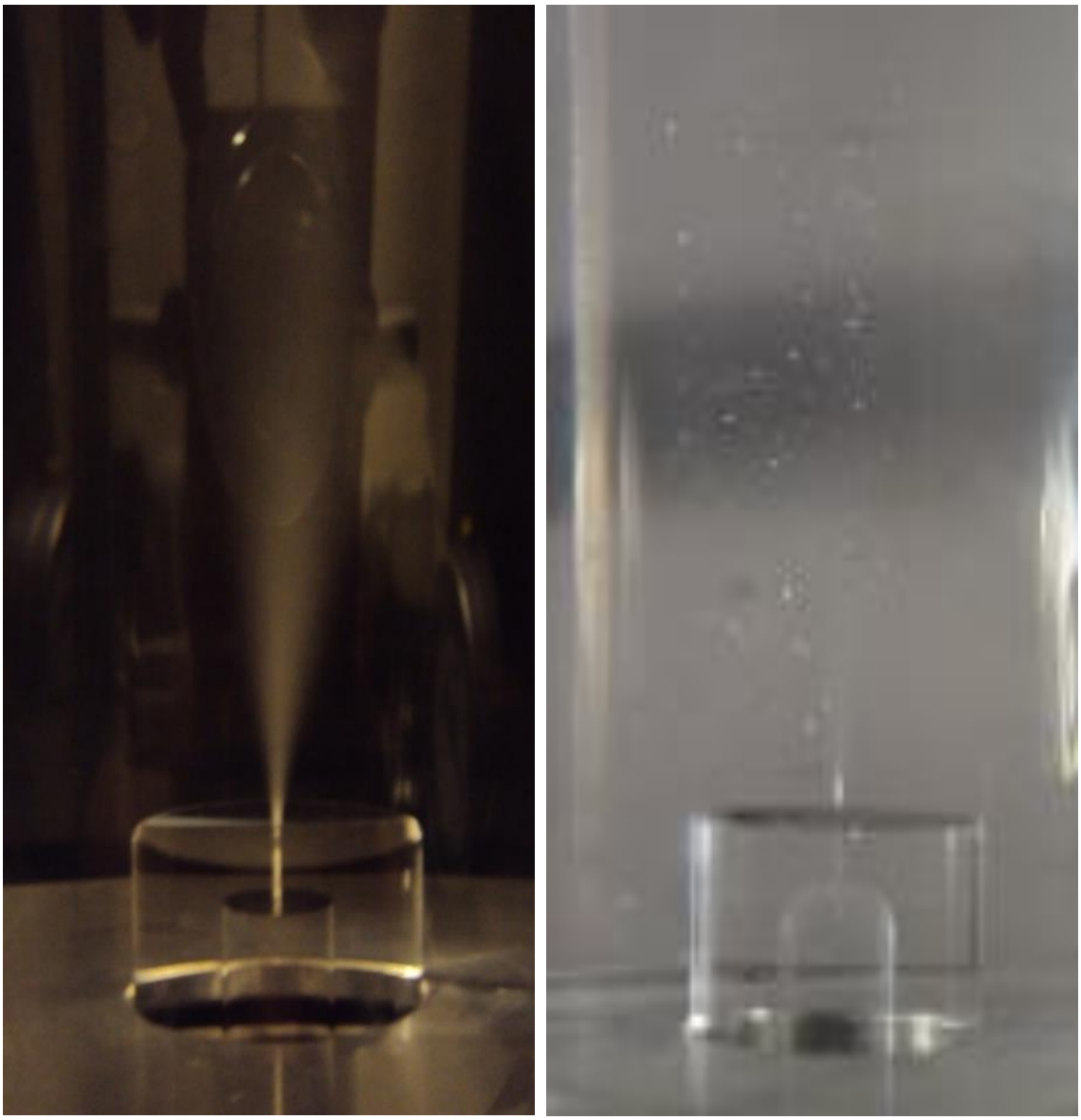

Figure A 9 - 1 Non turbulent and turbulent cavitated jet

The jet as shown on the left hand-side of picture displays the start of turbulence. The right hand-side of the picture depicts a fully turbulent jet.

APPENDIX B

B.1. High Pressure Sustained hydrodynamic cavitation of diesel and biodiesel fuels Rig – Operational Procedures

The rig, made up of mechanical and electrical components, was purposely built insitu for the hydrodynamic study of Fuel A, RME and GTL hydrocarbon fuels. A comprehensive Risk Assessment was done to underline the risks associated with the use of Fuel A, RME and GTL at high temperatures and pressures.

To start off, it was imperative to make sure that all operating machineries were turned off:

All electrical equipment was switched off – the rig main plug was removed in order to process with the draining procedure.

B.1.1. Draining of the rig

The drainage was done in two steps: ***Firstly***, a pipeline that connects one end to the filter and the other end to the first Drainage Bottle in order to drain the tank, the LPP, the injection cylinder and the piping system, was made use of making sure that the valve allowing the return of the fuel to the tank was "on" in order to completely drain the fuel contained in the piping system as well as partially drain the filter. The return to the tank was then set back to "off" position as the drainage took place.

Thereafter**,** the different stapes followed were:

- Closing the valve to the LPP, removing the pipeline connected to the filter, opening the valve to the HPP and placing a Second Drainage Bottle under the filter to drain the HPP and the rest of the fuel left inside the filter.
- Opening the valve that lead to the cooling units, enabling at least 2.5L of fuel to be drained from the cooling unit to the Third Drainage Bottle

Secondly, draining the injection cylinder by placing the Fourth Drainage Bottle at the end of the pipe – this was performed by opening the valve that led to the injector and slowly unscrewing the air-hole at the cylinder top to allow the air to enter the cylinder – the mechanism helped to drain the fuel as the pressurized air pushed the fuel out.

As the filter, cooler and measuring cylinder were already drained, it was vital to make sure that the valves connected to them were set to an "off "position, and to ensure that the return to tank was still set to an "off" position.

Hence, as the valves to the inlet/exit of the injection cylinder were set to an "on" position it was possible to flush the fuel contained inside the high pressure piping and pump as well as the fuel contained inside the common rail.

As the drainage took place, it was paramount to properly label each fuel bottle used, clearly marking sure to highlight from which part of the rig the fuel was drained from and making sure to include the date that the draining took place.

B.1.2. Flushing/Filling the rig

Before filling the rig with the next experimental fuel, a number of steps were followed:

- A first check was done on the valves in order to make sure that they are still off.
- A second check was done on the rest of system to make sure that the draining procedures were followed accordingly.

3.5 L of 95% n-Hexadecane was used for to flush the rig where an injection temperature of 40 ^{0}C and a pressure of 300 bar were set. The procedure took around 30 minutes.

The LPP was run before the flushing took place, filling up the pump and the piping system in order to remove the air cavities located inside them– the rig was filled starting with the pipping system and

the filter. The rest of the fuel was then directly pored inside the rig. At this stage the HPP was turned on to a maximum of 20 bar to fill the injection cylinder. As the injection cylinder was filled, the HPP was turned off. The LPP was then turned back on to evenly circulate the fuel through the rig.

The next steps were, to set the rig's 3way valve to n "on" position in order to empty the rig externally – A Drainage Bottle was placed under the 3way valve in order to collect the fuel.

The Flushing procedures were repeated for a second time. The rig was ready to be filled at this stage and as it was ready for the next experiment 3.5 L of fuel was made use of.

Hence the rig was run by carefully following the system running procedures. At the end of the experiment, the fuel was drained following the draining procedures.

B.1.3. Running of the Rig

Before running the rig, it was necessary to check all vales settings – Checks were performed to verify whether the fuel system was properly filled. The fuel level inside the tank was also verified as a change in temperature could easily lead to an increase in the fuel level.

The different steps followed were: Making sure that the water supplied to the system was turned on' checking that all electric system in connection to the rig are were switched on from the main supply. Turning the PC Link 2 Software on – as the Power button was selected, it was vital to make sure that the software was recalibrated if and necessary in order to avoid the accumulation of incorrect data. Hence, it was possible to set the duration as indicated on the software to 60 second, and to set the pressure and the emergency control.

At this stage the LPP was turned on, making sure that all emergency stops were lifted.

Following that, the operating key was turned clockwise, holding on the same position for about 20 seconds making sure that the LPP was properly turned on. Hence the start button was pressed on and the operating key was released.

The return valve connected to the top of the fuel tank was turned on and off for a number of times in order to get rid of the bubbles which may have been locked inside the pipes.

The next step was to power the 405 mm laser, enabling appropriate readings to be displayed. The first set of readings were noted as the system stabilized.

The following step was to set the required temperature at the LPP, HPP and pump inlet by pressing the rotation error.

At this stage, a note of the temperature reading at the inlet of the HPP was required – It was important to make sure that Course AN0 was fully clockwise fully.

A final check was made on the pressure regulators to ensure that they were all set to zero by turning them in an anticlockwise motion. Another check was done on the LLP, to ensure that it was still on – At this stage, the HPP could be turned on.

The following steps were followed when turning on the HPP: Turning the operating key clockwise and holding it, pressing the HPP button to start the pump, tune the regulator clockwise to the required pressure.

Here the start time was noted bearing in mind that approximately 15 minutes were needed to stabilize the 1st cooling cycle – Close attention was directed toward the temperature at the inlet of the HPP.

In case of an emergency, the LPP was halted by hitting the emergency stop button, ensuring that the laser was powered out and shutting down the computer system starting with the laser, following by

the rig – In the interest of safety, all spillages were contained with the use of absorbent sand and/or fuel absorbent paper.

At the end of the experiment (10 hours each day), all machines (i.e. electric motor and pump) were turned off allowing the rig temperature to be reduced to ambient. The fuel was left inside the rig where it was once more tested the following day for 10 hours, this during a 3-day period.

B.2. High pressure Sustained Hydrodynamic Cavitation Rig

Additional pictures of the Sustained Hydrodynamic Cavitation Rig were taken.

Figure B 2 - 1 Continuous Flow Sustained Hydrodynamic Cavitation Rig

Figure B 2 - 2 Components of the needless 0.4 mm hole diameter HB X 6965489 single hole Cylindrical nozzle

A fan was used to cool down the rig due to the high pressures considered during the expriment.

B.3. Optical Set Up

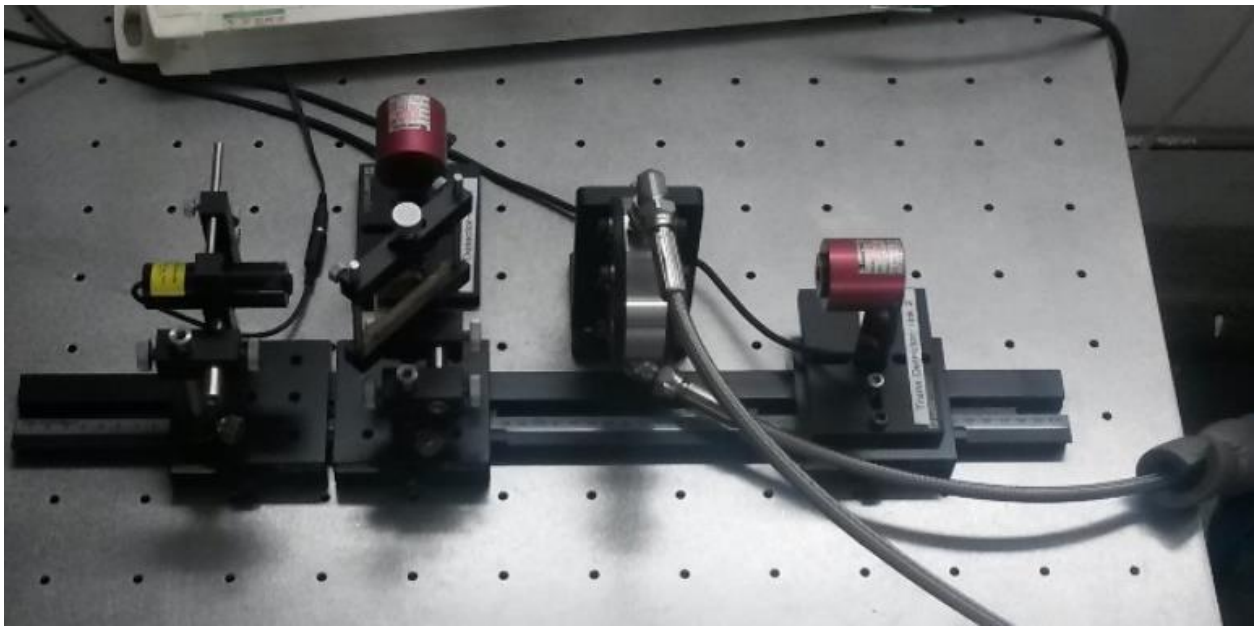

Figure B 3 - 1 Positioning of the Optical Instruments

When positioning the optical instruments, the laser, the Neutral Density Filter, the Reflective Detector, the Optical Cell and the Transmission Detector where place at variable distances to each other.

The Attenuation Coefficient was obtained used Equation B.3

$$\alpha_{(t)} = \frac{ln\dfrac{(t^2_{FusedSilica}\left(\dfrac{1-r_{fuel}}{r_{fuel}}\right)\ r_{mirror)}I_{Ref}}{I_{Dect2}}}{l}\ , Equation\ B.3$$